Anisotropic Colloids in Soft Matter Environments: Particle Synthesis and Interaction with Interfaces

By

Nicholas Ballard

A Thesis Submitted in Fulfilment of the Requirements for the Degree of Doctor of Philosophy

UNIVERSITY OF WARWICK

SEPTEMBER 2012

Table of Contents

Figures

Tables

Acknowledgments

Firstly, I would like to thank all the people who I have had the pleasure of working with over the last four years. A lot of the work described in this thesis would not have come to fruition if it were not for the helpful advice and words of wisdom of past and current members of the Bon group and aside from work I am very grateful for the friendship and support of the whole group. In particular, I would like to thank Andy, Yunhua, Roberto and Gabit who have kept me company on countless coffee breaks.

I would also like to thank my industrial sponsor Unilever for their financial support for the project and to Ezat Khoshdel and Angela Thomas who were very supportive and gave me the scientific freedom to undertake some of the less practical aspects of this work.

I would like to pay a special mention to my supervisor Dr. ir. Stefan Bon who gave me the opportunity to work in his lab and without whom there would undoubtedly be no thesis. I am immensely appreciative of his help, advice and friendship over the course of my time at Warwick and I cannot express my gratitude to him enough.

I would like to thank my family, especially my parents, Philip and Gillian Ballard for their continuing emotional (and financial!) support over the last few years and Mark and Louise Hallam who have welcomed me into their family and have been kind enough to let me stay in their home as I finished this thesis. I would also like to express my gratitude to the rest of my family with particular mention to Ian and Gladys Bulmer, Bernard and Marion Ballard, Peter and Eileen Crawley and my brothers Andy and Dave.

Finally, I would like to thank my beautiful wife, Emily, who has put up with the seemingly never-ending process of writing this thesis and has barely complained despite

the additional stress of me making her move to a foreign country in which neither of us speak the language. To her I am forever indebted.

Declaration

I declare that I am the major contributor to all work in this thesis except the work in chapter 4 which was done in collaboration with Madeleine Hodgson. In addition, Adam Morgan synthesized the cubic particles used in chapter 5. Any work previously published or in preparation for publication is referenced on the opening page of each chapter. All work contained herein was conducted in the Department of Chemistry at the University of Warwick, between October 2008 and October 2012. No material contained in this thesis has been submitted for any other degree, or at any other institution.

Signed _____ Date _____

Nicholas Ballard

Abstract

We have shown new applications and synthetic routes for polymer colloids in the field of home and personal care products by controlling polymer and/or colloidal architectures. Our initial aim was to develop functional particles that imparted beneficial properties to fibrous substrates and as such our first goal was to develop a method for depositing particles onto such surfaces. **Chapter 2** describes the method by which we achieved this goal, namely adding a small amount of a low glass transition polymer to an otherwise non-adhesive polymer to enhance colloidal deposition.

Following on from this work we looked into ways in which to impart desirable characteristics from the particles onto fibres. In **Chapter 3** we describe how the use of a hydrazide functional monomer in polymer gels can provide a continuing slow release of fragrance molecules that reacts to the environment it is held in such that if the local fragrance concentration is low then more is released. In **Chapter 4** we describe the synthesis of highly porous particles with controlled pore sizes and the use of such particles in oil absorption for applications in water-free cleaning systems. The particles are capable of carrying many times their own weight in oil and are shown to be reusable.

In **Chapter 5** we describe a computational model that predicts the ability of a particle to stabilize emulsions. The model is highly adaptable and can be used to predict the surface activity of almost any particle morphology. **Chapter 6** builds on this work and described the synthesis of highly anisotropic polymer particles by templating pre-existing structures and explains their surface activity, or lack thereof.

Publication List

Hybrid biological spores wrapped in a mesh composed of interpenetrating polymer nanoparticles as “patchy” Pickering stabilizers Nicholas Ballard, and Stefan A. F. Bon, *Polym.Chem*., **2011**, 2(4), 823-827.

High internal phase emulsion gels (HIPE-gels) from polymer dispersions reinforced with quadruple hydrogen bond functionality Yunhua Chen, Nicholas Ballard, Florence Gayet, and Stefan A. F. Bon *Chem. Comm.* **2012**, 48(8), 1117-1119

A simple microfluidic device for fabrication of double emulsion droplets and polymer microcapsules Gabit Nurumbetov, Nicholas Ballard, and Stefan A. F. Bon *Polym. Chem*. **2012**, 3 (4), 1043 - 1047.

Waterborne polymer nanogels non-covalently crosslinked by multiple hydrogen bond arrays Yunhua Chen, Nicholas Ballard, Stefan A. F. Bon *Polym. Chem*. **2012**, advance article

Understanding the Multiple Orientations of Isolated Superellipsoidal Hematite Particles at the Oil-Water Interface Adam R. Morgan, Nicholas Ballard, Luke A. Rochford, Gabit Nurumbetov, Thomas S. Skelhon, and Stefan A. F. Bon *under review* **2012**

Functional Polymer Materials. Nicholas Ballard, Stefan A. F. Bon **UK Patent Application No. 1215531.3**

Abbreviations

ACVA	4,4'azobis(4-cyanopentanoic acid)
AFM	Atomic force microscopy
AIBN	Azobisisobutyronitrile
BA	n-Butyl acrylate
CMC	Critical Micelle Concentration
C_p	Monomer concentration in particle (mol.dm^{-3})
CTAB	Cetyl trimethylammonium bromide
DLS	Dynamic light scattering
DVB	Divinylbenzene
ΔG_{ad}	Free energy change for particle adsorption at liquid liquid interface
F	Initiator efficiency
FEG-SEM	Field emission gun scanning electron microscope
GPC	Gel permeation chromatography
HD	Hexadecane
HEMA	2-hydroxyethyl methacrylate
IPA	Propan-2-ol
k_B	Boltzmann constant (1.386 x 10^{-23} J.K^{-1})
k_d	Initiator decomposition rate coefficient (s^{-1})
k_p	Monomer propagation rate coefficient (L.mol^{-1}.s^{-1})
k_t	Termination rate coefficient (L.mol^{-1}.s^{-1})

MAA	Methacrylic acid
MBIS	*N-N*' methylene bisacrylamide
MH	Methacryloyl hydrazide
MMA	Methyl methacrylate
n	Average number of radicals per particle
N_A	Avogadro's constant ($6.23 \times 10^{23} mol^{-1}$)
N_c	Number concentration of particles ($particles.L^{-1}$)
NMR	Nuclear magnetic resonance
PBA	Poly(n-butyl acrylate)
PDI	Polydispersity index
PDMS	Polydimethylsiloxane
PMH	Poly(methacryloyl hydrazide)
PMMA	Poly(methyl methacrylate)
PSt	Polystyrene
PVA	Polyvinyl alcohol
PVP	Poly(vinyl pyrrolidone)
QD	Quantum dot
SDS	Sodium dodecyl sulphate
St	Styrene
TEM	Transmission electron microscope

T_g	Glass transition temperature
Tol	Toluene
X_M	Fractional monomer conversion
Z_{ave}	Intensity average diameter
σ	Interfacial tension ($mN.m^{-1}$)

Chapter 1: Introduction

The ability to easily synthesize polymeric materials with controllable, application specific properties has revolutionized the world in which we live to an extent that it is difficult to find commercial products, for example in the area of home and personal care, which the field of polymer chemistry has not touched in some way or other.[1,2] Of the thousands of synthetic polymers that exist commercially those synthesized by heterogeneous (radical) polymerization make up a large proportion, primarily due to the low cost of synthesis and the ease in which the resulting polymer dispersion can be handled.[3] Heterogeneous radical polymerization techniques usually result in two phase systems of the polymer finally dispersed in an immiscible liquid and can be subdivided into a series of specific techniques that vary in the initial state of the reaction medium, particle formation mechanism and/or the reaction kinetics.[4] The aim of this chapter is to provide the reader with a concise overview of the techniques that are used to synthesize polymer particles and their current and potential uses in home and personal care products.

1.1. Synthesis of Polymeric Particles

1.1.1. The development of heterogeneous polymerization

Natural rubber, a suspension of poly(isoprene) suspended in an aqueous medium, had been used for centuries by the natives of south America[5] before its remarkable properties were discovered by European scientists in the mid 18th century. Commercial exploitation of the desirable water-resistant and viscoelastic properties meant that rubber rapidly became an important commodity and its chemical nature intrigued many of the great chemists of the time, including Joseph Priestly who is credited as being the

first to use it as a 'rubber' and Michael Faraday who discovered it to have an empirical formula of C_2H_5.[6] The demand for rubber grew substantially after the discovery of the vulcanization process by Charles Goodyear and a huge array of applications in which rubber was essential, from tires to the soles of shoes, were discovered.[7,8] In the late 19th century the British scientist Henry Wickham gathered thousands of rubber tree seeds from Brazil and smuggled them back to Kew Gardens, London from where they were later exported across the world to British colonies such as Singapore, Indonesia and Malaya (which was later to become the world's largest producer of natural latex). It was rapidly discovered that the rubber tree was significantly more productive in Asia than in the Brazils and the Asian rubber plantations soon surpassed the South American market in productivity.

Figure 1. 1 *(Left)* Natural rubber latex being tapped and collected from rubber tree. Source: *Kew Gardens, London*. *(Right)* Synthetic rubber plant under construction at Auschwitz-Monowitz 1945. Source *Bildarchiv Preußischer Kulturbesitz Collection.*

The first major efforts to manufacture *synthetic* rubber were conducted in the early part of the 20th century.[9,10] While the commercial synthesis of synthetic rubber was implemented by Germany during the first world war as supplies of natural rubber were cut off by the allies, these initial efforts were hampered by the high cost of production and inferiority of the synthetic product compared to that of natural latex. In the period between the two great wars of the last century significant steps in the

development of a commercially viable synthesis were made as the export restrictions of natural rubber imposed by the British in Malaya led countries such as Germany and Russia to develop methods to produce rubber without the need for imports.

During the 1930s, IG Farben, a German conglomerate, invested huge amounts of money, partly funded by the Nazi government, and manpower into the development of a replacement for natural rubber in case of war. The initial method involved polymerization of butadiene using metallic sodium as a catalyst but was later substantially modified to use free radical initiators in aqueous suspension and was termed 'Emulsion Polymerization'.[11–13] By the time the 2nd World War began Germany had several operational plants producing synthetic rubber and were constructing many more including the infamous plant at Auschwitz-Monowitz, largely built by concentration camp inmates but never actually operational (**Figure 1. 1**).

After the United States entered the war they quickly found themselves running low in rubber supplies as the Japanese prevented the transport of natural rubber from south-east Asia. In 1940 the US had the highest annual consumption of rubber in the world (600,000 tons *per annum*) and no means by which to fulfil this demand. What followed was an incredible collaborative effort, directed by the US government, involving Universities and companies nationwide, who pooled patents and knowledge in order to develop the emulsion polymerization process into a scalable industrial process capable of supplying the army and the nation with all the rubber that they would need. [14–16] The 'mutual recipe' which was decided upon for the production of general rubber is shown in table 1 and does not significantly differ from what one might expect to be used today.[17,18]

Table 1. 1 'Mutual Recipe' for general purpose rubber (1942)

Ingredient	Parts
Butadiene	75
Styrene	25
Potassium Persulfate	0.3
Lauryl mercaptan	0.5
Water	180
Soap	5

The development of emulsion polymerization as an industrially viable synthetic process meant that after the war significant research into heterogeneous polymerization was conducted and as the number of applications for polymeric materials grew so did the field of colloidal particle synthesis. What follows is a brief description of the techniques by which polymeric particles can be synthesized by free radical polymerization.

1.1.2. Heterogeneous radical polymerization techniques

Heterogeneous radical polymerization techniques can be divided into several classes with different features that allow for a wide range of monomers and particle sizes to be obtained (**Figure 1. 2**).[4]

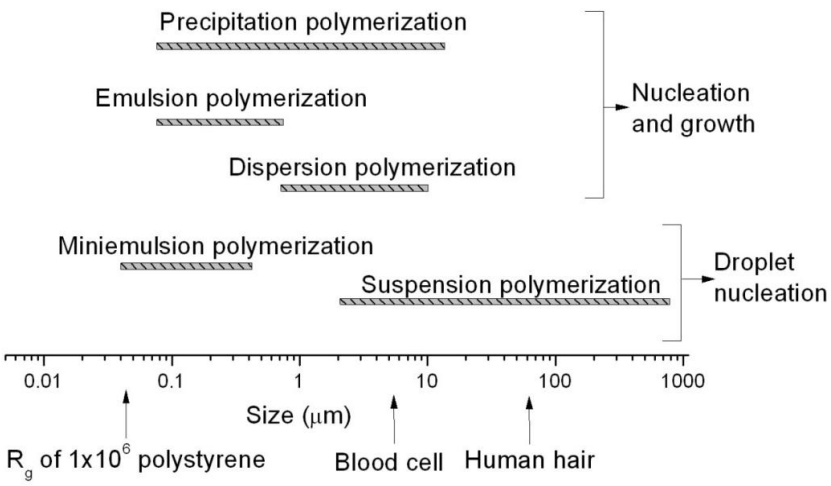

Figure 1. 2 Illustration of the particle size range achievable by various heterogeneous free radical polymerization techniques.

Heterophase polymerizations are often more complicated than their homogeneous counterparts because they depend on an interplay between the kinetics of polymerization and the kinetics that govern particle nucleation and growth. In order to synthesize particles that contain complex functional groups and intricate morphologies we must first understand the factors that control their formation.

1.1.2.1. Suspension Polymerization

Perhaps the most conceptually simple heterogeneous polymerization technique is suspension polymerization. In this case a monomer containing a soluble initiator is dispersed, usually by mechanical stirring, in a non-miscible solvent aided by a surfactant and/or protective colloids that prevent droplet coalescence (**Figure 1. 3**).[19,20] The polymerization is then conducted by raising the temperature (in the case of a thermal initiator) and is stirred throughout the reaction.

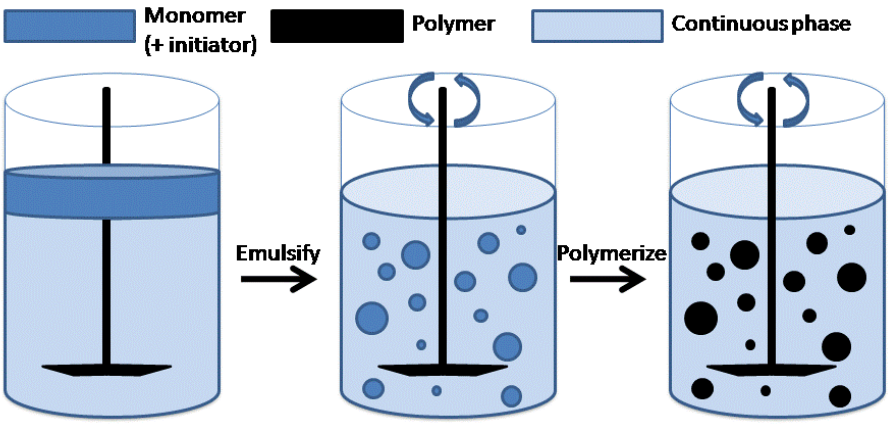

Figure 1. 3 Schematic illustrating typical suspension polymerization reaction. An immiscible monomer is dispersed by mechanical agitation and subsequently polymerized using a free radical initiator.

In this case the droplets produced during the initial emulsification are the loci of polymerization and polymerization is assumed to proceed with kinetics similar to that of bulk (or solution) polymerization with each droplet acting as a microreactor.[21–24] This type of nucleation mechanism is termed droplet nucleation for obvious reasons and typically results in a particle size and size distribution similar to that of the initial

emulsion in the absence of any coalescence of the droplets. The size range for this type of polymerization is limited by the amount of shear that can be applied to induce droplet breakup so that typical particle sizes are on the order of 10-500 μm and the particle size distribution is usually broad. The average particle size can be roughly tuned by altering the stir rate, emulsifier concentration and viscosity but is largely unaffected by changes to temperature and initiator concentration.[4]

One of the more desirable properties of suspension polymerization is the simplicity of the system which allows for multiple components to be loaded into the dispersed phase without much consideration of the partitioning that will occur during the reaction as with other heterogeneous polymerization techniques. For example, Qiu *et al.* showed the production of folded microparticles that were produced by suspension polymerization of styrene/divinylbenzene mixture in the presence of large amounts of toluene that would cause coagulation in most other heterogeneous polymerization techniques (see **Figure 1. 4**).[25] The shape of the particles could be tailored by varying the ratio of monomer to solvent.

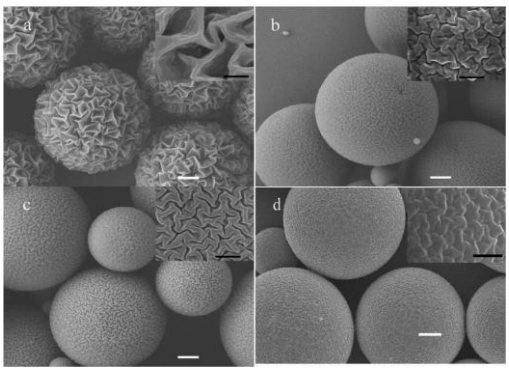

Figure 1. 4 Scanning electron microscope (SEM) images of different solvent-to-monomer ratios of toluene/St/DVB (w/w/w) after polymerization for 8 h: (a) 10:2:1, (b) 10:3:1.5, (c) 10:4:2, and (d) 10:6:3. The scale bar is 1 μm. (Inset) At higher magnification. The scale bar is 300 nm.[25]

1.1.2.2. Emulsion Polymerization

Emulsion polymerization is the most studied and industrially relevant heterogeneous polymerization technique although it can also be considered one of the more

complicated theoretically. The essential components of an emulsion polymerization are almost identical to those of the suspension polymerization system above. Initially there is a monomer which is agitated mechanically in a non-miscible liquid, with or without the aid of an emulsifier, to form an emulsion. In this case however the initiating species is generally contained in the continuous phase. Upon decomposition of the initiating species into free radicals propagation with the small amount of monomer which is dissolved in the continuous phase occurs.[16] The resulting oligoradicals can nucleate polymer particles by two distinct mechanisms. The extent to which one is dominant is dependent on the components used in the reaction mixture (see **Figure 1. 5**).

1.1.2.2.1. Micellar nucleation[16,26,27]

If surfactant is present above the critical micelle concentration (CMC) then there will exist surfactant micelles that can solubilise the growing oligoradical. The radical is said to undergo entry into the monomer swollen surfactant micelle. Radical entry into the monomer droplets that are present in the system is unlikely due to the low relative surface area of the substantially larger (5μm), and less abundant monomer droplets meaning that droplet nucleation is suppressed. Nucleation of new particles from micelles will continue to occur until all of the radicals that are formed are captured by pre-existing particles.

1.1.2.2.2. Homogeneous nucleation[28–31]

Primary particles may also be formed by the precipitation of the growing oligoradical chain. In this case the initiating radical grows to a critical chain length above which it is insoluble in the continuous medium and will precipitate out of solution. These primary particles may or may not be stable to coagulation. In the latter case the primary particles will undergo collision through Brownian motion, stick together and fuse and will continue to do so until there is enough surface

charge, either from surfactant or initiator derived polymer end groups, to stabilize the particles against coalescence.[32]

This nucleation stage is often termed 'Interval I' and is typically completed before the reaction reaches 10% monomer conversion. Following this period no new particles are produced (assuming no secondary nucleation) and hence the particles obtained often have a monomodal size distribution.

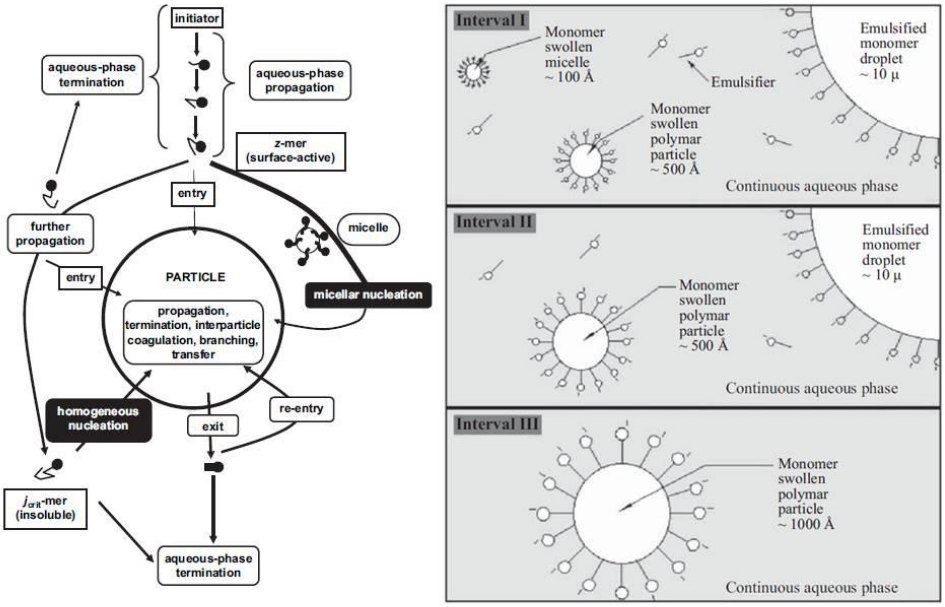

Figure 1. 5 *(Left)* Kinetic processes that can occur in an emulsion polymerization. Reproduced from Gilbert *et al.*[33] *(Right)* Schematic showing the three stages of a typical emulsion polymerization. Reproduced from Schork *et al.*[34]

Following interval I the nucleated particles swell with monomer which is transported through the water phase from the monomer droplets and is subsequently polymerized as the particles continue to capture radicals from solution in what is termed interval II.[35] During this period the monomer concentration in the particles stays approximately constant as the consumed monomer is balanced by the monomer transferred from the monomer droplets. As small latex particles cannot accommodate more than 1 radical without undergoing rapid termination many reactions follow 'zero-

one' kinetics.[36] In this type of kinetic model entry into the swollen polymer particles results in growth until such time as a new radical enters and termination occurs almost instantaneously. In this case the average number of radicals (***n***) in any particle is 0.5. These kinetics may be slightly skewed in the case of a substantial rate of radical exit from the particle (***n***<0.5) or if the particle can accommodate more than one radical due to high viscosity or large particle volume (***n***>0.5). The overall fractional conversion rate of monomer (dX_M/dt) is given by **Equation 1. 1**.

$$\frac{dX_M}{dt} = \frac{k_p C_p \boldsymbol{n} N_c}{n_M^0 N_A}$$ **Equation 1. 1**

Where t is time k_p is the rate of monomer propagation, C_p is the concentration of monomer within the polymer particles, N_c is the number concentration of particles in the reaction n_M^0 is the number of moles of monomer present per unit volume of water in the reactor and N_A is the Avogadro constant.

The particle will continue to grow as monomer is transported across the water phase from monomer droplets until no monomer droplets remain (approximately 40% conversion depending on the reaction conditions) corresponding to the onset of interval III. At this point the concentration of monomer in the particle decreases as it is consumed by the polymerization process and is accompanied by a change in rate. Often the viscosity inside the particle increases allowing for more than one radical to be accommodated and this is coupled with a substantial increase in the rate of polymerization, a phenomenon referred to as the Trommsdorff-Norrish or gel-effect.

The rate of emulsion polymerization is substantially faster than the equivalent solution polymerization due to the effect of compartmentalization. Radicals that are in separate latex particles cannot 'see' each other and hence the overall rate of termination is lower than in a typical bulk or solution free radical polymerization. This also allows

polymers with high molecular weight to be formed.[33] Particles produced by emulsion polymerization often have a monodisperse particle size distribution if interval I is sufficiently short and subsequent nucleation is suppressed and have a particle size on the order of 100 nm (see **Figure 1. 6**).

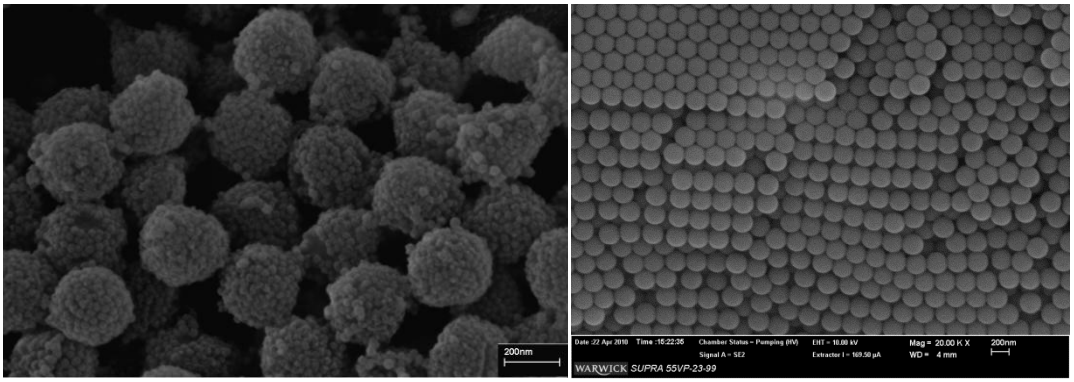

Figure 1. 6 Representative images of particles produced by emulsion polymerization ***(****Left)* FEG-SEM image of a poly(ethyl methacrylate) latex armoured with Ludox TM-40 prepared via solid-stabilized emulsion polymerization at pH 5.5.[37] *(Right)* FEG-SEM image of a poly(styrene-*co*-styrene sulfonate) latex produced by surfactant free emulsion polymerization.

1.1.2.3. Miniemulsion Polymerization

The concept of miniemulsion polymerization was conceived by Ugelstad and co-workers as they explored the extent to which droplet nucleation occurs in emulsion polymerization.[38] As explained above, under standard reaction conditions droplet nucleation is unlikely due to the low surface area of the monomer droplets but it was postulated that if the initial emulsion droplet size could be substantially reduced droplet nucleation could become the dominant mechanism for particle formation.

In order to reach a small enough droplet size the (mini)emulsion is generated using high shear, usually by a sonicator, and a surfactant/cosurfactant system that prevents coalescence and Ostwald ripening of the system. Typically, the average droplet size is on the order of 100 nm and can be controlled to an extent by the surfactant concentration employed and the shear strength. In this case when radicals are generated

in the aqueous phase the droplets successfully compete for their capture and droplet nucleation is the dominant method for particle formation.[34]

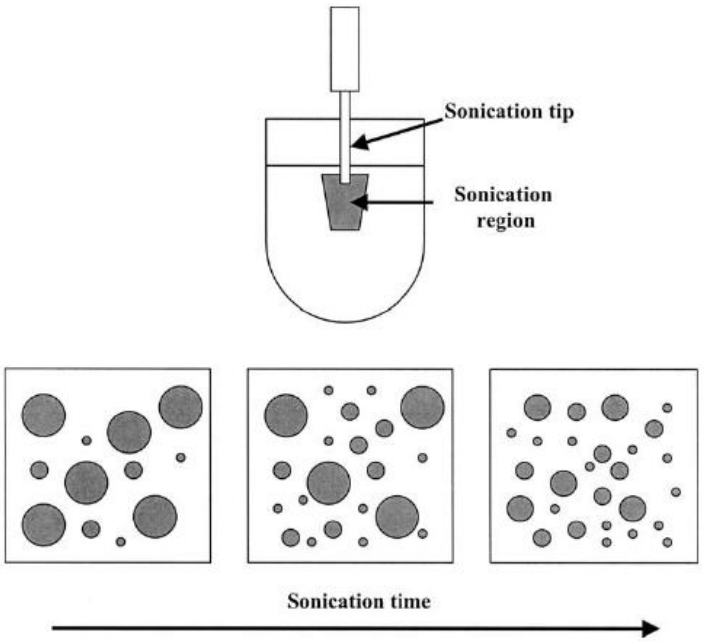

Figure 1. 7 Schematic demonstrating generation of a miniemulsion using ultrasonic waves.[39]

Miniemulsion polymerization can be initiated from both the continuous phase and from the dispersed phase. In the latter case because of the small volume of the droplets if there exists more than one radical in the polymerizing droplet rapid termination by coupling can occur. This has led researchers to the conclusion that either rapid desorption of one radical occurs before termination or that even with oil soluble initiators free radicals that initiate polymerization originate in the aqueous phase.[40] Where initiation is from the continuous phase entry to the monomer droplets by initiator derived radicals can occur. Now it is likely that a single propagating radical exists in the monomer droplet and as such termination is suppressed until another radical enters. The rate of termination is now considerably reduced and the polymerization can occur rapidly and the resulting polymers are of high molecular weight.

While droplet nucleation is the main cause of particle formation in miniemulsion polymerizations it should be noted that not all droplets are necessarily nucleated and this can lead to some complications in the reaction kinetics.[41] Monomer transport from the monomer droplets that are not nucleated is inhibited by the stabilizer (also referred to as cosurfactant) and this prohibits the complete disappearance of miniemulsion droplets even at high conversion.[42] It has also been demonstrated that the rate of entry of radicals in miniemulsion systems is substantially slower than in a corresponding emulsion polymerization.[43] In many cases all droplets are nucleated and the final particle size distribution is similar to the initial miniemulsion.[44–47]

The fact that you can, in ideal cases, preserve the identity of the initial miniemulsion droplets and obtain a "1:1 copy" in miniemulsion polymerization is very desirable[48] and allows for the synthesis of particles containing pigments or active ingredients that cannot be easily produced with other techniques that depend extensively on monomer transport simply by dispersing the active ingredient into the monomer before emulsification (see **Figure 1. 8**).[49] This fact coupled with the wide range of monomers that can be synthesized using miniemulsion polymerization make it a useful tool for polymer colloid scientists.

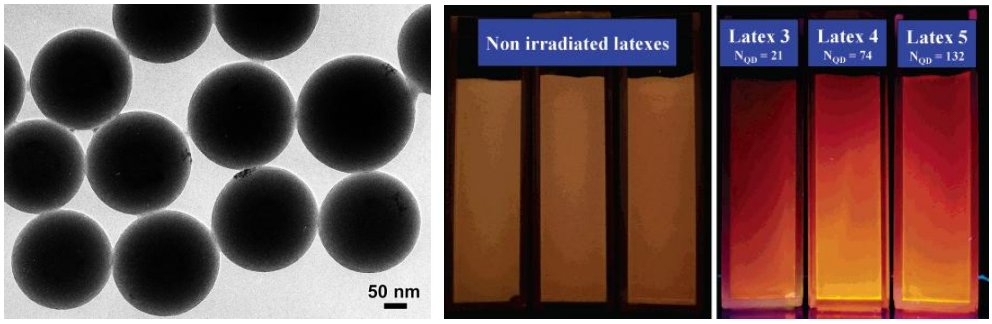

Figure 1. 8 ***(Left)*** TEM photos of quantum dot encapsulated with polystyrene particles by miniemulsion polymerization Dispersion polymerization. ***(Right)*** Photographs of latexes prepared with increasing concentrations of QDs, without and under irradiation (λ_{exc} = 365 nm).

1.1.2.4. Dispersion Polymerization

In contrast to the methods mentioned above dispersion polymerization systems begin as a homogeneous mixture in which the monomer is completely soluble but results in a polymer dispersion due to the insolubility of the polymer in the reaction medium. This encompasses a wide range of monomers and solvents and for the sake of brevity what is discussed herein is limited to the case of styrene and acrylates in alcoholic media which is more relevant to this thesis.

The reaction begins as a homogeneous mixture of monomer, initiator, stabilizer and solvent. Upon initiation of the polymerization oligomeric radicals are formed which grow to a critical chain length before precipitating from solution and forming a primary particle. Typically the particle will adsorb stabilizer from the reaction medium and undergo coagulation and aggregation until a stable particle is formed.[50,51] This aggregation is heavily influenced by the grafting by chain transfer of the growing polymer chain to the stabilizer.[52,53] Particle nucleation in dispersion polymerization is rapid and typically is stopped before 1% of monomer conversion so the polymerization kinetics in the initial stage of the reaction are vital in determining the final particle size and size distribution.[54,55] The monomer is subsequently partitioned between the reaction medium and the polymer particles. For the case of polystyrene in ethanol the majority of monomer resides in the continuous phase.[56,57] For this reason the kinetics of dispersion polymerization for polystyrene in ethanol largely follow solution polymerization kinetics although there is evidence of polymerization occurring in the polymer particles as well.[58,59] Growing radicals are captured by the polystyrene particles and the concentration of styrene in the continuous phase slowly decreases with conversion (see **Figure 1. 9**).

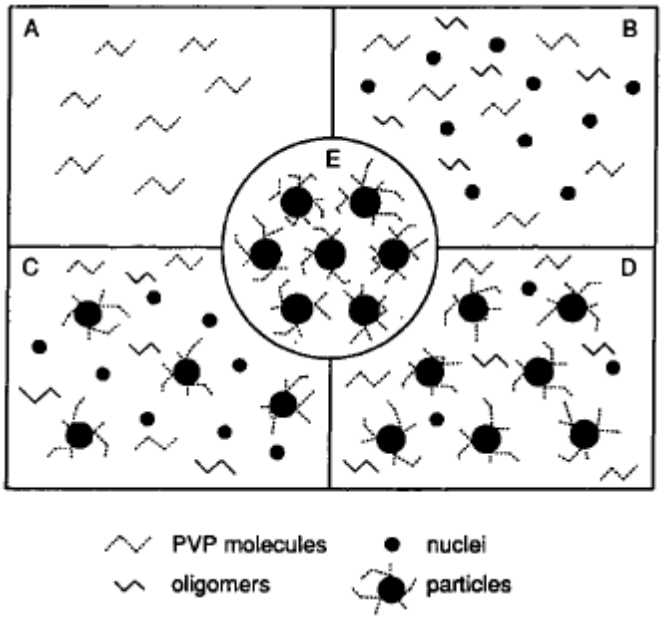

Figure 1. 9 Schematic showing particle formation in dispersion polymerization. (A) Homogeneous solution of stabilizer (PVP) dissolved in medium prior to polymerization. (B) Precipitation of oligomeric chain generates particle nuclei. (C) Mature particles formed by aggregation and stabilization of nuclei. (D) Coexistence of nuclei and mature particles during particle growth stage. (E) Only mature particles observed at the end of the reaction.[51]

In dispersion polymerization the particles are relatively large (~1 μm) and hence the number of particles is low compared to emulsion and miniemulsion polymerization. As the average number of radicals per particle is quite high this results in low molecular weight polymer and the low monomer concentration means that the average rate of polymerization is also substantially slower than the above cases.[56]

Dispersion polymerization can be rather sensitive to the reaction conditions but with careful tweaking of the reaction recipe the particle size distribution can be very narrow (see **Figure 1. 10**). The average particle size (1-10 μm) is an order of magnitude larger than that of emulsion and miniemulsion polymerizations making it of huge interest to the colloid synthesis community.

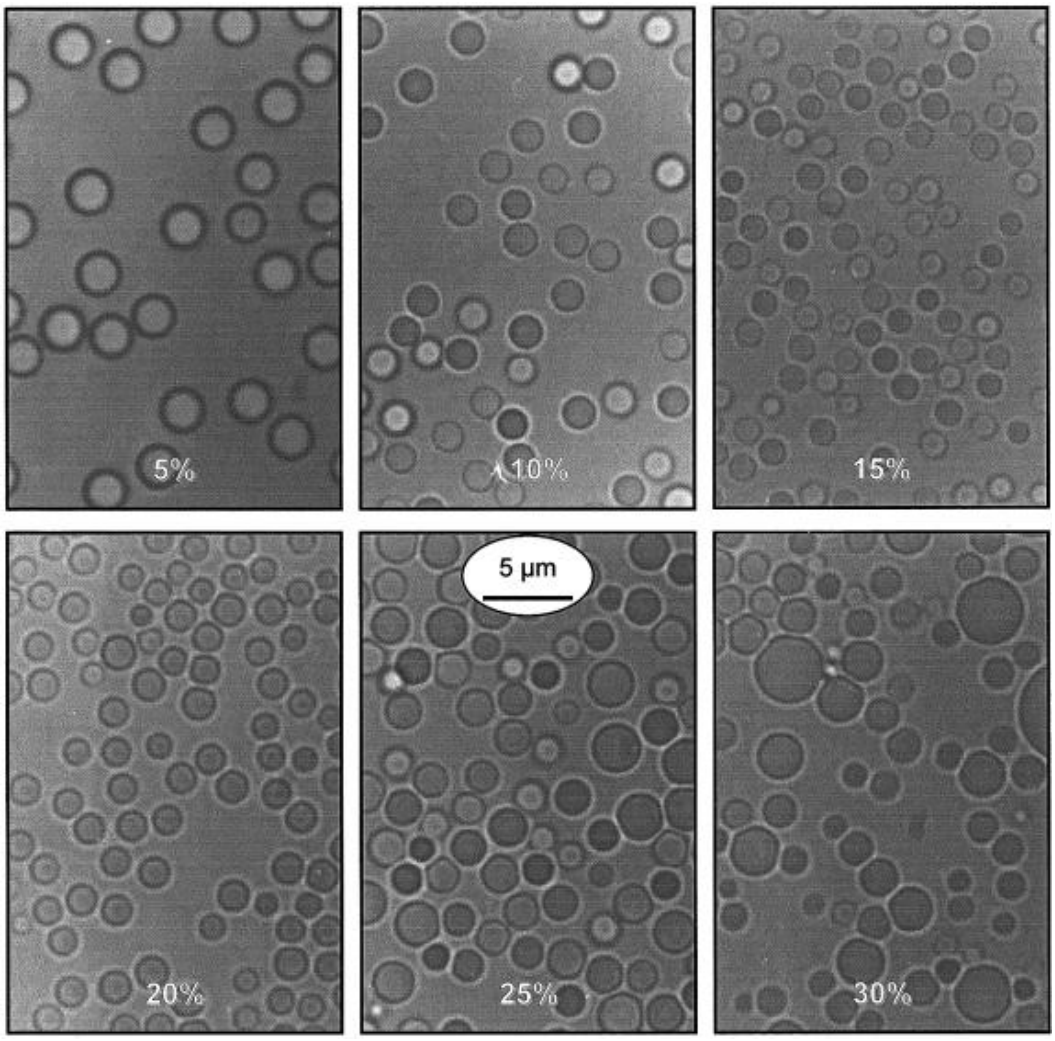

Figure 1. 10 Optical micrographs of poly(butyl acrylate) particles prepared by dispersion polymerization in 90/10 methanol/water medium using different monomer concentrations (wt% *n*-butyl acrylate on total).[60]

1.1.2.5. Precipitation polymerization

Precipitation polymerization is similar to dispersion polymerization in the respect that the initial reaction mixture is homogeneous. The way in which particles are nucleated is also similar and proceeds by the homogeneous nucleation mechanism.[61] The main difference between precipitation and dispersion polymerization is that there is little or no monomer in the particle phase, often because the polymer is heavily crosslinked, causing the polymerization kinetics to follow those of solution polymerization.[61,62] Subsequent growth of the particles occurs by precipitation of the oligomeric chains onto the polymer surface imparting a surface roughness to the

particles. It is often possible to use no stabilizer in this method and the resulting particles are typically on the order of a few microns and under certain conditions can be monodisperse in size.

1.1.2.6. Seeded polymerizations

It has been shown above that the particle nucleation stage in certain heterogeneous polymerization techniques is highly complex and depends heavily on a mixture of polymerization kinetics and the colloidal stability of the nucleated particles. For this reason it is commonplace to 'seed' a reaction mixture, that is to add a small amount of preformed latex particles to the initial feed in order to circumvent the nucleation stage. In doing so results of reactions, in terms of particle size and size distribution, are often more repeatable and it allows for a degree of control over the particle size since it can be assumed the monomer will be divided equally between the number of seed particles.[63–65] Seeded reactions also allow for complex particle morphologies to be produced with anisotropy in shape and chemical nature by using incompatible and/or crosslinked polymers opening up a wealth of new structures that can have interesting physical properties (see **Figure 1. 11**).[66–71]

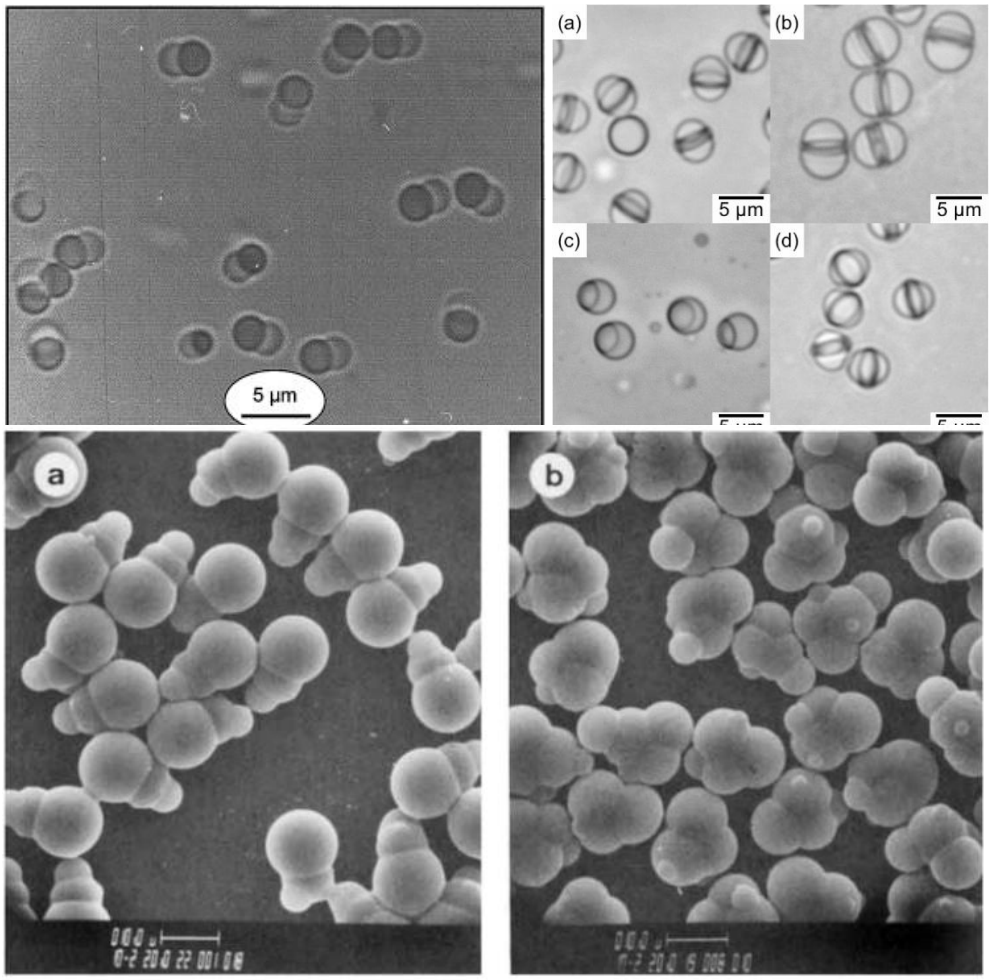

Figure 1. 11 Anisotropic particles synthesized by seeded polymerizations. *(Top left)* Polystyrene/poly(butyl acrylate) dumbbell particles produced by seeded dispersion polymerization.[70] *(Top right)* Polystyrene/poly(2-ethyl hexyl methacrylate) particles with disc-like and 'hamburger' morphologies produced by seeded dispersion polymerization.[67] *(Bottom)* 'Ice-cream cone' and 'popcorn' like polystyrene particles produced by sequential seeded emulsion polymerization of crosslinked polystyrene (scale bar = 10 μm).[72]

1.2. Colloids and polymer colloids in cosmetic and personal care products

Cosmetic and personal care products are almost invariably dependant on some kind of colloidal system, be it in the form of an emulsion, a suspension or a mixture of the two. The role of the colloid in question can differ substantially between products and the ability of colloids to perform a myriad of functions has led to their increasing use in commercial applications. Herein is discussed a selection of key applications in which colloidal particles play an invaluable role.

1.2.1. Pigments

Mineral pigments ground into fine powders are commonly used in cosmetics in order to add colour to the product. Historically pigments were obtained from natural sources and have been used for centuries but modern pigments tend to be made synthetically in order to alleviate problems with toxicity and reduce cost. Pigments are essential components of many make up products such as mascara, blushers, liquid foundation, face powders and lipstick.[73,74] The scope for polymeric pigments is limited by the lack of light absorbance of most acrylic and styrenic polymers and the high cost of incorporating UV/vis absorbing monomeric units into the polymer but there are reports of the use of photonic colloidal crystals for use as pigments (see **Figure 1. 12**).[75]

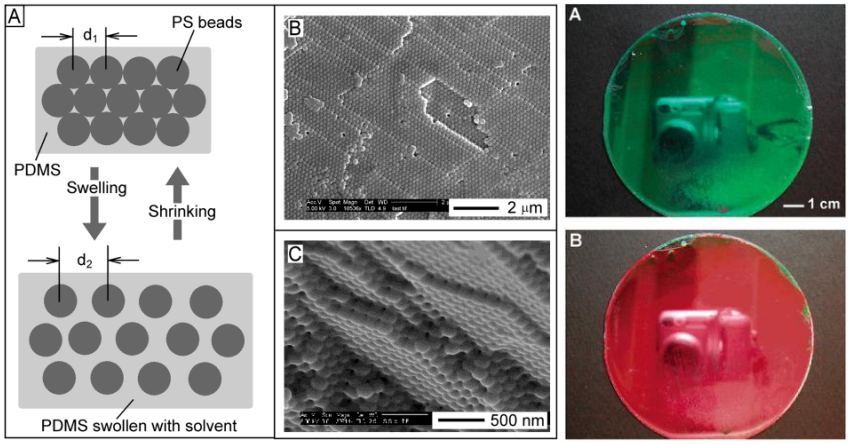

Figure 1. 12 *(Left)* (A) Colloidal crystal of polystyrene imbedded in PDMS and variation of lattice spacing d upon swelling PDMS network. (B) Top view SEM of colloidal crystal of polystyrene embedded in PDMS matrix. (C) Cross sectional SEM of the same sample. *(Right)* Photograph of 'photonic paper' before (A) and after (B) swelling with isopropanol.

1.2.2. Viscosity modifiers

Most commercial products contain viscosity modifiers in order to improve the feel of the product and it is common to use synthetic or biological polymers in order to induce desirable viscoelastic properties. Synthetic and mineral clays are also used extensively often in tandem with molecular viscosity modifiers in order to enhance performance. Colloidal gels are often stronger at lower concentrations, exhibit shear thinning and thixotropic behaviour and are tolerant to a wide range of electrolyte

concentrations. These features make particulate viscosity modifiers essential additives in a wide range of commercial areas including toothpastes,[76] hair styling products,[77] skin cleansers,[78] nail lacquers[79] and shampoos.[80] The particle shape plays a major role in its rheological behaviour and the ability to tune particle shape is key to enhancing rheological properties of suspensions.

1.2.3. Encapsulation agents

The ability to encapsulate active agents offers the opportunity for better storage and triggered/selective release. The core of the microcapsule is isolated from the continuous medium making it possible to store either hydrophilic or hydrophobic compounds in large quantities. Typically these capsules are made by either forming a double emulsion in which the middle phase can be solidified,[81-83] or alternatively by an interfacial reaction that forms a skin around the active ingredients (see **Figure 1. 13**).[84] These type of capsules have applications in a wide range of products but are most commonly found in laundry products which contain expensive active ingredients such as enzymes.[85]

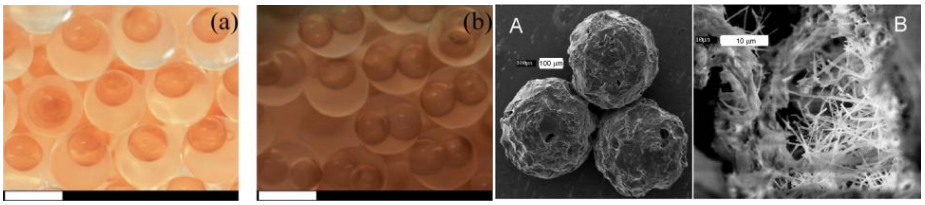

Figure 1. 13 ***(Left)*** Microcapsules containing single(A) or multiple cores(B) synthesized by producing a double emulsion of water in isobornyl methacrylate in water and subsequently polymerizing the middle phase.[86] ***(Right)*** Polyurethane microcapsules produced by interfacial polymerization of monodisperse oil in water droplets produced via a microfluidic device.[84]

1.2.4. UV blockers

High refractive index materials such as titanium dioxide are a key ingredient in sunblock formulations and other UV sensitive products. They provide a barrier that can prevent the penetration of UV light and are typically stabilized by polymeric surfactants.[87–89] Use of microcapsules containing a polymer shell with UV

photoprotectants embedded within has been shown to enhance the protection of photosensitive compounds contained within the capsule (see **Figure 1. 14**).[90,91] In this respect hybrid inorganic-organic polymers colloids can provide enhanced photoprotective properties and the controlled synthesis of such hybrids is key to unlocking their potential in this area.

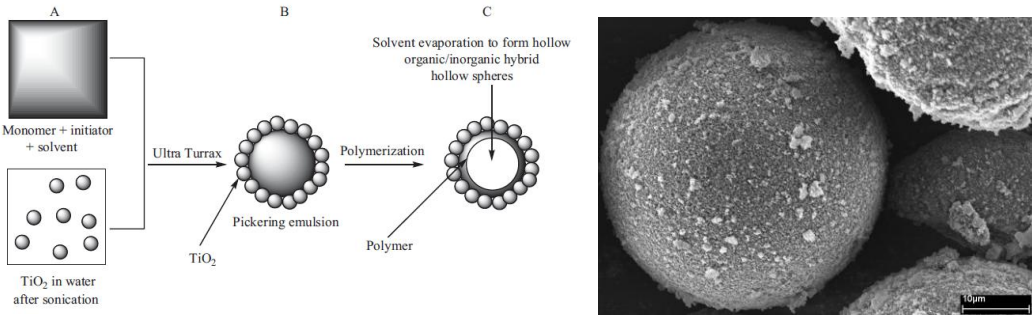

Figure 1. 14 *(Left)* Method of synthesizing TiO_2 armoured microcapsules. Emulsion of monomer and solvent in water containing TiO_2 is formed by mechanical mixing and subsequently polymerized to yield microcapsules with UV photoprotectants embedded in the wall. *(Right)* SEM of TiO_2 armoured microcapsule.[91]

1.2.5. Emulsion and foam stabilizers

It has been known for over a century that colloidal particles can efficiently stabilize emulsions.[92,93] More recently the ability to produce long lasting stable foams has been demonstrated.[94,95] It has also been shown that colloidal particles can be effective as antifoaming agents which have use in the processing of products, especially those that contain large amounts of surfactants.[96–99]

The physical basis of this phenomenon is described in more detail in chapters 5 and 6. It is common to find emulsions stabilized by biological colloids in many food based systems such as mayonnaise which is stabilized by egg-yolk proteins and butter which are stabilized by fat crystals.[100,101] Despite this the potential of colloidal particles as surfactants in home and personal care products has not been fully exploited.

1.2.6. Abrasive agents

Colloidal abrasive agents are commonly found in toothpastes and other cleaning products in order to gently clean and remove dirt from the substrate. Calcium phosphates are commonly used, dispersed in a viscous, aqueous surfactant solution, to provide this functionality.[102,103] The abrasive efficiency is dependent on both surface interactions with the substrate and the particle-substrate surface area[104] so exploiting the ability to tailor polymeric particles shape and surface chemistry offers the potential for far superior colloidal abrasives than are currently used.

1.3. Conclusions and scope of this thesis

This thesis concerns the design, synthesis and application of colloidal polymer particles for application in cosmetic and personal care products. It has been shown above that there exists a multitude of methods by which polymer colloids of various shapes, sizes and chemical functionality can be synthesized and a pre-existing range of products that make use of speciality colloidal particles. The aim of this thesis is to exploit our ability to synthesize colloids that are tailored to a specific task in order to identify ways in which products can be either improved or new application areas discovered.

Chapter 2 concerns the use of biphasic particles to enhance deposition of colloids onto fibrous substrates from solution. Particles that are comprised of a two compartments, one a sticky, low T_g polymer that encourages deposition and the other a model hard polymer, are shown to significantly increase the rate and extent to which particles are deposited. **Chapter 3** describes the synthesis of microgel particles of a hydrazide containing polymer that is used for fragrance release. It is demonstrated that the reversible covalent binding of the fragrance to the hydrazide moiety prolongs the release profile and can be controlled by pH. **Chapter 4** focuses on routes towards the

fabrication of particles that are capable of absorbing large amounts of oil by capillary action for application in water free cleaning products. Suspension polymerization is used to produce highly porous particles using a combination of solvent and polymeric pore forming agents. The effect of the particle microstructure and surface chemistry on the ability to uptake oil is discussed. **Chapters 5 and 6** deal with the use of polymer colloids as emulsion surfactants. In **Chapter 5** a computational model that describes the effect of particle shape and orientation on stability is developed. From this we deduce a set of general guidelines for the synthesis of colloidal particles tailored to act as emulsion stabilizers. In **Chapter 6** we describe the synthesis highly anisotropic particles that are templated from biological colloids and discuss their interfacial activity. Finally **Chapter 7** provides a brief conclusion and outlook for the future.

1.4. References

1. Hargreaves, T. *Chemical Formulation*. (Royal Society of Chemistry: Cambridge, 2003).

2. Tadros, T.F. *Colloids in Cosmetics and Personal Care*. (Wiley-VCH: 2007).

3. Fitch, R.M. *Polymer Colloids: A Comprehensive Introduction*. (Academic Press: 1997).

4. Arshady, R. Suspension , emulsion , and dispersion polymerization - A methodological survey. *Colloid & Polymer Science* **270**, 717-732 (1992).

5. Hosler, D., Burkett, S.L. & Tarkanian, M.J. Prehistoric Polymers- Rubber Processing in Ancient Mesoamerica. *Science* **284**, 1988-1991 (1999).

6. Faraday, M. *Experimental Researches in Chemistry and Physics*. (Taylor and Francis: London, 1859).

7. Goodyear, C. Improvement in India-Rubber Fabrics. US Patent 3633. (1844).

8. Dunlop, J.B. Pneumatic Tire. US Patent 523270. (1893).

9. Hofmann, F., Coutelle, C., Delbruck, K. & Meisenburg, K. Caoutchouc Substance and Process of Making the Same. US Patent 1062913. (1913).

10. Hofmann, F. & Coutelle, C. Caoutchouc Substance and Process of Making the Same. US Patent 1069951. (1913).

11. Harries, C. Caoutchouc Substance and Process of Making the Same. US Patent 1058056. (1913).

12. Staudinger, H. Polymerized Styrene. US Patent 2089444. (1937).

13. Starck, W. & Freudenberger, H. Aqueous emulsions of polymerization products and a process of preparing them. US Patent 2227163. (1940).

14. Dinsmore, R.P. Synthetic Rubber and Method of Making it. US Patent 1732795. (1929).

15. Semon, W. Polymerization of butadienes-1,3. US Patent 2376390. (1945).

16. Harkins, W.D. A general theory of the mechanism of emulsion polymerization. *Journal of the American Chemical Society* **69**, 1428-44 (1947).

17. Frank, R., Adams, C., Blegen, J., Deanin, R. & Smith, P. Effect of Impurities on Copolymerization of Isoprene and Styrene. *Industrial and Engineering Chemistry* **39**, 887-893 (1947).

18. Marvel, C.S., Coleman, L.F., Scott, G.P., Taft, W.K. & Labbe, B.G. Copolymers of Pyridine Analogs of Chalcone with Butadiene. *Industrial & Engineering Chemistry* **48**, 214-218 (1956).

19. Tanaka, M. & Hosogai, K. Suspension Polymerization of Styrene with Circular Loop Reactor. *Journal of Applied Polymer Science* **39**, 955-966 (1990).

20. Vivaldo-lima, E., Wood, P.E., Hamielec, A.E. & Penlidis, A. An Updated Review on Suspension Polymerization. *Industrial & Engineering Chemistry Research* **36**, 939-965 (1997).

21. Trommsdorff, V.E., Kohle, H. & Lagally, P. Zur Polymerisation des Methacrylsauremethylesters. *Die Makromolekulare Chemie* **1**, 169-198 (1947).

22. Hopff, V.H., Lussi, H. & Hammer, E. Zur Kenntnis der Perlpolymerisation. *Die Makromolekulare Chemie* **82**, 184-189 (1965).

23. Hopff, V.H., Lussi, H. & Hammer, E. Zur Kenntnis der Perlpolymerisation. *Die Makromolekulare Chemie* **78**, 175-183 (1964).

24. Hohenstein, W.P. & Mark, H. Polymerization of olefins and diolenfins in suspension and emulsion. *Die Makromolekulare Chemie* **1**, 127-145 (1946).

25. Zhao, T. & Qiu, D. One-pot synthesis of highly folded microparticles by suspension polymerization. *Langmuir* **27**, 12771-4 (2011).

26. Odian, G. *Principles of Polymerization*. (John Wiley & Sons: New Jersey, 2004).

27. Chern, C.S. Emulsion polymerization mechanisms and kinetics. *Progress in Polymer Science* **31**, 443-486 (2006).

28. Hansen, F.K. & Ugelstad, J. Particle Nucleation in Emulsion Polymerization . II . Nucleation in Emulsifier-Free Systems Investigated by Seed Polymerization. *Journal of Polymer Science: Polymer Chemistry Edition* **17**, 3033-3045 (1979).

29. Hansen, F.K. & Ugelstad, J. Particle Nucleation in Emulsion Polymerization . IV . Nucleation in Monomer Droplets. *Journal of Polymer Science: Polymer Chemistry Edition* **17**, 3069-3082 (1979).

30. Hansen, F.K. & Ugelstad, J. Particle Nucleation in Emulsion Polymerization . III . Nucleation in Systems with Anionic Emulsifier Investigated by Seeded and Unseeded Polymerization. *Journal of Polymer Science: Polymer Chemistry Edition* **17**, 3047-3067 (1979).

31. Hansen, F.K. & Ugelstad, J. Particle Nucleation in Emulsion Polymerization . I . A Theory for Homogeneous Nucleation. *Journal of Polymer Science: Polymer Chemistry Edition* **16**, 1953-1979 (1978).

32. Fitch, R.M. Latex Particle Nucleation and Growth. *Emulsion Polymers and Emulsion Polymerization* 1-29 (1981).

33. Thickett, S.C. & Gilbert, R.G. Emulsion polymerization: State of the art in kinetics and mechanisms. *Polymer* **48**, 6965-6991 (2007).

34. Schork, F.J. *et al.* Miniemulsion Polymerization. *Advances in Polymer Science* **175**, 129-255 (2005).

35. Gardon, J.L. Emulsion Polymerization. VI. Concentration of Monomers in Latex Particles. *Journal of Polymer Science Part A-1* **6**, 2859-2879 (1968).

36. Smith, W.V. & Ewart, R.H. Kinetics of Emulsion Polymerization. *The Journal of Chemical Physics* **16**, 592-599 (1948).

37. Colver, P.J., Colard, C. a L. & Bon, S. a F. Multilayered nanocomposite polymer colloids using emulsion polymerization stabilized by solid particles. *Journal of the American Chemical Society* **130**, 16850-1 (2008).

38. Ugelstad, J., Vanderhoff, J.W. & El-Aasser, M.S. Emulsion Polymerization - Initiation of Polymerization in Monomer Droplets. *Journal of Polymer Science: Polymer Letters Edition* **11**, 503-513 (1973).

39. Kohut-svelko, N., Pirri, R., Asua, J.. & Leiza, J.R. Redox Initiator Systems for Emulsion Polymerization of Acrylates. *Journal of Polymer Science Part A: Polymer Chemistry* **47**, 2917-2927 (2009).

40. Luo, Y. & Schork, F.J. Emulsion and miniemulsion polymerizations with an oil-soluble initiator in the presence and absence of an aqueous-phase radical scavenger. *Journal of Polymer Science Part A: Polymer Chemistry* **40**, 3200-3211 (2002).

41. Choi, Y.T., El-Aasser, M.S., Sudol, E.D. & Vanderhoff, J.W. Polymerization of Styrene Miniemulsions. *Journal of Polymer Science: Polymer Chemistry Edition* **23**, 2973-2987 (1985).

42. Delgado, J., El-Aaser, M.S., Silebi, C.A. & Vanderhoff, J.W. Miniemulsion Copolymerization of Vinyl Acetate and Butyl Acrylate . III . Experimental Evidence for the Role of the Cosurfactant. *Journal of Polymer Science Part A: Polymer Chemistry* **27**, 193-202 (1989).

43. Napper, H., Chamberlain, B.J. & Gilbert, R.G. Polymerization within Styrene Emulsion Droplets. *Journal of the Chemical Society, Faraday Transactions 1* **78**, 591-606 (1982).

44. Asua, J.M. Miniemulsion polymerization. *Progress in Polymer Science* **27**, 1283-1346 (2002).

45. Miller, C.M., Sudol, E.D., Silebi, C.A. & El-Aasser, M.S. Polymerization of Miniemulsions Prepared from Polystyrene in Styrene Solutions. 3. Potential Differences between Miniemulsion Droplets and Polymer Particles. *Macromolecules* **28**, 2772-2780 (1995).

46. Miller, M., Sudol, E.D., Silebi, C.A. & El-Aasser, M.S. Polymerization of Miniemulsions Prepared from Polystyrene in Styrene Solutions. 2. Kinetics and Mechanism. *Macromolecules* **28**, 2765-2771 (1995).

47. Miller, C.M., Sudol, E.D., Silebi, C.A. & El-Aasser, M.S. Polymerization of Miniemulsions Prepared from Polystyrene in Styrene Solutions . 1 . Benchmarks and Limits. *Macromolecules* **28**, 2754-2764 (1995).

48. Landfester, K., Bechthold, N., Forster, S. & Antonietti, M. Evidence for the preservation of the particle identity in miniemulsion polymerization. *Macromolecular Rapid Communications* **20**, 81-84 (1999).

49. Landfester, K. & Weiss, C.K. Encapsulation by Miniemulsion Polymerization. *Advances in Polymer Science* **229**, 1-49 (2010).

50. Tseng, C.M., Lu, Y.Y., El-Aasser, M.S. & Vanderhoff, J.W. Uniform polymer particles by dispersion polymerization in alcohol. *Journal of Polymer Science Part A: Polymer Chemistry* **24**, 2995-3007 (1986).

51. Shen, S., Sudol, E.D. & El-Aasser, M.S. Dispersion Polymerization of Methyl Methacrylate: Mechanism of particle Formation. *Journal of Polymer Science Part A: Polymer Chemistry* **32**, 1087-1100 (1994).

52. Winnik, F.M. & Paine, A.J. Dispersion polymerization of styrene in polar solvents. Characterization of stabilizer in ordinary and precipitated particles by fluorescence quenching. *Langmuir* **5**, 903-910 (1989).

53. Paine, A.J., Deslandes, Y., Gerroir, P. & Henrissat, B. Dispersion Polymerization of Styrene in Polar Solvents II Visualization of Surface Layers of Steric Stabilizer on Dispersion-Polymerized and Precipitated Polystyrene Latex Particles by Transmission Electron Microscopy. *Journal of Colloid and Interface Science* **138**, 170-181 (1990).

54. Paine, A.J. Dispersion Polymerization of Styrene in Polar Solvents. 7. A Simple Mechanistic Model To Predict Particle Size. *Macromolecules* **23**, 3109-3117 (1990).

55. Paine, A.J. Dispersion Polymerization of Styrene in Polar Solvents. IV. Solvency Control of Particle Size Stabilized Polymerizations. *Journal of Polymer Science Part A: Polymer Chemistry* **28**, 2485-2500 (1990).

56. Lu, Y.Y., El-Aasser, M.S. & Vanderhoff, J.W. Dispersion Polymerization of Styrene in Ethanol - Monomer Partitioning Behavior and Locus of Polymerization. *Journal of Polymer Science: Part B: Polymer Physics* **26**, 1187-1203 (1988).

57. Ober, C.K., van Grunsven, F., McGrath, M. & Hair, M.L. Partitioning of monomer during dispersion polymerisation. *Colloids and Surfaces* **21**, 347-354 (1986).

58. Ahmed, S.F. & Poehlein, G.W. Kinetics of Dispersion Polymerization of Styrene in Ethanol. 1. Model Development. *Industrial & Engineering Chemistry Research* **36**, 2597-2604 (1997).

59. Ahmed, S.F. & Poehlein, G.W. Kinetics of Dispersion Polymerization of Styrene in Ethanol. 2. Model Validation. *Industrial & Engineering Chemistry Research* **36**, 2605-2615 (1997).

60. Wang, D., Dimonie, V.L., Sudol, E.D. & El-Aasser, M.S. Dispersion polymerization of n-butyl acrylate. *Journal of Applied Polymer Science* **84**, 2692-2709 (2002).

61. Downey, J.S., Frank, R.S., Li, W.-H. & Stover, H.D.H. Growth Mechanism of Poly(divinylbenzene) Microspheres in Precipitation Polymerization. *Macromolecules* **32**, 2838-2844 (1999).

62. Yan, Q., Bai, Y., Meng, Z. & Yang, W. Precipitation polymerization in acetic acid: synthesis of monodisperse cross-linked poly(divinylbenzene) microspheres. *The Journal of Physical Chemistry. B* **112**, 6914-22 (2008).

63. Wang, D., Dimonie, V.L., Sudol, E.D. & El-Aasser, M.S. Effect of PVP in dispersion and seeded dispersion polymerizations. *Journal of Applied Polymer Science* **84**, 2721-2732 (2002).

64. Lee, C.F. & Chiu, W.Y. Kinetic Study on the Poly (methyl methacrylate) Seeded Soapless Emulsion Polymerization of Styrene . I. Experimental Investigation. *Journal of Applied Polymer Science* **56**, 1263-1274 (1995).

65. Kang, K., Kan, C., Du, Y. & Liu, D. Synthesis and properties of soap-free poly(methyl methacrylate-ethyl acrylate-methacrylic acid) latex particles prepared by seeded emulsion polymerization. *European Polymer Journal* **41**, 439-445 (2005).

66. Okubo, M., Fujibayashi, T., Yamada, M. & Minami, H. Micron-sized, monodisperse, snowman/confetti-shaped polymer particles by seeded dispersion polymerization. *Colloid and Polymer Science* **283**, 1041-1045 (2005).

67. Fujibayashi, T. & Okubo, M. Preparation and Thermodynamic Stability of Micron-Sized , Monodisperse Composite Polymer Particles of Disc-like Shapes by Seeded Dispersion Polymerization. *Langmuir* **23**, 7958-7962 (2007).

68. Okubo, M., Miya, T., Minami, H. & Takekoh, R. Morphology of micron-sized, monodisperse, nonspherical polystyrene/poly(n-butyl methacrylate) composite particles produced by seeded dispersion polymerization. *Journal of Applied Polymer Science* **83**, 2013-2021 (2002).

69. Du, Y.Z., Tomohiro, T. & Kodaka, M. Synthesis of Hemispherical Poly (2-hydroxylethyl methacrylate) Composite Particles with Heterobifunctional Groups by Soap-Free Seeded Emulsion Polymerization. *Macromolecules* **37**, 803-812 (2004).

70. Wang, D., Dimonie, V.L., Sudol, E.D. & El-Aasser, M.S. Seeded dispersion polymerization. *Journal of Applied Polymer Science* **84**, 2710-2720 (2002).

71. Mock, E.B., De Bruyn, H., Hawkett, B.S., Gilbert, R.G. & Zukoski, C.F. Synthesis of anisotropic nanoparticles by seeded emulsion polymerization. *Langmuir* **22**, 4037-43 (2006).

72. Sheu, H.R., El-Aasser, M.S. & Vanderhoff, J.W. Phase separation in polystyrene latex interpenetrating polymer networks. *Journal of Polymer Science Part A: Polymer Chemistry* **28**, 629-651 (1990).

73. Kamen, M.E. & Bernstein, P. Method for Preparing Cosmetic Products and the Products Obtained Thereby. US Patent 5066486. (1991).

74. Kamen, M.E., Philip Bernstein & Shah, A. Polymer Supported Cosmetic Products and Methods. US Patent 5093110. (1992).

75. Fudouzi, H. & Xia, Y. Colloidal Crystals with Tunable Colors and Their Use as Photonic Papers. *Langmuir* **19**, 9653-9660 (2003).

76. Watson, C.A. Visually Clear Toothpaste. US Patent 3864470. (1975).

77. Giles, C.C. & Soubiran, L.M. Hair Treatment Composition. US Patent 2006/0134154. (2006).

78. Goodwin, W.D. Skin Conditioning Composition. US Patent 3819825. (1974).

79. Poterie, V. de L. Aqueous Nail Polish Containing as Film-Forming Substance Particles of Polyester-Poluurehtane Which Are Anionic in Dispersion. US Patent 5538717. (1996).

80. Giles, C.C. & Treesilvattanakul, K. Hair treatment composition. US Patent 2010/0221206. (2010).

81. Utada, A.S. *et al.* Monodisperse double emulsions generated from a microcapillary device. *Science* **308**, 537-41 (2005).

82. Shah, R.K., Kim, J.W., Agresti, J.J., Weitz, D.A. & Chu, L.Y. Fabrication of monodisperse thermosensitive microgels and gel capsules in microfluidic devices. *Soft Matter* **4**, 2303 (2008).

83. Lee, D. & Weitz, D.A. Double Emulsion-Templated Nanoparticle Colloidosomes with Selective Permeability. *Advanced Materials* **20**, 3498-3503 (2008).

84. Quevedo, E., Steinbacher, J. & McQuade, D.T. Interfacial polymerization within a simplified microfluidic device: capturing capsules. *Journal of the American Chemical Society* **127**, 10498-9 (2005).

85. Lei, Y., Popplewell, L.M. & Huang, X. Microcapsules Containing Active Ingredients. US Patent 2010/0247660. (2010).

86. Nurumbetov, G., Ballard, N. & Bon, S.A.F. A simple microfluidic device for fabrication of double emulsion droplets and polymer microcapsules. *Polymer Chemistry* **3**, 1043-1047 (2012).

87. Galley, E. & Elsom, N.A. Titanium Dioxide Sunscreens.US Patent 5817298. (1998).

88. SenGupta, A.K. & Lin, I. Stable Sunscreen Composition Containing Zinc Oxide. US Patent 2006/0280702. (2006).

89. Traynor, D.H., Markowitz, S.M., Compton, D.L., Traynor, H.G. & Dulak, M. Sunscreen Compositions and Methods of Use. US Patent 2006/0188458. (2006).

90. Shirley, I., Heming, A.M., Bon, S.A.F. & Cauvin, S.M.P. Microencapsulation of pesticides for photoprotection. WO 2008032022. (2008).

91. Chen, T., Colver, P.J. & Bon, S.A.F. Organic–Inorganic Hybrid Hollow Spheres Prepared from TiO2-Stabilized Pickering Emulsion Polymerization. *Advanced Materials* **19**, 2286-2289 (2007).

92. Pickering, S.U. CXCVI.—Emulsions. *Journal of the Chemical Society, Transactions* **91**, 2001-2021 (1907).

93. Ramsden, W. Separation of Solids in the Surface-layers of Solutions and ' Suspensions ' (Observations on Surface-membranes, Bubbles, Emulsions, and Mechanical Coagulation). — Preliminary Account. *Proceedings of the Royal Society of London* **72**, 156-164 (1903).

94. Binks, B.P. & Horozov, T.S. Aqueous Foams Stabilized Solely by Silica Nanoparticles. *Angewandte Chemie* **117**, 3788-3791 (2005).

95. Gonzenbach, U.T., Studart, A.R., Tervoort, E. & Gauckler, L.J. Ultrastable particle-stabilized foams. *Angewandte Chemie* **45**, 3526-30 (2006).

96. Denkov, N.D. Mechanisms of Action of Mixed Solid–Liquid Antifoams. 2. Stability of Oil Bridges in Foam Films. *Langmuir* **15**, 8530-8542 (1999).

97. Denkov, N.D., Marinova, K.G., Christova, C., Hadjiiski, A. & Cooper, P. Mechanisms of Action of Mixed Solid-Liquid Antifoams. 3 . Exhaustion and Reactivation. *Langmuir* **16**, 2515-2528 (2000).

98. Denkov, N.D., Cooper, P. & Martin, J.Y. Mechanisms of Action of Mixed Solid-Liquid Antifoams . 1 . Dynamics of Foam Film Rupture. *Langmuir* **15**, 8514-8529 (1999).

99. Marinova, K.G., Denkov, N.D., Branlard, P., Giraud, Y. & Deruelle, M. Optimal Hydrophobicity of Silica in Mixed Oil-Silica Antifoams. *Langmuir* **18**, 3399-3403 (2002).

100. Dickinson, E. Protein-stabilized emulsions. *Journal of Food Engineering* **22**, 59-74 (1994).

101. Dickinson, E. Food colloids — An overview. *Colloids and Surfaces* **42**, 191-204 (1989).

102. Dromard, A. & Lavault, S. Toothpaste Compostion with Abrasive Calcium-Based Particles Having a Coating Comrsing An Hydrophobic Product. US Patent 2002/0001569. (2002).

103. Gitomer, T.J. & Dlaton, P.E. Body Scrub Cosmetic Composition. US Patent 2004/0028630. (2004).

104. Lu, Z., Lee, S.-H., Babu, S.V. & Matijević, E. The use of monodispersed colloids in the polishing of copper and tantalum. *Journal of Colloid and Interface Science* **261**, 55-64 (2003).

Chapter 2: Soft-hard polymer hybrids for improving wet deposition

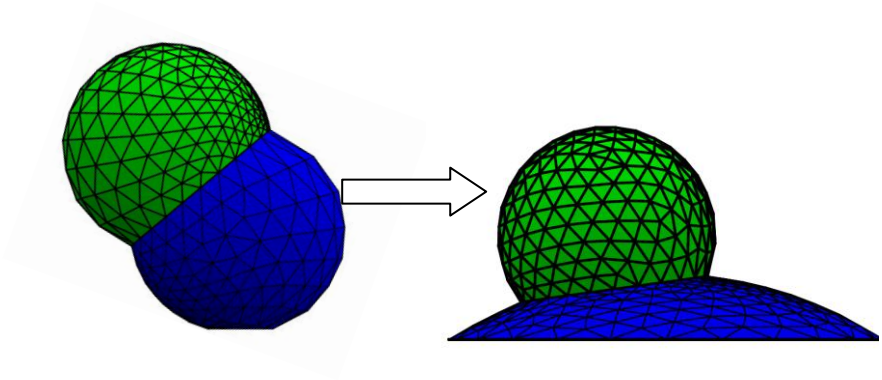

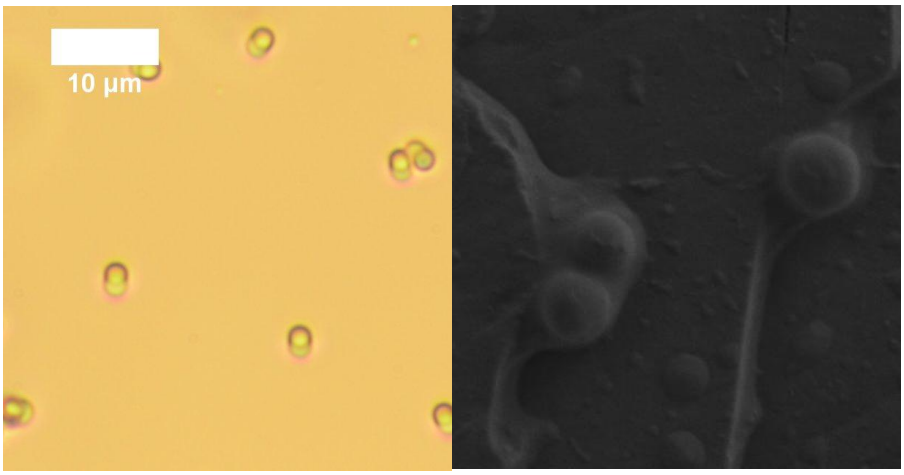

2.1. Abstract

In this chapter we describe the synthesis of biphasic Janus-type dumbbell or peanut-shaped particles consisting of one soft, low T_g polymer lobe and one hard polystyrene lobe for enhanced colloidal deposition onto solids substrates from solution. The presence of the soft part causes a significant increase in the rate and extent of wet deposition. It effectively acts as a glue to prevent desorption after collision, in other words it omits reversible surface adhesion. It is demonstrated that the geometry of the particle strongly influences the deposition efficacy. Moreover, due to the unique film forming properties of the low T_g lobe, some spatial deposition control can be accomplished.

2.2. Introduction

2.2.1. Applications of deposited polymer particles

Colloidal deposition is a subject of interest in a host of industries where product/process efficiency is often determined by the ability of a colloid to deposit onto the surface of a solid macroscopic substrate. In paper manufacturing, for example, pulp fibres are coated with film forming polymer particles in order to bind pigments, impart water resistance and increase strength.[1–3] Aside from this many functional products involve the deposition of colloidal particles or capsules onto solid surfaces, in laundry detergent applications for example, and as such the extent to which colloids can be deposited from wet solution determines their efficacy. In this chapter we look at a new method to deposit colloidal particles onto fibrous substrates.

In home and personal care products colloids are frequently used to influence and improve the physical properties of various fibres. Perhaps the most common of these cases are emulsion-based systems, that is a liquid dispersed in the form of droplets in a second liquid, where the dispersed phase exhibits some effect that enhances the consumer experience. Hair conditioner for example functions as a product due to the deposition of silicone oil droplets onto the hair surface aided by cationic surfactants that interact favourably the anionic surface of hair fibers.[4] Since this improvement in texture and appearance is only apparent if the dispersed phase is deposited it is essential to maximize the adhesion of the colloids. This work focuses on suspensions of solid particles in a liquid. This is another area of great importance since many commercial products contain particulates. If one looks at the composition of a typical mascara formulation, for example, it is easy to see the importance of colloidal particles in personal care products. Colloidal carbon black is used as a pigment, with a dispersed

wax acting to affect the eyelash enhancing effect and film forming latex is used to bind the ingredients to the surface.[5]

In the case of human hair, the prime substrate in this chapter, the surface is more complicated than the majority of biological and synthetic fibres. A comprehensive review by Bhushan contains a detailed description on the structure of hair and its physical properties and the following paragraph is a very basic summary of this review.[6] The surface can be seen as a series of overlapping cells mainly composed of a cysteine rich protein called keratin, which has an alpha helical structure (see **Figure 2. 1**). The cysteine residues can form disulphide bonds with each other and result in structural changes to the hair, resulting in a change to the overall physical properties. The outer layer of the hair surface is covered in a thin layer of covalently attached fatty acids (mainly 18-methyl eicosanoic acid). This surface is also negatively charged and therefore most commercial products which adsorb to the surface contain cationic surfactants. The zeta potential of the surface of hair has been measured by streaming potential measurements and for untreated hair it is calculated at ~ -90 mV which allows for the potential adsorption of cationic colloidal particles by heterocoagulation.[7] The majority of other fibres of interest such as cotton, nylons and polyesters which are of prime importance in washing detergent applications are also negatively charged though to a lesser extent.[4]

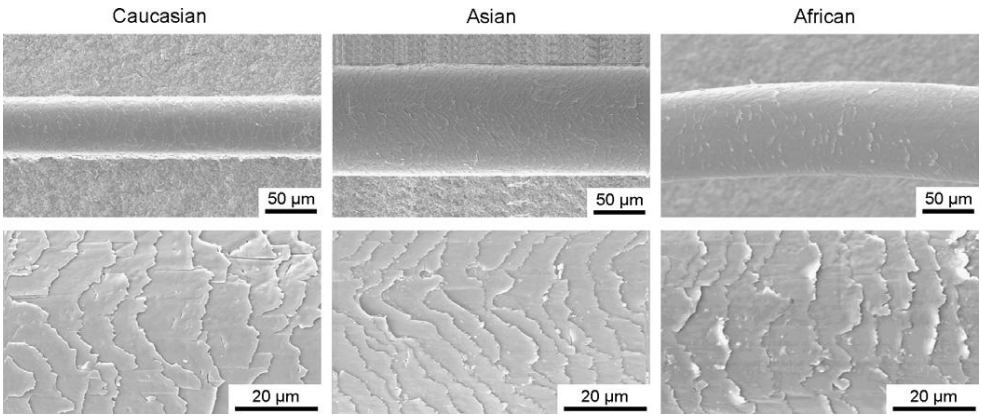

Figure 2. 1 SEM images of the surface of various types of hair.[8]

2.2.2. Latex deposition: Particle-fibre interactions

The underlying principles of particle adsorption to solid surfaces has long been of great interest to colloid scientists, especially with respect to the interaction forces involved. The majority of works to date are fundamental studies which explore the extent of interactions between electrostatically stabilised colloidal particles and a charged surface although there are reports of the effect of steric stabilizers on deposition rates.

2.2.2.1. Heterocoagulation of electrostatically stabilized colloids and fibres

The most studied interaction between colloids and fibres is based on an extension of the DLVO theory.[9] Many groups have used this theory to explain the observed effects of the adsorption rates of charged latex particles with varying surface charge and chemical functionality in media of different ionic strength and pH with various fibres including wool, nylons and cotton.[10–15] The DLVO theory explains colloidal stability by combining the attractive energy from van der Waals interactions and the Coulombic interaction energy between the double layers. An equation describing the overall interaction energy between colloidal particles with dissimilar electrical double layers was later described by Hogg. [16] From this the interaction energy due to electrostatic forces, V_R, between a plate and a sphere has been derived (see **Equation 2. 1**).[17]

$$V_R = \pi\epsilon_r\epsilon_0 a\left[(\psi_1^2 + \psi_2^2)ln\left(\frac{e^{2\kappa H_0} - 1}{e^{2\kappa H_0}}\right) + 2\psi_1\psi_2 ln\left(\frac{e^{\kappa H_0} + 1}{e^{\kappa H_0} - 1}\right)\right]$$

Equation 2. 1

Where ε_r is the dielectric permittivity of the solvent, ε_0 is the permittivity in vacuum, a is the particle radius, ψ_1 and ψ_2 are the surface potentials of the sphere and the plate respectively, κ is the reciprocal of the Debye length and H_0 is the separation distance between sphere and particle. To calculate the van der Waals interaction, V_a, between a plate and a sphere **Equation 2. 2** is used.

$$V_A = \frac{A_{12/3}}{6}\left[\frac{2a(H_0 + a)}{H_0(H_0 + a)} + ln\frac{H_0}{H_0 + 2a}\right]$$

Equation 2. 2

Where $A_{12/3}$ is the Hamaker constant for the interactions of objects 1 and 2 dispersed in a medium 3. The sum of these two energies yields the total interaction energy at a defined distance. **Figure 2. 2** shows the total interaction energy V_T as a function of distance H_0 at varying ionic strengths for the interaction of a latex particle with a fibre for a cationic and an anionic latex. It is clear that there is a large barrier to heterocoagulation for the case of an anionic latex particle and as such deposition is less likely. For the cationic latex there is no barrier and the interaction between the surface and the particle is high.

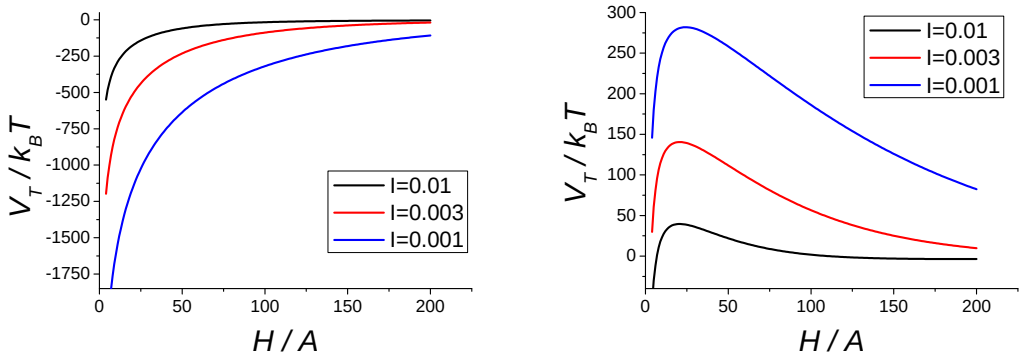

Figure 2. 2 Heterocoagulation of a cationic *(left)* polystyrene latex particle and an anionic polystyrene latex particle *(right)* of 100 nm radius with a nylon fibre at varying ionic strengths. Hamaker constant for polystyrene was taken as 4×10^{-21} J and for nylon 4.2×10^{-20} J. T=298 K

The use of electrostatic interactions in practical systems is often hindered because most substrates of commercial interest, hair, wool, pulp, cotton *etc.* contain negative charges and the majority of commercially available latexes that are capable of depositing onto such surfaces via electrostatic interactions contain tertiary amines which are only protonated at low pH values where stability issues with other components occurs (and potentially protonation of anionic surfaces resulting in a decrease in electrostatic interaction).

2.2.2.2. Polymer induced flocculation

Colloidal particles that are stable in their dispersion medium can be induced to flocculate and deposit by addition of soluble polymers and /or polyelectrolytes. For example Alince and co-workers have shown that clay particles can be induced to deposit onto pulp fibres by addition of poly(ethylenimine).[18] The positively charged polymer adsorbs onto the surface of the two negative surfaces and promotes interactions between them. In these cases the deposition kinetics are usually determined by the rate of polymer adsorption onto the surfaces in question and under certain conditions can be incredibly rapid.[19] However, the complex kinetics involved in adsorption of the polymer onto multiple substrates and their subsequent interactions make prediction of the timescales involved in deposition by flocculation a challenging prospect.

2.2.2.3. Heterocoagulation of sterically stabilized colloids and fibres

An alternative to electrostatic stabilization can be achieved by using polymer brushes which adsorb or are fixed to the particle surface and are solvated by the continuous phase.[20–24] In this case the van der Waals attraction energy, V_a, is identical to the case in section 2.2.2.1. The steric interaction force, V_s, is predicted to be the sum of the increase in free energy caused by interpenetration of the polymer brushes resulting in a decrease in the Gibbs free energy for mixing and a second term arising from the compression of the polymer brushes as the particle and fibre approach. For this work the main method of colloid synthesis is via dispersion polymerization in alcoholic media and colloidal stability is provided by a thin layer of a water soluble polymeric surfactant which is grafted to the particle surface during the polymerization.[25,26]

There are reports in the literature of the use of these 'hairy' latexes to encourage colloidal deposition.[27–29] Hairy latex particles synthesized by surfactant free emulsion polymerization were thought to deposit onto surfaces because the hairs were capable of coming into close contact with the substrate despite the large interaction energy upon close approach. However, reversible adhesion was seen to occur due to the presence of electrostatic interactions such that particle residence time was, even in the best cases, on the order of minutes.

We have described above the main methods by which colloids are deposited from solution and shown that each one has associated problems, often due to the reversibility of the deposition process. We describe herein a method by which to prevent reversible adhesion by synthesis of a Janus-type dumbbell particle containing two distinct lobes, one of which is comprised of a low T_g polymer that encourages deposition and adhesion of the second, non-adhesive lobe.

2.3. Results and Discussion

2.3.1. Wet deposition of sterically stabilized particles

We focused our initial efforts into the use of polystyrene sterically stabilized by poly(vinyl pyrrolidone) (PVP) as a model system to observe deposition effects onto fibrous substrates. Monodisperse sterically stabilized latex particles of 1.8 µm diameter were produced by dispersion polymerization of polystyrene in ethanol.[30,31] A representative optical microscope image is shown in **Figure 2. 3**.

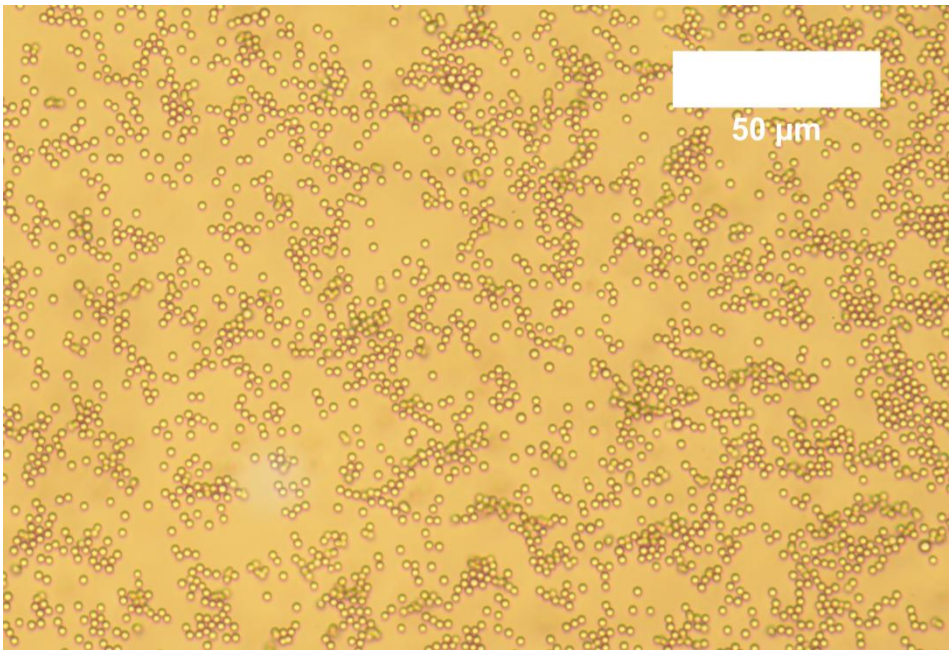

Figure 2. 3 Optical microscope image of polystyrene particles produced by dispersion polymerization in ethanol. [Styrene]=30 vol% [AIBN] = 1 wt% to monomer [PVP] = 6.6 wt% to monomer.

Latex deposition on fibres was performed by immersing samples of hair fibres in colloidal suspensions and mixing gently. The polymer concentration in the aqueous phase was monitored by turbidity measurements comparing to samples of known solid content. For polystyrene latexes we observed no deposition by this method but when we performed the same experiment with poly(butyl acrylate) (PBA) synthesized under similar conditions[32] we observed significant deposition (**Figure 2. 4**).

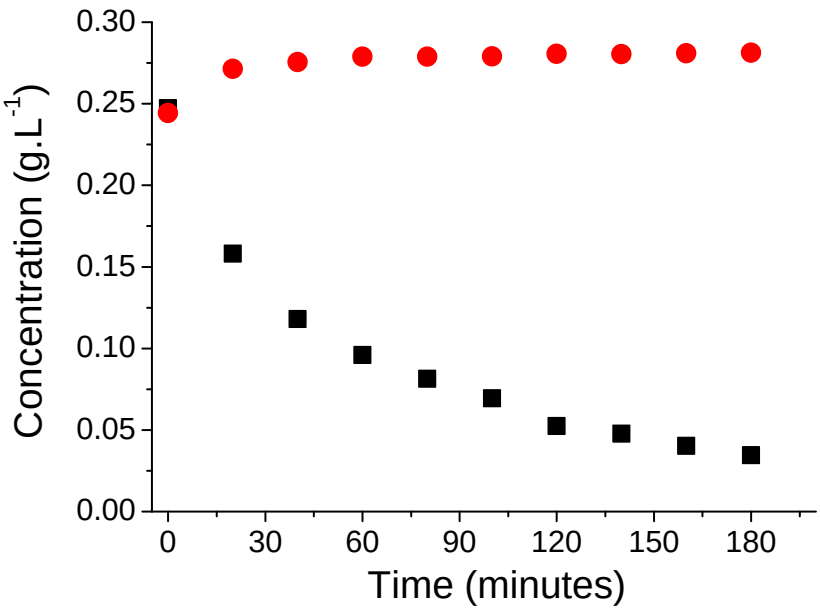

Figure 2. 4 Concentration of particles in the aqueous phase over time as deposition occurs for sterically stabilized particles of 1.8 µm polystyrene (●) and 1.3 µm poly(butyl acrylate) (■) particles on hair fibres monitored by turbidity measurements.

This experiment led us to believe that poly(butyl acrylate) a soft, low T_g polymer (T_g= -54 °C) had enhanced wet adhesive properties and we undertook experiments into imparting the same behaviour in the non-adhesive polystyrene particles, especially given that the difference in Hamaker constants of the two materials is expected to be negligible (the Hamaker constants for PMMA and polystyrene are 7.56×10^{-20} J and 9×10^{-20} J respectively).[33] To achieve this we synthesized particles which were biphasic in nature, consisting of a soft part of poly(butyl acrylate) and a hard polystyrene part by a seeded dispersion polymerization of the polystyrene particles using varying quantities of butyl acrylate (BA) to change the soft lobe volume (see **Figure 2. 5**).[34] At higher weight fractions of butyl acrylate, when the weight ratio of monomer:seed particles exceeded 1, large amounts of coagulum formed. The obtained particles were dialyzed into water to prevent aggregation that occurred when purification by centrifugation and redispersion was used.

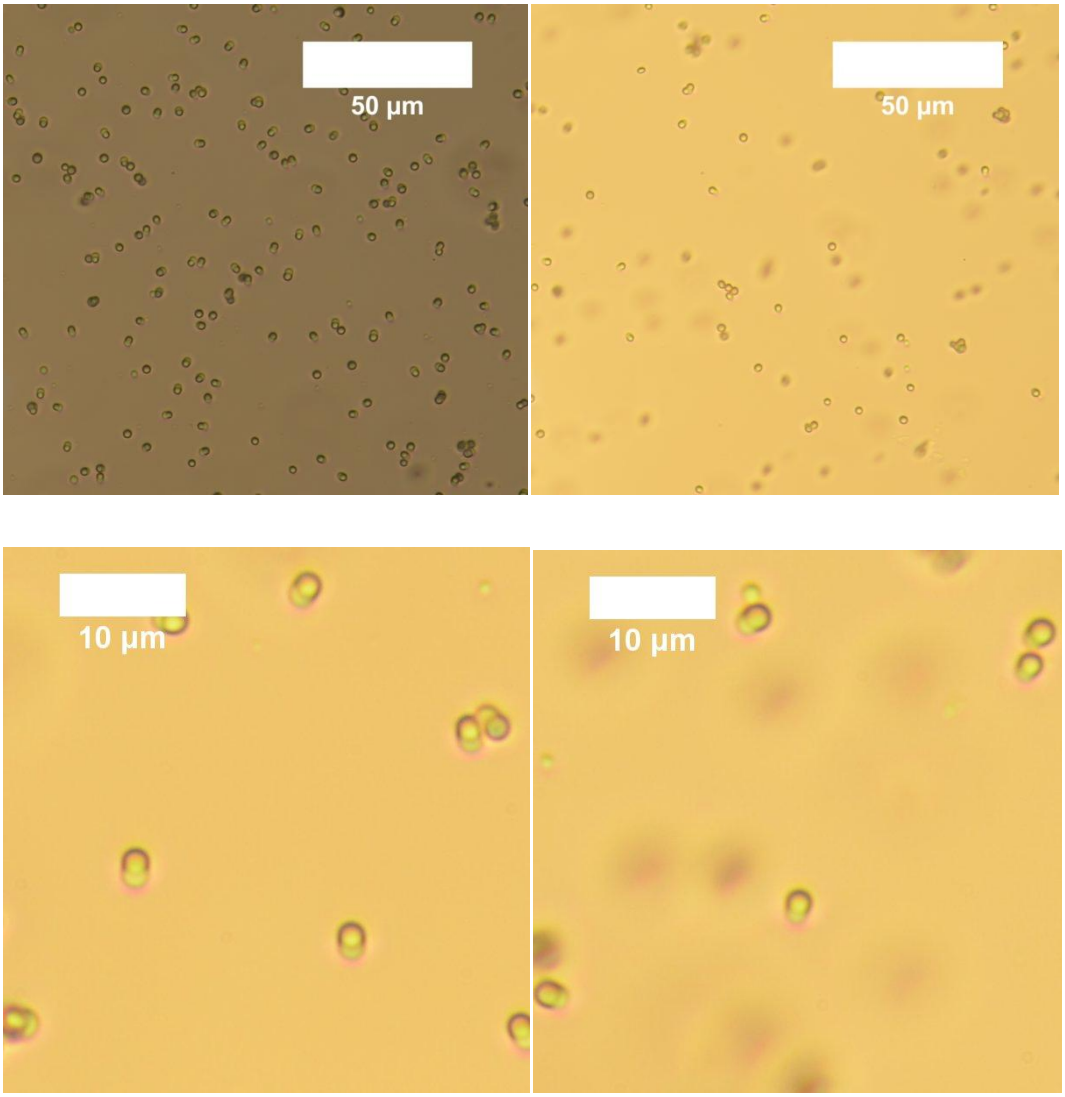

Figure 2. 5 Optical microscopy images of soft-hard biphasic particles synthesized by seeded dispersion polymerization of butyl acrylate using polystyrene seed particles at (a,c) 1:1 seed:BA weight ratio and (b,d) 1:0.5 seed:BA weight ratio.

The biphasic particles with varying ratio of poly(butyl acrylate) to polystyrene were tested by the same method as before to see the effect of adding the soft lobe to a non-adhesive colloid (see **Figure 2. 6**). It can be seen that by attaching the soft adhesive poly(butyl acrylate) part then deposition is substantially increased compared to the seed polystyrene particle alone. Upon varying the lobe size a small change in rate is observed with the slowest rate being for the case with lowest poly(butyl acrylate) to polystyrene ratio (1:3) and the fastest rate with the highest lowest poly(butyl acrylate) to polystyrene ratio(1:1).

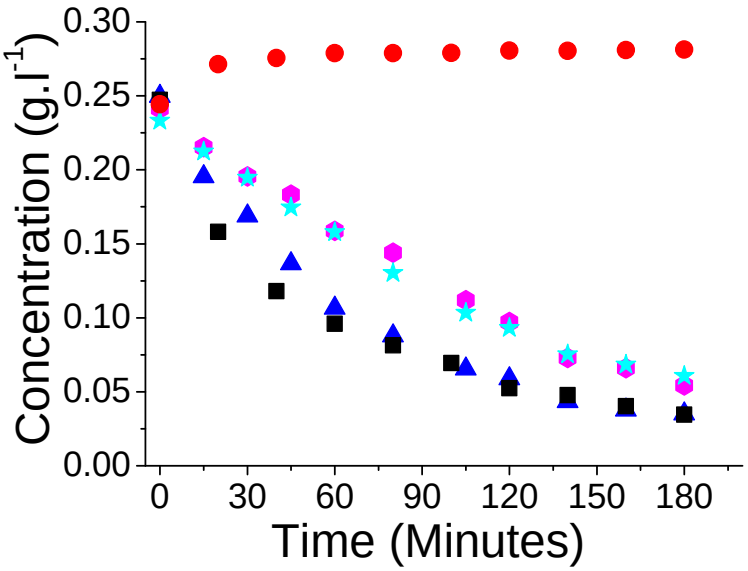

Figure 2. 6 Concentration of particles in the aqueous phase over time as deposition occurs for sterically stabilized particles of 1.8 µm polystyrene (●), 1:1(▲), 0.6:1(★), 0.3:1(⬢) poly(butyl acrylate):polystyrene biphasic particles and 1.3 µm poly(butyl acrylate)(■) particles on hair fibres monitored by turbidity measurements.

One surprising result from this experiment is that even with small amounts of butyl acrylate in the system deposition is hugely increased. We predicted that if the rate of deposition is purely based on collision of the soft part with the hair fibre then the angle of orientation upon approaching the fibre determines the success of a collision. The range of angles at which the butyl acrylate lobe will come into contact with the solid surface can be determined by geometrical constraints for particles of different shapes and morphologies. For the peanut shape particles used in this work the particle shape can be described by the relative size of the two lobes and the distances between them. The initial particle is simply described as a sphere with volume, V_1, and radius, R_1. The second lobe with radius, R_2, and volume, V_2, is separated by a distance d which is quantified in a dimensionless form, ε, such that $\varepsilon = d/(R_1+R_2)$. The volume of the second lobe is complicated by overlapping volumes with the first lobe such that $V_2=4/3\pi R_2^3-V_{overlap}$ (see **Figure 2. 7**).

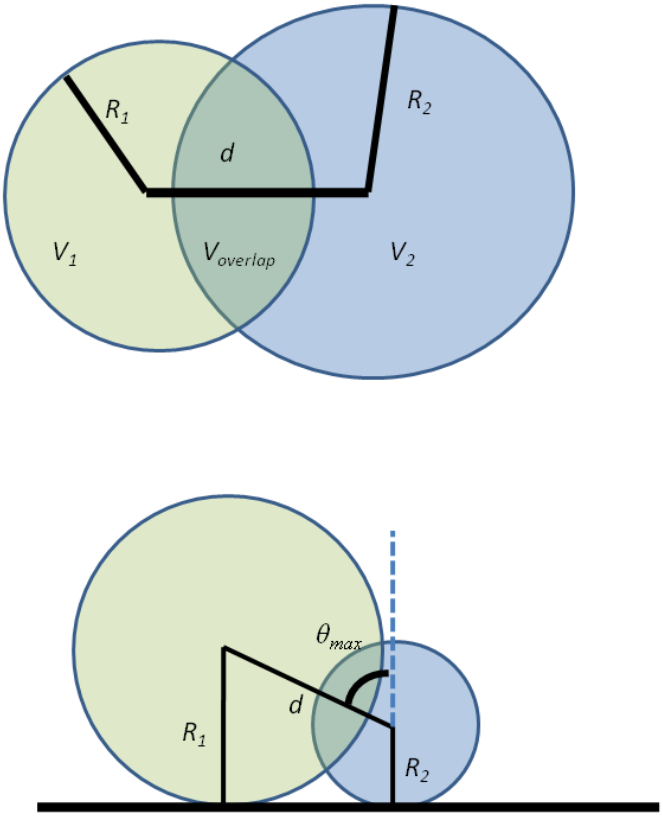

Figure 2. 7 *(Top)* Particle geometry used to calculate collision angles. The first lobe has volume, V_1, given by $V_1=4/3\pi R_1^3$ and the second lobe is attached with volume $V_2=4/3\pi R_2^3-V_{overlap}$. The distance between particle centres is given by *d*. *(Bottom)* Maximum deposition angle θ_{max} is calculated from the slope of the line between the two sphere centre points at the point at which both radii are in surface contact.

We set the initial volume of the two lobes and the dimensionless separation distance, ε, and solve the volume equations to give R_2. From the values of R_1, R_2 and the separation distance it is possible to calculate the maximum angle at which a successful collision of the soft lobe is possible at varying volumes and interparticle separation distances (see **Figure 2. 8**). The fractional range of angles (X_θ) for which deposition can occur can be given by θ_{max} / 180. As θ_{max} approaches 180° then the likelihood of a collision of the soft lobe is increased assuming a random rotation upon particle approach to the hair fibre. The rate of deposition, assuming no deposition from the hard non-adhesive part will be a function of the fraction of collisions that occur with the poly(butyl acrylate) part, X_θ, and the barrier to heterocoagulation imparted by the steric stabilizer.

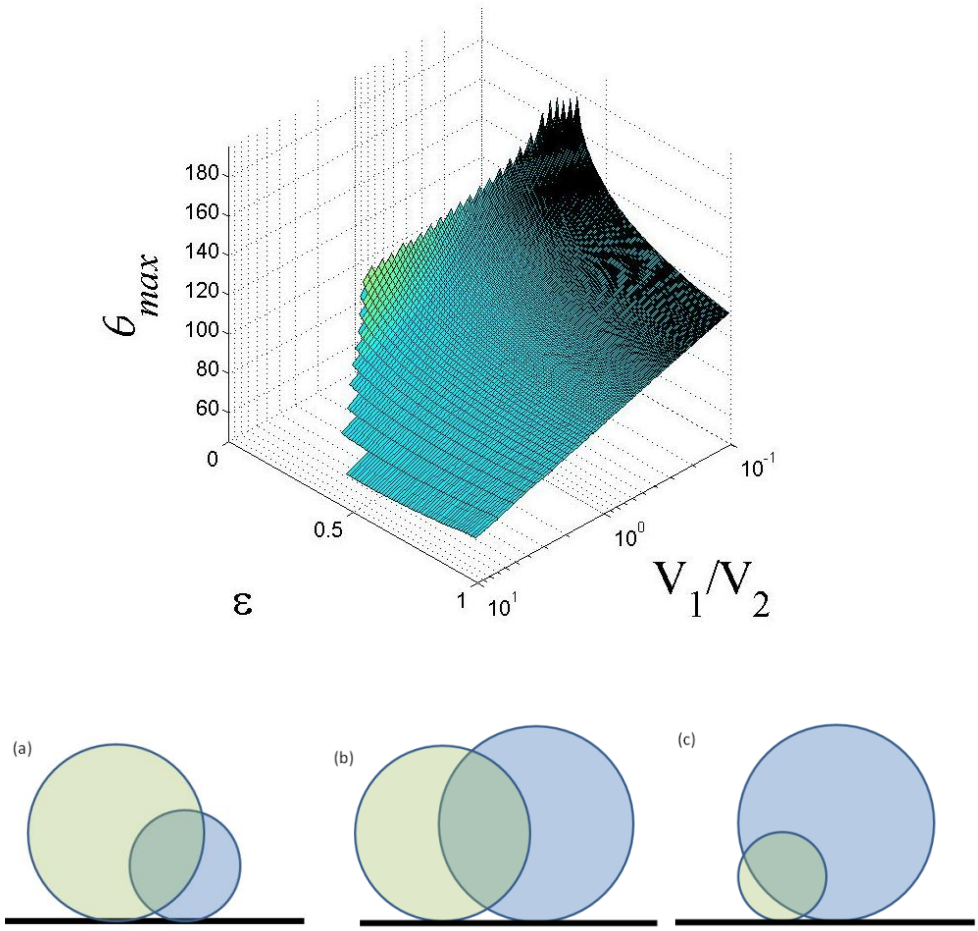

Figure 2. 8 *(Top)* Maximum deposition angles (θ_{max}) as a function of the relative lobe volume (V_1/V_2) and dimensionless separation distance (ε). *(Bottom)* Schematics showing deposition angles for constant ε=0.5 and varying (V_1/V_2) (a) V_1/V_2=10 (b) V_1/V_2=1 (c) V_1/V_2=0.1.

The plot shows that even for quite low volume ratios the range of deposition angles is quite large indicating that with very low volumes of the soft butyl acrylate lobe substantial deposition effects may be gained. For example for a constant ε = 0.5 the value of $\theta_{\text{max changes}}$ from 63° to 96° to 139° upon changing the volume ratio of the hard and soft lobes from V_1/V_2 = 10 to V_1/V_2 = 1 to V_1/V_2 = 0.1. This suggests that increasing the volume of the second lobe by 100 times would only increase the rate by a factor of approximately 2. For the experiment shown in **Figure 2. 6** the values of V_1/V_2 used were 1, 1.6 and 3.3 corresponding to theoretical θ_{max} values of 96°, 85° ,78° and X_θ=0.53, 0.47, 0.43. The rate of deposition would be therefore be expected to change by a factor of only 1.2 between the V_1/V_2=1 and V_1/V_2=3.3 and by a factor of 1.1 between the

V_1/V_2=1.6 and V_1/V_2=3.3 particles and this is roughly borne out in the data. Perhaps more surprising is the similarity between the rate of deposition for the poly(butyl acrylate) particles and the biphasic particles in which V_1/V_2=1. We believe this is due to the larger mass of the biphasic particles which, given the particles are under constant shear force, will result in larger deformation of the particles upon close contact with the fibre and increase deposition rates.

2.3.2. Adhesive properties of biphasic particles

It has been shown above that addition of the poly(butyl acrylate) lobe enhances the wet deposition properties of otherwise non-depositing polymer latexes. The synthesized particles also exert interesting film properties due to the difference in the T_g of the two phases of the particles. SEM images of deposited particles of the surface of hair fibres showed that the low T_g, poly(butyl acrylate) spread on the surface and the polystyrene parts lay flat on the fibre (see **Figure 2. 9**).

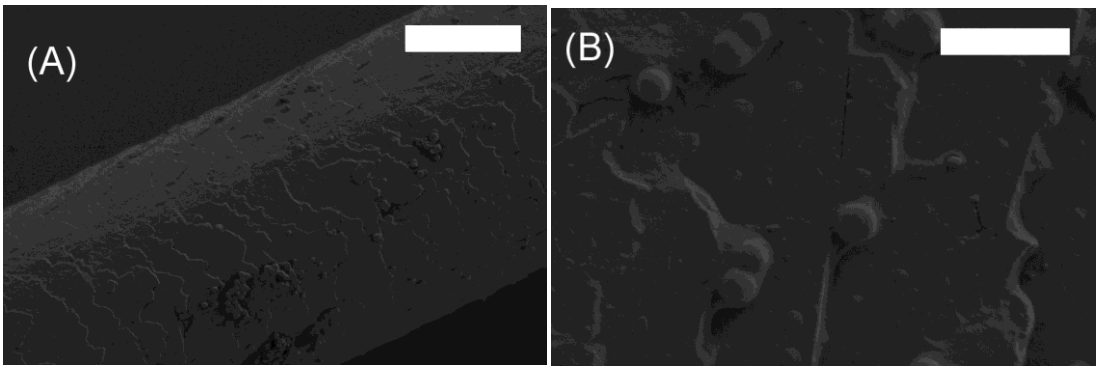

Figure 2. 9 Film forming of deposited polystyrene-poly(butyl acrylate) (1:1) particles on hair fibres. *(Top)* Scale bar is 25 μm. *(Bottom)* Scale bar is 5 μm.

The ability of the poly(butyl acrylate) to deform and spread on the surface makes deposition irreversible and strongly binds the polystyrene part to the fibre surface. The extent to which the poly(butyl acrylate) spreads will affect the resulting fibre properties. For small V_1/V_2 the poly(butyl acrylate) will have a large area over which it spreads and will leave the hair with an adhesive layer of sticky polymer on it. For large V_1/V_2 it

should be possible to have a small adhesive area which sticks the polystyrene to the substrate without excess polymer spreading on the surface.

The SEM images also indicated that in every case the polystyrene lay flat with respect to the fibre surface. In order to explain this we developed a Surface Evolver model using similar geometric parameters as shown in **Figure 2. 7**.[35] The hard part has constrained edges that maintained the spherical shape and was initiated at a certain angle with respect to the substrate. The radius of the area of contact of the soft part with the substrate was initially set at $R_2/10$ and gradually increased, evolving the surface after each step to minimize the interfacial energy to simulate the effect of deformation and spreading of the soft butyl acrylate part (see **Figure 2. 10**).

	θ_0=60°		θ_0=0°	
R_1/R_2	**Before**	**After**	**Before**	**After**
1/1	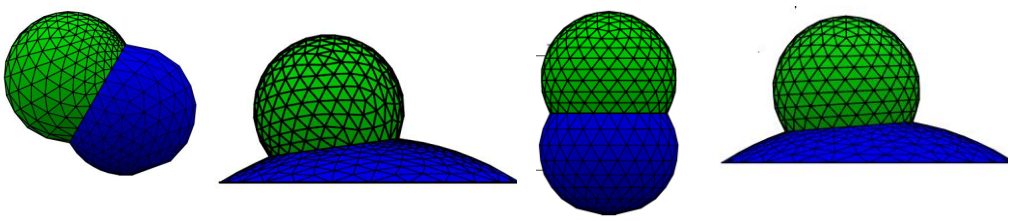			
1/0.75	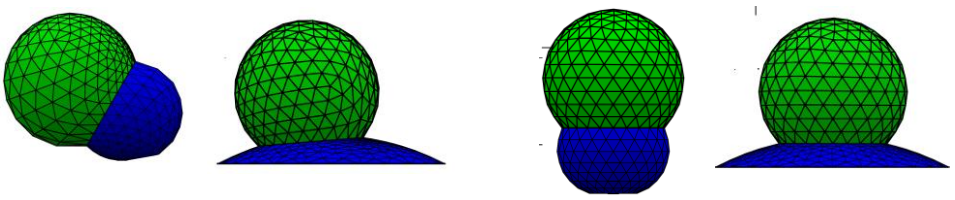			
1/0.5				

Figure 2. 10 Surface Evolver simulations of adhesive properties of biphasic particles in which one part is capable of deformation and the other consists of a hard non-deformable part at varying lobe size ratios and initial angles. ε=0.5 in all cases.

It can be seen that the final orientation of the polystyrene part is not hugely dependant on the initial deposition angle. As the soft part undergoes film formation the polystyrene part aligns vertically with respect to the interface in order to minimize the energy of the system. The extent to which the soft part film forms will depend on the polymer contact angle with the substrate. Where the ratio of soft:hard parts are roughly equal the soft part spreads far beyond the radii of the hard polystyrene part and will cause the formation of an adhesive polymer layer on the substrate surface. Where the particles are fairly concentrated during the film formation process we predicted that this would cause an interpenetrating film network in which the hard polystyrene lobes will be embedded. The extent to which the interpenetrating film will be connected will therefore be dependent on the relative volume of the two lobes. In order to test this theory we left a dilute suspension of the biphasic particles to dry on a glass side and observed the resulting surface (see **Figure 2. 11**).

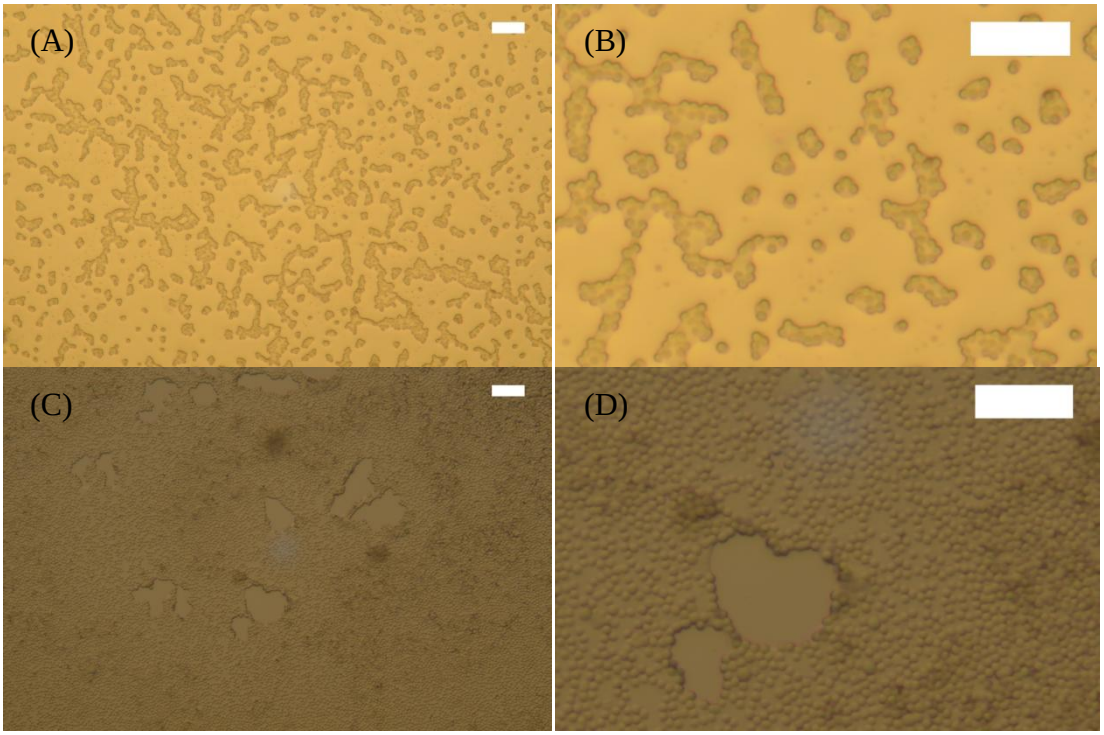

Figure 2. 11 Optical microscope images of adhesive properties of biphasic particles with equal volume of poly(butyl acrylate) and polystyrene left to dry on a glass slide. (A), (B) Low particle concentration (C), (D) High particle concentration. Scale bar is 20 μm in all cases.

It can be seen from **Figure 2. 11a** and **Figure 2. 11b** that where the concentration of particles is low upon deformation the poly(butyl acrylate) part becomes attached to nearby particles and forms a link between the two particles. **Figure 2. 11b** demonstrates the linking of particles to form unimers, dimers, trimers, tetramers *etc*. that do not interact with other particles that are beyond the reach of the film forming polymer. Where the concentration was higher (**Figure 2. 11c** and **Figure 2. 11d**) a self assembled interpenetrating film is formed that links all the particles and adheres them to the surface. The concentration at which it is possible to form such a structure will be determined by the volume of poly(butyl acrylate) and its ability to spread on the substrate.

2.4. Conclusion

In conclusion, we have shown that attachment of a small amount of adhesive polymer to a non-adhesive colloidal particle can significantly improve the rate and extent of deposition from solution. The resulting deposition is not based on specific chemical interactions but rather on the irreversible nature of soft polymer adhesion. We have demonstrated that even for low relative volumes of adhesive polymer appreciable deposition rates can be obtained and developed a model to explain the film forming properties of such biphasic particles.

2.5. Experimental

2.5.1. Materials

Styrene (>99%), and butyl acrylate (99%) were purchased from Sigma-Aldrich and were filtered through a short column of basic alumina before use to remove inhibitor. Poly(vinyl pyrrolidone) (K-90, M_W=360,000 g.mol^{-1}) and 4,4'azobis(4-cyanopentanoic acid) (ACVA, 75% remainder water) was purchased from Sigma-

Aldrich and used without further purification. Azobisisobutyronitrile (AIBN) was purchased from Wako and used without further purification. All solvents were of reagent grade purity and were purchased from Fisher Scientific. Virgin hair fibres were provided by Unilever.

2.5.2. Equipment

Particle size was determined by static light scattering using a Malvern Mastersizer 2000 with a Hydro 2000s aqueous dispersion unit attached. The particle size and size distribution were calculated from Mie theory. Scanning electron microscopy was performed on a Zeiss supra 55VP FEGSEM. Particles were coated with a thin layer of platinum prior to scanning. Optical microscope images were taken on a Leica DM2500M using a Nikon D5100 camera. Tumbling experiments were performed in a SciGene Model 777 Microarray Oven consisting of two steel plates attached to a rotor in a thermostatted chamber.

2.5.3. Dispersion polymerization

Monodisperse latex particles of polystyrene and poly(butyl acrylate) were synthesized by dispersion polymerization in alcoholic media using poly(vinyl pyrrolidone) (PVP) as stabilizer according to the amounts given in **Table 2. 1** and **Table 2. 2**. PVP was dissolved in the water/alcohol mixture with stirring and the sample was purged with nitrogen for 30 minutes then heated to the reaction temperature. Initiator, AIBN or ACVA, was dissolved in the monomer and injected by syringe. The reaction mixture was stirred for 24 hours and then cleaned by centrifugation and redispersed in ethanol twice then in water twice. The poly(butyl acrylate) latexes were purified by dialysis into water due to the coalescence of particles at high centrifugation speeds.

Table 2. 1 Recipe for synthesis of 1.8 µm polystyrene microspheres by dispersion polymerization

Ingredient	Weight (g)
Ethanol	70
PVP K90	2
AIBN	0.30
Styrene	30

Table 2. 2 Recipe for synthesis of 1.3 µm poly(butyl acrylate) microspheres by dispersion polymerization

Ingredient	Weight (g)
MeOH/Water (90:10)	100
PVP K90	2
AC**V**A	0.10
BA	10

2.5.4. Seeded dispersion polymerizations

The polystyrene seed particles were synthesized as above and used in the form of a dry powder. The particles were dispersed a methanol water mixture and PVP was added. The suspension was placed in an ultrasound bath for 10 minutes to ensure dispersion of the particles and butyl acrylate and ACVA was added. The reaction vessel was sealed and purged with nitrogen for 30 minutes then heated to the reaction temperature. The reaction mixture was stirred for 20 hours at this temperature then the resulting particles were transferred into water by dialysis.

Table 2. 3 Recipe for synthesis of biphasic particles by seeded dispersion polymerization

Ingredient		V_1/V_2	
	1	***1.6***	***3.3***
MeOH/Water (90:10) (g)		8	
PVP K90 (g)		0.013	
ACVA (g)		0.010	
Polystyrene seed (g)		1	
Butyl Acrylate (g)	1.00	0.60	0.30

2.5.5. Deposition experiments

The amount of latex that was deposited on samples of hair was determined by turbidity. A calibration curve was made by analyzing the absorbance at 540 nm of the latex at known solids contents. For deposition analysis 10 ml of 0.25 $g.l^{-1}$ latex was added to a sample of 100 mg of human hair cut into 5 cm pieces. The mixture was sealed in a glass vial and tumbled end over end at room temperature in a rotary oven at 30 rpm.

2.6. References

1. Alince, B. Cationic Latex Interaction with Pulp Fibers . 11 . Modification of Sheet Properties by Styrene- Butadiene Latex with Quaternized Amino Groups. *Journal of Applied Polymer Science* **23**, 549–560 (1979).

2. Alince, B., Inoue, M. & Robertson, A. A. Cationic latex interaction with pulp fibers. I. Deposition of styrene-butadiene latex having quaternized amino groups. *Journal of Applied Polymer Science* **23**, 539–548 (1979).

3. Alince, B. Colloidal Particle Deposition on Pulp Fibers. *Colloids and Surfaces* **39**, 39–51 (1989).

4. Berthiaume, M. D. & Jachowicz, J. The Effect of Emulsifiers and Oil Viscosity on Deposition of Nonionic Silicone Oils from Oil-in-Water Emulsions onto Keratin Fibers. *Journal of Colloid and Interface Science* **141**, 299–315 (1991).

5. Kljuic, A. & Kanji, M. Mascara composition with self-emulsifying waxes and latex polymers. European Patent EP 1 832 277 A1. **1**, 1–11 (2007).

6. Bhushan, B. Nanoscale characterization of human hair and hair conditioners. *Progress in Materials Science* **53**, 585–710 (2008).

7. Guthrie, J. T., Kazlauciunas, A., Rongong, L. & Rush, S. The Characterisation of Treated and Dyed Hair. *Dyes and Pigments* **29**, 23–44 (1995).

8. Wei, G., Bhushan, B. & Torgerson, P. M. Nanomechanical characterization of human hair using nanoindentation and SEM. *Ultramicroscopy* **105**, 248–66 (2005).

9. Verwey, E. J. W. & Overbeek, J. T. G. *Theory of the stability of lyophobic colloids*. (Elsevier: 1948).

10. Tamai, H., Hakozaki, T. & Suzawa, T. Deposition of polymethyl methacrylate latex on fibers. *Colloid and Polymer Science* **258**, 870–876 (1980).

11. Hisashi Tamai, Hamada, A. & Suzawa, T. Deposition of Cationic Polystyrene Latex on Fibers. *Journal of Colloid and Interface Science* **88**, 378–384 (1982).

12. Tamai, H. & Suzawa, T. Latex Deposition on Fibers: Effect of Electrolytes on Rate and Interaction Energy. *Journal of Colloid and Interface Science* **88**, 372–377 (1982).

13. Alince, B., Robertson, A. A. & Inoue, M. Deposition of Cationic Styrene and Styrene-Butadiene Latex Particles on Cellulose Fibers. *Journal of Colloid and Interface Science* **65**, 98–107 (1978).

14. Tamai, H., Nagai, Y. & Suzawa, T. Latex Deposition on Fibers VI Deposition State and Interaction Energy. *Journal of Colloid and Interface Science* **91**, 464–471 (1983).

15. Tamai, H. & Suzawa, T. Rate of deposition and interaction energy on deposition of polymethyl meth- acrylate latex on fibers. *Colloid and Polymer Science* **259**, 1100–1104 (1981).

16. Hogg, B., Healy, T. W. & Fuerstenau, D. W. Mutual Coagulation of Colloidal Dispersions. *Transactions of the Faraday Society* **33**, 1638–1651 (1965).

17. Voorn, D. J. *et al.* Plate–sphere hybrid dispersions: Heterocoagulation kinetics and DLVO evaluation. *Colloids and Surfaces A: Physicochemical and Engineering Aspects* **294**, 236–246 (2007).

18. Alince, B. & van de Ven, T. G. M. Kinetics of colloidal particle deposition on pulp fibers 2. Deposition of clay on fibers in the presence of poly(ethylenimine). *Colloids and Surfaces A: Physicochemical and Engineering Aspects* **71**, 105–114 (1993).

19. Van de Ven, T. Orthokinetic Heteroflocculation in Papermaking. *Highlights in Colloid Science.* 1–20 (2008).

20. Napper, D. H., Smitham, J. B. & Evans, R. Analytical Theories of the Steric Stabilization of Colloidal Dispersions. *Journal of the Chemical Society, Faraday Transactions 1* **71**, 285–297 (1975).

21. Evans, R. & Napper, D. H. Steric Stabilization I. *Kolloide-Zeitschrift und Zeitschrift fur Polymere* **251**, 409–414 (1973).

22. Napper, D. H. Steric Stabilization. *Journal of Colloid and Interface Science* **58**, 390–407 (1977).

23. Evans, R. & Napper, D. H. Steric Stabilization II. *Kolloide-Zeitschrift und Zeitschrift fur Polymere* **251**, 329–336 (1973).

24. Zhulina, E. B., Borisov, O. V. & Priamitsyn, V. A. Theory of Steric Stabilization of Colloid Dispersions by Grafted Polymers. *Journal of Colloid and Interface Science* **137**, 495–511 (1990).

25. Paine, A. J., Deslandes, Y., Gerroir, P. & Henrissat, B. Dispersion Polymerization of Styrene in Polar Solvents II Visualization of Surface Layers of Steric Stabilizer on Dispersion-Polymerized and Precipitated Polystyrene Latex Particles by Transmission Electron Microscopy. *Journal of Colloid and Interface Science* **138**, 170–181 (1990).

26. Paine, A. J. Dispersion Polymerization of Styrene in Polar Solvents I. Grafting Mechanism of Stabilization by Hydroxypropyl Cellulose. *Journal of Colloid and Interface Science* **138**, 157–169 (1990).

27. Thun, C. & van de Ven, T. G. M. Deposition of hairy latex particles onto a glass surface. *Colloids and Surfaces A: Physicochemical and Engineering Aspects* **145**, 205–212 (1998).

28. Thun, C. & van de Ven, T. G. M. Effect of dextran on the deposition of latex on a glass surface. *Colloids and Surfaces A: Physicochemical and Engineering Aspects* **146**, 19–24 (1999).

29. Rijnaarts, H. H. M., Norde, W., Lyklema, J. & Zehnder, A. J. B. DLVO and steric contributions to bacterial deposition in media of different ionic strengths. *Colloids and Surfaces B: Biointerfaces* **14**, 179–195 (1999).

30. Tseng, C. M., Lu, Y. Y., El-Aasser, M. S. & Vanderhoff, J. W. Uniform polymer particles by dispersion polymerization in alcohol. *Journal of Polymer Science Part A: Polymer Chemistry* **24**, 2995–3007 (1986).

31. Paine, A. J., Luymes, W. & McNulty, J. Dispersion Polymerization of Styrene in Polar Solvent. 6. Influence of Reaction Parameters on Particle Size and Molecular Weight in Poly(N-vinylpyrrolidone)-Stabilized Reactions. *Macromolecules* **23**, 3104–3109 (1990).

32. Wang, D., Dimonie, V. L., Sudol, E. D. & El-Aasser, M. S. Dispersion polymerization of n-butyl acrylate. *Journal of Applied Polymer Science* **84**, 2692–2709 (2002).

33. Fritz, G., Scha, V., Willenbacher, N. & Wagner, N. J. Electrosteric Stabilization of Colloidal Dispersions. *Langmuir* **18**, 6381–6390 (2002).

34. Wang, D., Dimonie, V. L., Sudol, E. D. & El-Aasser, M. S. Seeded dispersion polymerization. *Journal of Applied Polymer Science* **84**, 2710–2720 (2002).

35. Brakke, K. A. Surface Evolver. *Experimental Mathematics* **1**, 141–165 (1992).

Chapter 3: Synthesis and application of poly(methacryloyl hydrazide) microgels in aqueous dispersions*

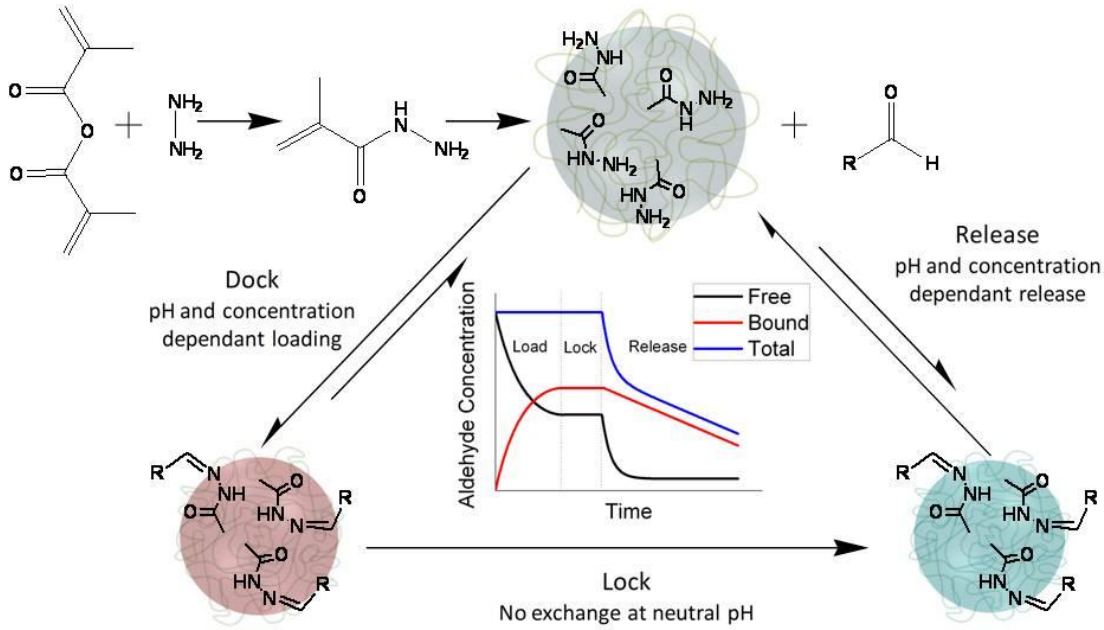

3.1. Abstract

The synthesis of poly(methacryloyl hydrazide) microgels via dispersion polymerization for the controlled release of carbonyl containing compounds is described. The kinetics of the reaction between the colloidal particles and aldehyde compounds are explored and it is shown that the subsequent release profile at conditions of physiological significance indicate a dynamic balance between the reaction components. It is demonstrated that the polymer has applications in drug delivery and in the slow release of fragrant compounds.

---

* Parts of this chapter have been published elsewhere: Ballard N, Stefan, A. F. Bon; Functional Polymer Materials **UK Patent Application No. 1215531.3**

3.2. Introduction

The use of polymers as delivery vehicles for controlled release has been studied extensively for a wide array of end applications.[1–5] In the majority of cases the desired effect of the polymer in question is to prolong the release of some active ingredient and increase the efficiency of the substance in question. This may be achieved by slow degradation or stimuli induced contraction of a polymer matrix in which the compound is encapsulated or alternatively,[6–10] cleavage of a covalent bond to release the active compound.[11–14] In either case the rate of release can often be tuned to some extent by the physiological conditions under which it is employed (pH, temperature, light *etc.*).

The controlled release of fragrance has the same fundamental challenges as drug delivery and control over the release profile is key to improving product efficiency. The release profile of volatile fragrances from a pool of liquid is given by **Equation 3. 1**.[15]

$$E \propto k_e[F]$$ **Equation 3. 1**

Where E is the evaporation rate k_e is the evaporation rate constant which depends on mass transfer (wind and chemical dependent), the area of the pool, temperature and the vapour pressure of the fragrance and $[F]$ is the concentration of fragrance in the liquid pool. The net effect of this is that evaporation is a first order process with respect to the volatile compound and the release profile decays exponentially resulting in a burst of fragrance followed by a very slow stream. Traditionally this problem has been overcome by the addition of multiple compounds with varying vapour pressures that contribute to the long life of fragrances (see **Figure 3. 1**).

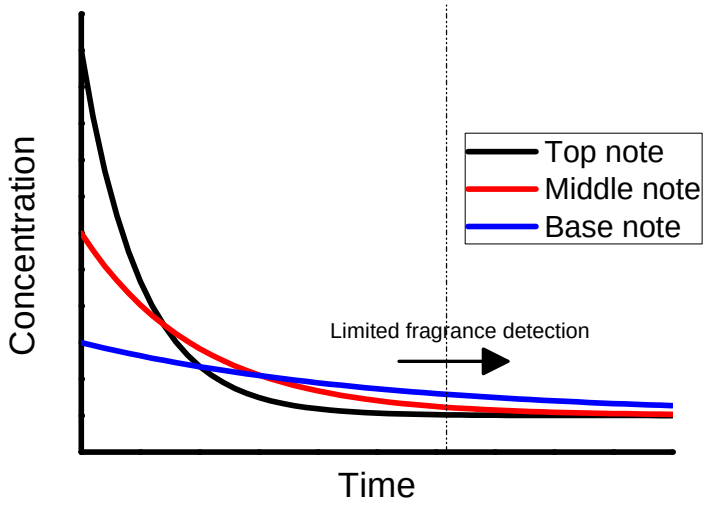

Figure 3. 1 Graph demonstrating the classical method of prolonging fragrance by use of multiple compounds of varying vapour pressure.

To a certain extent the vapour pressure of fragrances can be controlled by altering the molecular weight of the fragrance compound but doing so is costly, control is limited and the fragrance can be negatively altered. Pro-fragrances, that is compounds that degrade to yield the desired compound, are a feasible alternative that allow for fragrance release to be controlled by external stimuli such as light and pH but still limited control over the general release profile is obtained.[16,17] In order to maximize control over the release the pro-fragrance must be sensitive to relative concentration such that only when the detection of fragrance is limited, is more released. In this chapter we describe the use of dynamic polymers to achieve this effect.

3.2.1. 'Click' Chemistry and Dynamic Polymers

The advent of click chemistry has undoubtedly enhanced the ease and efficiency of the production of functional polymer materials.[18] Of the selection of 'good reactions' originally put forward by Sharpless and coworkers[19] the most widely used has been the azide-alkyne cycloaddition made popular due to the remarkable reliability of the copper catalyzed system.[20] The desirability of this process stems not only from its

ability to access new materials but the fact that the coupling process does not involve any protection/deprotection steps and opens up the possibility of the synthesis of a wealth of products from a single starting material. The impressive potential of this concept has been demonstrated by Lehn *et al.* in their seminal work on dynamic combinatorial libraries who used a pool of interchanging compounds in the presence of a molecular target to discover which have a significant binding affinity.[21,22] As shown in **Figure 3. 2** below the binding molecules to the target molecule causes a shift in equilibrium and results in amplification of the library constituents that are good potential candidates for the receptor/substrate in question.

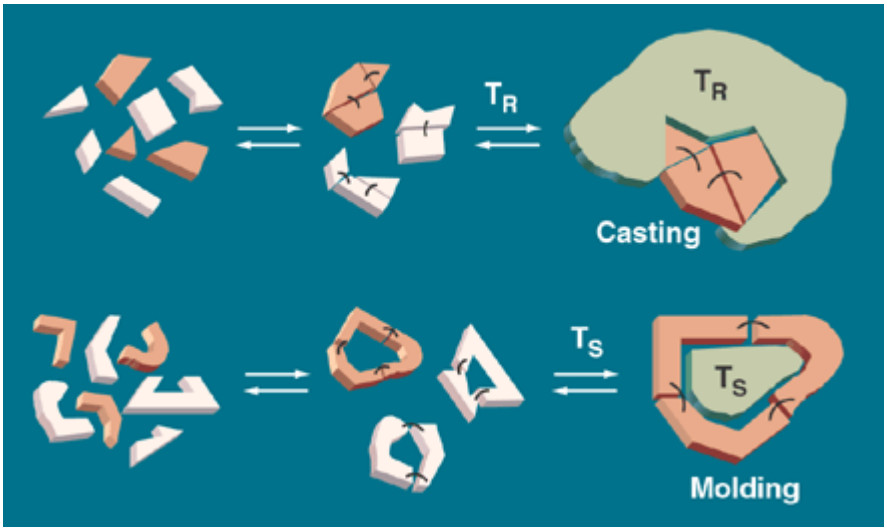

Figure 3. 2 Moulding and casting processes in dynamic combinatorial libraries. The moieties that bind strongly to the receptor (TR) or substrate (TS) cause a shift in the equilibrium and their number amplifies in order to balance the shift. Figure reproduced from Lehn *et al.*[22]

The advantage of dynamic combinatorial libraries stems from the reversible nature of the chemistry involved which is something that is uncommon in click chemistry, with the exception of a few examples such as Diels-Alder type reactions. Lehn *et al.* later undertook groundbreaking work in applying these reversible type reactions to polymer chemistry. Dynamic polymers, or 'dynamers', exhibit the ability to undergo component exchange thus providing configurational diversity.[23,24] One particularly desirable property of this type of dynamic system is that the equilibrium and

exchange process can be controlled by physical conditions such as pH and temperature.[25] The stimuli responsive properties that make these materials so inherently interesting can be derived from a variety of functional groups. Takahara *et al.* utilized the labile alkoxyamine group to scramble two well defined polymers containing 2,2,6,6-tetramethylpiperidine-1-oxy (TEMPO)-based derivatives in the polymer backbone to implement macromolecular crossover upon application of heat[26] (see **Figure 3. 3**) while Chen *et al.* have described the use of coumarin dynamers in the polymer backbone to produce light responsive polyurethanes.[27] Aside from these notable examples there is a plethora of work in the literature describing the dynamic activity of polymers including by Diels-Alder chemistry,[28] transesterification reactions,[29] and through boranate ester linkages.[30]

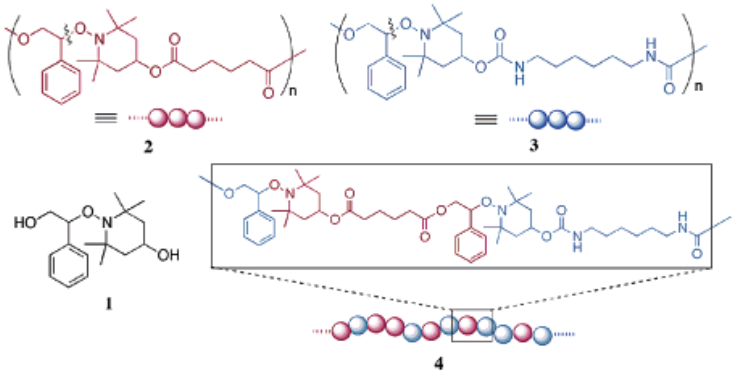

Figure 3. 3 Polymer scrambling of TEMPO containing polymers by application of heat. Reproduced from Takahara *et al.*[26]

Reports of dynamers are not limited solely to covalent interactions with various groups having reported on the use of difunctional hydrogen bond containing monomers to introduce dynamic properties to supramolecular polymers.[31,32]

3.2.2. Polyhydrazides and Polyhydrazones

One of the most widely used functionalities for covalent assemblies, and the group upon which this research is based, is the imine group and its closely related compounds.[33,34] Polyacylhydrazones, for example, contain a reversible, covalent

hydrazone linkage between monomer units. This presents the possibility of dynamic exchange with other dialdehydes/dihydrazides into the polymer backbone and subsequent alteration of the materials physicochemical properties (see **Figure 3. 4** and **Figure 3. 5**).[35,36]

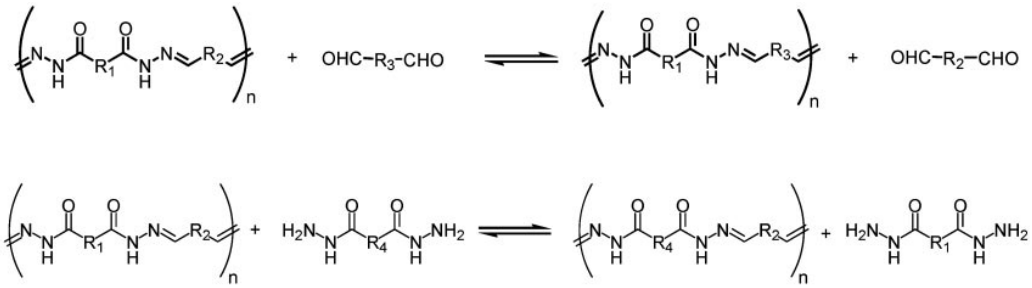

Figure 3. 4 Scrambling of polyacylhydrazones by dialdehyde and dihydrazide exchange. Reproduced from Lehn *et al*.[24]

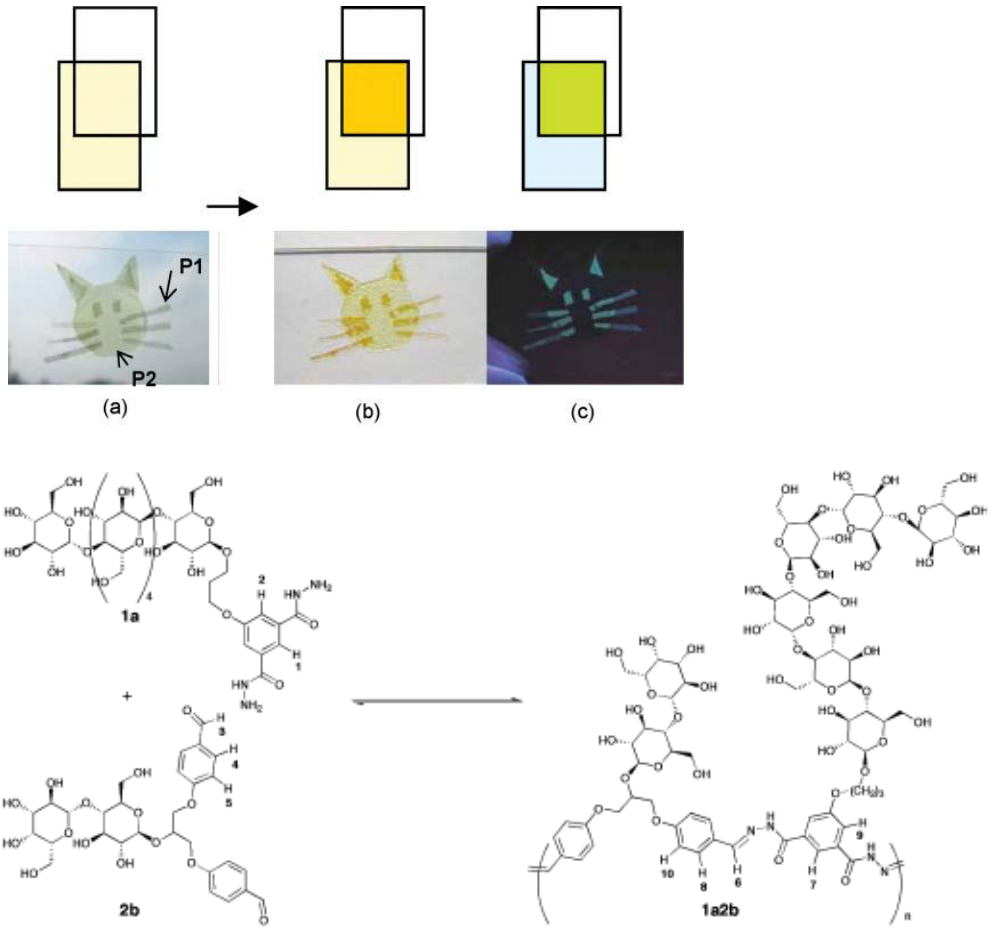

Figure 3. 5 Dynamic polymers based on polyhydrazones. *(Top)* Optodynamers – Two hydrazone containing films are brought into contact and dynamic exchange between the two results in differences in colour and fluorescent properties. *(Bottom)* Glycodynamers – Dynamic glycopolymers formed from sugar functionalized dihydrazides/dialdehydes. Reproduced from Lehn *et al.*[35,36]

On the molecular scale the hydrazone linkage has previously been used to control the release profile of aromatic aldehydes and some anti-cancer anthracyclines. [11,37,38] In the latter example the hydrazide moiety was not in the polymer backbone but as a pendant group that allowed for subsequent functionalization. The ease of reversibility and the pH dependence of the exchange reaction makes the hydrazone link especially desirable for drug delivery where pH can act as a trigger for release.

However, despite the well known reactivity of the hydrazide functional group and its 'clickability' its use in polymer chemistry has been limited due to the associated problems in synthesis and stability of the methacryloyl hydrazide polymer. The homopolymer of methacryloyl hydrazide has usually been produced by boiling poly(methyl methacrylate) in hydrazine.[39,40] This reaction is almost the antithesis of click chemistry with low yields, harsh reaction conditions and complex side reactions occurring. The alternative of synthesizing the monomer and subsequently polymerizing it has been explored although to a lesser extent.[41,42] The stability of the homopolymer of methacryloyl hydrazide in solution is hindered by the rapid transamidation that occurs in both air and water and causes gel formation preventing its application in commercial systems.[43–45] This problem of gelation due to transamidation can be negated in a microgel type system shown here where the polymer network is already crosslinked through difunctional acrylic monomers and allows the potential of the hydrazide functional group to be fully exploited. In addition problems with solubility after formation of the hydrophobic hydrazone are avoided because the particles are colloidally stable.

In this chapter we present the one step synthesis of a hydrazide functional monomer in high yield and the subsequent synthesis of the corresponding polymer microgel via dispersion polymerization. It is our aim to illustrate that by confining the

reactive hydrazide functional group to colloidal particles we can obtain reactive microgels that will dynamically uptake and release functional aldehyde compounds according to external stimuli with a degree of effortlessness that would previously have been unavailable. We believe the versatility of this system could prove of immense interest in numerous applications.

3.3. Results and Discussion

3.3.1. Synthesis of methacryloyl hydrazide

A water soluble hydrazide functional monomer, methacryloyl hydrazide (MH), was synthesized by the reaction of methacrylic anhydride and hydrazine monohydrate in chloroform according to a modified method of Okawara *et al.*.[46] The product was purified by recrystallization from a 10:1 toluene:DCM mixture and obtained in 79% yield. Previous syntheses of this molecule had described the use of equimolar amounts of hydrazine monohydrate and methacrylic anhydride but the yield in this case is low, typically less than 20%, with a large amount of the divinyl species being formed. The formation of this is due to the high reactivity of the target molecule, methacryloyl hydrazide, which can undergo a second addition to methacrylic anhydride. In order to minimize the occurrence of this a large excess of hydrazine typically 10 molar equivalents is used (see **Figure 3. 6**). Under these conditions the monomer was formed in high yield.

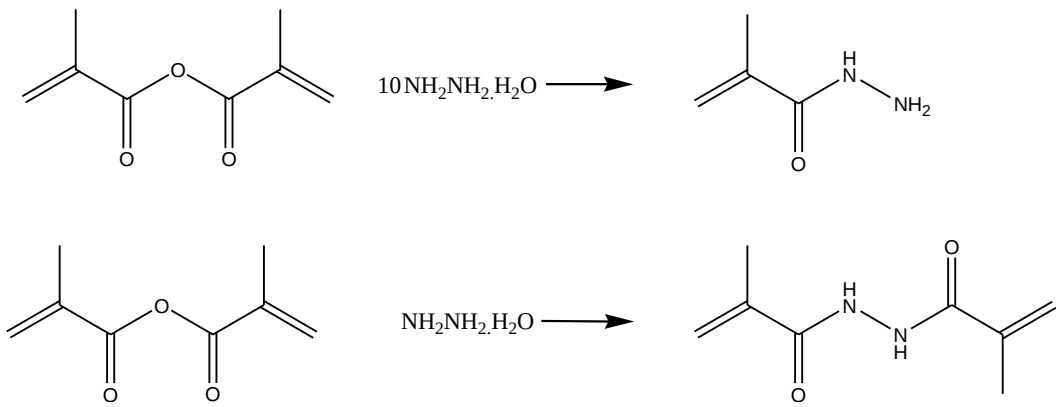

Figure 3. 6 Synthesis of methacryloyl hydrazide demonstrating undesired divinyl species formed at equimolar ratios.

3.3.2. Dispersion polymerization of methacryloyl hydrazide

3.3.2.1. Effect of reaction parameters in dispersion polymerization of methacryloyl hydrazide

Methacryloyl hydrazide was polymerized by dispersion polymerization in alcoholic media which has been shown to be a good method for the production of hydrophilic poly(acrylamides) and other acrylic polymers.[47–52] The particle size and size distribution in dispersion polymerization is particularly sensitive to reaction parameters and only under certain reaction conditions it is possible to obtain monodisperse particles. We investigated the key parameters in the synthesis of poly(methacryloyl hydrazide) microgel particles in propan-2-ol(IPA)/water mixtures using poly(vinyl pyrrolidone) (PVP) as stabilizer, *N*-*N'*methylene bisacrylamide (MBIS) as crosslinker and azobisisobutyronitrile (AIBN) as initiator and the summary of these results are presented in **Table 3. 1**.

Table 3. 1 Effect of reaction parameters in the dispersion polymerization of methacryloyl hydrazide

Code	MH / mg	MBIS / mg	PVP / mg	AIBN / mg	IPA / g	Water / g	Z_{ave} † / nm	PDI	X_m
A_W_50	240	12	240	12	2.25	2.25	N/A	N/A	0.72
A_W_60	240	12	240	12	2.75	1.75	161±3	0.424	0.69
A_W_65	240	12	240	12	3	1.5	332±4	0.375	0.70

† Intensity average diameter measured by DLS. Errors are the standard deviation of 3 measurements.

A_W_70	240	12	240	12	3.25	1.25	315±6	0.162	0.63
A_W_75	240	12	240	12	3.5	1	276±2	0.05	0.64
PVP_0	280	14	0	14	3.2	1.4	N/A	N/A	0.71
PVP_100	280	14	100	14	3.2	1.4	238±1	0.483	0.73
PVP_200	280	14	200	14	3.2	1.4	260±5	0.336	0.92
PVP_300	280	14	300	14	3.2	1.4	349±7	0.262	0.80
PVP_450	280	14	450	14	3.2	1.4	334±4	0.239	0.71
PVP_600	280	14	600	14	3.2	1.4	312±5	0.219	0.73
AIBN_3	280	14	280	3	3.2	1.4	277±2	0.183	0.81
AIBN_6	280	14	280	6	3.2	1.4	317±6	0.047	0.83
AIBN_12	280	14	280	12	3.2	1.4	413±6	0.221	0.95
AIBN_18	280	14	280	18	3.2	1.4	336±7	0.361	0.75
AIBN_24	280	14	280	24	3.2	1.4	410±4	0.497	0.85
AIBN_30	280	14	280	30	3.2	1.4	344±5	0.415	0.91
MH_5	410	20	410	20	3.2	1.4	375±8	0.175	0.74
MH_4	328	16	328	16	3.2	1.4	406±8	0.256	0.81
MH_3.5	287	14	287	14	3.2	1.4	289±3	0.231	0.78
MH_3	246	12	246	12	3.2	1.4	327±2	0.337	0.63
MH_2.5	205	10	205	10	3.2	1.4	293±11	0.536	0.72
MH_2	164	8	164	8	3.2	1.4	201±5	0.321	0.68
MH_1	82	4	82	4	3.2	1.4	104±2	0.218	0.64

3.3.2.1.1. Effect of medium polarity

Table 3.1 presents the results of dispersion polymerization reactions under various conditions. It can be seen that upon increasing the alcohol/water ratio the dispersity of the particles was reduced. At propanol volume fractions lower than 50% v/v the polymerization was conducted entirely in solution. The reaction conducted at 50% propanol was slightly turbid with the turbidity of the resulting particle suspension increasing as the propanol volume fraction was increased. At low alcohol concentrations

the polymer formed is more soluble in the reaction medium and no particles were observed.

3.3.2.1.2. Effect of stabilizer concentration

Poly(vinyl pyrrolidone) is a common stabilizer in dispersion polymerization reactions in alcoholic media. The concentration required in this set of experiments is significantly higher than usual for dispersion polymerization of styrene, for example. Where no poly(vinyl pyrrolidone) was used the polymerization went to high conversion as observed by ^{1}H NMR but no precipitation of the polymer was observed. This indicates that the PVP is not only essential to stabilize the resulting particles but it also serves to encourage phase separation of the polymer from the reaction medium. Increasing the stabilizer content resulted in lower PDI which is common in dispersion polymerization systems.

3.3.2.1.3. Effect of initiator concentration

Increasing the concentration of the initiator resulted in a general increase in the particle size. The size distribution was at a minimum for 5% by weight of AIBN. Whilst the polymer yield does not correlate with increasing initiator concentration the rate of polymerization is known to play an important role in the particle formation, particularly in the early stages of the reaction and such variability is common in dispersion polymerization systems.[53,54]

3.3.2.1.4. Effect of monomer concentration

Monomer concentration has a notable affect of the PDI of the resulting polymer dispersion and only at the higher concentrations was a narrow dispersity index obtained. This is likely due to the slow rate of polymerization and subsequent slow nucleation rate at low monomer concentration resulting in broad PDI.

3.3.2.2. Properties of microgel particles

The stability of the resulting microgel particles under different conditions is of vital importance in order to assess their viability in specific applications. We tested the microgel particles synthesized at highest monomer content (MH_5) under conditions of interest. The particles were found to be stable to a wide range of electrolyte concentrations and to both low and high pH values. In addition following lyophilisation the particles were capable of redispersion into aqueous and alcoholic solvents. The size and zeta potential of a typical poly(methacryloyl hydrazide) microgel dispersion as a function of pH is shown in **Figure 3. 7**. Below pH 4 the particle size increases with a concomitant increase in the zeta potential. The pH range at which this occurs is in good agreement with the pKa of the hydrazide group and indicates that protonation and increased swelling by water occurs below pH 4.

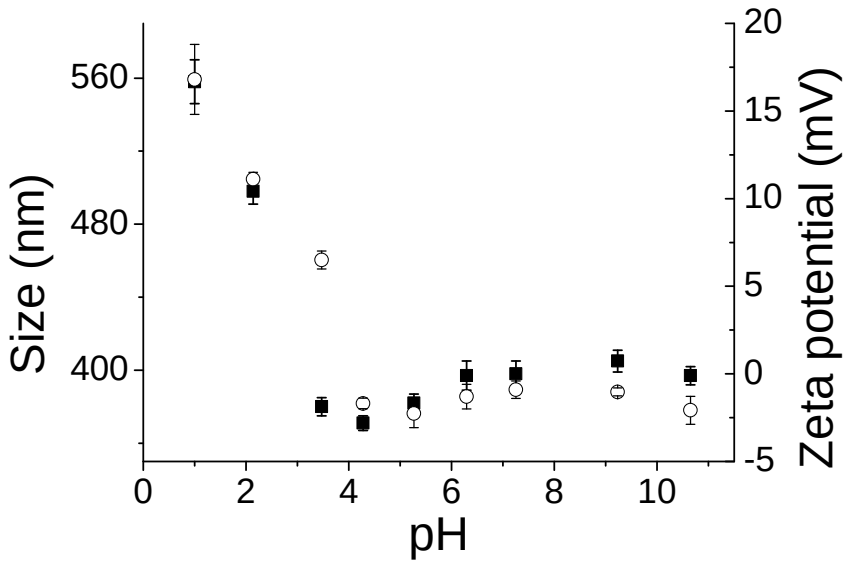

Figure 3. 7 Effect of pH on particle size (■) and zeta potential (○)

3.3.3. Dynamic behaviour of poly(methacryloyl hydrazide)

Poly(methacryloyl hydrazide) was synthesized by dispersion polymerization in 80/20 vol/vol isopropanol water mixture using AIBN as initiator, PVP as stabilizer and methylene bisacrylamide as crosslinker as described above. Following polymerization at

60°C for 24 hours the reaction mixture was centrifuged and redispersed in water 3 times then freeze dried and resuspended as a 5wt% solution in water. We proceeded to investigate the reversibility between the microgel particles, aldehydes and their respective hydrazone.

3.3.3.1. Kinetics of hydrazone formation

The rate and extent to which the hydrazone is formed from the respective aldehyde and hydrazide is of prime importance to the end application. As a model compound we looked into the kinetics of hydrazone formation using benzaldehyde (see **Figure 3. 8**).

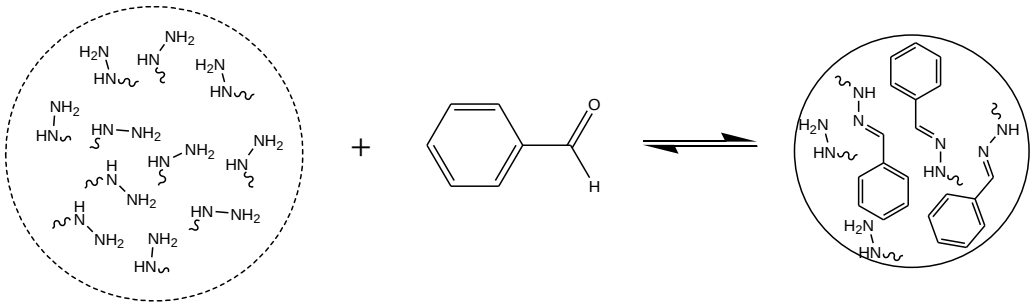

Figure 3. 8 Schematic illustrating reversible hydrazone formation from poly(methacryloyl hydrazide) microgel and benzaldehyde

3.3.3.1.1. Effect of pH on rate and equilibrium of reaction

The effect of pH on the rate and equilibrium position of hydrazone formation was examined by mixing the microgel particles and benzaldehyde at an equimolar ratio in buffered solution and monitoring the extent of reaction over time by UV/vis spectroscopy (see **Figure 3. 9**).

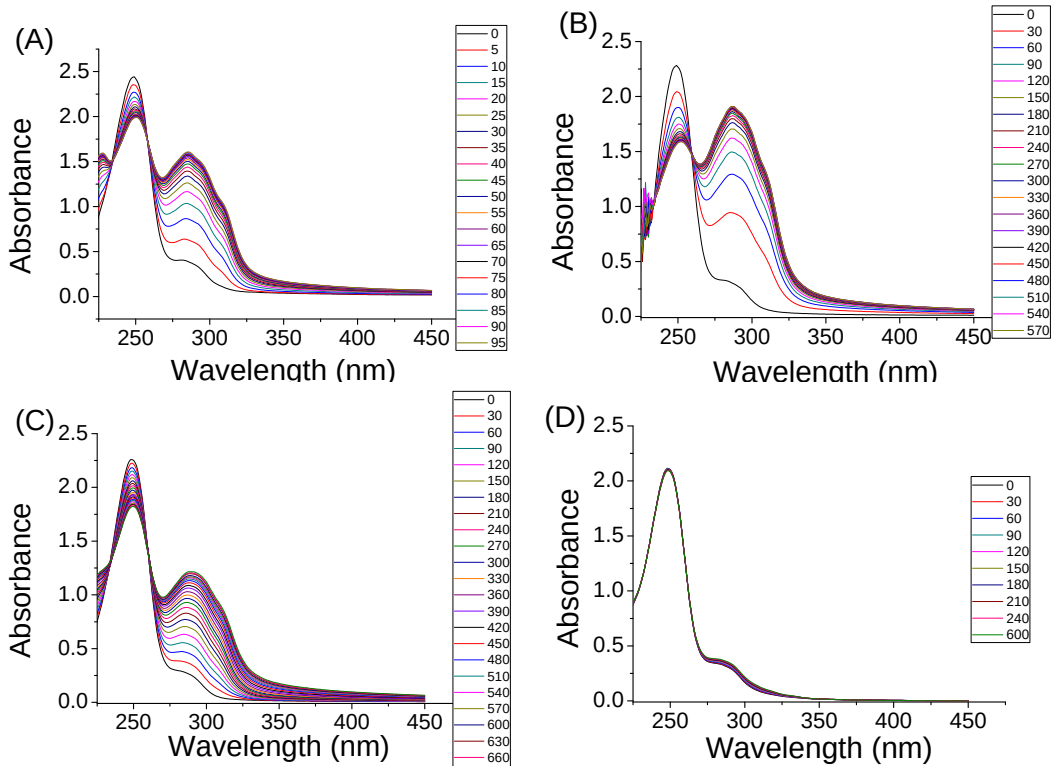

Figure 3. 9 UV/visible spectra of equimolar amounts of methacryloyl hydrazide and benzaldehyde at (A) pH 1.89 (B) pH 3.86 (C) pH 5.01 (D) pH 7.03. The figure legends denote the corresponding time in minutes.

The rate of reaction was calculated by plotting the concentration of free aldehyde at time t against the concentration at time $t+\Delta t$ (*Kezdy–Mangelsdorf–Swinbourne* method)[55] the slope being equal to $e^{-k'\Delta t}$. The concentration of aldehyde bound to the microgels at equilibrium was determined by subtracting the final aldehyde concentration, calculated by first-derivative spectrophotometry (comparing *dA/dL* at 259 nm to a set of benzaldehyde standards), from the initial aldehyde concentration. The equilibrium kinetic data for the reaction of equimolar amounts of benzaldehyde and poly(methacryloyl hydrazide) microgel particles at varying pH is given in **Table 3. 2**.

Table 3. 2 The effect of pH on pseudo first order rate constant, *k'*, and the equilibrium position

pH	$[Aldehyde]_{BOUND}/[Aldehyde]_{FREE}$	k' / s^{-1}
1.86	1.45	$6.83 \pm 0.46 \times 10^{-4}$
3.87	5.79	$2.29 \pm 0.05 \times 10^{-4}$
5.01	0.99	$0.49 \pm 0.05 \times 10^{-4}$
7.00	0.04	-

As shown above the reaction kinetics and the position of equilibrium varied drastically with pH. At low pH the time taken for the equilibrium to be established was much faster but the position of equilibrium was only slightly in favour of the hydrazone formation. At neutral pH the rate of hydrolysis and formation are so slow that there is essentially no exchange. This is of notable interest because it allows for the loading of particles at acidic pH and subsequent locking of the equilibrium at pH 7. It should be noted that due to the position of equilibrium lying almost entirely on the side of the free carbonyl no experiments with ketone compounds were conducted.

3.3.3.1.2. Effect of relative concentration on rate and equilibrium position

The effect of relative concentration on the rate and equilibrium position of hydrazone formation was examined by mixing the microgel particles and varying quantities of benzaldehyde at in pH 1.87 buffered solution and monitoring the extent of reaction over time by UV/vis spectroscopy. The reaction rate and equilibrium was calculated as described in section 3.3.3.1.1.

Table 3. 3 Effect of initial aldehyde concentration on pseudo first order rate constant, *k'*, and the equilibrium position

$[Aldehyde]_{t=0}$ / mol.dm^{-3}	$[Aldehyde]_{BOUND}/[Aldehyde]_{FREE}$	k' / s^{-1}
2.13×10^{-4}	1.45	$6.83 \pm 0.46 \times 10^{-4}$
1.79×10^{-4}	2.11	$6.49 \pm 0.51 \times 10^{-4}$
1.21×10^{-4}	1.98	$5.43 \pm 0.43 \times 10^{-4}$
8.62×10^{-5}	1.47	$4.47 \pm 0.43 \times 10^{-4}$
4.73×10^{-5}	0.72	$9.68 \pm 1.16 \times 10^{-4}$

It can be seen in **Table 3. 3** that upon decreasing the aldehyde content there is a decrease in the pseudo first order rate constant as expected when decreasing concentration. For the lowest concentration of benzaldehyde used the rate was significantly increased perhaps due to the equilibrium lying in more in favour of the free aldehyde at this low concentration. The reaction at highest benzaldehyde concentration contains more free aldehyde than one would expect but this may be due to being in slight excess with respect to the number of hydrazide groups in the polymer which was estimated based on weight of the polymer and does not take into account any side reactions that occur during the polymerization steps that could result in deactivation of the hydrazide functionality.

3.3.3.2. Dynamic fragrance release from hydrazide functionalized microgel particles

Having studied the kinetics of the reaction of microgel particles with aldehydes we then investigated the potential of the microgel particles as mediators for the controlled release of active substances. This offered the opportunity to explore the dynamic behaviour of the particles when a concentration gradient of the free aldehyde was introduced. Due to the dynamic nature of the hydrazone bond we can vastly alter the release profile of functional aldehydes by tuning the pH.

As an initial investigation into the dynamic activity of the microgel particles we looked at the evaporation of benzaldehyde in the presence of the microgel particles. Lehn *et al.*[20,21] have previously illustrated that molecular hydrazones can be deposited onto cotton surfaces and slowly release the fragrance but this required alcoholic solvents due to the relative insolubility of the hydrazones in water. In our case the microgels are colloidally stable after addition of the hydrophobic aldehydes with small amounts of surfactant. 25 ml of a phosphate buffered benzaldehyde solution (0.25 wt% benzaldehyde, pH 1.89, 0.5 wt% CTAB) was placed in a Schlenk tube. Compressed air at a constant pressure was blown over the sample. At selected time intervals the UV spectrum of the suspension was recorded to measure concentration.

Alternatively a suspension of poly(methacryloyl hydrazide) microgel particles (1.25 ml, 5 wt%) was added to 25 ml of the benzaldehyde solution and left overnight to ensure equilibrium is reached. The suspension was then placed in a Schlenk tube and subjected to the same air flow as before. The concentrations of bound and free aldehyde were calculated by first derivative spectrophotometry at a wavelength of 317 and 259 nm respectively compared to standards. The amount of benzaldehyde released was calculated using **Equation 3. 2**).

$$Release = 1 - \frac{[RCHO]_{bound} + [RCHO]_{free}}{[RCHO]_{t=0}}$$ **Equation 3. 2**

Where [RCHO] is the concentration of benzaldehyde and the subscripts refer to the amount of bound benzaldehyde at time *t*, the amount of free benzaldehyde at time *t* and the concentration of benzaldehyde initially added to the sample at *t*=0.

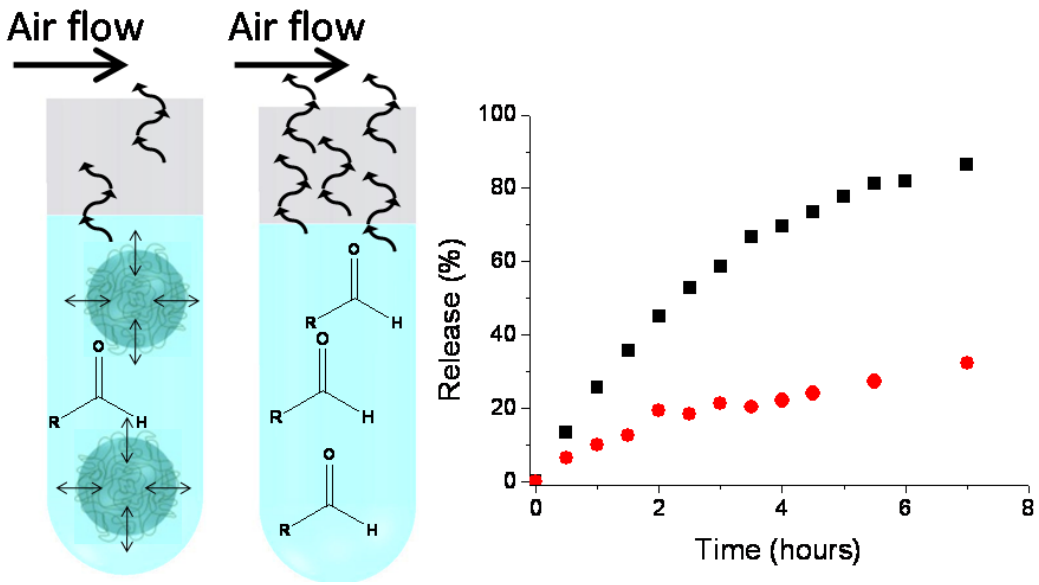

Figure 3. 10 *(Left)* Schematic demonstrating experiment used to determine release of fragrance. *(Right)* Plot showing the release of benzaldehyde over time in the absence (■) and in the presence (●) of poly(methacryloyl hydrazide) particles at pH 1.87.

The plot of the concentration of free benzaldehyde against time for the two cases is plotted in **Figure 3. 10** along with a schematic of the reaction set up. It can clearly be seen that the addition of the microgel particles induces a fairly linear release profile in addition to reducing the rate of evaporation substantially. Addition of the microgel particles significantly lowers the concentration of free aldehyde in water and hence the evaporation rate according to the scheme below.

$$\text{R-CHO}_{(g)} \xleftarrow{k_{evap}} \text{R-CHO}_{(aq)} \underset{k_h}{\overset{\text{R'-NH-NH}_2,\ k_f}{\rightleftharpoons}} \text{R'-NH-N=CH-R}$$

$$-\frac{d[R-CHO]_{(aq)}}{dt} = k_{evap}[R-CHO]_{(aq)} + k_f[R-CHO]_{(aq)}[R'-NH-NH_2] - k_h[R-C=N-NH-R']$$

Figure 3. 11 Schematic showing the rate of release of aldehyde. k_{evap}, k_f and k_h are the rate constants for evaporation, hydrazone formation and hydrazone hydrolysis respectively.

As the aldehyde in the aqueous phase evaporates the microgel releases aldehyde in order to maintain equilibrium. This has the effect of 'topping up' the free aldehyde concentration and allows for the decay in concentration to occur in a more linear fashion thus providing a more steady flow of the evaporating substance. This dynamic balance

allows fragrance to be released from the microgels only when the fragrance is diminished and can also be controlled by pH.

3.3.3.3. Dynamic release of small molecules from hydrazide functionalized microgel particles

Following this we looked into the possibility of using the microgel particles as general delivery vehicles for aldehyde containing compounds. There are very few molecules containing aldehyde groups that are used for therapeutic applications, primarily because of the high toxicity and reactivity of the aldehyde functionality so the fact that the particles mask that reactive group could prove immensely interesting to the field of drug discovery. We used, as a model compound, streptomycin sulphate, a hydrophilic, aldehyde containing antibiotic (see **Figure 3. 12**).

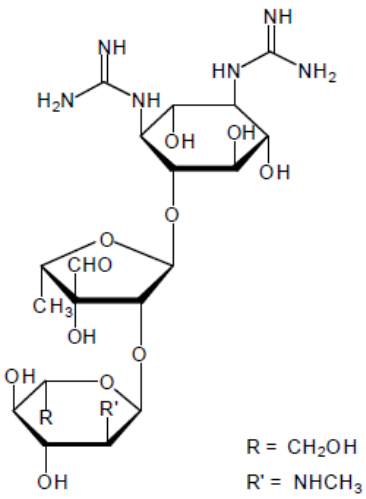

Figure 3. 12 Molecular structure of streptomycin sulphate

The microgel suspension was placed inside a dialysis membrane and submerged in a streptomycin sulphate solution in buffer and left for 24 hours to equilibrate. At selected time intervals an aliquot of the exterior solution was removed and the concentration of streptomycin was determined by the chemical assay developed by Leghorn *et al.*[56] The reaction mixture was topped up with buffer solution having the effect of diluting the streptomycin solution, similar to what one would expect to occur

in the body as the antibiotic is used up. **Figure 3. 13** shows the decrease in concentration of total streptomycin concentration over time when different amounts of the microgel particles were used. As expected at higher concentrations of microgel particles the release rate was significantly slower due to the increase in the bound streptomycin. Any free aldehyde is rapidly removed from the system and subsequent release follows a steady profile that is related to the rate of hydrolysis of the hydrazone bond, itself a function of the relative aldehyde and microgel particle concentrations. The net effect of this is to slow down release when the concentration of free aldehyde is high and speed up release when aldehyde concentration is low allowing for dynamic, concentration dependant release of the aldehyde compound.

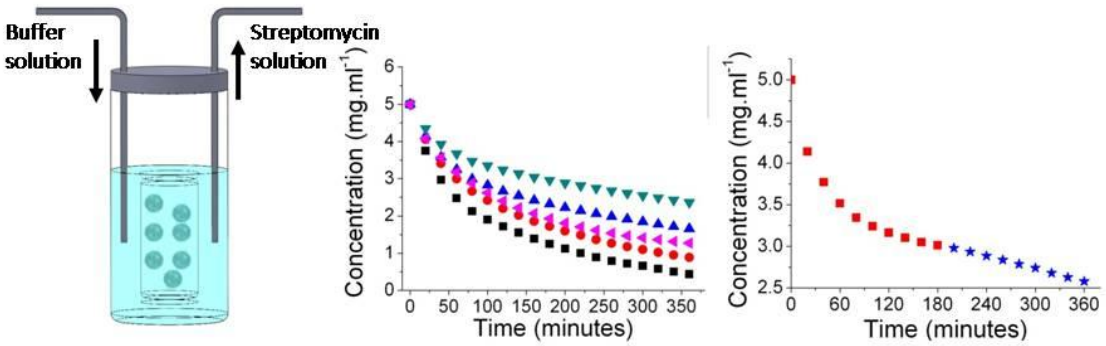

Figure 3. 13 *(Left)* Schematic of reaction set up. *(Middle)* Release profile of streptomycin sulfate in the presence of equimolar concentration of poly(methacryloyl hydrazide) microgel particles at pH 3.86(▲) pH 5.01(◀) and at a pH of 3.86 with 0(■), 0.5(●) and 2(▼) molar equivalents of hydrazide functional groups to aldehyde. *(Right)* Release profile of streptomycin sulphate in the presence of equimolar concentration of poly(methacryloyl hydrazide) microgel particles with changing pH from 7(■) to pH 3.86(★) where symbols change.

Having demonstrated that the microgel particles can be effective mediators in drug delivery we looked to investigate the ability of the particles to offer a pH sensitive delivery profile. **Figure 3. 13** illustrates that the release profile is heavily dependent on the pH of the reaction mixture. At pH 5 the equilibrium lies less to the side of the hydrazone formation so the concentration of free streptomycin is significantly higher than the analogous situation at pH 4 and thus the rate of release is faster. To test the

ability of the particles to respond dynamically to pH changes we first loaded the microgel particles with streptomycin at pH 3.86 and then froze the system by altering the pH to 7. At pH 7, where there is no exchange, the concentration of free streptomycin decreases rapidly and then tails off as the bound streptomycin cannot be released. Reverting the pH back to 3.86 where exchange can occur we saw an increase in the rate of release as bound streptomycin can once again be hydrolyzed. This result indicates the remarkable activity of the microgel particles on the release profile of carbonyl containing compounds, namely that the release profile is sensitive to both the concentration of the released species and pH which prevents overloading the concentration of the compounds in one area. We believe that the ability of these microgel particles to react and respond to changes in pH under conditions of physiological significance could have an immense impact on the use of dynamic polymers in biological and chemical applications.

3.4. Conclusion

In conclusion, we have described the synthesis of hydrazide functionalized microgel particles and demonstrated their dynamic equilibrium with carbonyl compounds in aqueous suspensions. The results of kinetic experiments showed that a complex relationship between bound and free aldehyde that is affected heavily by pH and concentration. We have shown potential application of the particulate materials in release of fragrances and other small molecules and demonstrated the ability of the particles to react in a dynamic fashion to their chemical environment. The present results indicate that the microgels can provide an efficient means of slow, controlled release of organic compounds, the release profile being determined by both pH and concentration.

3.5. Experimental

3.5.1. Materials

Methacrylic anhydride (92%), hydrazine monohydrate (98%), poly(vinyl pyrrolidone) (PVP, K-30 M_w 40,000 g.mol^{-1}), benzaldehyde (≥99.5%), streptomycin sulphate salt (M_w 728.69 g.mol^{-1}) and *N*, *N*'-methylene bisacrylamide (99%) were purchased from sigma Aldrich and were used without further purification. Azobisisobutyronitrile was purchased from Wako and used without further purification. All solvents were of reagent grade purity and were purchased from Fisher Scientific.

3.5.2. Equipment

Particle size was determined by dynamic light scattering performed on a Malvern Zetasizer ZS using a scattering angle of 173° at a standard temperature of 25°C unless otherwise stated. Zeta-potential measurements were performed on a Malvern Zetasizer ZS and were calculated from the electrophoretic mobility of the colloids using the Smoluchowski relationship. NMR measurements were performed on a Bruker DPX-400 400 MHz spectrometer and the spectrum was analysed with Mestrec v2.3a. UV spectra were recorded using a Perkin Elmer Lambda-45 UV-vis spectrometer. Melting points were recorded using a Stuart SMP3 melting point apparatus at a rate of 2°C per minute. X-ray crystallography data were measured on a Siemens SMART three-circle system with CCD area detector using the Oxford Cryosystems Cryostream Cooler. FT-IR spectra were recorded on a Perkin Elmer Spectrum 100. Microanalysis was performed by Warwick Analytical Services and high resolution mass spectrometry was performed at the Mass Spectroscopy Facility at the University of Warwick.

3.5.3. Synthesis of methacryloyl hydrazide

A solution of methacrylic anhydride (51.75 g, 0.34 mol) in chloroform (250 ml) was added dropwise to a stirred solution of hydrazine monohydrate (70 ml, 1.44 mol) at

0 °C. After addition the mixture was left to stir at room temperature for 10 minutes. The organic layer was removed and the aqueous layer washed three times with chloroform. The volatiles were removed from the organic fraction by rotary evaporation to yield a white solid. This was recrystallized from a mixture of 10:1 toluene:dichloromethane to yield fine needle like crystals (26.86 g, 79%).

Melting point range: 83-84 °C;

IR (υ_{max}/cm^{-1}, neat) 3204, 3021, 1661, 1606, 1520, 1344, 1238, 1135, 1022, 922;

^{1}H NMR (400.03 MHz, $CDCl_3$, 298 K): δ = 1.90 (s, 3H), δ = 3.91(s, 2H), δ = 5.30(s, 1H), δ = 5.68 (s,1H), δ = 7.69(s, 1H);

^{13}C NMR (100.59 MHz, $CDCl_3$, 298 K): δ = 16.4, 120.4, 138.1, 169.4;

High resolution MS-ES calc. for $C_4H_8NaN_2O$ $[M + Na]^+$: 123.0534 ; found: 123.0531;

Anal. Cald. For $C_4H_8N_2O$: C, 47.99; H, 8.05; N, 27.98; Found: C, 47.19; H, 7.95; N, 26.96

X-ray crystal structure data for methacryloyl hydrazide

Compound reference	Methacryloyl Hydrazide
Chemical formula	$C_4H_8N_2O$
Formula Mass	100.12
Crystal system	Monoclinic
a/Å	6.2801(6)
b/Å	3.9793(5)
c/Å	11.0189(12)
α/°	90.00
β/°	96.105(9)
γ/°	90.00
Unit cell volume/Å^3	273.80(5)
Temperature/K	293(2)
Space group	*P*2(1)
No. of formula units per unit cell, *Z*	2
No. of reflections measured	2674
No. of independent reflections	769
R_{int}	0.0287
Final R_1 values ($I > 2\sigma(I)$)	0.0381
Final $wR(F^2)$ values ($I > 2\sigma(I)$)	0.0866
Final R_1 values (all data)	0.0620
Final $wR(F^2)$ values (all data)	0.0923

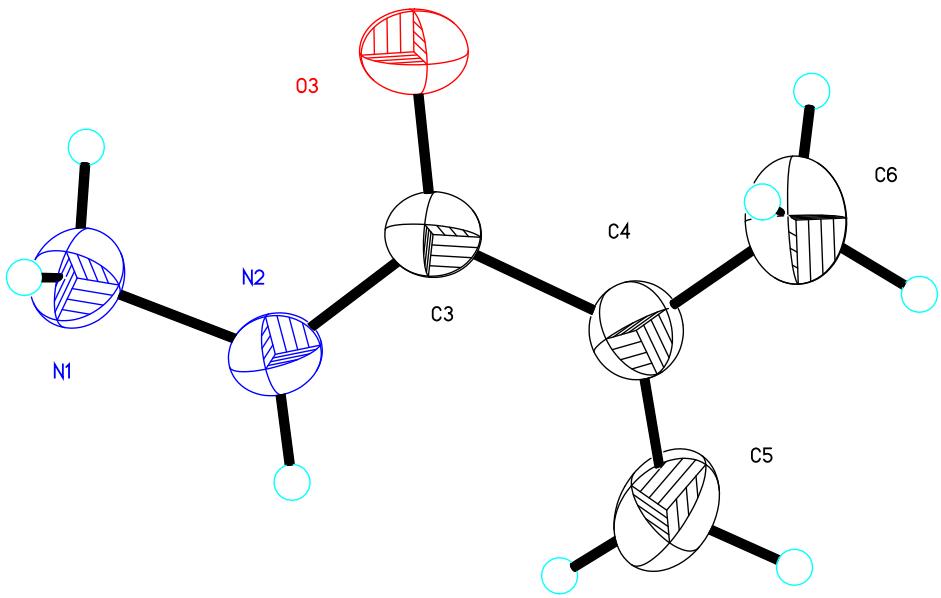

Figure 3. 14 Molecular structure by X-ray of methacryloyl hydrazide.

3.5.4. Dispersion polymerization of methacryloyl hydrazide

In a typical experiment methacryloyl hydrazide (3 g), PVP-K30 (3 g), *N, N'*methylenebisacrylamide (300 mg) and AIBN (60 mg) were dissolved in a mixture of propan-2-ol (40 ml) and water (10 ml). The mixture was purged of oxygen by bubbling with nitrogen then sealed with a slight overpressure of nitrogen and heated to 60°C overnight. The resulting milky suspension was centrifuged and redispersed in ethanol 3 times to remove excess PVP then freeze-dried and suspended in water at 5 wt%.

3.5.5. Polymer aldehyde binding kinetics

To phosphate buffer(2 ml, pH 1.89, 0.15 M) containing 0.5 wt% CTAB was added 200 μl of a suspension of poly(methacryloyl hydrazide) microgel (0.025 wt%, 2.5×10^{-3} M) and varying amounts of a benzaldehyde solution (40-200 μl, 2.36×10^{-3} M). The UV spectrum was recorded every 5 minutes for 100 minutes. Alternatively a citric acid buffer (pH 3.86, 0.15 M), an acetic acid/sodium acetate buffer (pH 5.01, 0.15 M) or a phosphate buffer (pH 7, 0.15 M) were used and the time interval was 30 minutes until equilibrium was established. The concentration of aldehyde bound to the microgels at any given time was determined by first-derivative spectrophotometry (comparing *dA/dL* at 259 nm to a set of benzaldehyde standards), from the initial aldehyde concentration

3.5.6. Dynamic release of fragrances under air flow

Release of volatile compounds: 25 ml of a phosphate buffered benzaldehyde solution (0.25 wt% benzaldehyde, pH 1.89, 0.5 wt% CTAB) was placed in a Schlenk tube. Compressed air at a pressure of 20 psi was blown over the sample. At selected time intervals 50 μl of the solution was removed and made up to 5 ml and the UV/Vis spectrum was recorded. Alternatively a suspension of poly(methacryloyl hydrazide) microgel particles (1.25 ml, 5 wt%) was added to 25 ml of the benzaldehyde solution

and left overnight to ensure equilibrium was reached. The suspension was then placed in a Schlenk tube and subjected to the same air flow as before. The concentrations of bound and free aldehyde were calculated by first derivative spectrophotometry at a wavelength of 317 and 259 nm respectively compared to standards. The amount of benzaldehyde released was calculated using

$$Release = 1 - \frac{[RCHO]_{bound} + [RCHO]_{free}}{[RCHO]_{t=0}}$$

Where [RCHO] is the concentration of benzaldehyde and the subscripts refer to the amount of bound benzaldehyde at time *t*, the amount of free benzaldehyde at time *t* and the concentration of benzaldehyde initially added to the sample at *t*=0.

3.5.7. Dynamic release of organic molecules by applied concentration gradients

Release after dilution: 5 ml of a suspension of microgel particles at varying concentrations (0-2 molar equivalents of streptomycin sulphate) in buffer was placed inside a dialysis membrane. The dialysis membrane was submerged in a 5 ml solution of streptomycin sulphate (10 $mg.ml^{-1}$, 0.013 $mmol.ml^{-1}$) and left for 24 hour under light stirring at room temperature to achieve equilibrium. At twenty minute intervals 2.5 ml of the reaction mixture on the outside of the dialysis membrane was removed and 2.5 ml of the appropriate buffer was added to replace it. The concentration of streptomycin sulphate in the removed sample was determined by a colorimetric method. To 2.5 ml of the test solution 0.5 ml of NaOH (2 M) was added. This was heated in a test tube in a water bath at 95°C for 3 minutes then removed and cooled in water for 3 minutes. 2 ml of iron ammonium sulphate solution (1 wt% in 0.75 M HCl) was added and the colour was allowed to develop for 10 minutes before the UV absorption at 540 nm was

measured. The concentration was determined from a calibration curve of known streptomycin concentrations.

3.6. References

1. Khandare, J. & Minko, T. Polymer–drug conjugates: Progress in polymeric prodrugs. *Progress in Polymer Science* **31**, 359-397 (2006).

2. Chacko, R.T., Ventura, J., Zhuang, J. & Thayumanavan, S. Polymer nanogels: a versatile nanoscopic drug delivery platform. *Advanced Drug Delivery Reviews* **64**, 836-51 (2012).

3. Gupta, P., Vermani, K. & Garg, S. Hydrogels: from controlled release to pH-responsive drug delivery. *Drug Discovery Today* **7**, 569-79 (2002).

4. Uhrich, K.E., Cannizzaro, S.M., Langer, R.S. & Shakesheff, K.M. Polymeric systems for controlled drug release. *Chemical Reviews* **99**, 3181-98 (1999).

5. Allen, T.M. & Cullis, P.R. Drug delivery systems: entering the mainstream. *Science* **303**, 1818-22 (2004).

6. Xu, Q. *et al.* Preparation of monodisperse biodegradable polymer microparticles using a microfluidic flow-focusing device for controlled drug delivery. *Small* **5**, 1575-81 (2009).

7. Soppimath, K.S., Tan, D.C.-W. & Yang, Y.-Y. pH-Triggered Thermally Responsive Polymer Core-Shell Nanoparticles for Drug Delivery. *Advanced Materials* **17**, 318-323 (2005).

8. Oh, J.K. *et al.* Biodegradable nanogels prepared by atom transfer radical polymerization as potential drug delivery carriers: synthesis, biodegradation, in vitro release, and bioconjugation. *Journal of the American Chemical Society* **129**, 5939-45 (2007).

9. Cha, Y. & Pitt, C.G. The Acceleration of Degredation-Controlled Drug Delivery from Polyester Microspheres. *Journal of Controlled Release* **8**, 259-265 (1989).

10. Qiu, Y. & Park, K. Environment-sensitive hydrogels for drug delivery. *Advanced drug delivery reviews* **53**, 321-39 (2001).

11. Etrych, T., Chytil, P., Jelínková, M., Říhová, B. & Ulbrich, K. Synthesis of HPMA Copolymers Containing Doxorubicin Bound via a Hydrazone Linkage. Effect of Spacer on Drug Release and in vitro Cytotoxicity. *Macromolecular Bioscience* **2**, 43-52 (2002).

12. Wiwattanapatapee, R., Lomlim, L. & Saramunee, K. Dendrimers conjugates for colonic delivery of 5-aminosalicylic acid. *Journal of controlled release* **88**, 1-9 (2003).

13. Soyez, H., Schacht, E. & Vanderkerken, S. The crucial role of spacer groups in macromolecular prodrug design. *Advanced Drug Delivery Reviews* **21**, 81-106 (1996).

14. Thue, P., Godwin, A., Hartenstein, M., Müller, A.H.E. & Brocchini, S. Narrow Molecular Weight Distribution Precursors for Polymer - Drug Conjugates. *Angewandte Chemie* **113**, 614-617 (2001).

15. Kawamura, P.I. & MacKay, D. The Evaporation of Volatile Liquids. *Journal of Hazardous Materials* **15**, 343-364 (1987).

16. Levrand, B. & Herrmann, A. Light induced controlled release of fragrances by Norrish type II photofragmentation of alkyl phenyl ketones. *Photochemical & Photobiological Sciences* **1**, 907-919 (2002).

17. Laumer, J.Y. de S., Frerot, E. & Herrmann, A. Controlled Release of Perfumery Alcohols by Neighboring-Group Participation . Comparison of the Rate Constants for the Alkaline Hydrolysis of 2-Acyl- , 2- (Hydroxymethyl) - , and 2-Carbamoylbenzoates. *Helvetica Chemica Acta* **86**, 2871-2899 (2003).

18. Hawker, C.J., Fokin, C.V.V., Finn, B.M.G. & B, K.B.S. Bringing Efficiency to Materials Synthesis - The Philosophy of Click Chemistry. *Australian Journal of Chemistry* **60**, 381-383 (2007).

19. Kolb, H.C., Finn, M.G. & Sharpless, K.B. Click Chemistry: Diverse Chemical Function from a Few Good Reactions. *Angewandte Chemie* **40**, 2004-2021 (2001).

20. Wu, P. *et al.* Efficiency and fidelity in a click-chemistry route to triazole dendrimers by the copper(i)-catalyzed ligation of azides and alkynes. *Angewandte Chemie* **43**, 3928-32 (2004).

21. Huc, I. & Lehn, J.M. Virtual combinatorial libraries: dynamic generation of molecular and supramolecular diversity by self-assembly. *Proceedings of the National Academy of Sciences of the United States of America* **94**, 2106-10 (1997).

22. Lehn, J.-M. & Eliseev, A.V. Dynamic Combinatorial Chemistry . *Science* **291** , 2331-2332 (2001).

23. Lehn, J.-M. Supramolecular polymer chemistry - scope and perspectives. *Polymer International* **51**, 825-839 (2002).

24. Skene, W.G. & Lehn, J.-M.P. Dynamers: polyacylhydrazone reversible covalent polymers, component exchange, and constitutional diversity.

Proceedings of the National Academy of Sciences of the United States of America **101**, 8270-5 (2004).

25. Otsuka, H., Aotani, K., Higaki, Y. & Takahara, A. A dynamic (reversible) covalent polymer: radical crossover behaviour of TEMPO-containing poly(alkoxyamine ester)s. *Chemical communications* 2838-9 (2002).

26. Otsuka, H., Aotani, K., Higaki, Y. & Takahara, A. Polymer scrambling: macromolecular radical crossover reaction between the main chains of alkoxyamine-based dynamic covalent polymers. *Journal of the American Chemical Society* **125**, 4064-5 (2003).

27. Chen, Y. & Chen, K.H. Synthesis and Reversible Photocleavage of Novel Polyurethane Containing Coumarin Dimer Components. *Journal of Polymer Science Part A: Polymer Chemistry* **35**, 613-624 (1997).

28. Reutenauer, P., Buhler, E., Boul, P.J., Candau, S.J. & Lehn, J.-M. Room temperature dynamic polymers based on Diels-Alder chemistry. *Chemistry - A European Journal* **15**, 1893-900 (2009).

29. Kricheldorf, H.R. Macrocycles. 21. Role of Ring–Ring Equilibria in Thermodynamically Controlled Polycondensations. *Macromolecules* **36**, 2302-2308 (2003).

30. Nakazawa, I., Suda, S., Masuda, M., Asai, M. & Shimizu, T. pH-dependent reversible polymers formed from cyclic sugar- and aromatic boronic acid-based bolaamphiphiles. *Chemical Communications* **1**, 881-882 (2000).

31. De Greef, T.F.A. *et al.* Supramolecular polymerization. *Chemical Reviews* **109**, 5687-754 (2009).

32. Kolomiets, E. & Lehn, J.-M. Double dynamers: molecular and supramolecular double dynamic polymers. *Chemical Communications* 1519-21 (2005).

33. Fujii, S. & Lehn, J.-M. Structural and functional evolution of a library of constitutional dynamic polymers driven by alkali metal ion recognition. *Angewandte Chemie* **48**, 7635-8 (2009).

34. Cho, E.-B., Han, O.H., Kim, S., Kim, D. & Jaroniec, M. Multifunctional periodic mesoporous organosilicas with bridging groups formed via dynamic covalent chemistry. *Chemical Communications* **46**, 4568-70 (2010).

35. Ono, T., Fujii, S., Nobori, T. & Lehn, J.-M. Optodynamers: expression of color and fluorescence at the interface between two films of different dynamic polymers. *Chemical Communications* 4360-2 (2007).

36. Ruff, Y. *et al.* Glycodynamers: dynamic polymers bearing oligosaccharides residues--generation, structure, physicochemical, component exchange, and

lectin binding properties. *Journal of the American Chemical Society* **132**, 2573-84 (2010).

37. Levrand, B., Ruff, Y., Lehn, J.-M. & Herrmann, A. Controlled release of volatile aldehydes and ketones by reversible hydrazone formation--classical" profragrances are getting dynamic. *Chemical Communications* 2965-7 (2006).

38. Levrand, B., Fieber, W., Lehn, J.-M. & Herrmann, A. Controlled Release of Volatile Aldehydes and Ketones from Dynamic Mixtures Generated by Reversible Hydrazone Formation. *Helvetica Chemica Acta* **90**, 2281-2314 (2007).

39. R Vartan-BoghossianDederichs, B. & Klesper, E. Reaction of Syndiotactic poly(methacrylic acid hydrazide) with Functional Carboxylic Acids. *European Journal of Organic Chemistry* **22**, 23-36 (1986).

40. Thevissen, J., Klein, L., Dederichs, B. & Klesper, E. Tactic poly(methacrylic acid hydrazides). *European Polymer Journal* **24**, 201-207 (1988).

41. Iwasaki, Y., Tabata, E., Kurita, K. & Akiyoshi, K. Selective cell attachment to a biomimetic polymer surface through the recognition of cell-surface tags. *Bioconjugate Chemistry* **16**, 567-75 (2005).

42. Iwasaki, Y., Maie, H. & Akiyoshi, K. Cell-Specific Delivery of Polymeric Nanoparticles to Carbohydrate Tagging Cells. *Biomacromolecules* **8**, 3162-3168 (2007).

43. Kern, V.W., Hucke, T., Hollander, R. & Schneider, R. Uber Hydrazide von Polyacrylsauren. II. Mitt. Darstellung und Eigenschaften von Polyacrylsaurehydrazonen. *Die Makromolekulare Chemie* **22**, 39-46 (1957).

44. Kern, V.W., Hucke, T., Hollander, R. & Schneider, R. Uber Hydrazide von Polyacrylsauren. I. Mitt. Darstellung und Eigenschaften der Polyacrylsaurehydrazide. **51**, 31-38 (1956).

45. Kobayashi, M. & Yabuhara, T. Process for Stabilizing Aqueous Solution of Acrylic or Methacrylic Hydrazide Polymers US Patent 4195007. (1980).

46. Endo, T., Inoue, T. & Okawara, M. Syntheses and Reactions of Functional Polymers, 74. *Die Makromolekulare Chemie* **169**, 109-116 (1973).

47. Ray, B. & Mandal, B.M. Dispersion Polymerization of Acrylamide. *Langmuir* **13**, 2191-2196 (1997).

48. Cho, M.S., Yoon, K.J. & Song, B.K. Dispersion polymerization of acrylamide in aqueous solution of ammonium sulfate: Synthesis and characterization. *Journal of Applied Polymer Science* **83**, 1397-1405 (2002).

49. Ni, H. & Kawaguchi, H. Mechanism of preparing monodisperse poly(acrylamide/methacrylic acid) microspheres in ethanol. I. *Journal of Polymer Science Part A: Polymer Chemistry* **42**, 2823-2832 (2004).

50. Ni, H. & Kawaguchi, H. Mechanism of preparing monodispersed poly(acrylamide/methacrylic acid) microspheres in ethanol. II. *Journal of Polymer Science Part A: Polymer Chemistry* **42**, 2833-2844 (2004).

51. Shapoval, P. & Horak, D. Reactive Poly (Glycidyl Methacrylate) Microspheres Prepared by Dispersion Polymerization. *Journal of Polymer Science Part A: Polymer Chemistry* **38**, 3855-3863 (2000).

52. Zhou, L.M., Shi, S., Kuroda, S.I. & Kubota, H. Nonspherical and Octopus-like Poly(methyl methacrylate) Particles Prepared by Seeded Dispersion Polymerization. *Chemistry Letters* **35**, 248-249 (2006).

53. Chen, Y. & Yang, H.W. Hydroxypropyl Cellulose (HPC) - Stabilized Dispersion Polymerization of Styrene in Polar Solvents - Effect of Reaction Parameters. *Journal of Polymer Science Part A: Polymer Chemistry* **30**, 2765-2772 (1992).

54. Uyama, H. & Kobayashi, S. Dispersion Polymerization of Styrene in Aqueous Alcohol Solution - Effects of Reaction Parameters on the Polymer Particle Formation. *Polymer International* **34**, 339-344 (1994).

55. Swinbourne, E. S. Method for obtaining the Rate Coeficient and Final Concentration of a First-order Reaction. *Journal of the Chemistry Society* 2371 (1960).

56. Boxer, G.E., Jelinek, V.C. & Leghorn, P.M. The Colorimetric Determination of Streptomycin in Clinical Preparations, Urine and Broth. *Journal of Biological Chemistry* **169**, 153 (1947).

Chapter 4: Controlling the microstructure of high porosity polymer particles for oil absorption

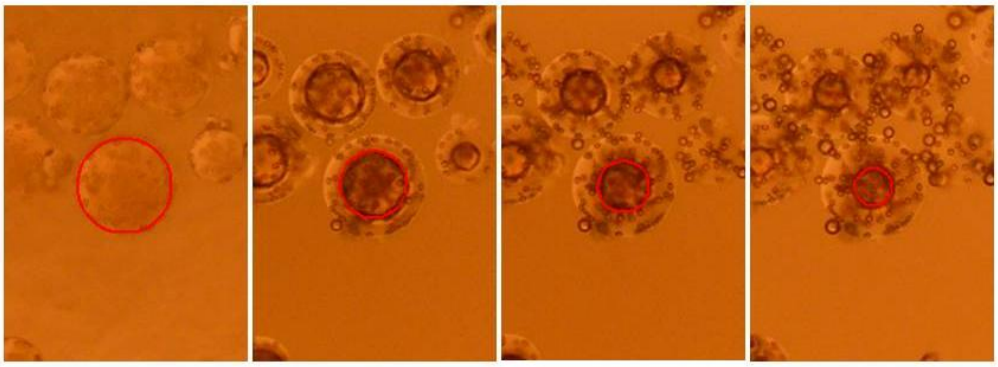

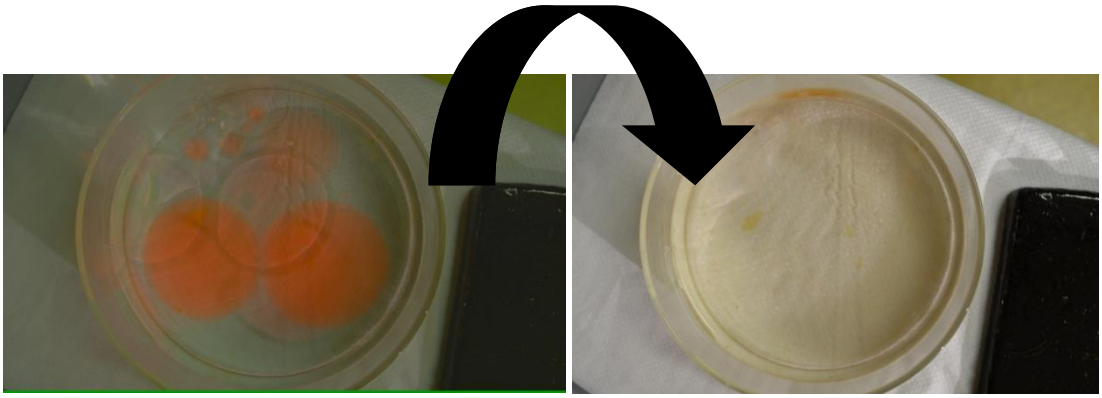

4.1. Abstract

The synthesis of particles capable of removing oil either from solution and solid surfaces is described. Highly porous particles produced by suspension polymerization of divinylbenzene in the presence of a mixture of solvating and polymeric porogens yielded particles with very high surface area which were capable of absorbing oil via capillary action, the rate of absorbance being a factor of the both the pore size and pore volume. We demonstrate the application of these particles in oil recovery from solution.

4.2. Introduction

Oil removal presents itself as a problem that is ubiquitous in the modern world. Some cases such as crude oil spills are a huge problem that impact on our lives and the delicate ecosystem in which we live. Whilst advances in production and refining oil have been rapid there has been little attention paid to efficient and environmentally friendly ways of cleaning it up in the case of spills. In the recent BP *Deepwater Horizon* incident in the Gulf of Mexico, for example, 2.1 million gallons of the 'dispersant chemical' anionic surfactant DOSS (dioctyl sodium sulfosuccinate) was deployed by aircraft to break up the slick into smaller droplets.[1] Thus the use of dispersants does not solve the problem but rather diverts it away from our view.

Figure 4. 1 A plane releases dispersant dioctyl sodium sulfosuccinate over the oil spill in the Gulf of Mexico. Source*: Reuters*

The removal of oil from fibres is commonplace in personal care products and forms the basis of many products that we use every day. Detergents in washing powders and shampoo use dispersants that are capable of removing grease and dirt from clothing fibers.[2] Despite the obvious success of these products they do have some issues associated with them. One of the world's biggest problems currently is lack of water and any product that relies on dispersants to remove oil requires substantial amounts to

be effective hence there is a drive towards cleaning products that are capable of removing oil and grease in the complete absence of water. Currently there are few products that can be marketed as water-free and those that are are often wrought with problems. Dry shampoo is one such product that has immense potential but has yet to be perfected. Currently the products consist of silica or cellulose based powders that are contained in an aerosol and work by coating/absorbing the layers of grease on the hair and preventing the greasy look and feel.[3–6] Such measures, however, are only temporary as the oil is still stuck on the fibres and in some cases, due to the white powders used, can leave the hair looking worse than before. In this chapter we describe the synthesis and application of porous polymeric particles that are capable of physically adsorbing oil by capillary action and can subsequently be removed from the fibre surface by external forces.

4.2.1. Synthesis of porous polymer particles

The synthesis of porous particles is a well researched topic due to the wide ranging application of such particulate materials.[7–11] There exists a great many techniques in the literature tailored towards synthesis of porous particles with varying porosities and pore sizes largely dependent on the porogen that is used in the reaction. What follows is a brief discussion on methods by which porosity can be introduced to polymer particles.

4.2.1.1. Generating porosity by multiple emulsions

Polymerization of monomer droplets that contain a second nonmiscible interior phase results in particles containing voids where the porosity is controlled by the size and frequency of the nonmiscible interior phase droplets. The most common way of achieving this is by a creating a multiple emulsion, *i.e.* a water in monomer in water system, and subsequently polymerizing it. In particular if the interior phase is high

(>74%) compared to the monomer phase it is termed a high internal phase emulsion (HIPE) and subsequent polymerization often produces a highly porous interconnected structure. Flowing the high internal phase emulsion into a third miscible phase before polymerizing allows production of macroporous emulsion templated polymer beads.[12] For example, Bon *et al* generated monodisperse water in glycidyl methacrylate HIPE droplets in a third aqueous phase by a microfluidic device and polymerized the monomer phase by free radical polymerization to give highly porous polymers with pore sizes of several hundred microns (see **Figure 4. 3**).[8] Ma *et al.* developed a method by which the multiple emulsion can be formed spontaneously in an oil in water suspension polymerization in which the monomer phase contained a large amount of surfactant that formed reverse micelles and absorbed water from the continuous phase. Polymerization yielded highly porous microspheres with a surface area of 200 m^2/g and average pore sizes of 50 nm.[13,14]

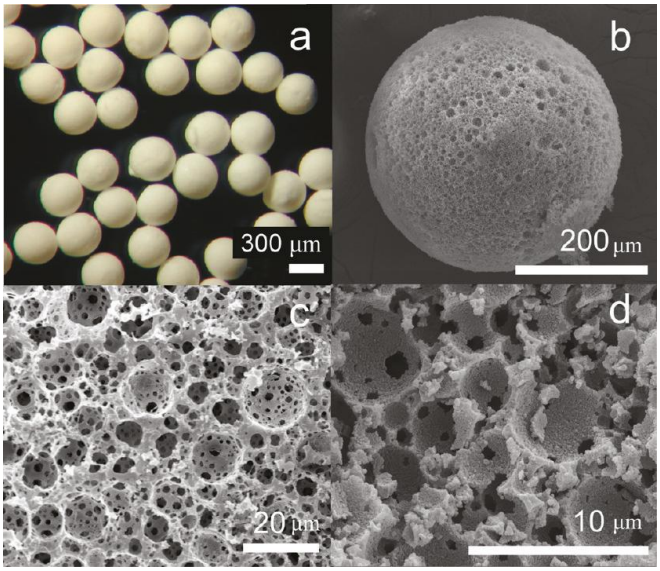

Figure 4. 2 Porous, size-monodisperse near-spherical poly(HIPE) beads:(a) optical microscopy image showing size monodispersity; SEM images of (b) a whole bead, (c) surface of a bead, and (d) inner part of a broken bead. Figure from Bon *et al.*[8]

4.2.1.2. Molecular pore forming agents

Using emulsion droplets as templates has severe limitations in accessing smaller pore sizes due to the templating process. Molecular pore forming agents are therefore more common in the synthesis of porous polymeric particles. These particles are most commonly produced via heterogeneous polymerization techniques where the porosity is generated by porogenic materials incorporated into the reaction mixture. Typically this is achieved using monomer droplets that contain a mixture of mono and difunctional vinyl species in the presence of a porogen that induces phase separation at some point in the reaction. The phase separation process and hence the average pore size and surface area are determined by the type of porogen used.[15,16]

4.2.1.2.1. Good solvents as pore forming agents

Using a good solvent for the polymer species as porogen results in the polymer network being solvated up to high levels of conversion and when phase separation occurs, in the latter stages of the reaction, the resulting microgel particulates are still swollen with residual monomer. At higher levels of conversion the small gel like particles are fused together and pores are generated in the spaces between the particulate materials. The surface area of the resulting particles is typically high (up to 750 m^2g^{-1}).[17] For styrene–DVB mixtures, porogens such as toluene and xylene are useful in this respect but they must be used with relatively high levels of DVB (>50%) in order to achieve satisfactory phase separation.[18]

4.2.1.2.2. Poor solvents as pore forming agents

Alternatively, using a solvent that has poor thermodynamic compatibility with the polymer results in phase separation in the early stages of polymerization as the polymer precipitates inside the monomer/porogen droplets. The resulting nuclei fuse and aggregate and residual monomer is precipitated throughout the polymerization and fills

in gaps between already aggregated particles. This coarsening process creates pores with large average diameter (macropores) but the particles have a lower surface area (<50 m^2g^{-1}).[16,17] Some polymerisations undergo a 'self porogen' effect in this way if the monomer is immiscible with its corresponding polymer.[19]

4.2.1.2.3. Polymers as pore forming agents

More recently the effect of linear polymers as coporogen materials has been investigated. Commonly used polymeric porogens include: poly(styrene), poly(methyl methacrylate) and poly(ethylene oxide).[20–23] Sherrington *et al.* reported a bimodal pore size distribution using DVB as crosslinking monomer and a mixture of toluene and PDMS as the pore forming agents in a suspension polymerization system.[17] They demonstrated that by using toluene, a good solvent, microporosity could be obtained but PDMS, the polymeric porogen, gave the resulting particles macroporosity giving the result of a particle with high surface area and large pore volume simultaneously (see **Figure 4. 3**).

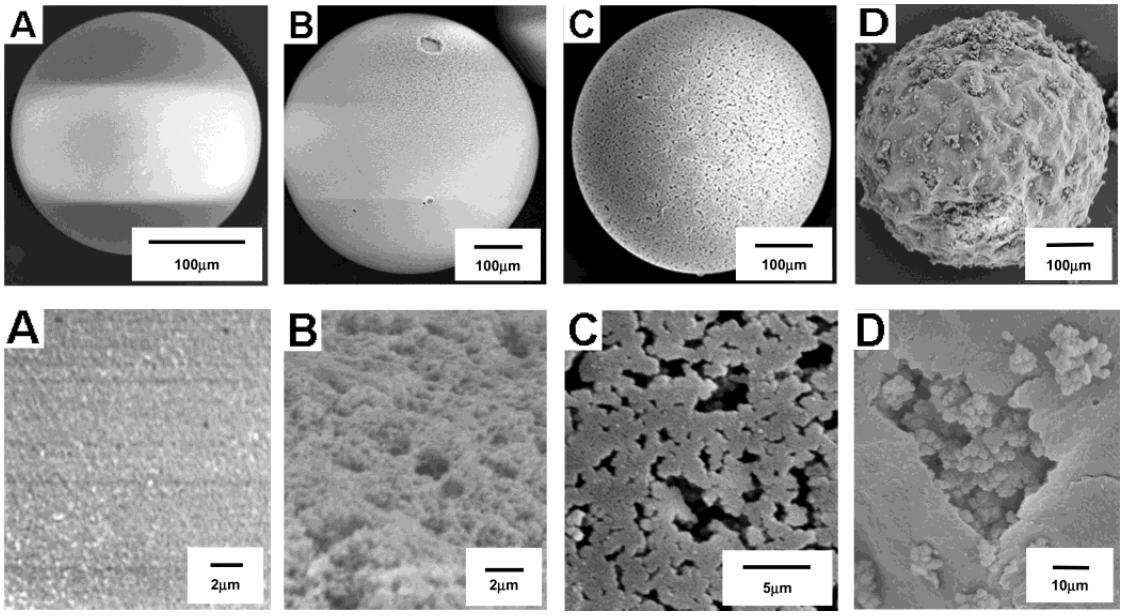

Figure 4. 3 Scanning electron micrographs of poly(DVB) resins prepared using (A) toluene porogen 100 vol %, (B) PDMS coporogen 6 vol %, (C) PDMS coporogen 20 vol %, and (D) PDMS porogen 100 vol %.[17]

Numerous groups have investigated the combined effects of polymeric and small molecule porogens in the production of macroporous polymers with both high surface area and large pore volume. For example, Gong and co-workers used suspension polymerisation to synthesise uniform porous p(DVB) spheres and compared the effects of two porogens – heptanes(a non-solvent) and toluene(a good solvent for styrenic polymers). The specific surface areas obtained were up to 706.6 m^2g^{-1} and 937.5m^2g^{-1} respectively and indicated a synergetic effect between the polymeric and molecular pore forming agents.[21]

4.2.1.3. Enhancing porosity after reaction – hypercrosslinked polymers

There are reports in the literature of using chemical functionalization to increase surface area post polymerization by creating hypercrosslinked systems. These hypercrosslinked polymers were first reported by Davankov and co-workers who functionalized polystyrene by chloromethylation and subsequently converted these into crosslinking methylene bridges.[24] This work has since been developed by other groups to synthesize the hypercrosslinked networks in a single step.[25,26] For example, Cormack *et al*. synthesized crosslinked poly(vinylbenzyl chloride) particles and subsequently performed the Lewis acid catalyzed hypercrosslinking reaction in dichloroethane (see **Figure 4. 4**). They also showed that these hypercrosslinked particles can act as amphipathic sponges, absorbing large quantities of both oils and water.[27]

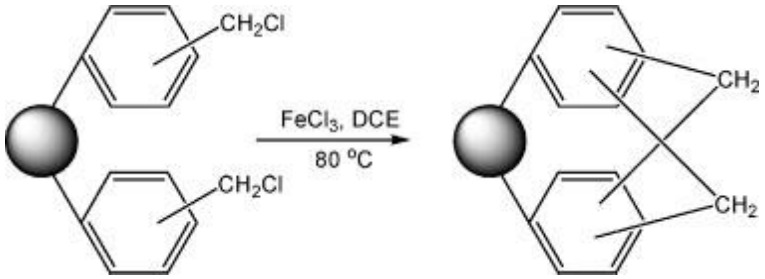

Figure 4. 4 Schematic representation of Lewis acid catalyzed 'internal' hypercrosslinking of VBC-DVB precursor particles. Reproduced from Cormack *et al.*[27]

4.2.2. Oil absorption by capillary action

It has been known for many centuries that thin tubes are capable of drawing liquids up within against the direction of gravity. Perhaps the first to observe this was Leonardo da Vinci who postulated (incorrectly!) that mountain springs are due to a series of interconnected fine capillaries that are capable of lifting water. The underlying physical basis of this phenomenon is due to the lowering of surface energy if the capillary is wet. The combination of surface tension and adhesive forces between the capillary and liquid acts to draw liquid into the tube while the force of gravity is acting in the reverse direction. The net effect of this is that as the capillary radius is reduced the height to which a liquid column will rise within it increases as seen from Jurin's law for capillary rise (**Equation 4. 1**).[28]

$$h = \frac{2\gamma\cos\ \theta}{r\rho g}$$ **Equation 4. 1**

Where h is the liquid height, γ is the liquid surface tension, θ is the contact angle, ρ is the liquid density, r is the tube radius, *and* g is the gravitational acceleration. Jurin's law is valid if the tube radius is smaller than the capillary length.

Absorption of fluid into porous media is driven by this capillary action and in order to optimize the use of porous particulates both the extent to which liquid is absorbed and the rate at which the absorption occurs is of paramount importance. Based on the Washburn equation, which approximates a porous body as an ensemble of individual, small, cylindrical capillaries perpendicular to the absorbate liquid, the mass of fluid absorbed per unit area, normal to the direction of flow, m_s, is expressed by **Equation 4. 2**.[29,30]

Equation 4. 2

$$m_s = \rho\left(\frac{\gamma cos\theta}{2\mu}\right)^{1/2}\left(\frac{\varepsilon^*}{\tau}r^{1/2}\right)t^{1/2}$$

Where ρ is the fluid density, γ is the surface tension, μ is its viscosity, θ is the contact angle, ε* is the effective porosity (considered until the material is saturated), r is the average pore radius, t is time and τ is the tortuosity factor (dimensionless correction term for pores not being completely uniform and vertical, which reduces the rate of absorption). This equation demonstrates that the rate of liquid uptake is at a maximum when contact angle is at a minimum and radius is larger.[31,32]

The two equations above show the balance required in order to maximize absorption. The contact angle between the inner pore surface and the absorbent must be minimized while the radius must be large enough to allow rapid flow but small enough to ensure a reasonable amount of capillary rise.

4.3. Results and Discussion

In order to synthesize highly porous particles in which both the porosity and contact angle of the resulting particles could be tailored to maximise the rate of oil absorption into the polymer particles we conducted the suspension polymerization of divinyl benzene (DVB) using a combination of toluene and linear polystyrene as the pore forming agents.

4.3.1. Synthesis of porous particles

4.3.1.1. Effect of polystyrene coporogen

To investigate the effect of the polystyrene coporogen used in the reaction we performed a set of suspension polymerizations using a constant DVB:toluene ratio of 1:5 and at constant shear rate. Following polymerization the particles were filtered and washed with water extensively followed by ethanol and finally soaked in acetone

overnight to remove any residual linear polymer and toluene and dried. The porosity of the particles was examined by SEM and by porosimetry.

The SEM images indicate a trend in increasing pore size upon increasing the polystyrene coporogen content (see **Figure 4. 5**). This effect is well documented in the literature and is ascribed to earlier phase separation induced by the polymeric porogen. At higher concentrations of polystyrene there are visible holes in the particles that arise due to incomplete or slow dissolution of the polystyrene microspheres used as coporogen. This unexpected result serves to increase the overall surface area in addition to creating large macropores and increasing the connectivity of the porous polymer network. The effect of linear polymer is also shown more quantitatively in the porosimetry data where pore size distributions are in the mesopore region for low polystyrene contents and in the macropore region at higher concentrations (see **Figure 4. 6**).

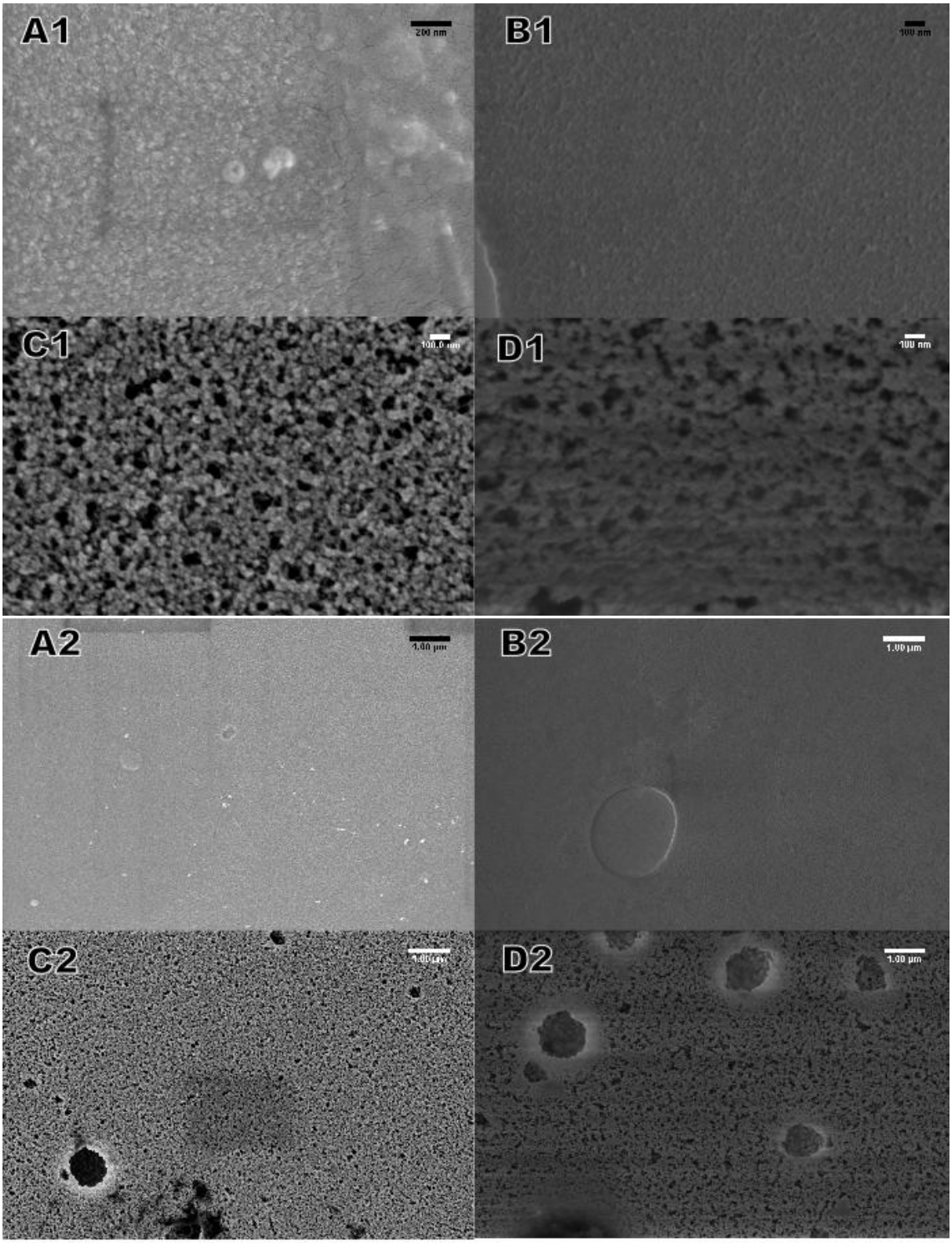
A1
200 nm
B1
100 nm
C1
100.0 nm
D1
100 nm
A2
1.00 µm
B2
1.00 µm
C2
1.00 µm
D2
1.00 µm

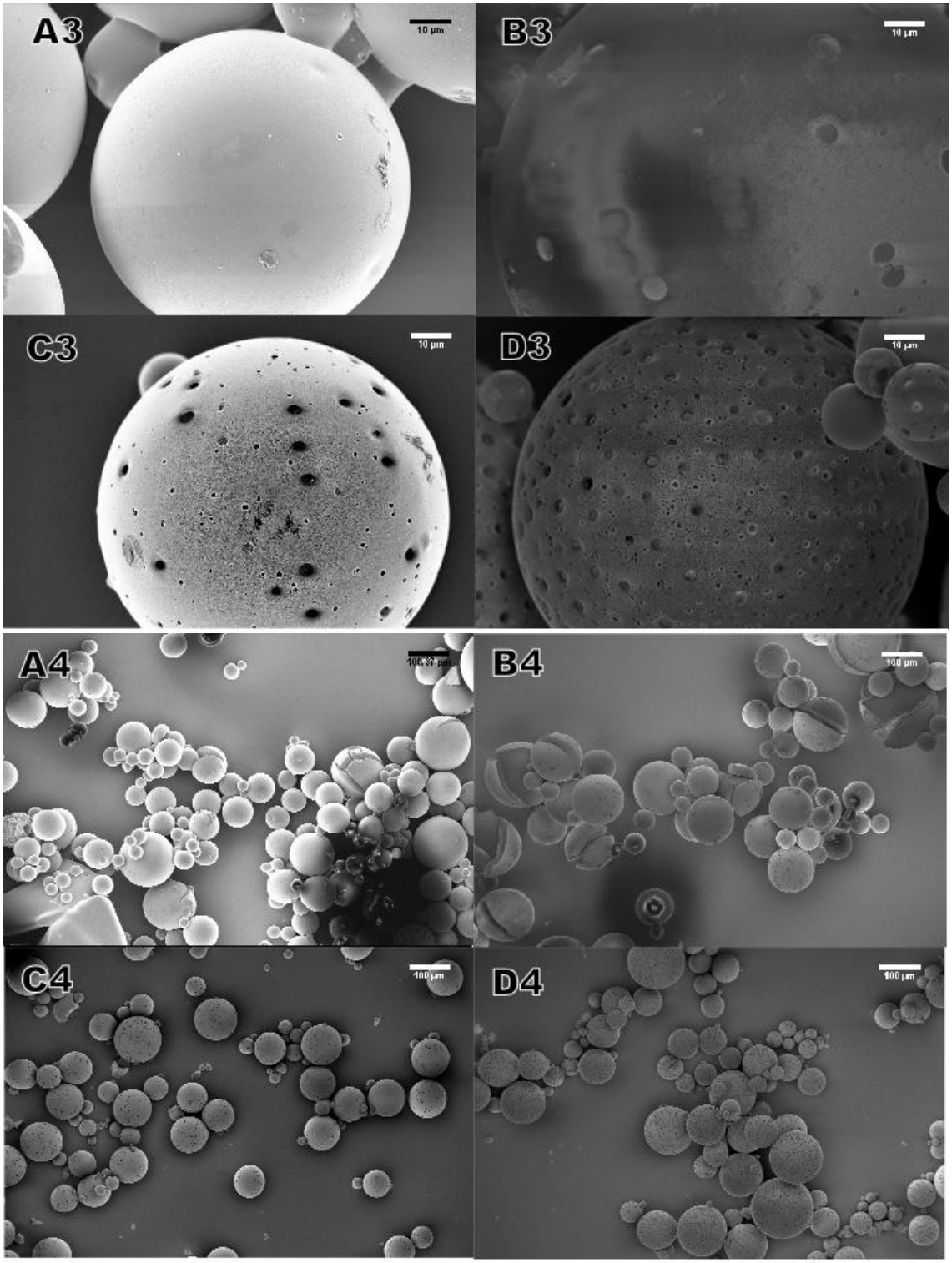

Figure 4. 5 SEM images at 50,000x, 10,000x, 1,000x and 100x magnification of porous poly(DVB) microspheres produced by suspension polymerization of DVB in the presence of toluene at a 1:5 DVB:toluene ratio and increasing linear polystyrene coporogen content in the monomer feed (A) 1% polystyrene (B) 2% polystyrene (C) 5%polystyrene and (D) 10% polystyrene.

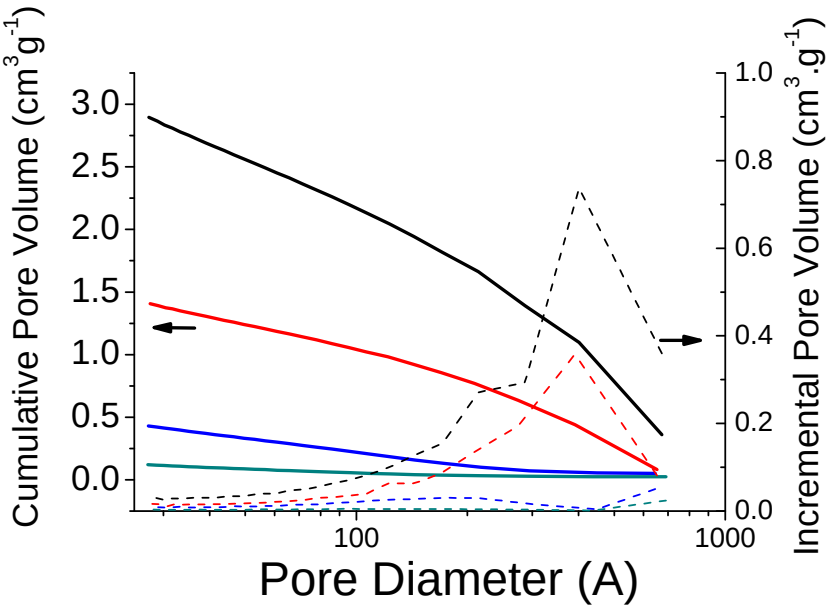

Figure 4. 6 Cumulative(straight lines) and incremental(dashed lines) pore volumes obtained using BJH theory from N_2 adsorption isotherm for poly(DVB) particles at 5:1 toluene to DVB ratio and varying the content of polystyrene as coporogen 1% (--) 2%(--) 5%(--) and 10%(--)

The introduction of polystyrene increases the average pore diameter and also the accessible pore volume but it also hugely increases the surface area of the resulting particles. This effect can be seen in **Table 4. 1** where the surface area calculated by BET theory increases over times as the concentration of linear polymer is increased. This result demonstrates that using linear polystyrene as a porogenic agent in suspension polymerization of divinyl benzene we can tune pore size distributions and porosity to suit the purpose.

Table 4. 1 Effect of linear polymer and solvent porogen on particle size distribution and particle surface area

Tol/DVB	PSt content / %	Size* / µm	S_{BET} / m^2g^{-1}
5	1	58±28	118
5	2	79±38	489
5	5	41±21	684
5	10	40±22	1558
3	5	50±34	581
1	5	64±34	532

4.3.1.2. Effect of solvent porogen monomer ratio

The effect of the polymeric porogen has been demonstrated in section 4.3.1.1 and it was expected that the solvent porogen would exert similar effects on the porosity of the resulting particles. We therefore synthesized a series of particles in which the linear polystyrene to divinyl benzene ratio was kept constant while the ratio of toluene to divinylbenzene was altered.

Table 4. 1 shows the effect of altering the toluene content on the surface area and particle size distribution. The surface area increased upon increasing toluene concentration because of the change in phase separation behaviour. The increase in toluene results in an increase in the overall accessible pore volume and subsequently an increase in total surface area. The effect on average pore size could be seen using SEM (see **Figure 4. 7**) in which the average pore size increases with increasing toluene content. It is apparent that the synergistic effects of the polymeric porogen and solvent porogen lead to particles with very high surface area and large pore sizes making this system ideally suited to synthesis of absorbent particles.

*Average Radius - size and size distributions measured by optical microscopy. Error denotes one standard deviation.

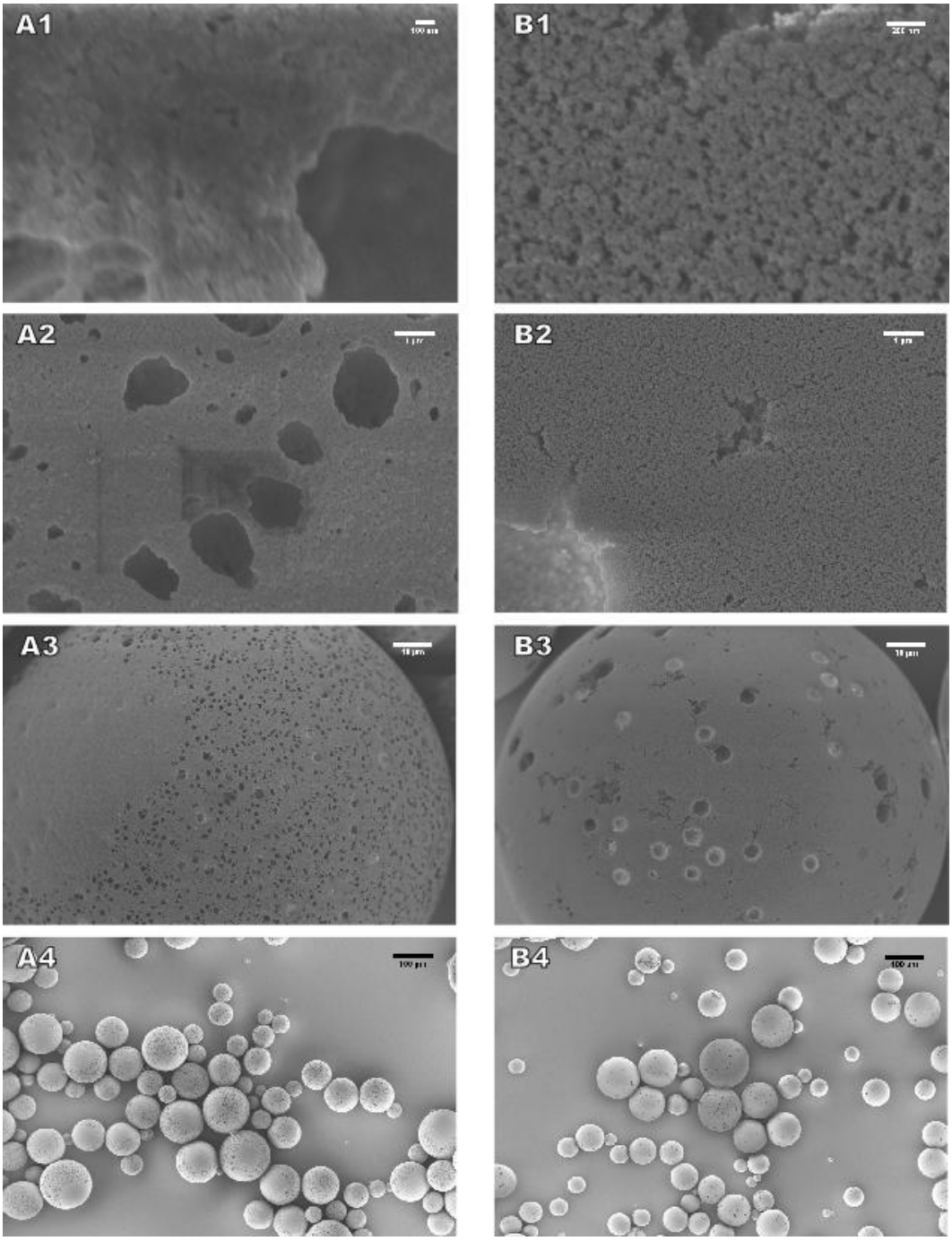

Figure 4. 7 SEM images of porous poly(DVB) microspheres synthesized using polystyrene as a coporogen (5 wt% to DVB) and varying toluene ratio (A) Toluene:DVB = 1 (B) Toluene:DVB = 5

4.3.1.3. Synthesis of highly porous magnetic particles

In order to manipulate the particles at a macroscopic level we introduced magnetic nanoparticles into the initial monomer feed in order to synthesize magnetically responsive porous polymer particles. The toluene to divinylbenzene ratio was 5 and 5 wt% of linear polystyrene as coporogen was used in the monomer feed to which was

added a ferrofluid at 5 wt% dispersed in toluene corresponding to a total Fe_3O_4 content of 2.5 wt% compared to monomer.

The resulting particles exhibited a similar porosity to the equivalent reaction in the absence of ferrofluid except some particles (~10%) were of a core-shell morphology (see **Figure 4. 1**). This core shell morphology is thought to be due to spontaneous formation of double emulsion type structures due to the large amount of surfactant employed to disperse the ferrofluid in organic solvent creating a similar effect to the reverse micelle method reported by Ma *et al*.[13]

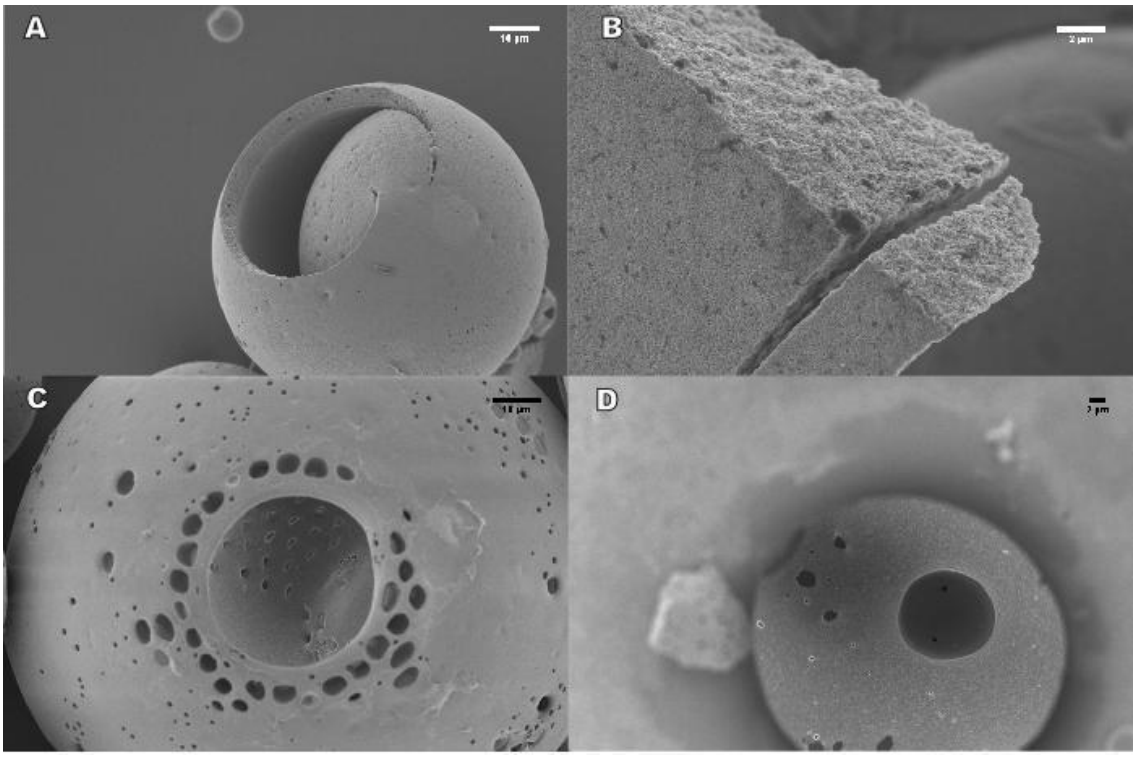

Figure 4. 8 SEM images of ferrofluid containing poly(DVB) particles synthesized by suspension polymerization in the presence of polystyrene (5 wt% to monomer) and toluene(toluene:monomer=5 $g.g^{-1}$) demonstrating core shell appearance of some particles.

4.3.2. Oil absorption of porous particles

4.3.2.1. Oil absorbance by porous particles

The solvent uptake of the synthesized porous particles was measured by a gravimetric method and are shown in **Figure 4. 9**. As expected, upon increasing the concentration of toluene porogen and keeping the linear polystyrene content the same

the absorbance is drastically increased corresponding to a larger pore volume. The blank measurement recorded with no toluene in the monomer feed exhibits a tendency to absorb small amounts of oil due to combined capillary and swelling effects. The variation of absorbance with polystyrene content shows that at lower levels (1,2 wt%) then absorbance is fairly low but at higher concentrations (5,10 wt%) the amount of oil that can be absorbed is increased dramatically. This increase is due to the greater interconnectivity of the pores as demonstrated in section 4.3.1.1 that allows solvent to travel freely within the particle. It can be seen that the higher polystyrene content particles are capable of absorbing approximately 4-5 times their own volume for solvents with a favourable contact angle with the pore walls.

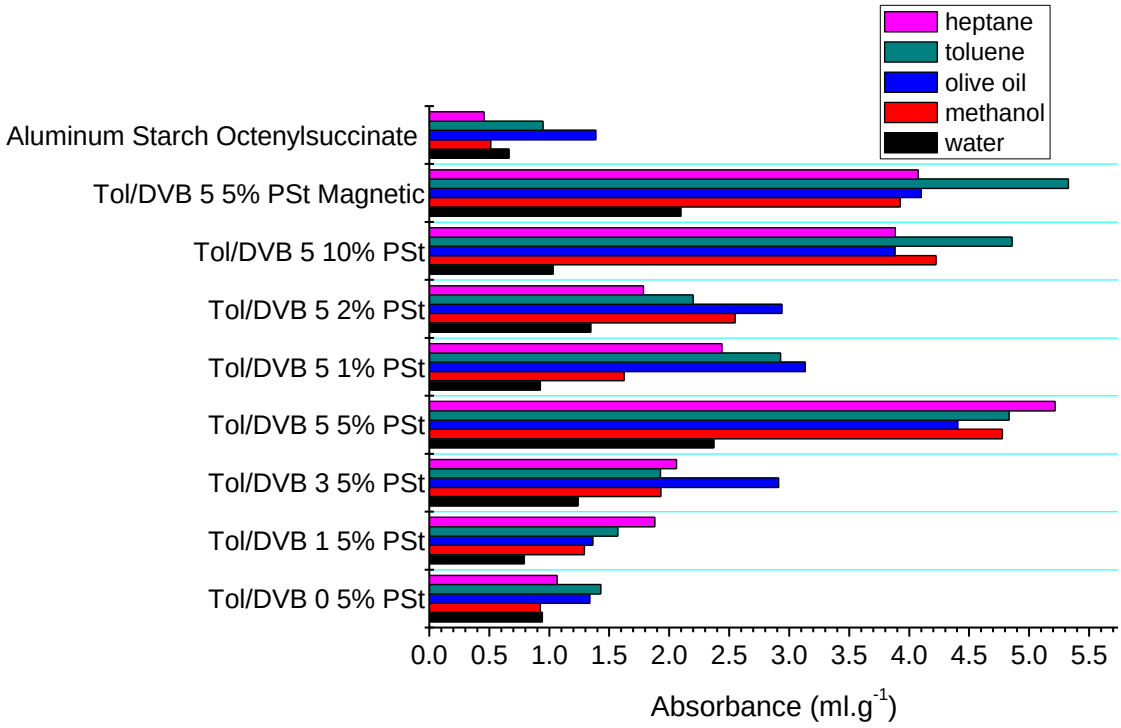

Figure 4. 9 Solvent uptake of porous particles at varying toluene to DVB weight ratios in the monomer feed and varying polymeric coporogen polystyrene (expressed as wt% compared to monomer)

The variation between solvents is negligible with toluene being absorbed to a slightly greater extent due to its ability to swell the polymer network. In the case of water absorbance was low in every case. The contact angle of water on poly(DVB) and hence the pore walls is expected to exceed 90° and it can be seen from **Equation 4. 1**

that where *cos(θ)*<0 then capillary rise does not occur. For comparison the absorbance of aluminium starch octenyl succinate, a commonly used absorbent, was measured. It can be seen that the porous particles synthesized here hugely outperform by up to 10 times in the case of the higher polystyrene and toluene content particles.

4.3.2.2. Reversibility of oil absorbance

It was postulated that these macroporous particles could exhibit reversible absorption behaviour by washing through with volatile solvents and drying. In order to test this, the particles were subjected to several cycles of absorption of olive oil, subsequently washed in acetone then dried in air (see **Figure 4. 10**). The particles were not observed to experience any deterioration in performance after several cycles indicating that the particles are in principal reusable which is no doubt desirable in several application areas. In addition the removed oil can be obtained by removing the volatile solvent used to wash the particles and hence absorbed oil can be recovered.

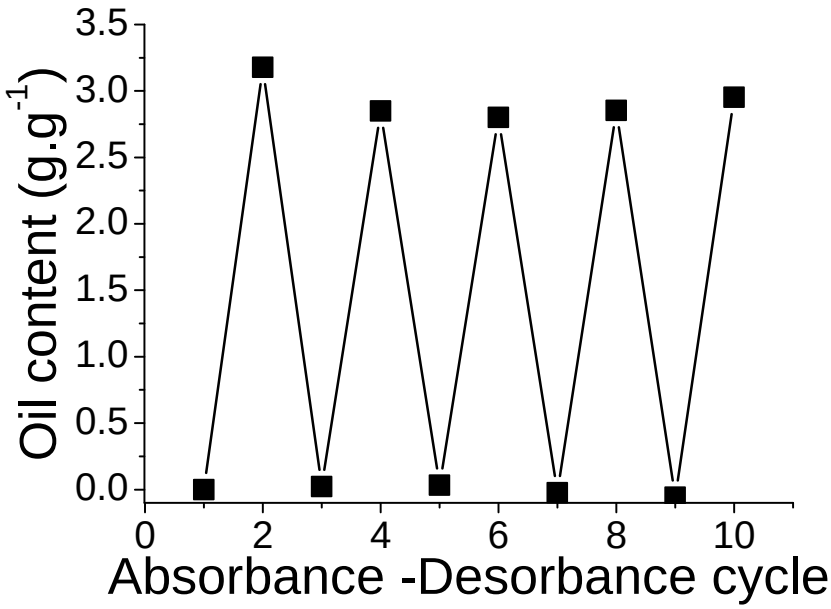

Figure 4. 10 Reversible behaviour of porous particles synthesized using toluene / DVB = 5 and 10% PSt coporogen. Each cycle consists of soaking in oil then washing with acetone and drying.

4.3.2.3. Rate of oil absorbance

In addition to the extent to which the particles are able to absorb oil the rate is of prime importance in numerous applications. The rate of oil absorption was measured by optical microscopy, immersing the particles in oil and monitoring the disappearance of the air void inside (see **Figure 4. 15**). The radius of the measured circle was used to calculate the ratio between the shell volume (V_{SHELL}) and the total particle volume (V_{TOT}).

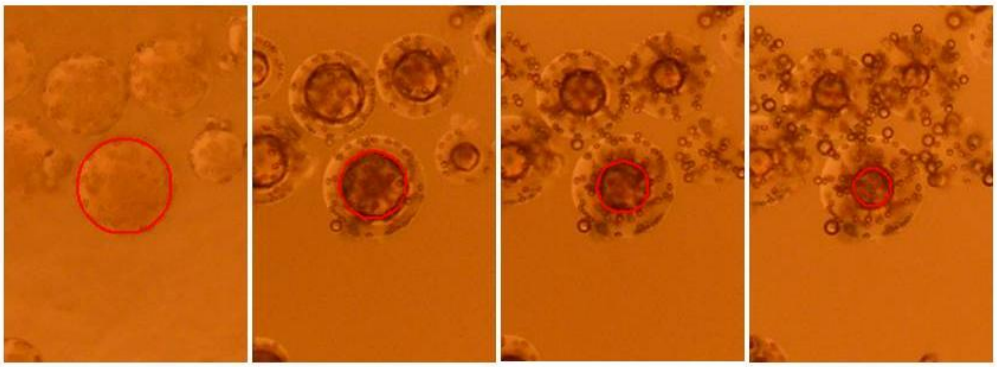

Figure 4. 11 Optical microscope images at 20x magnification demonstrating disappearance of air void inside porous particles at t=0,0.8,1.6,2.4 seconds as olive oil becomes imbibed.

For the higher contents of polystyrene used as porogen the rate of imbibition was rapid and where non-viscous organic liquids (toluene, heptane, methanol) were used as test liquid complete absorption had occurred in under half a second making measurement of the absorption rate on a particle by particle basis by this method impossible. With more viscous organic liquids such as olive oil it was however possible to measure the rates and in these cases both 5 and 10% linear polymer content particles absorbed at similar rates (see **Figure 4. 12**).

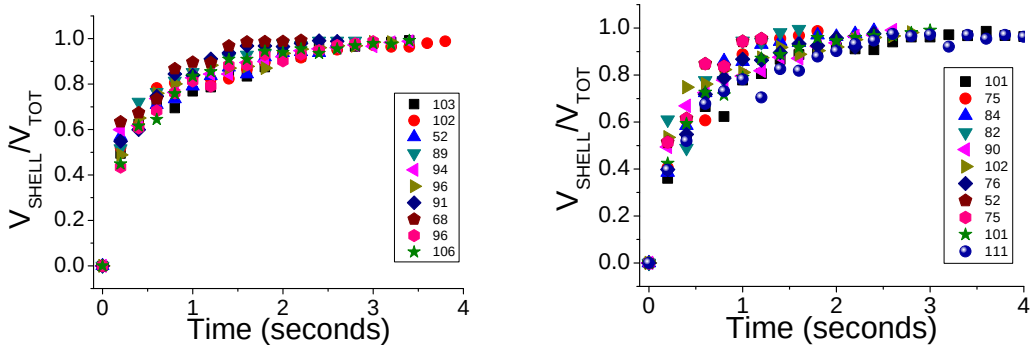

Figure 4. 12 Absorption curves of olive oil using porous particles synthesized at a toluene:DVB ratio of 5 and varying amounts of the linear polystyrene coporogen (*left)* 5 wt% (*right)* 10 wt%. Legend shows the diameter of the measured particles in micrometers.

For lower polystyrene content particles the rate of imbibition was significantly slower, in the case of viscous oils very little absorption was observed even at long time scales, probably due to low pore interconnectivity. Using olive oil and other low viscosity oils it was possible to observe absorbance but this occurred on a much longer time scale than in the case observed for higher polystyrene contents. The severe decrease in oil absorption and rate can be explained by examining the microstructure of the polymer network. At higher polystyrene contents the pore radii and interconnectivity of pores was substantially increased. The wider pores will imbibe the oil at a faster rate and deliver oil to the smaller microchannels within the network.

In addition to this the 2.5 μm diameter microspheres of polystyrene that are used as the source of linear polystyrene provide an unexpected benefit. At higher concentrations of polystyrene incomplete dissolution occurs and large holes appear on the surface and throughout the particle. The large holes provide a space through which it is possible for displaced air to build up and be released from the particle surface continuously as more oil is absorbed. In the absence of these large voids the air has no viable escape route and is strongly absorbed in the particle. This can be evidenced in both the higher polystyrene content particles where void space can be seen to nucleate

bubbles (see **Figure 4. 13**). In contrast at lower polystyrene content the voids are significantly less frequent and in this case the air released after solvent uptake comes exclusively from one or two voids on the surface. The slow rate of air removal from the interior hinders uptake and results in slow rates of oil absorption (see **Figure 4. 13**).

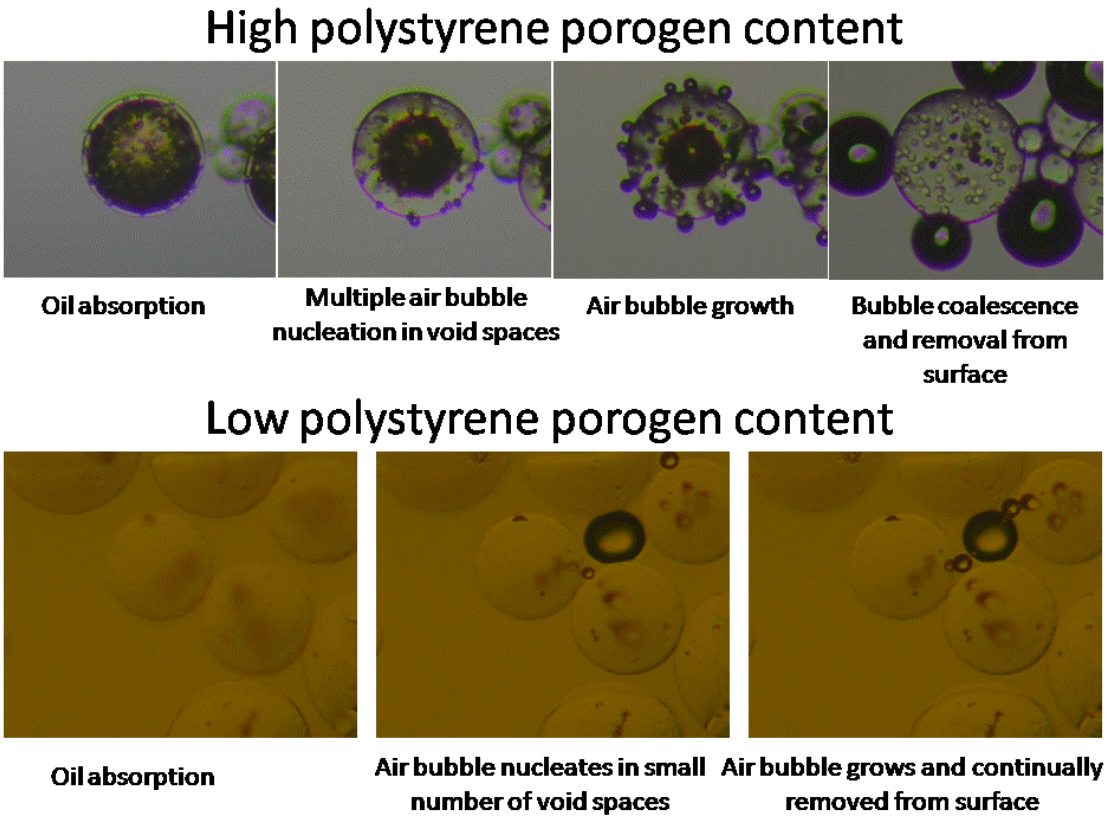

Figure 4. 13 Optical microscopy images demonstrating the effect of micron sized surface voids caused by polystyrene porogen on the rate of oil absorption.

4.3.3. Porous particles for use in oil recovery

In order to investigate the potential of the particles for use in oil recovery we performed an experiment that simulated the effect of an oil spill by adding olive oil directly into water (see **Figure 4. 14**). The oil spread across the water surface in thick globules almost immediately. The dry, ferrofluid containing particles were spread on the surface corresponding to a weight ratio of oil to particles of 4:1. The particles were left for 10 minutes to allow for maximum absorption and agitated gently then removed using a magnetic force. The particles were washed with acetone and the acetone

washings were dried to recover any absorbed oil. The amount of recovered oil was in excess of 80% demonstrating the potential use of the particles in bulk clean up of oil spills. The dried particles could potentially be reused as required as shown in section 4.3.2.2.

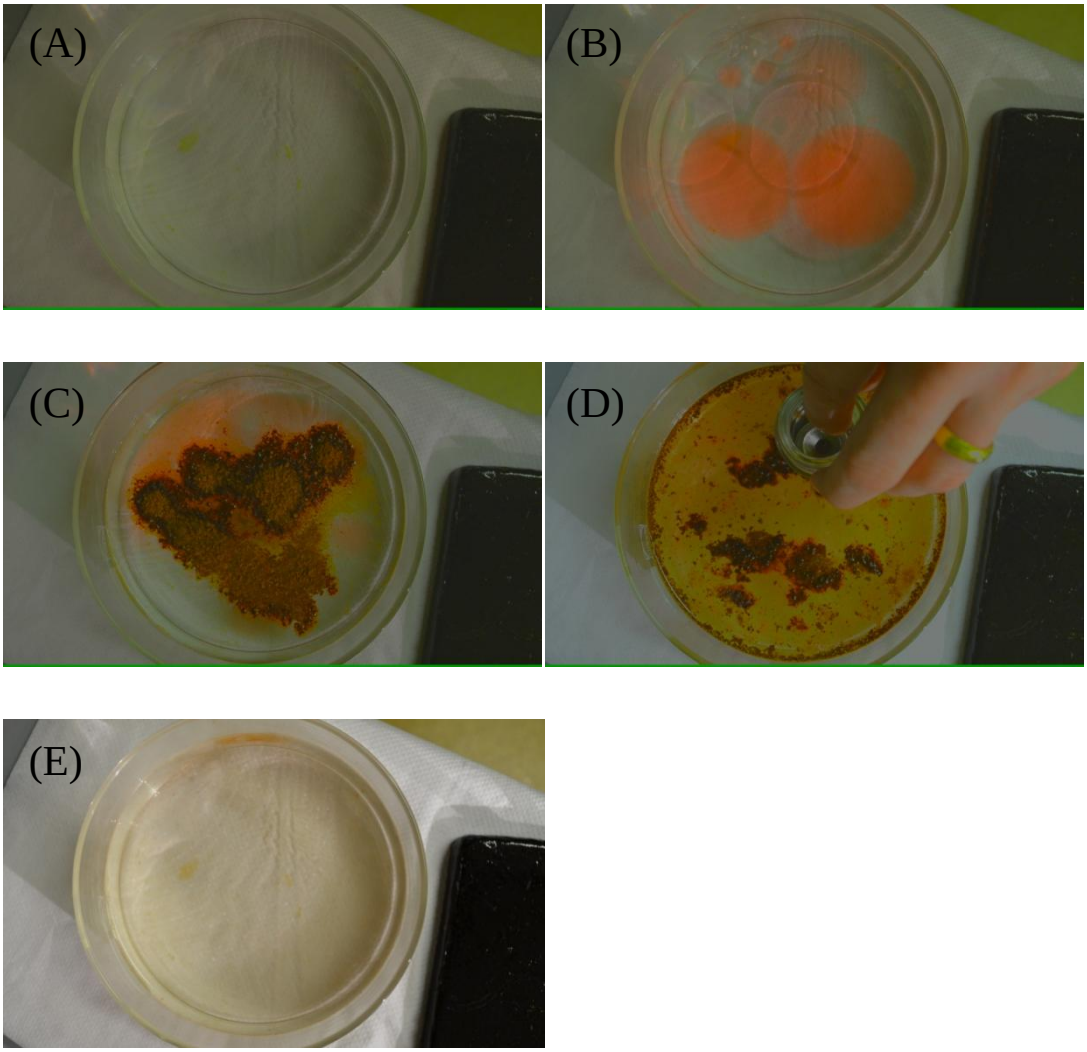

Figure 4. 14 Optical images demonstrating cleanup of an oil spill by magnetic porous particles (polystyrene = 5 wt% to monomer, toluene:DVB=5 $g.g^{-1}$ Fe_2O_3=2.5 wt%) (A) Water before oil addition. (B) Water after addition of 4 g olive oil labelled with a small amount of nile red fluorescent dye (C) Addition of 1 g particles to soak up oil (D) Removal of oil soaked particles by magnetic force (E) 'Clean' water after removal of oil soaked particles.

4.4. Conclusion

In conclusion, we have developed a method by which porous particles with controllable porosity can be synthesized using toluene and polystyrene as coporogens in the suspension polymerization of divinylbenzene. At high concentrations of both linear

polymer and toluene in the monomer feed particles with a very high surface area (>1500 $m^2.g^{-1}$) and with large pore radii can be obtained. The effect of the porogens on both the rate and extent of oil absorption has been measured and was shown to be greatest when pore volume and average pore radii were highest. It has been demonstrated that the absorption behaviour of these particles greatly exceeds the performance of standard absorbing materials and is reversible. Finally, we have demonstrated the use of these particles in oil recovery applications.

4.5. Experimental

4.5.1. Materials

DVB (80% technical grade), Mowiol 40-88 (88-90% hydrolysis M_w~205,000 $g.mol^{-1}$), $NaNO_2$ (>97%), and styrene (99%) was purchased from Sigma Aldrich and used as received. AIBN (97%) was purchased from Wako and used as received. SDS and Na_2SO_4 were purchased from Fisher and used as received. Poly(vinyl pyrrolidone) (PVP K90, M_w=360,000 $g.mol^{-1}$) was purchased from Fluka and used as received. Ferrofluid was purchased from e-magnets UK and used as received. All solvents were purchased from Fisher and used as received.

4.5.2. Equipment

Scanning electron microscopy was performed on a Zeiss supra 55VP FEGSEM. Particles were coated with a thin layer of platinum prior to scanning. For quantitative particle size, light microscopy images were taken of the particles which were then analysed by computer software program 'ImageJ' to give an average particle size and size distribution for each type of particle synthesised. A Micromeritics ASAP 2020 porosimeter was used to determine the surface area and pore size distribution of the

particles. The surface area was calculated by the software using BET theory and pore size distributions from the BJH method.

4.5.3. Synthesis

4.5.3.1. Synthesis of linear polystyrene by dispersion polymerization

Dispersion polymerisation of styrene was carried out in a 250 ml round bottom flask. 2 g of PVP K90 was added to the flask along with 70 ml ethanol. This was stirred for ten minutes to dissolve. 300 mg of AIBN in 30 ml of styrene was added to the reaction mixture. The reaction mixture was degassed with nitrogen for ten minutes. The solution was polymerised under constant stirring for 24 hours at 70°C. The PS obtained was centrifuged and washed with ethanol three times before the final supernatant was dried in a vacuum oven at 60°C for 24 hours. The PS synthesised was used later as a coporogen in the synthesis of porous p(DVB) spheres. A GPC of the PS gave the M_n and M_w to be 20500 and 42700 g.mol^{-1} respectively. M_w/M_n was 2.08.

4.5.3.2. Synthesis of porous DVB particles

Porous particles were made by suspension polymerisation of DVB in a double walled glass reactor equipped with overhead stirrer and nitrogen inlet according to the recipes shown in **Table 4. 2**. The discrete phase liquid was added to the reaction vessel containing 150 ml aqueous continuous phase. The lid was sealed and the heterogeneous reaction mixture was degassed in nitrogen for ten minutes whilst being stirred at 500 rpm to emulsify the discrete phase. The nitrogen source was then raised above the height of the solution and the stir rate was dropped to a desired number (typically 350 rpm). The water jacket was filled and the solution was polymerised at 70°C for 24 hours. The resulting microspheres from every suspension polymerisation were collected by Buchner filtration using a number 1 frit filter. The particles were washed twice with distilled water, followed by twice in ethanol and finally twice in acetone. The particles

were collected in a vial and left in an acetone solution overnight to completely remove any linear polymer. They were then filtered once again and dried for 24 hours in a vacuum oven at 60°C.

Table 4. 2 Suspension polymerisation reaction mixture

	Particle type	**1:1**	**1:3**	**1%**	**2%**	**5%**	**10%**
Discrete phase	DVB / g	3.50	1.75	1.15			
	Toluene / g	3.50	5.25	5.85			
	% PSt	5	5	1	2	5	10
	PSt / mg	175	88	12	23	58	115
Continuous phase	Distilled water / ml	150					
	SDS / g	0.0675					
	Na_2SO_4 / g	0.0340					
	$NaNO_2$ / g	0.0375					
	Mowiol 40-88 / g	3.00					

4.5.3.3. Magnetic particles

To modify the particles so that they can be easily removed from hair, they were made magnetic by the incorporation of iron particles into the structure of the microspheres. This was achieved by adding magnetic ‘ferrofluid’ to the discrete phase droplets of the suspension polymerisation.

Table 4. 3 –chemical quantities for magnetic particles by suspension polymerisation

Discrete phase	DVB / g	1.150
	Toluene / g	5.265
	% PS	5
	PSt / mg	58
	Ferrofluid / g	0.585
Continuous phase	Distilled water / ml	150
	SDS / g	0.0675
	Na_2SO_4 / g	0.0340
	$NaNO_2$ / g	0.0375
	Mowiol 40-88 / g	3.00

4.5.4. Oil absorption

4.5.4.1. Extent of oil absorption

The extent of oil absorption was determined gravimetrically using a modified version of a previously published procedure.[27] The particle to be tested were loaded into a syringe fitted with a non-absorbent cotton wool filter and weighed. The test liquid was added and the particles were immersed for 20 minutes before the liquid was removed by vacuum. The weight absorbed was determined from subtracting the final wet weight from the initial particle weight.

4.5.4.2. Rate of oil absorption

Using a light microscope and a camera, video footage of individual particles absorbing oil were obtained. A cover slip with a drop of oil on top was placed over the microscope lens. The particles were adhered to a glass microscope slide using adhesive tape. This was turned upside down and placed onto the stage above the cover slip. The lens was slowly raised up to meet the slide and a video was recorded as the oil displaced

the air inside the particles. The rate at which oil was imbibed was monitored by measuring the diameter of the shrinking air phase (**Figure 4. 15**).

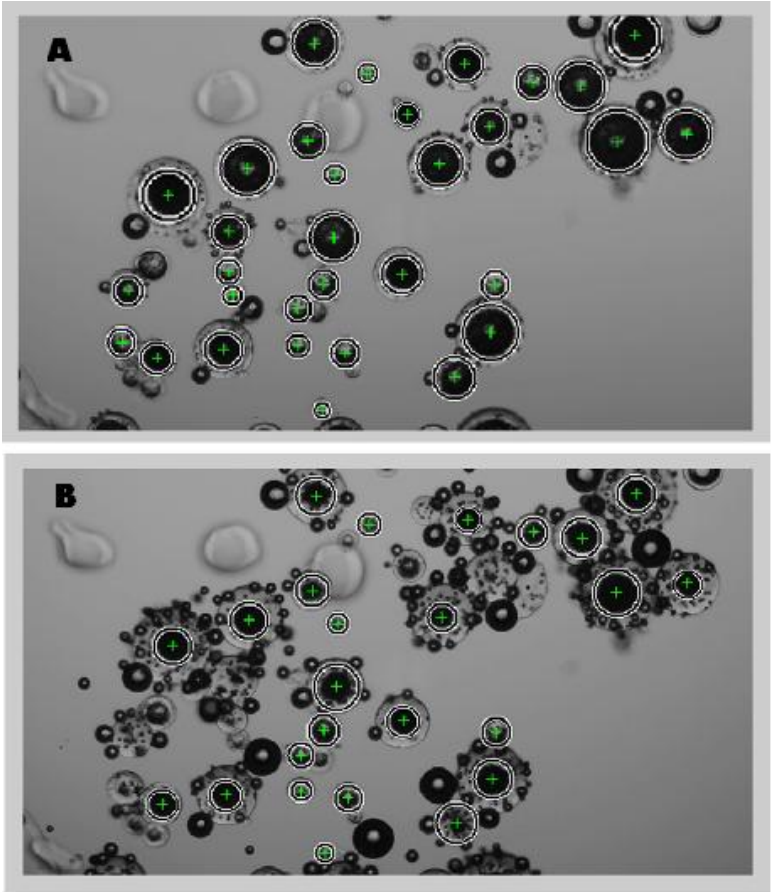

Figure 4. 15 Frame by frame monitoring of air displacement by oil. The decrease in the air void is monitored by measuring the diameter at constant time intervals.

4.6. References

1. Kujawinski, E. B. *et al.* Fate of Dispersants Associated with the Deepwater Horizon Oil Spill. *Environmental Science & Technology* **45**, 1298–1306 (2011).

2. Hargreaves, T. *Chemical Formulation*. (Royal Society of Chemistry: Cambridge, 2003).

3. Jager, J. de Self Pressurized Aerosol Spot Dry Cleaning Compositions US Patent 5269958. (1993).

4. Gleckler, G. C. & Goebel, J. C. Dry Shampoo Using Chitin Powder US Patent 4035267. (1976).

5. Wittwer, J. J. Dry Shampoo Composition US Patent 1208069. (1916).

6. Roulier, V., Mellul, M., Gabin, G. & Holz, J. Expanded Solid Composition Whose Matrix Comprises a Starch Based Cellular Network and Which Contains Expanded Thermoplastic Hollow Particles and its Uses in Topical Application. US Patent 5925380. (1996).

7. Choi, S.-W., Zhang, Y. & Xia, Y. Fabrication of Microbeads with a Controllable Hollow Interior and Porous Wall Using a Capillary Fluidic Device. *Advanced Functional Materials* **19**, 2943–2949 (2009).

8. Gokmen, M. T., Van Camp, W., Colver, P. J., Bon, S. a. F. & Du Prez, F. E. Fabrication of Porous "Clickable" Polymer Beads and Rods through Generation of High Internal Phase Emulsion (HIPE) Droplets in a Simple Microfluidic Device. *Macromolecules* **42**, 9289–9294 (2009).

9. Cheng, C. M., Micale, F. J., Vanderhoff, J. W. & El-Aasser, M. S. Synthesis and characterization of monodisperse porous polymer particles. *Journal of Polymer Science Part A: Polymer Chemistry* **30**, 235–244 (1992).

10. Gokmen, M. T. & Du Prez, F. E. Porous polymer particles—A comprehensive guide to synthesis, characterization, functionalization and applications. *Progress in Polymer Science* **37**, 365–405 (2012).

11. Li, W. & Stover, H. D. H. Porous Monodisperse Poly (divinylbenzene) Microspheres by Precipitation Polymerization. *Journal of Polymer Science Part A: Polymer Chemistry* **36**, 1543–1551 (1998).

12. Zhang, H. & Cooper, A. I. Synthesis of Monodisperse Emulsion-Templated Polymer Beads by Oil-in-Water-in-Oil (O / W / O) Sedimentation Polymerization. *Chemistry of Materials* **14**, 4017–4020 (2002).

13. Zhou, W.-Q., Gu, T.-Y., Su, Z.-G. & Ma, G.-H. Synthesis of macroporous poly(styrene-divinyl benzene) microspheres by surfactant reverse micelles swelling method. *Polymer* **48**, 1981–1988 (2007).

14. Zhou, W.-Q., Gu, T.-Y., Su, Z.-G. & Ma, G.-H. Synthesis of macroporous poly(glycidyl methacrylate) microspheres by surfactant reverse micelles swelling method. *European Polymer Journal* **43**, 4493–4502 (2007).

15. Svec, F. & Frechet, J. M. J. Kinetic Control of Pore Formation in Macroporous Polymers. Formation of "Molded" Porous Materials with High Flow Characteristics for Separations or Catalysis. *Chemistry of Materials* **7**, 707–715 (1995).

16. Sherrington, D. C. Preparation, structure and morphology of polymer supports. *Chemical Communications* 2275–2286 (1998).

17. Macintyre, F. S. & Sherrington, D. C. Control of Porous Morphology in Suspension Polymerized Poly(divinylbenzene) Resins Using Oligomeric Porogens. *Macromolecules* **37**, 7628–7636 (2004).

18. Garcia-Diego, C. & Cuellar, J. Synthesis of Macroporous Poly (styrene-co-divinylbenzene) Microparticles Using n-Heptane as the Porogen - Quantitative Effects of the DVB Concentration and the Monomeric Fraction on Their Structural Characteristics. *Industrial & Engineering Chemistry Research* **44**, 8237–8247 (2005).

19. Alexopoulos, A. H. & Kiparissides, C. On the prediction of internal particle morphology in suspension polymerization of vinyl chloride. Part I: *Chemical Engineering Science* **62**, 3970–3983 (2007).

20. Horak, D., Labsky, J., Pilar, J., Bleha, M. & Pelzbauer, Z. The effect of polymeric porogen on the properties of macroporous poly (glycidyl methacrylate-co-ethylene dimethacrylate). *Polymer* **34**, 3481–3489 (1993).

21. Hao, D.-X. *et al.* Porogen effects in synthesis of uniform micrometer-sized poly(divinylbenzene) microspheres with high surface areas. *Journal of Colloid and Interface Science* **323**, 52–9 (2008).

22. Bigan, M. & Blondeau, D. Optimization of a polymeric HPLC phase - poly (glycidyl Influence of the polymerization conditions on the pore structure of macroporous beads. *Reactive and Functional Polymers* **56**, 123–136 (2003).

23. Kanamori, K., Hasegawa, J., Nakanishi, K. & Hanada, T. Facile Synthesis of Macroporous Cross-Linked Methacrylate Gels by Atom Transfer Radical Polymerization. *Macromolecules* **41**, 7186–7193 (2008).

24. Davankov, V. a. & Tsyurupa, M. P. Structure and properties of hypercrosslinked polystyrene—the first representative of a new class of polymer networks. *Reactive Polymers* **13**, 27–42 (1990).

25. Veverka, P. & Jeřábek, K. Influence of hypercrosslinking on adsorption and absorption on or in styrenic polymers. *Reactive and Functional Polymers* **59**, 71–79 (2004).

26. Ahn, J.-H. *et al.* Rapid Generation and Control of Microporosity, Bimodal Pore Size Distribution, and Surface Area in Davankov-Type Hyper-Cross-Linked Resins. *Macromolecules* **39**, 627–632 (2006).

27. Fontanals, N., Manesiotis, P., Sherrington, D. C. & Cormack, P. a. G. Synthesis of Spherical Ultra-High-Surface-Area Monodisperse Amphipathic Polymer Sponges in the Low-Micrometer Size Range. *Advanced Materials* **20**, 1298–1302 (2008).

28. Gennes, P.-G. de, Brochard-Wyart, F. & Quere, D. *Capillarity and Wetting Phenomenom - Droplets, Bubbles, Pearls, Waves*. (Springer: 2004).

29. Washburn, E. W. The Dynamics of Capillary Flow. *The Physical Review* **17**, 273–283 (1921).

30. Navas, J., Alcántara, R., Fernández-Lorenzo, C. & Martín-Calleja, J. Pore Characterization Methodology by Means of Capillary Sorption Tests. *Transport in Porous Media* **86**, 333–351 (2010).

31. Benltoufa, S., Fayala, F. & Bennasrallah, S. Capillary Rise in Macro and Micro Pores of Jersey Knitting Structure. *Journal of Engineered Fibers and Fabrics* **3**, 47–54 (2008).

32. Dullien, F. Rate of capillary rise in porous media with nonuniform pores. *Journal of Colloid and Interface Science* **60**, 497–506 (1977).

Chapter 5: A computational toolbox for examining the efficiency of anisotropic particles as surfactants*

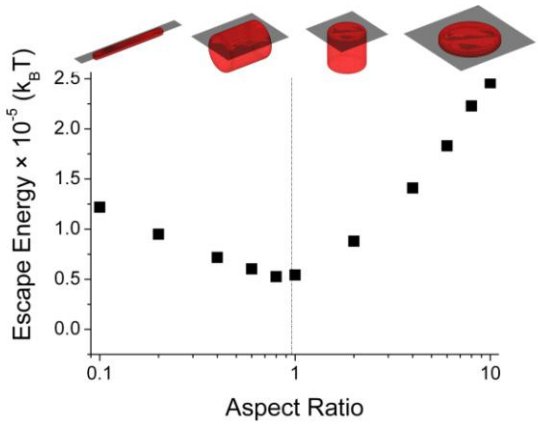

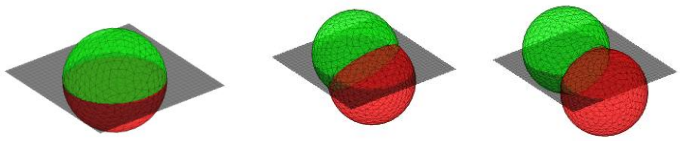

5.1. Abstract

We present a user-friendly computational model that can be used to determine equilibrium orientations of colloidal particles at liquid-liquid interfaces, a phenomenon known as Pickering stabilization which allows for particle stabilized emulsion droplets. Particle morphologies to be tested can be selected by the user to produce any superellipsoidal structure (rods, spheres, cubes *etc.*) or can be imported from CAD software. The software determines the free energy profile of particle adsorption at liquid-liquid interfaces using a triangular tessellation scheme. We demonstrate the use of the program for a variety of anisotropic particles and demonstrate its ability to predict and explain experimental observations of particle behaviour at interfaces.

---

* Parts of this chapter have been submitted for publication elsewhere: Morgan, A. R.,Ballard, N., Rochford, L. A., Nurembetov, G., Skelhon, T. S., Bon, S. A. F.; Understanding the Multiple Orientations of Isolated Superellipsoidal Hematite Particles at the Oil-Water Interface *Under Review*

5.2. Introduction

Surfactants are omnipresent in home and personal care products where they perform multiple roles, primarily in emulsifying and cleaning. Their use has been documented for centuries, but in terms of chemical composition there have not been any major changes during that period. More recently, especially since the development of polymer chemistry, tailored surfactants with variable hydrophilic to hydrophobic blocks have allowed for unprecedented control over the emulsifying ability of molecular compounds. In tandem with this development there has been a great deal of research performed in the area of surfactants not stabilized on a molecular level but rather with colloidal particles.

The ability of particles to adsorb onto biphasic interfaces and stabilize emulsion droplets has been studied in great detail since the inception of the topic over 100 years ago by Ramsden and Pickering.[1,2] They found, quite independently, that inorganic particulates were capable of emulsifying oils in the absence of any molecular surfactant and noted that particle stabilized emulsions were often superior in terms of resistance to de-emulsification to their soluble counterparts. The first quantitative theoretical description of this effect was given by Pieranski for the case of a sphere of uniform surface tension in the absence of any imposed external force fields.[3] He demonstrated that the main cause of particle adhesion to the interface was due to energy minimization as a result of removal of an area of liquid-liquid interface (see **Figure 5. 1**) and that as a result of this the energy to remove a particle from the interface is typically on the order of many thousands of k_BT rendering particle adhesion effectively irreversible.

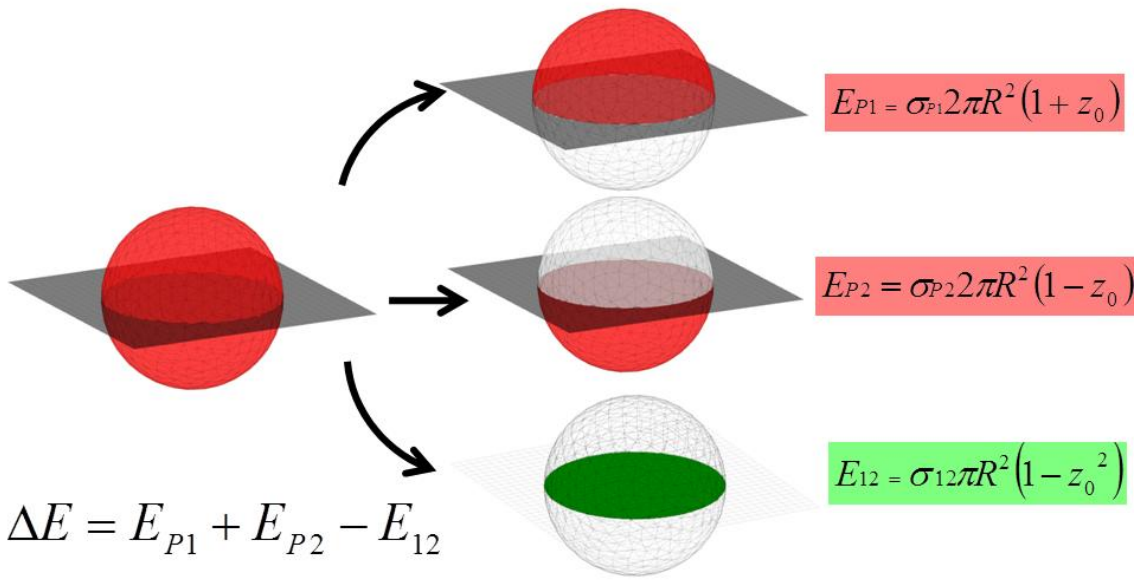

Figure 5. 1 Free energy change upon adsorption of colloidal particle of radius, *R*, at the liquid-liquid interface. The interface energy, *E*, depends on the particle position with respect to the interface given by z_0 (where z_0=1 it is immersed in phase 1 and where z_0=-1 it is immersed in phase 2) and the various interfacial tension, σ, values.

This knowledge has been exploited by many academic and industrial researchers in the synthesis of new materials with interesting physical properties. In the field of heterogeneous polymer synthesis for example, our group and others have shown that clay and silica nanoparticles can be used in place of the more traditional surfactants in emulsion and miniemulsion polymerizations to produce composite materials that exhibit vastly improved adhesive properties.[4–7] Our group was the first to show that colloidal particles can been used to stabilize high internal phase emulsions (HIPEs). We subsequently polymerized the continuous phase to form a porous polymeric monolith and demonstrated the irreversible nature of particle adhesion.[8] It has since been shown that these materials can be synthesized with very low solid content and that the colloidal particles can reinforce the network offering enhanced mechanical resistance.[9–13] More recently it has been shown that colloidal particles are capable of stabilizing both aqueous and oil based foams for incredibly long periods of time (see **Figure 5. 2**).[14–16]

Figure 5. 2 *(Left)* Free-flowing powder passing through a glass funnel, made by aerating 5 g of silica particles possessing 20% SiOH and 95 g of water (φ_w =0.056). *(Right)* Foam extruded through a serrated metal nozzle prepared by aerating 5 g of silica particles possessing 32% SiOH and 95 g of water (φ_w =0.056). Scale bars=1 cm.[17]

One important factor in the stability of the emulsions and foam materials listed above is the particle morphology and surface chemistry which govern the overall particle wettability and the strength with which it is adhered to the interface.[18] Whilst spheres are the most studied particulate emulsifier there have also been reports of discs,[19,20] cylinders,[21,22] ellipsoids,[23] cubes,[24] dumbbells[25] and hemispheres[26] amongst a multitude of others being used as emulsifying agents. In addition new synthetic routes to complex nanoparticles have allowed us to explore the use of chemically anisotropic 'Janus' particles as surfactants. For example, Weitz *et al.* used colloidal dumbbells synthesized through a seeded emulsion polymerization to stabilize hydrocarbon in water emulsions and illustrated the ability of these particles to outperform their spherical particles of the same surface groups.[25] Muller *et al.* synthesized Janus cylinders by self assembly of block copolymers and demonstrated that they are capable of reducing the interfacial tension of liquid-liquid interfaces more than the homogeneous analogues.[27] Okubo and coworkers demonstrated 'mushroom-like' particles which were amphiphilic

were capable of stabilizing octanol in water emulsions and by incorporating functional polymers they were able control the stability of the emulsion by application of an external stimulus (see **Figure 5. 3**).[28]

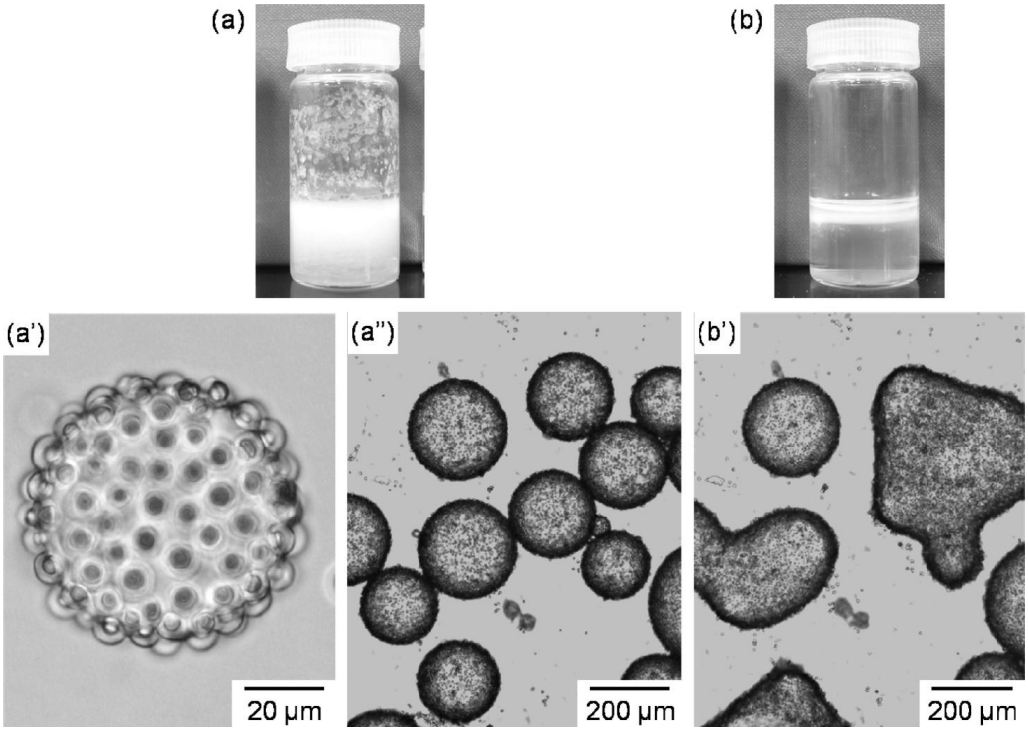

Figure 5. 3 (a, b) Photographs of 1-octanol/water mixture after vigorous stirring in the presence of PMMA/P(S-BIEM)-g-PDM Janus particles and (a', a", b') optical micrographs of 1-octanol-in-water emulsion droplets stabilized by the Janus particles at pH 7.2 at (a, a', a") 25°C and (b, b') after rising to 60°C. Both micrographs of (a") and (b') are on the same visual field.[29]

The theoretical description of how such complicated nanoparticles orientate at liquid-liquid interfaces is of the upmost importance and governs the extent to which they are adsorbed, the type of emulsion and ultimately their ability to stabilize an emulsion. While the theoretical case for a sphere has been extensively researched[30–32] more complicated shape and chemically anisotropic particles have largely been ignored due to the extensive derivations that are required for analytical solutions as the particle shape deviates from a sphere. The case for a chemically anisotropic sphere has been studied by several groups who have shown that amphiphilic spheres orientate to minimize free energy and can potentially give thermodynamically stable emulsion systems.[33–35] Cubic particles have been shown to sit in one of many orientations at the

liquid interfaces due to the existence of multiple energy minima in the free energy profile which greatly effects emulsion stability.[36] Ellipsoidal and cylindrical particles have been shown to orientate according to capillary interactions between particles at interfaces and their orientation is guided by such adhesive bonds.[23,37,38] Recently the effects of both chemical and shape anisotropy has been observed in simulations on amphiphilic cylinders and dumbbells with the orientation being dictated by the balance of shape and chemical nature of the particle surfaces.[39] We present here a program that allows users to predict surface activity of particles of any shape or chemistry in a simple user-friendly manner. The calculation is based on a triangular tessellation scheme originally introduced by Dijkstra *et al.*[40] which allows for the free energy profile of a particle at an interface to be determined from which equilibrium orientations can be predicted. We show the application of the program to a broad spectrum of particle morphologies in the hope that it will aid in the synthesis by design of colloidal surfactants.

5.3. Model Development

The free energy upon forming an emulsion (ΔG_{em}) using particulate surfactants can be calculated using **Equation 5. 1**.[30,33]

$$\Delta G_{em} = n_d\{A_{ow}\sigma_{ow} + n_p(\Delta G_{ad} - T\Delta S_{ad})\}$$ **Equation 5. 1**

Where n_d is the number of droplets, A_{ow} is the area of the oil water interface, σ_{ow} is the oil water interfacial tension n_p is the number of particles stabilizing the droplet ΔG_{ad} is the free energy change upon particle adsorption and ΔS_{ad} is the entropy change upon particle adsorption. If the entropy change, which contributes only a small term, and effects due to surface curvature and particle interactions are ignored then the free energy change per unit area ΔG_u can be expressed according to **Equation 5. 2**.

$$\Delta G_u = A_{ow}^u \sigma_{ow} + N_p^u \Delta G_{ad}$$ **Equation 5. 2**

Where $A_{ow}{}^u$ is the area of oil water interface exposed per unit area and $N_p{}^u$ is the number of particles per unit area. This equation demonstrates that the ability of a particle to stabilize and emulsion is a direct function of the adsorption enthalpy and the maximum packing density of the particles. We set out herein a computational model that is capable of calculating the ΔG_{ad} for highly anisotropic particle morphologies using a triangular tessellation scheme for describing the particle.

5.3.1. Triangular tessellation model

The ground-breaking work of Pieranski demonstrated that the surface activity of spherical colloidal particles could be explained using surface tension arguments. In essence he described the adsorption free energy (ΔG_{ad}) of a colloidal particle being equal to the sum of the three areas shown in **Figure 5. 1**. While the case for a sphere can be easily solved, upon introducing anisotropy there is often no analytical solution but the general solution (**Equation 5. 3**) still holds.

$$\Delta G_{ad} = A_{P1}\sigma_{P1} + A_{P2}\sigma_{P2} - A_{12}\sigma_{12}$$ **Equation 5. 3**

Where A corresponds to area and σ is the interfacial tension and the subscripts correspond to the particle(P) and phases 1 and 2. Hence for a given particle position the free energy at this orientation can be calculated if the corresponding areas and interfacial tension values are known. In order to calculate the surface areas of the particle we use a triangular tessellation scheme in which the particle surface is divided into a series of tessellating of triangles define the surface.

5.3.2. Defining particle shape

Particles can be defined either as a single superellipsoid or as a composite of multiple superellipsoidal shapes, termed here shape elements.

5.3.2.1. Single shape elements

The particles are created from a series of points which all fit the unique expression for a superellipsoid (see **Equation 5. 4**)

Equation 5. 4

$$\left(\frac{x}{r_x}^{2/n_2} + \frac{y}{r_y}^{2/n_2}\right)^{n_2/n_1} + \frac{z}{r_z}^{2/n_1} = 1$$

Where x, y and z denote the coordinates of the point r_x, r_y, and r_z are the particles x, y and z radii and n_1 and n_2 acts as the "squareness" parameter in the z axis and the squareness parameter in the x-y plane respectively with $0<n_1,n_2<\infty$.

From the input parameters of r_x, r_y, r_z, n_1, n_2 and the number of points to be created the particle shape is computed. The point coordinates are obtained by first generating an evenly distributed set of points around a sphere with $r_x = r_y = r_z = 1$ using the golden section spiral method.

The x, y, z coordinates calculated are converted into spherical coordinates and the x, y, z values for the superellipsoid are calculated from **Equation 5. 5**.

Equation 5. 5

$$x = r_x \cos^{n_1}\theta \cos^{n_2}\varphi$$

$$y = r_y \cos^{n_1}\theta \sin^{n_2}\varphi$$

$$z = r_z \sin^{n_1}\theta$$

The values of θ and φ are taken from the sphere points initially obtained and r_x, r_y, r_z, n_1, n_2 are from the user inputted values. This has the effect of projecting the sphere points onto the corresponding superellipsoid and generates a set of data

points from which the surface can be determined (see **Figure 5. 4**).

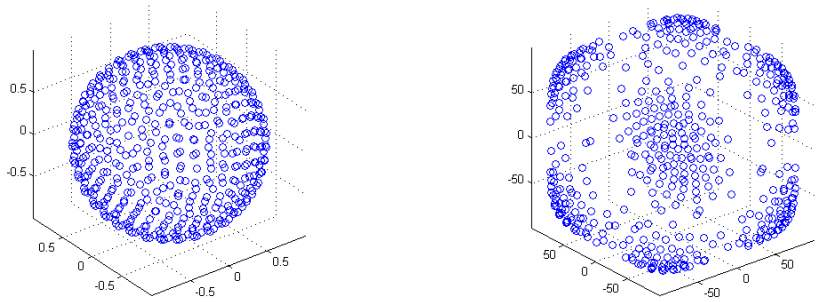

Figure 5. 4 Evenly distributed points on a sphere *(left)* and the same points projected onto a superellipsoid *(right)* with x=y=z=100, n_1=0.4, n_2=0.4.

The surface of the particle is obtained from this set of data points by taking the convex hull of the data set resulting in list *m* x 3 triangulation table where *m* is the number of triangles containing and the three columns correspond to the vertices of the triangle that are taken from the data point list (see **Figure 5. 5**).

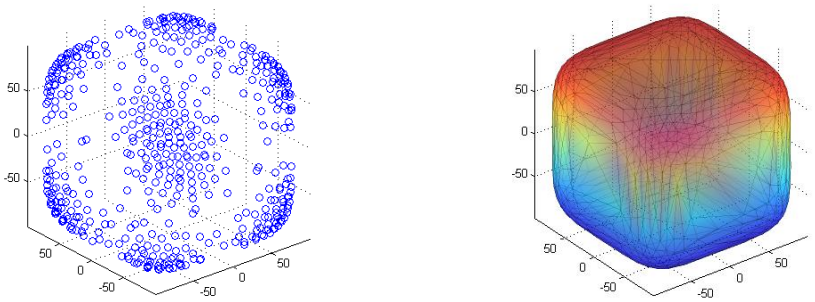

Figure 5. 5 Set of data points *(left)* and the surface created by taking the convex hull *(right)*

5.3.2.2. Multiple shape elements

Particles with anisotropic morphologies such as dumbbells can be created by merging one or more shape elements together. In this case the series of points for each element is determined as above and the elements are also shifted somewhat in the *x*, *y* or *z* direction as directed by the user. Points which overlap with other shape elements are removed from the point data. This is determined by the inequality in

Equation 5. 6.

$$\left(\frac{x_{test}}{r_x}^{2/n_2} + \frac{y_{test}}{r_y}^{2/n_2}\right)^{n_2/n_1} + \frac{z_{test}}{r_z}^{2/n_1} < 1$$

Equation 5. 6

Where the point to be destined has Cartesian coordinates (x_{test}, y_{test}, z_{test}) and the shape element is given by the parameters r_x, r_y, and r_z (the shape elements x, y, and z radii respectively), n_1 and n_2 act as the "squareness" parameters in the z axis and the x-y plane respectively, with $0<n_1,n_2<\infty$.

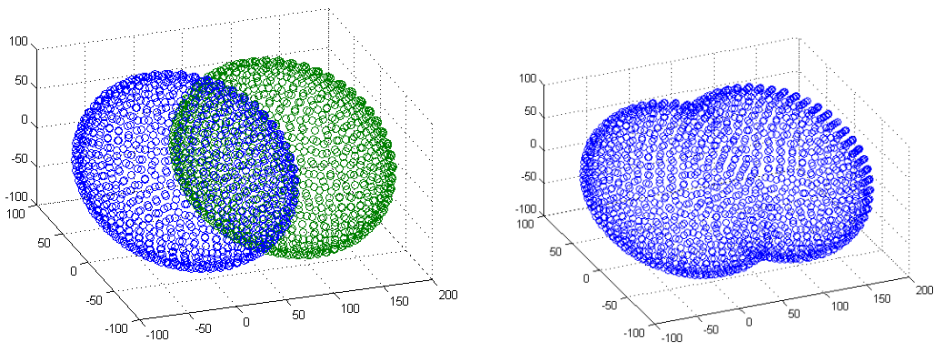

Figure 5. 6 Set of overlapping data points *(left)* and the same particle with overlapping points removed *(right).*

From this set of points the alpha hull is found. In order to accurately achieve this it is often necessary to subdivide the triangular tessellation to give a shorter distance between points. The alpha hull is used because such composite particles with multiple shape elements are often not concave. The alpha hull uses a resolution parameter to determine maximum triangle size and generates the triangular tessellation (see **Figure 5. 7**).

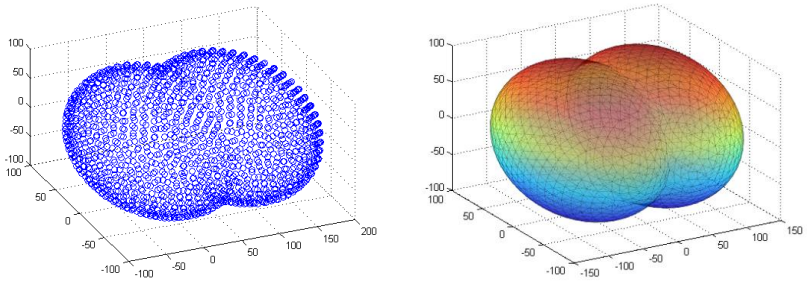

Figure 5. 7 Set of points *(left)* and the triangular tessellation created by taking the alpha hull *(right).*

5.3.2.3. Importing from .stl files

It is also possible to use a set of predefined points and its triangulation matrix in the form of Standard Tessellation Language (.stl) files. These files can be created in standard CAD programs and allow for particularly complicated particles (see **Figure 5. 8**) to be created without the need for specific shape parameters being called for.

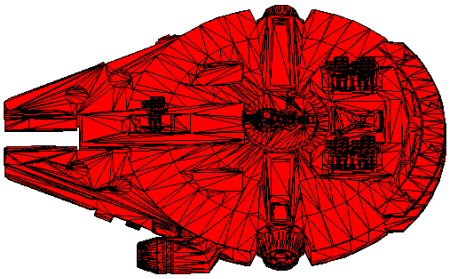

Figure 5. 8 Triangular tessellation model of highly anisotropic particle produced from .stl format.

5.3.3. Defining particle surfaces

In order to introduce chemical anisotropy into the system the model must have a way of determining the interfacial area of areas of differing chemical functionality. This is achieved by simply designating triangles that lie within such areas as of a different phase (see **Figure 5. 9**).

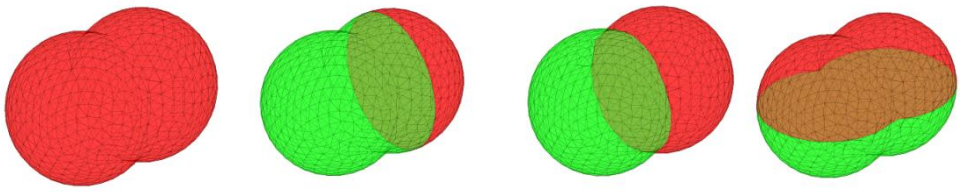

Figure 5. 9 Series of particles with identical shape but varying surface functionality by assigning triangles to different phases.

5.3.4. Computing the free energy profile

5.3.4.1. Defining orientations and z position

The free energy profile for a given particle morphology is determined iteratively by scanning through the user defined rotations and translations. In order to do this we need a consistent model to give the location of the particle. From the initial set of points centred around the origin a minimum bounding sphere with centre at the origin which contains all the points is determined (see **Figure 5. 10**).

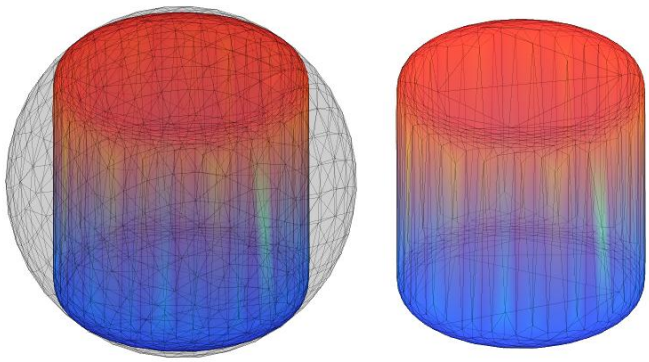

Figure 5. 10 Example of a minimum bounding sphere for a cylindrical particle that is used to calculate rotations and translations the z axis.

The height of the particle with respect to the z coordinate is given in terms of a vertical coordinate ž given by **Equation 5. 7**.

$$\check{z} = {}^{z}/_{r_{bounding}}$$ **Equation 5. 7**

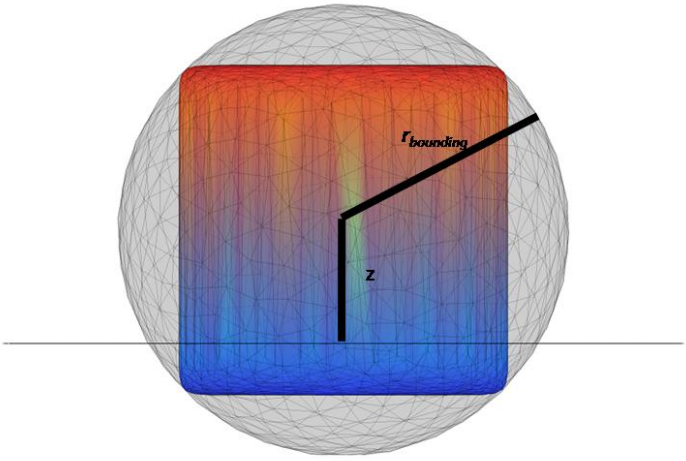

Figure 5. 11 Schematic demonstrating the how the location of the particle with respect to the z axis is defined

The particle can also be rotated about the y axis (θ_1) or the x axis (θ_2) to give multiple particle orientations. The program gets the set of points defined by (x ,y ,z) for a given rotation from the transformation matrix in **Equation 5. 8**.

$$\left(\begin{bmatrix} cos\theta_2 & 0 & sin\theta_2 \\ 0 & 1 & 0 \\ -sin\theta_2 & 0 & cos\theta_2 \end{bmatrix} \times \begin{bmatrix} 1 & 0 & 0 \\ 0 & cos\theta_1 & -sin\theta_1 \\ 0 & sin\theta_1 & cos\theta_1 \end{bmatrix} \times \begin{bmatrix} x \\ y \\ z \end{bmatrix}\right) + \begin{bmatrix} 0 \\ 0 \\ z_c \end{bmatrix} = \begin{bmatrix} \boldsymbol{x} \\ \boldsymbol{y} \\ \boldsymbol{z} \end{bmatrix}$$

Equation 5. 8

The triangulation matrix does not change since the position of the points with respect to each other does not change and therefore the tessellation pattern can remain the same.

5.3.4.2. Determining free energy at a given location

The free energy of the particle can be calculated using interfacial tension arguments according to **Equation 5. 9**.

$$\Delta G_{ad} = \sum_P A_{P1}\sigma_{P1} + \sum_P A_{P2}\sigma_{P2} - A_{12}\sigma_{12}$$

Equation 5. 9

After defining a particle position as described in the above section the program calculates the free energy at this position. In order to calculate the areas above, below and at the interface, A_{P1}, A_{P2} and A_{12} respectively the program needs to determine the surface area of each triangle and its location with respect to the interface. For simplicity the interface is always designated to lie in the z=0 plane. The surface area of the triangle is calculated using a stabilized version of Heron's formula. The length of the sides are ranked in order of size such that $a \geq b \geq c$ and the area A is given by **Equation 5. 10**.

$$A = \frac{1}{4}\sqrt{a + (b + c)\big(c - (a - b)\big)\big(c + (a - b)\big)(a + (b - c))}$$ **Equation 5. 10**

The program determines the location of the particle with respect to the interface by the sign of the z component of the three vertices and adds the area to either A_{P1} or A_{P2} accordingly. Where the signs are mixed and the triangle intersects the interface it is subdivided into three smaller triangles and the corresponding areas are added to A_{P1} or A_{P2} as usual (see **Figure 5. 12**).

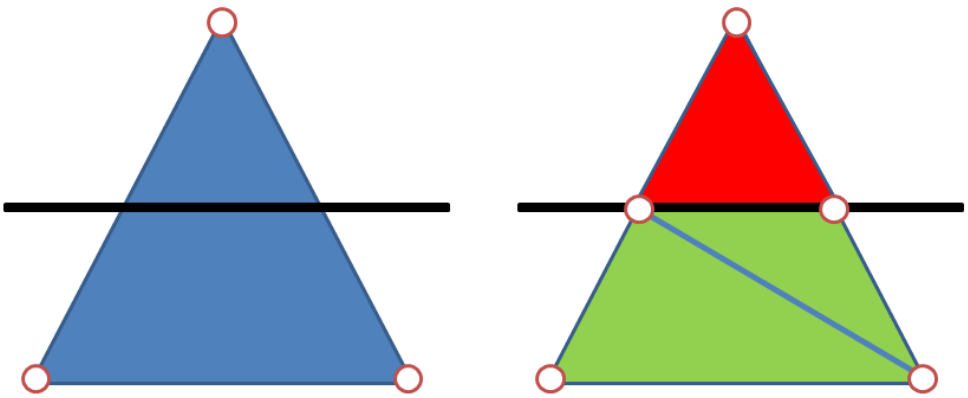

Figure 5. 12 Schematic demonstrating subdividing of triangles that intersect the interface.

The area of the interface, A_{12}, is calculated by using all the points that intersect the interface and the edges that connect them as constraints in a Delaunay

triangulation of the interface points. This allows the area of shapes that can be discontinuous at the interface such as dumbbells to be accurately calculated. A_{12} is subsequently found by summing the constituent triangles of the Delaunay triangulation. The free energy is thus simply calculated by multiplying the calculated areas by the inputted interfacial tension values.

5.3.4.3. The free energy profile

To obtain the free energy profile of adsorption for a variety of orientations the point matrix is multiplied by a rotation matrix and translated in the z-axis as required to give a new set of points with the same triangular tessellation pattern. The iterative process of calculating the areas A_{P1}, A_{P2} and A_{12} explained above is simply repeated for each set of points generated by the rotation matrix. The motion in the z axis and rotations are set depending on particle morphology. Where multiple rotations are unnecessary (i.e. the case of spheres) these can be left out.

5.3.5. Adsorption trajectories

5.3.5.1. The free energy landscape and its vector field

The process of calculating a free energy profile has been explained above but an important aspect of colloidal stabilization of interfaces is centred around the dynamics of the process. Since the adsorption energy is often so high that adsorption is rendered irreversible, kinetic minima can be observed in both experimental and theoretical systems. It is possible to estimate adsorption trajectories by looking at the change in free energy upon altering the particle orientation. Since the above methods give either a 1d (only z motion no rotations), 2d (z motion and 1 rotation) or 3d (z motion and 2 rotations) the model deals with each case slightly differently.

The 1d case is only interesting for a sphere and in this case adsorption trajectories do not provide extra detail that cannot be gained from simple observation of the ž vs. E graph and therefore they are not considered here. For a 2d case a 3d graph of $\check{z}$ vs. θ vs. E the gradient of the free energy can be given by **Equation 5. 11**.

Equation 5. 11

$$-\nabla E\,(\theta, z) = -\left(\frac{dE}{d\theta_1}\boldsymbol{i} + \frac{dE}{dz}\boldsymbol{j}\right)$$

Using this relationship the directional motion from a given point, P^0 ($\check{z}^0$, θ^0), can be found. The particle can be initiated from $\check{z}$ = ± 1 and follows the path of lowest energy until the gradient is negligible (see **Figure 5. 13**).

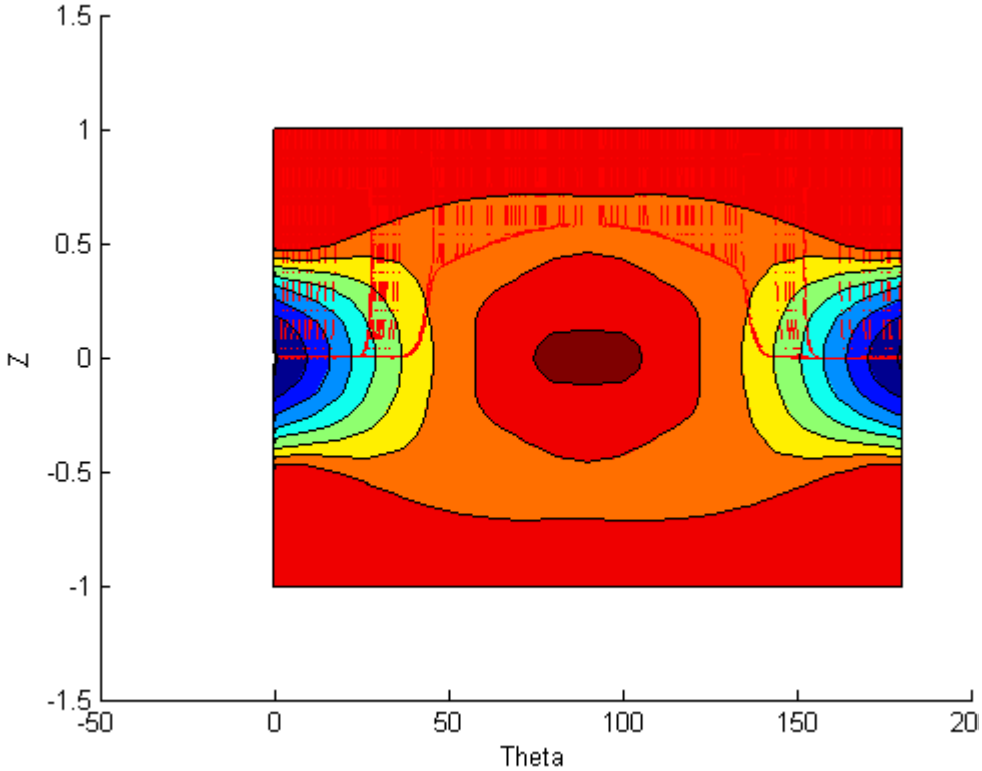

Figure 5. 13 Adsorption profile for 2 dimensional case illustrating the pathway towards energy minima. The contour plot reflects the relative energy levels at given orientations.

For the case the 3d case the gradient of the free energy is given by **Equation**

5. 12.

Equation 5. 12

$$-\nabla E\,(\theta_1, \theta_2, ž) = -\left(\frac{dE}{d\theta_1}\boldsymbol{i} + \frac{dE}{d\theta_2}\boldsymbol{j} + \frac{dE}{dž}\boldsymbol{k}\right)$$

Trajectories that follow the path of the steepest descent in terms of energy from an initial point $P^0(\theta_1^0, \theta_2^0, ž^0)$ are calculated by interpolating between the values of the gradient of the free energy profile and using the constituent $d\theta_1$, $d\theta_2$ and $dž$ values to determine the direction of particle motion. The particle can be initiated from $ž = \pm 1$ and follows the path of lowest energy until the gradient is negligible.

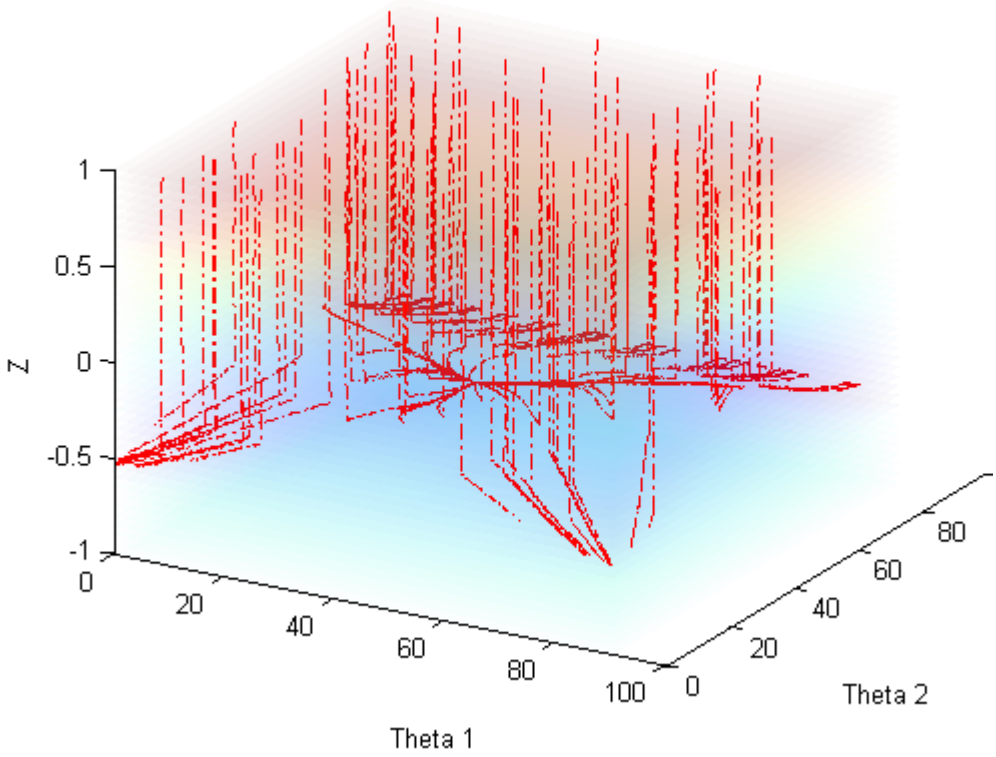

Figure 5. 14 Adsorption profile for 3 dimensional case illustrating the pathway towards minima in the free energy profile. The colour represents relative energy levels.

5.3.6. Adsorption model assumptions

It should be noted that our method falls in line with Pieranski's model,[3] and

does not take into account several factors which may contribute to the overall adsorption energy. We ignore effects due to gravity (such as interfacial deformation) because of the low energy involved compared to the adsorption energy in the low Bond number regime. The effect of capillarity on deforming the interface is also ignored. This assumption is somewhat validated by the negligible interfacial distortion observed in experimental measurements of colloidal particles in the region of 100 nm and above and the fact that we deal with isolated particles ruling out any capillary bridging. We also ignore the effects of line tension since the magnitude of this force is negligible for smooth particles with a characteristic size exceeding the order of 10 nm.

5.4. Results and Discussion

5.4.1. Effect of particle shape on adhesion energy and particle orientation

The effect of particle shape on the adhesion energy at liquid-liquid interfaces was determined for a series of ellipsoidal and discoid particles with constant volume by varying the particle aspect ratio. The escape energy for the series of polystyrene ellipsoidal particles at a hexadecane water interface with varying aspect ratio is shown in **Figure 5. 15** (σ_{P1}=32 mN.m^{-1}, σ_{P2}=14 mN.m^{-1} and σ_{12}=53 mN.m^{-1}). It can clearly be seen that upon increasing the aspect ratio, the energy required to escape from the interface, determined by subtracting the energy minima from the free energy of the particle immersed in the hexadecane phase is increased. This can be explained by the huge increase in the interfacial area of the 'removed' liquid interface, which contributes to the negative energy term in **Equation 5. 9**. Similarly, upon decreasing the aspect

ratio and forming a prolate type spheroid the particle orientates itself to maximize the negative energy term.

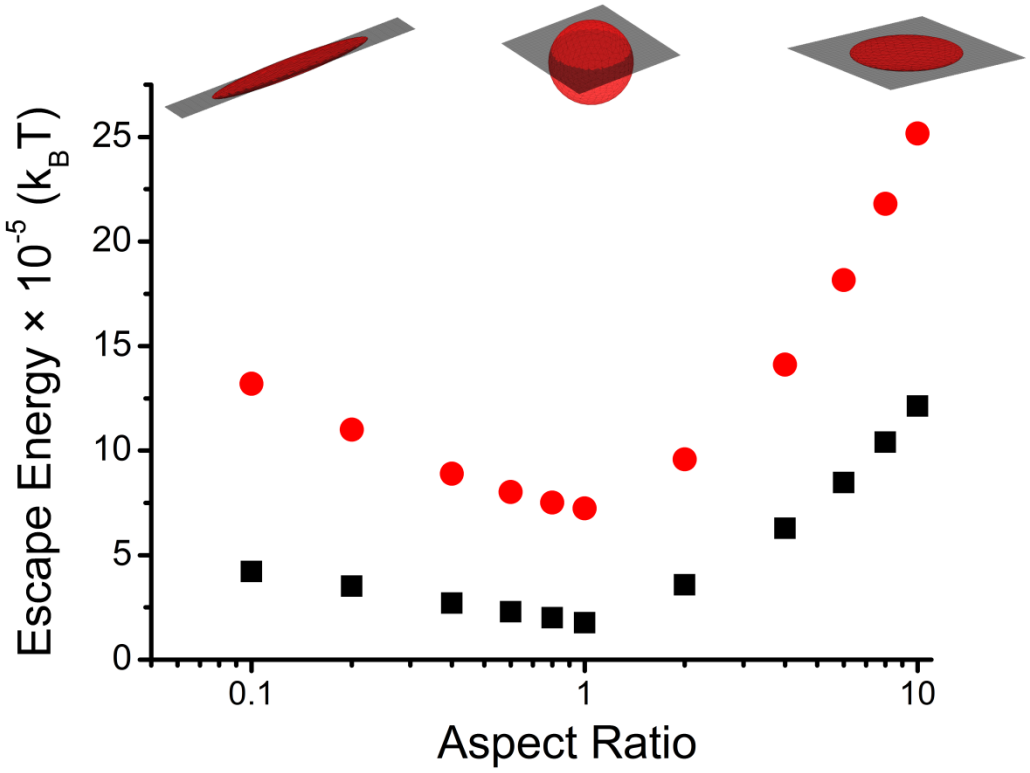

Figure 5. 15 Escape energy for polystyrene ellipsoids of varying aspect ratio but with constant particle volume ($V=4/3\pi(100)^3$ nm^3) into the n-hexadecane phase (■) and the aqueous phase(●). The upper images show the particles position at the liquid liquid interface at the most extreme aspect ratios.

A similar trend in adsorption free energy is seen for discoidal particles (see **Figure 5. 16**). In this case a sharp transition between lying upright and lying flat with respect to the interface can be observed upon decreasing the aspect ratio below 1. The net effect of particle shape can be generalized by saying that the particle will orientate itself to maximize area of the liquid-liquid interface taken up by the particle whilst minimizing unfavourable interactions with either liquid phase.

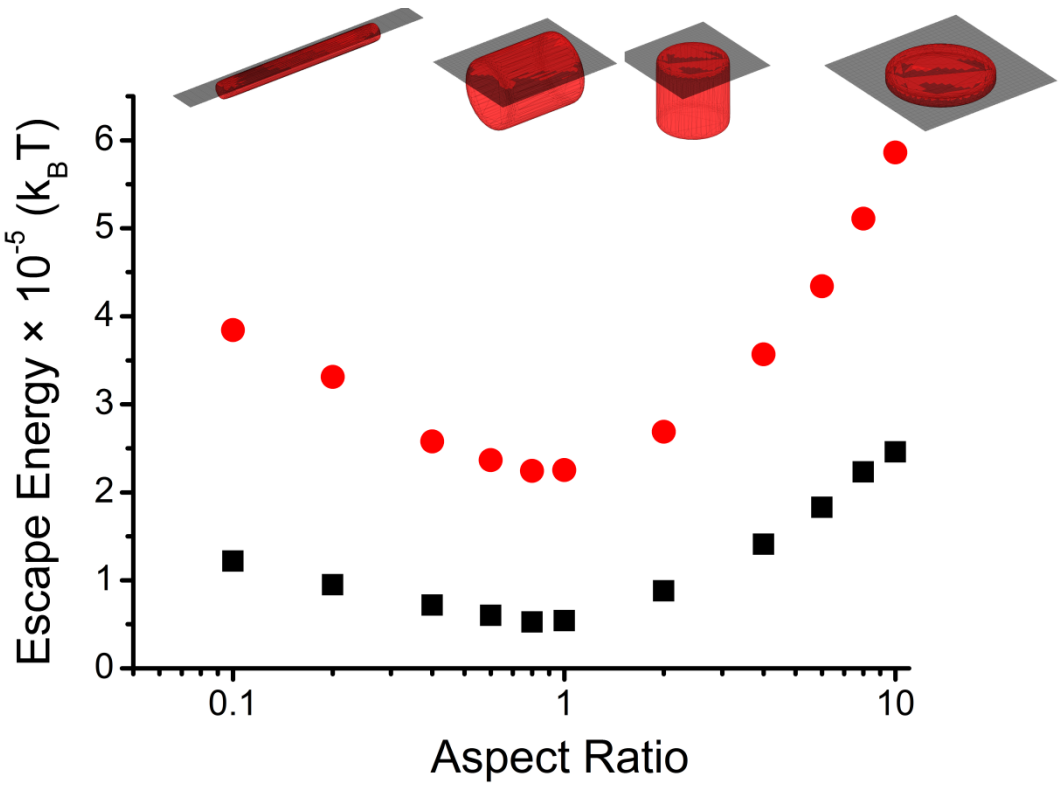

Figure 5. 16 Escape energy for polystyrene discoids of varying aspect ratio but with constant particle volume ($V=\pi(100)^2(10)$ nm^3) into the n-hexadecane phase (■) and the aqueous phase(●). The upper images show the particles position at the liquid liquid interface at the most extreme aspect ratios.

5.4.2. Synergistic and antagonistic effects of shape and chemical anisotropy

It has been shown above that by tuning the aspect ratio of colloidal particles their ability to adhere to liquid-liquid interfaces is greatly altered. The effect of adding chemical anisotropy to this and making analogues of molecular surfactants in which emulsion stability is imparted through differences in wettability throughout the molecular structure has the potential to greatly increase the efficiency of colloidal surfactants.

We simulated the effect of adding a hydrophilic face of 2-hydroxyethyl methacrylate (HEMA) to an ellipsoidal polystyrene particle with aspect ratio 0.4 (r_x=r_y=74 nm, r_z=184 nm). We achieved this by cutting along a plane in either the xy or xz axis at a designated value in the plane (v_{plane}) such that $X_{plane}=v_{plane}/r_{max}$ (see **Figure**

5. 17) and measured the escape energy at each value (see **Figure 5. 18**) from a hexadecane water interface.

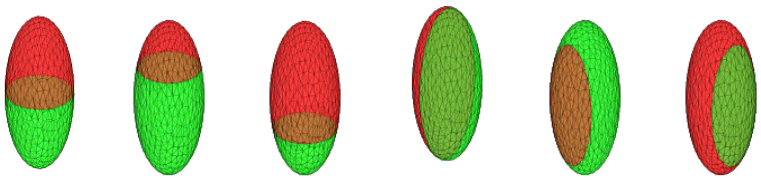

Figure 5. 17 Janus ellipsoids with aspect ratio of 0.4 from left to right X_{plane}=0, 0.5, -0.5 in the xy plane and X_{plane}=0, 0.5, -0.5 in the xz plane.

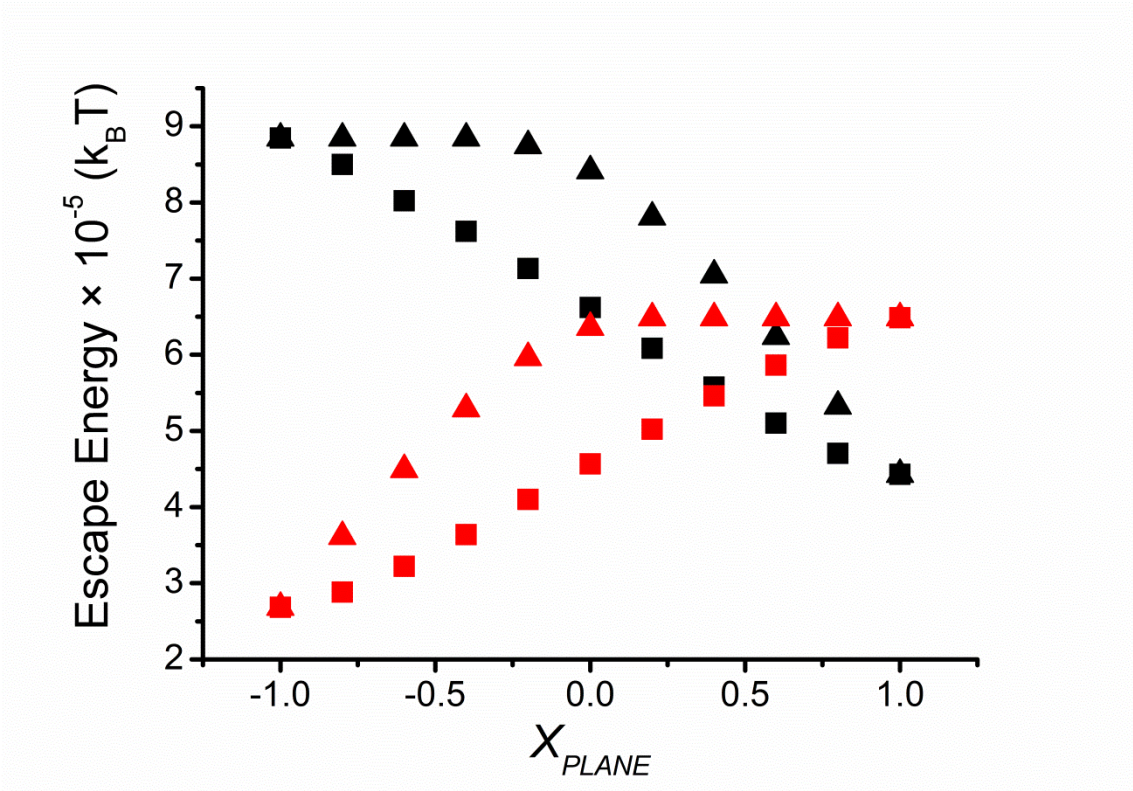

Figure 5. 18 Escape energy for polystyrene-poly(HEMA) Janus ellipsoids (aspect ratio= 0.4) of varying Janus character either intersected in the XY plane (squares) or the XZ plane (triangles). The colour of the point represents that the minimum energy for escape is into the oil phase (red) or aqueous phase (black). $\sigma_{HD/water}$=53.5 mNm^{-1} $\sigma_{HD/PSt}$=14 mNm^{-1} $\sigma_{water/PSt}$=32 mNm^{-1} $\sigma_{HD/PHEMA}$=18 mNm^{-1} $\sigma_{water/PHEMA}$=12 mNm^{-1} either calculated from the polymer surface energy or taken from literature.[41,42]

It can be seen from **Figure 5. 18** that where the XZ plane is used to impart the Janus character then the escape energy is significantly higher. This can be ascribed to the synergistic effects of particle shape and particle chemistry which both encourage the

particle to lie flat at the interface when. Conversely for where the XY plane is intersected the shape of the particle acts as a driving force to induce the particle to lie flat and maximize the interfacial area at the interface whereas the chemistry of the particle attempts to make the particle stand upright to encourage favourable interactions between the hydrophilic part of the particle and the aqueous phase and the hydrophobic part and the hexadecane phase. The net effect is a reduction in the amount of energy required to remove these particles from the interface.

In select cases for intersection in the XZ plane we observed that changing the value of X_{plane} did not induce any change in the escape energy of the particle. In these cases the particle was orientated such that the particle lay flat at the interface to maximize the interfacial area and the hydrophobic part of the particle was completely immersed in the hexadecane phase. In this instance, the polystyrene phase of the particle is not in contact with the aqueous phase and the free energy for the particle at the minimum and in the hexadecane phase is given by **Equation 5. 13**.

$$\Delta G_{min} = A_{PS}\sigma_{PS/HD} + Amin_{HEMA/Water}\sigma_{HEMA/Water} + Amin_{HEMA/HD}\sigma_{HEMA/HD} - Amin_{Water/HD}\sigma_{Water/HD}$$

Equation 5. 13

$$\Delta G_{HD} = A_{PS}\sigma_{PS/HD} + A_{HEMA}\sigma_{HEMA/HD}$$

Where *Amin* corresponds to the areas at the thermodynamic minima in the free energy profile. In these cases all the polystyrene phase (A_{PS}) is contained within the hexadecane phase, both at the minimum and, by necessity when the particle lies in the hexadecane phase, and therefore the escape energy can be given by **Equation 5. 14**.

Equation 5. 14

$$\Delta G_{ad} = \Delta G_{HD} - \Delta G_{min}$$
$$= A_{HEMA}\sigma_{HEMA/HD} - Amin_{HEMA/Water}\sigma_{HEMA/Water}$$
$$- Amin_{HEMA/HD}\sigma_{HEMA/HD} + Amin_{Water/HD}\sigma_{Water/HD}$$

Since the total area of the HEMA part of the particle (A_{HEMA}) is given by the sum of $Amin_{HEMA/Water}$ and $Amin_{HEMA/HD}$ then the adsorption escape energy reduces to **Equation 5. 15**.

Equation 5. 15

$$\Delta G_{ad} = Amin_{HEMA/Water}\,\sigma_{\frac{HEMA}{HD}} + Amin_{HEMA/HD}\,\sigma_{\frac{HEMA}{HD}}$$
$$- Amin_{HEMA/Water}\sigma_{HEMA/Water}$$
$$- Amin_{HEMA/HD}\sigma_{HEMA/HD} + Amin_{Water/HD}\sigma_{Water/HD}$$

$$\Delta G_{ad} = Amin_{HEMA/water}\left(\sigma_{\frac{HEMA}{HD}} - \sigma_{\frac{HEMA}{Water}}\right)$$
$$+ Amin_{Water/HD}\sigma_{Water/HD}$$

In cases where the polystyrene particle phase was immersed in the hexadecane phase and where the shape of the particle induces it to sit where the area at the liquid liquid interface is maximum then the two values of $Amin_{HEMA/water}$ and $Amin_{Water/HD}$ do not change upon changing the surface chemistry. This results in a scenario where changing the amphiphilic balance of the particle does not result in any net gain or loss of interfacial activity (see **Figure 5. 19**) and is somewhat contrary to logical thought. This also demonstrates a marked difference from molecular surfactants where the hydrophilic hydrophobic balance is a deciding factor in emulsion stabilization efficiency.

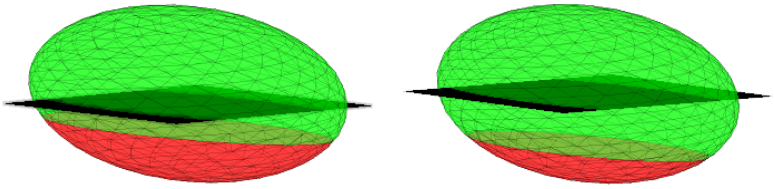

Figure 5. 19 Identical equilibrium orientations of two polystyrene (red) / poly(HEMA) (green) Janus ellipsoids with different intersection planes in the XZ axis *(left)* X_{plane}=0.4 and *(right)* X_{plane}=0.6 at a water (upper phase) hexadecane(lower phase) interface. The minimum escape energy for both is into the hexadecane phase and is identical (6.484 x 10^{-5} k_BT).

Thus we can conclude from these results that in order to maximise the particle adsorption energy the effects of surface chemistry, particle shape and their mutual effects should be considered. When designing colloidal particles to stabilize liquid-liquid interfaces the orientation in which the particle is most stable should be used to determine where the chemical anisotropy should lie to encourage synergistic effects.

5.4.3. Dumbbell particles at liquid liquid interfaces

Previous work within the group had shown that Janus dumbbell particles tend to sit at an angle with respect to the liquid liquid interface contrary to the original expectation of them lying upright (see **Figure 5. 20**). [43]

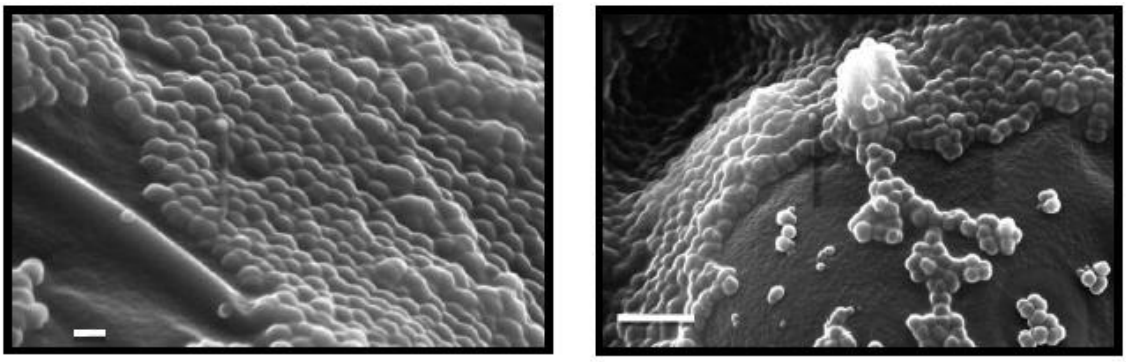

Figure 5. 20 SEM images of amphiphilic Janus particles comprised of polystyrene on one side and hairy poly(ethylene glycol methyl ether acrylate) on the other at a paraffin wax water interface. Scale bars represent 200 nm and 1 µm.

In order to explain these observations we performed a set of simulations using variations of the dumbbell morphology. Initially we varied the distance between the centres of the two spherical components of the dumbbell, one consisting of polystyrene

and the other of poly(2-hydroxyethyl methacrylate) and obtained the free energy profile of the particle at a water/hexadecane interface. Where the distance was zero and the particle was essentially a Janus sphere the particle orientation is as one would expect, with the hydrophilic lobe residing in the aqueous phase and the hydrophobic polystyrene lobe in the hexadecane phase. However as the distance between the spherical components of the dumbbell is increased the particle begins to orientate itself to lie flat with respect to the interface, in effect ignoring the chemical anisotropy (see **Figure 5. 21**). This can be explained by looking at the increasing area of the missing liquid liquid interface upon tilting the particle. The reduction in energy arising from this tilting outweighs the benefit of maximizing the hydrophilic and hydrophobic interactions of the particle and its medium.

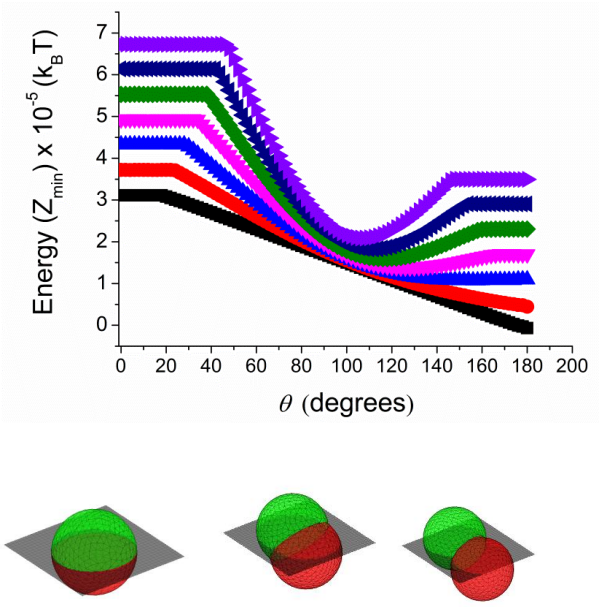

Figure 5. 21 *(Top)* Free energy change upon varying orientation angle demonstrating the effect of distance on the equilibrium orientation angle of Janus dumbbells with two spherical lobes of 100 nm radius. Symbols represent centre to centre distances of the two spheres that make up the Janus particle 0 nm(■),25 nm(●), 50 nm(▲), 75 nm(▼), 100 nm(◆), 125 nm(◀) and 150 nm(▶).$\sigma_{HD/water}$=53.5 mNm^{-1} $\sigma_{HD/PSt}$=14 mNm^{-1} $\sigma_{water/PSt}$=32 mNm^{-1} $\sigma_{HD/PHEMA}$=18 mNm^{-1} $\sigma_{water/PHEMA}$=12 mNm^{-1} either calculated from the polymer surface energy or taken from literature.[41,42] *(Bottom)* Equilibrium orientation of Janus dumbbells at hexadecane water interface for interlobe distances of (from left to right) 0 nm, 75 nm and 150 nm.

Following on from this we looked into the effect of varying the relative sizes of the two lobes that make up the dumbbell particle rendering it asymmetric in shape. The dimensionless separation distance $\varepsilon=d/r_0+r_1$ where d is the separation distance in nm and r_0 and r_1 are the radii of the two lobes is fixed at 0.5 and the radii of the two lobes were altered and for each, the free energy profile was calculated (see **Figure 5. 22**).

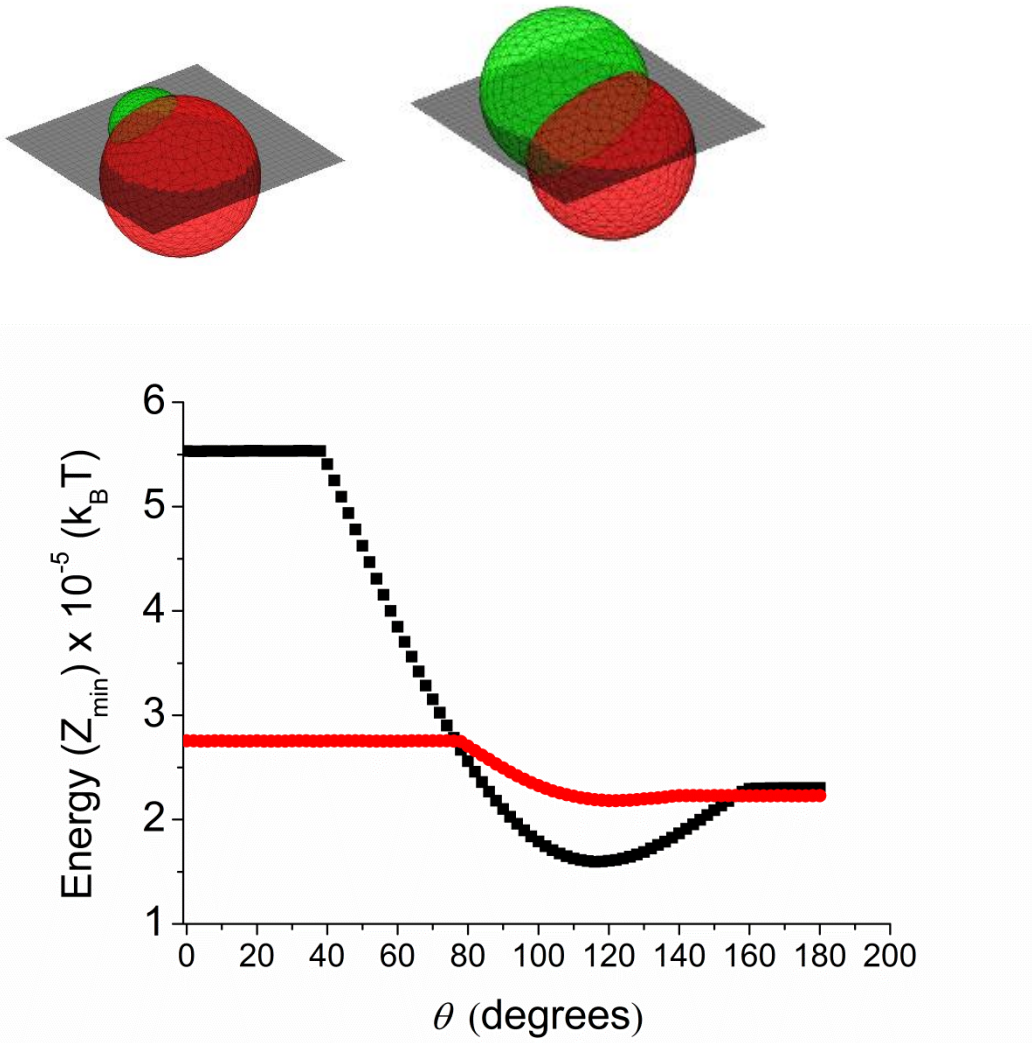

Figure 5. 22 Equilibrium orientations and barrier to rotation for Janus dumbbell particles consisting of polystyrene/poly(HEMA) for different lobe sizes. In both the polystyrene lobe has radius of 100 nm. The radius of the poly(HEMA) is 100 nm(■) and 50 nm(●). The separation distance $\varepsilon=d/r_0+r_1$ is 0.5 in both cases.

It can be seen that the size of the hydrophilic lobe has a strong influence on the rotational energy profile. Where it is large the particle is effectively fixed at a given angle and the barrier to rotation is very large. However when the hydrophilic lobe is

decreased in size then the free energy profile indicates that rotations may be possible as the energy loss caused by reducing the area the particle takes up at the interface is negligible for the near-spherical Janus particle with the smaller lobe.

We can deduce from these results that the delicate interplay between particle shape and chemistry hugely impacts upon particle orientations and therefore the ability of particle to stabilize emulsions. The latter results in which the barrier to rotation was fairly small led us to believe that metastable states may be present in experimental systems depending on particle morphology and we subsequently attempted to see if this was indeed the case.

5.4.4. Multiple energy minima – The case of cubic particles

The existence of more than one minima in the free energy profile was observed for several particle morphologies. In order to confirm this we synthesized cubic particles which were predicted from initial analysis of the free energy profile to have two energy minima. Superellipsoidal hematite particles of micron-scale dimensions (1.36 ± 0.12 μm average characteristic length) and with a monomodal particle size distribution, were prepared by a hydrothermal synthetic route (see **Figure 5. 23**). This approach allows for control of particle shape by varying the relative amounts of iron(III) chloride to sodium hydroxide, and other ionic species, used in the synthesis. Colloidal stability of the hematite particles was warranted through use of poly(vinyl pyrrolidone) as macromolecular surfactant, which is strongly adhered to the surface of the particles by physisorption. Coverage of the surface of the particles with the polymeric stabilizer masks underlying variations in wettability of the different crystal faces. This removes chemical anisotropy and provided us with straightforward set of three interfacial tension values to be used in the simulations.

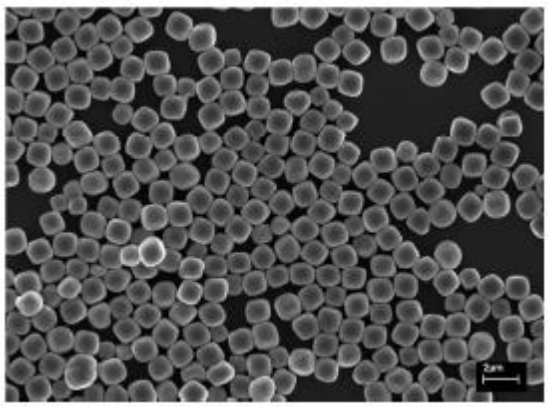

Figure 5. 23 SEM image of cubic hematite particles. Scale bar is 2 μm.

The orientation of isolated hematite particles with respect to *n*-hexadecane-water interface was determined by the gel trapping technique.[44] We analyzed the orientation of 100 isolated superellipsoidal hematite particles at the hexadecane-water interface through a combination of SEM and AFM analysis. Only isolated particles were studied in order to avoid complications as a result of particle-particle interactions, for example through capillary bridging, which potentially could alter their orientation. Following image analysis of all isolated particles it became evident that three orientations existed, two of which predominated (see **Figure 5. 24**). Overall, SEM analysis was more practical than AFM in assessing the orientation of a larger set of the hematite particles. From our set of 100 particles, 59 adopted a conformation where two of the faces lay parallel to the interface (flat), with an average penetration depth into the water phase of 1.05 ± 0.08 μm. 35 particles showed a titled orientation relative to the oil-water interface, with a tip to surface distance of 0.86 ± 0.08 μm. A small ternary population of 6 particles also exhibited a tilted orientation, but they were lying distinctly deeper into the oil phase, with a tip to surface distance of 0.54 ± 0.08 μm. AFM measurements were used to corroborate accurate particle penetration depths for the three orientations observed.

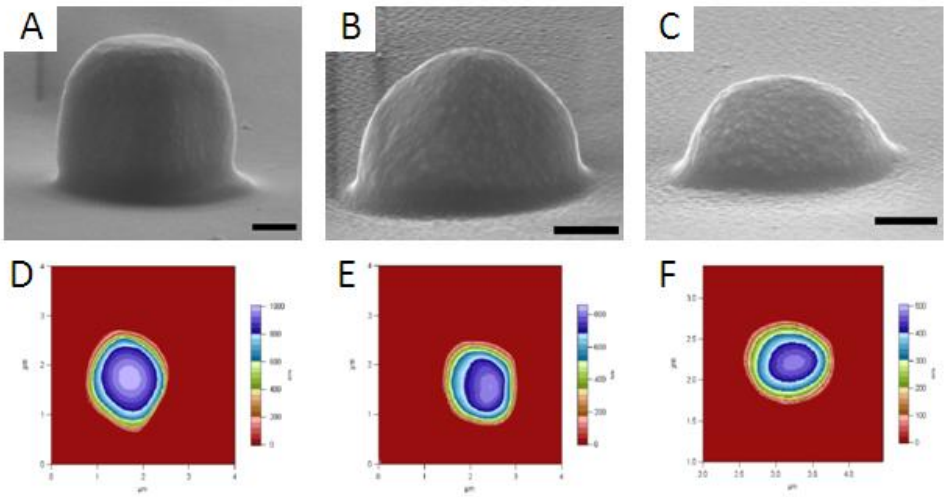

Figure 5. 24 Representative SEM Images of the three observed orientations (A) flat orientation – 59%, (B) tilted orientation – 35%, and (C) tilted but sunken orientation – 6%. Scale bar = 400nm. (D-F) AFM height contour maps of the three orientations.

In order to explain our experimental observations of three distinct particle orientations, we calculated the free energy landscape of superellipsoidal cubes. Firstly, we define mathematically the shape of a superellipsoid using **Equation 5. 16**.

Equation 5. 16

$$\left(\frac{x^{2/n_2}}{r_x}+\frac{y^{2/n_2}}{r_y}\right)^{n_2/n_1}+\frac{z^{2/n_1}}{r_z}=1$$

Where x, y, and z are Cartesian coordinates. r_x, r_y, and r_z are the particles x, y, and z radii respectively. n_1 and n_2 act as the "squareness" parameters in the z axis and the x-y plane respectively, with $0< n_1, n_2<\infty$. In our calculations we used values of $r_x= r_y= r_z=$ 680 nm, and $n_1 = n_2 = 0.5$, to be in agreement with the shape of the hematite particles used in our experiments, as determined from SEM image analysis.

The energy profile for the adhesion of our superellipsoidal hematite particles at the hexadecane-water interface calculated by our method predicts two energy minima, and thus two thermodynamic equilibrium orientations. These are in excellent agreement with two of our experimentally observed orientations; one lying flat with respect to the interface (θ_1=0, θ_2=0, ž=-0.52), which corresponds to the global energy minimum

(**Figure 5. 25a**), and the other lying at a tilted angle, corresponding to θ_1=45, θ_2=35, ž=-0.21 (**Figure 5. 25b**), being a local minimum. The overall energy contour plot as a function of the angles θ_1 and θ_2 for the minimum ž value, G(θ_1, θ_2, $ž_{min}$), is given (**Figure 5. 25c**).

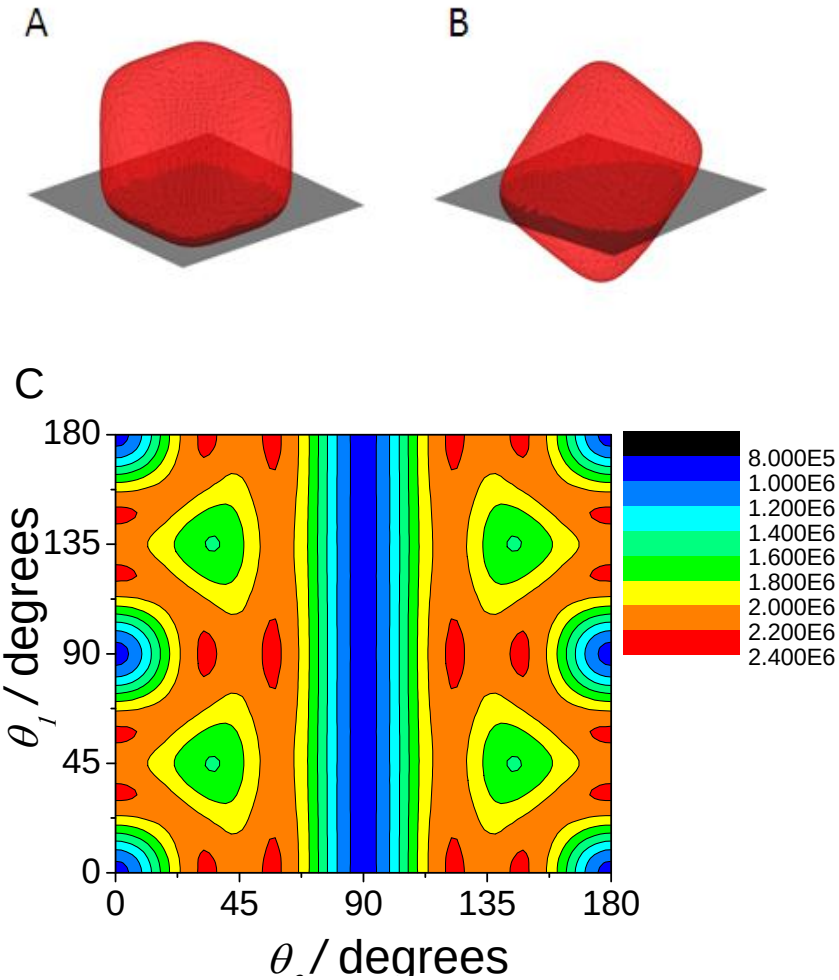

Figure 5. 25 (a) Representation of a particle trapped at the global energy minimum, corresponding to the observed flat orientation found at θ_1=θ_2=0, ž=-0.52 (b) A second thermodynamic metastable tilted state is also observed at the local minimum found at θ_1=45, θ_2=35, ž=-0.21 (c) Energy profile of a superellipsoidal hematite particle at the hexadecane-water interface at its minimum ž value as a function of θ_1 and θ_2. Scale bar is in units of k_bT.

A third orientation that was found experimentally could not be assigned to any minima in the free energy landscape as determined by our simulations. In order to understand the existence of this orientation we looked closer at the dynamics of the transition of the particle from the oil phase into the interface. For this we initialized the

particle at a random orientation in the hexadecane phase with respect to the interface and calculated the associated energy (see **Figure 5. 26**).

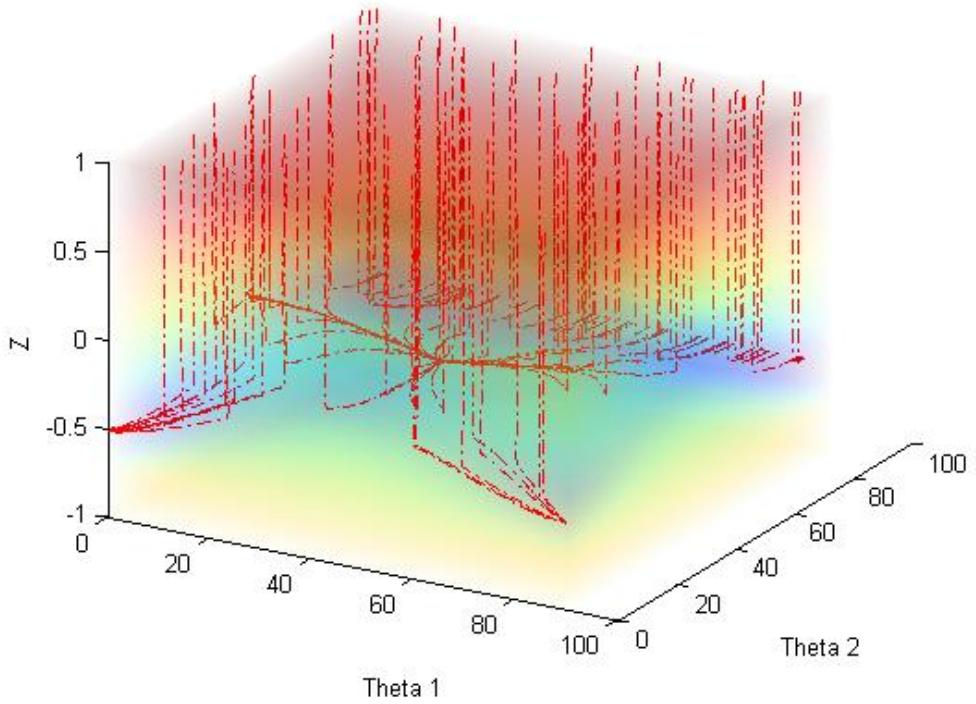

Figure 5. 26 Simulation of energetic trajectories taken by 100 particles dropped towards the interface from a random starting orientation in the oil phase.

Trajectories that follow the path of the steepest descent in terms of energy from an initial point $P^0(\theta_1^0, \theta_2^0, z^0)$ are calculated by interpolating between the values of the gradient of the free energy profile and using the constituent $d\theta_1$, $d\theta_2$ and dz values to determine the direction of particle motion. In all cases the simulated trajectories of the particle could be discerned into two separate stages. First, a rapid 'sinking' of the particles into the interface is observed, as the energy involved in translation of the particle from the oil phase into the interface (movement in the z axis) is significantly more favourable than the energy involved in particle rotation. Following this the particle undergoes a rotation into an orientation that corresponds to an energy minimum. In certain cases it was observed that the energy profile contained a region between these two stages in which the gradient was negligible, which would allow for a kinetically-

trapped state, or transition state (**Figure 5. 27**). Closer examination indicated that this region relates to the third 'unknown' orientation that had been observed experimentally.

The plateau region of the energy profile corresponds with the sunk and tilted state as was experimentally observed for a small population of particles. To the best of our knowledge this is the first report of such a kinetic metastable state being observed for particles at liquid-liquid interfaces.

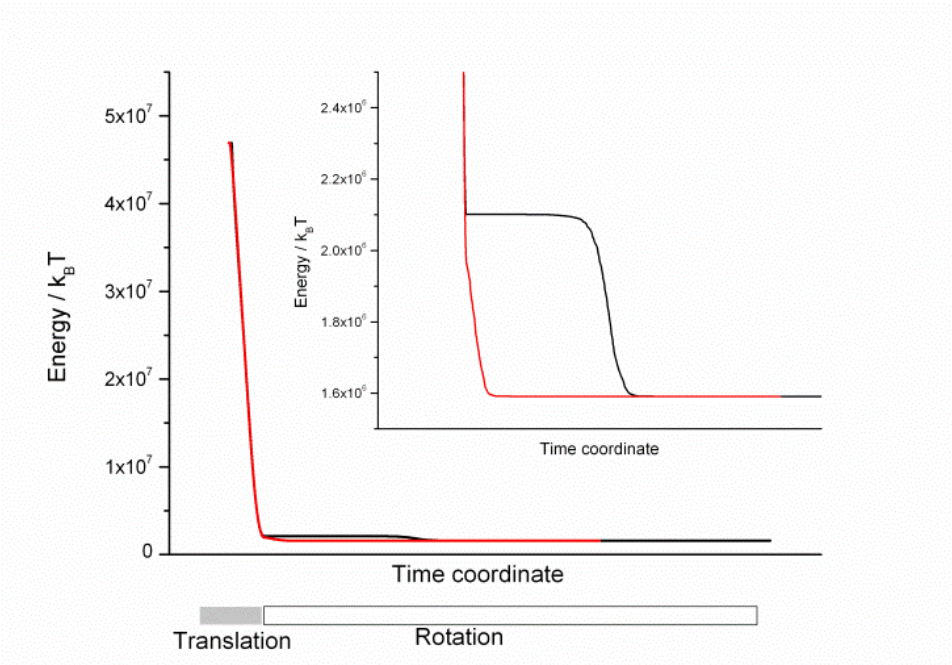

Figure 5. 27 Plot of the total free energies involved in two specific hematite superellipsoidal particle trajectories into a hexadecane-water interface. Some particles experience a negligible gradient in free energy when re-orientating (black energy trajectory vs. the red energy trajectory), corresponding to the third observed kinetically-trapped transition state

When we simulate a set of 100 different particles to fall into the interfacial energy wells and allow all of them to reach a thermodynamic equilibrium minimum (see **Figure 5. 26**), 56% of the particles fall into the global energy minimum and thus adopt the flat orientation, whereas 44% get trapped into the local minimum, corresponding to the tilted orientation. The experimental observations of 59% of particles lying flat, and the rest tilted, is in excellent agreement with this data. This implies that our initial assumption, that is that the particles can be modelled to have a random orientation prior

to contact with the interface, is valid. It was also observed that from very similar initial orientations the particles may travel to vastly different minima. For example, two particles that start their trajectories from similar orientations in the oil phase, being θ_1=20, θ_2=55, and θ_1=20, θ_2=65 respectively follow different pathways ending up in different final orientations. Thus the distribution of particle orientations observed once adhered to the oil-water interface is a result of the random tumbling of particles, the specific orientation the particle has when it comes into contact with the oil-water interface, and a potential plateau region in the energy profile of the trajectory, rather than a distribution predicted on the basis of the relative energy levels of the respective minima.

The population densities and relative energy levels of the multiple minima would be expected to have a huge impact on the ability of a particle to stabilize an emulsion, especially since the barrier to reorganization once adsorbed to the interface is so high. We have shown here that even relatively shallow energy minima in the free energy profile can attract a large population of particles and as such can influence greatly the ability of a particle to stabilize an emulsion.

5.5. Conclusion

In conclusion, we have developed a model for determining the adhesion energy for particles at liquid-liquid interfaces and used it to explain some experimental observations of the behaviour of anisotropic particles. From this work we can outline some guidelines by which particles should be designed in order to optimize emulsion stability:

1. The particle shape should be tailored in order to maximize the interfacial area of the particle at the liquid-liquid interface.

2. Where chemical anisotropy is introduced it should be orientated in such a way as to complement the orientation of the particle at the interface in the absence of any amphiphilic character.

3. The presence of multiple minima, even if shallow, in the free energy profile can result in inefficient stabilization and should be considered in particle design.

5.6. Experimental

5.6.1. Materials

Reagent grade iron(III) chloride hexahydrate, hexadecane, methanol, sodium hydroxide, phytagel, PDMS (200 fluid, 10 cSt), and PVP-K30 (40,000 g mol^{-1}) were all used as received from Sigma Aldrich. Phytagel was obtained from Sigma Aldrich. Deionized water was produced by a Milli-Q purification unit with a conductivity of 18MΩ. Beer bottles and their swing tops were obtained from JBC glassware.

5.6.2. Preparation of Hematite Superellipsoids

Iron(III) chloride hexahydrate (2.0 M, 100 mL) was added to a 200 mL beer bottle fitted with a ceramic swing top, and sealed with a Teflon-lined rubber seal. Sodium hydroxide solution (6.0 M, 90 mL) was slowly fed into the iron chloride solution under vigorous stirring over a period of 5 minutes before a small aliquot of deionized water (10 mL) was added. The bottle was sealed and transferred to an oven at 100°C where it was left for 8 days. The amber-colored supernatant was removed and the sediment re-dispersed in water before 3 rounds of centrifugation at 2000 rpm, re-dispersing in water each time. PVP-K30 (10.0 g) was added and the solution was allowed to stir for 48 hours to ensure complete absorption before they were cleaned by a further 3 rounds of

centrifugation/dispersion in water, and drying in an oven under vacuum at 60°C for 48 hours.

5.6.3. Gel-Trapping technique

A 2.0 wt% solution of phytagel was made up by dissolving in water at 80°C with vigorous stirring, and then left to cool to 50°C with light stirring, until no bubbles remained in the system. This solution was placed in a Petri dish and n-hexadecane at 50°C was layered on top. 100 µl of a 1.0 wt% hematite particle suspension in isopropanol was injected at the oil-water interface by syringe, and the Petri dish was left to cool for 30 minutes at room temperature until the aqueous phase gelled. The oil layer was gently removed by pipette and replaced by a Sylgard 184 elastomer at a mass ratio of 9:1 PDMS:curing agent ratio, which had previously been degassed in a vacuum. The liquid PDMS was gently poured over the gel surface and left to cure for 2 days at room temperature. At this point the PDMS layer was peeled from the hydrogel surface and immersed in hot water for two minutes to remove any residual phytagel.

Squares of PDMS (1cm x 1cm) were cut before cleaning in boiling deionized water for 2 minutes. Atomic force microscopy (AFM) images were obtained using an Asylum Research MFP-3D (Santa Barbara, USA) in AC mode using AC240TS cantilevers (Olympus). SEM samples were prepared by sputter-coating PDMS squares with platinum at a 45° angle. An operating voltage of 15 kV was used, calculated to give a surface thickness of 5 nm. Imaging was performed at a 14.1° angle with respect to the plane of the interface on a Zeiss Supra 55VP SEM, operated at 10 kV. Particle sizes were averaged over 100 isolated particles. A simple trigonometric correction factor was applied when measuring particle height in order to account for the tilt of the stage.

5.7. References

1. Ramsden, W. Separation of Solids in the Surface-layers of Solutions and ' Suspensions ' (Observations on Surface-membranes, Bubbles, Emulsions, and Mechanical Coagulation). — Preliminary Account. *Proceedings of the Royal Society of London* **72**, 156–164 (1903).

2. Pickering, S. U. CXCVI.—Emulsions. *Journal of the Chemical Society, Transactions* **91**, 2001–2021 (1907).

3. Pieranski, P. Two-Dimensional Interfacial Colloidal Crystals. *Physical Review Letters* **45**, 569–572 (1980).

4. Colver, P. J., Colard, C. A. L. & Bon, S. A. F. Multilayered nanocomposite polymer colloids using emulsion polymerization stabilized by solid particles. *Journal of the American Chemical Society* **130**, 16850–1 (2008).

5. Bon, S. A. F. & Colver, P. J. Pickering miniemulsion polymerization using Laponite clay as a stabilizer. *Langmuir* **23**, 8316–22 (2007).

6. Wang, T., Colver, P. J., Bon, S. A. F. & Keddie, J. L. Soft polymer and nano-clay supracolloidal particles in adhesives: synergistic effects on mechanical properties. *Soft Matter* **5**, 3842 (2009).

7. Schmid, A., Armes, S. P., Leite, C. A. P. & Galembeck, F. Efficient preparation of polystyrene/silica colloidal nanocomposite particles by emulsion polymerization using a glycerol-functionalized silica sol. *Langmuir* **25**, 2486–94 (2009).

8. Colver, P. J. & Bon, S. A. F. Cellular Polymer Monoliths Made via Pickering High Internal Phase Emulsions. *Chemistry of Materials* 1537–1539 (2007).

9. Chen, Y., Ballard, N., Gayet, F. & Bon, S. A. F. High internal phase emulsion gels (HIPE-gels) from polymer dispersions reinforced with quadruple hydrogen bond functionality. *Chemical Communications* **48**, 1117–9 (2012).

10. Menner, A., Ikem, V., Salgueiro, M., Shaffer, M. S. P. & Bismarck, A. High internal phase emulsion templates solely stabilised by functionalised titania nanoparticles. *Chemical Communications* 4274–4276 (2007).

11. Haibach, K., Menner, a, Powell, R. & Bismarck, a Tailoring mechanical properties of highly porous polymer foams: Silica particle reinforced polymer foams via emulsion templating. *Polymer* **47**, 4513–4519 (2006).

12. Sun, G., Li, Z. & Ngai, T. Inversion of particle-stabilized emulsions to form high-internal-phase emulsions. *Angewandte Chemie* **49**, 2163–6 (2010).

13. Menner, A., Powell, R. & Bismarck, A. A new route to carbon black filled polyHIPEs. *Soft Matter* **2**, 337 (2006).

14. Binks, B. P. & Horozov, T. S. Aqueous Foams Stabilized Solely by Silica Nanoparticles. *Angewandte Chemie* **117**, 3788–3791 (2005).

15. Binks, B. P., Rocher, A. & Kirkland, M. Oil foams stabilised solely by particles. *Soft Matter* **7**, 1800 (2011).

16. Gonzenbach, U. T., Studart, A. R., Tervoort, E. & Gauckler, L. J. Ultrastable particle-stabilized foams. *Angewandte Chemie* **45**, 3526–30 (2006).

17. Binks, B. P. & Murakami, R. Phase inversion of particle-stabilized materials from foams to dry water. *Nature Materials* **5**, 865–9 (2006).

18. Binks, B. P. & Lumsdon, S. O. Influence of Particle Wettability on the Type and Stability of Surfactant-Free Emulsions. *Langmuir* **16**, 8622–8631 (2000).

19. Ashby, N. P. & Binks, B. P. Pickering emulsions stabilised by Laponite clay particles. *Physical Chemistry Chemical Physics* **2**, 5640–5646 (2000).

20. Salonen, A., Muller, F. & Glatter, O. Dispersions of internally liquid crystalline systems stabilized by charged disklike particles as pickering emulsions: basic properties and time-resolved behavior. *Langmuir* **24**, 5306–14 (2008).

21. Alargova, R. G., Warhadpande, D. S., Paunov, V. N. & Velev, O. D. Foam superstabilization by polymer microrods. *Langmuir* **20**, 10371–4 (2004).

22. Noble, P. F., Cayre, O. J., Alargova, R. G., Velev, O. D. & Paunov, V. N. Fabrication of "hairy" colloidosomes with shells of polymeric microrods. *Journal of the American Chemical Society* **126**, 8092–3 (2004).

23. Madivala, B., Fransaer, J. & Vermant, J. Self-assembly and rheology of ellipsoidal particles at interfaces. *Langmuir* **25**, 2718–28 (2009).

24. Morris, G., Neethling, S. J. & Cilliers, J. J. The effects of hydrophobicity and orientation of cubic particles on the stability of thin films. *Minerals Engineering* **23**, 979–984 (2010).

25. Kim, J.-W., Lee, D., Shum, H. C. & Weitz, D. A. Colloid Surfactants for Emulsion Stabilization. *Advanced Materials* **20**, 3239–3243 (2008).

26. Kim, S.-H., Abbaspourrad, A. & Weitz, D. a Amphiphilic crescent-moon-shaped microparticles formed by selective adsorption of colloids. *Journal of the American Chemical Society* **133**, 5516–24 (2011).

27. Ruhland, T. M., Gröschel, A. H., Walther, A. & Müller, A. H. E. Janus cylinders at liquid-liquid interfaces. *Langmuir* **27**, 9807–9814 (2011).

28. Okubo, M., Ikegami, K. & Yamamoto, Y. Preparation of micron-size monodisperse polymer microspheres having chloromethyl group. *Colloid & Polymer Science* **267**, 193–200 (1989).

29. Tanaka, T., Okayama, M., Kitayama, Y., Kagawa, Y. & Okubo, M. Preparation of "mushroom-like" Janus particles by site-selective surface-initiated atom transfer radical polymerization in aqueous dispersed systems. *Langmuir* **26**, 7843–7 (2010).

30. Aveyard, R., Clint, J. H. & Horozov, T. S. Aspects of the stabilisation of emulsions by solid particles: Effects of line tension and monolayer curvature energy. *Physical Chemistry Chemical Physics* **5**, 2398 (2003).

31. Binks, B. P. Particles as surfactants - similarities and differences. *Current Opinion in Colloid & Interface Science* **7**, 21–41 (2002).

32. Aveyard, R., Binks, B. P. & Clint, J. H. Emulsions stabilised solely by colloidal particles. *Advances in Colloid and Interface Science* **102**, 503–546 (2003).

33. Aveyard, R. Can Janus particles give thermodynamically stable Pickering emulsions? *Soft Matter* **8**, 5233–5240 (2012).

34. Sacanna, S., Kegel, W. & Philipse, a. Thermodynamically Stable Pickering Emulsions. *Physical Review Letters* **98**, 13–16 (2007).

35. Binks, B. P. & Fletcher, P. D. I. Particles Adsorbed at the Oil-Water Interface : A Theoretical Comparison between Spheres of Uniform Wettability and " Janus " Particles. *Langmuir* 4708–4710 (2001).

36. Morris, G., Neethling, S. J. & Cilliers, J. J. A model for investigating the behaviour of non-spherical particles at interfaces. *Journal of Colloid and Interface Science* **354**, 380–5 (2011).

37. Lewandowski, E. P. *et al.* Orientation and self-assembly of cylindrical particles by anisotropic capillary interactions. *Langmuir* **26**, 15142–54 (2010).

38. Botto, L., Lewandowski, E. P., Cavallaro, M. & Stebe, K. J. Capillary interactions between anisotropic particles. *Soft Matter* (2012).

39. Park, B. J. & Lee, D. Equilibrium orientation of nonspherical janus particles at fluid-fluid interfaces. *ACS Nano* **6**, 782–90 (2012).

40. de Graaf, J., Dijkstra, M. & van Roij, R. Triangular tessellation scheme for the adsorption free energy at the liquid-liquid interface: Towards nonconvex patterned colloids. *Physical Review E* **80**, 1–19 (2009).

41. Binks, B. P. & Clint, J. H. Solid Wettability from Surface Energy Components: Relevance to Pickering Emulsions. *Langmuir* **18**, 1270–1273 (2002).

42. Çaykara, T., Yerlikaya, Z. & Kantoglu, Ö. The Effect of Copolymer Composition on Surface Free-Energy of Poly(2-Hydroxyethyl Methacrylate-Crotonic Acid) Copolymers. *Journal of Macromolecular Science, Part A* **40**, 1173–1182 (2003).

43. Alzhrani, A. Fabrication of Anisotropic Polymer Colloid Particles. PhD Thesis. *University of Warwick, UK* (2011).

44. Paunov, V. N. Novel Method for Determining the Three-Phase Contact Angle of Colloid Particles Adsorbed at Air-Water and Oil-Water Interfaces. *Langmuir* **19**, 7970–7976 (2003).

Chapter 6: Synthesis of anisotropic microparticles from biological templates and their interfacial activity*

6.1. Abstract

This chapter describes the synthesis of shape anisotropic particles by polymer templating of pre-existing particulate materials. We describe a new method for the decoration of the intricate morphology of spore particles with polymer nanoparticles and investigate the behaviour of these hybrids at liquid-liquid interfaces. We find a large difference in the interfacial activity between spherical microspheres and the anisotropic particles synthesized here and describe this in terms of particle wettability.

* Parts of this chapter have previously been published Ballard, N., Bon, S. A. F, Hybrid biological spores wrapped in a mesh composed of interpenetrating polymer nanoparticles as "patchy" Pickering stabilizers. *Polymer Chemistry* **2** 823-827 (2011)

6.2. Introduction

In previous chapters in this thesis the ability of asymmetric and chemically anisotropic particles to outperform their isotropic counterparts has been discussed. The ability to synthesize particulate materials of a controlled shape and surface chemistry is therefore of great interest to colloid scientists but it remains a huge challenge due to the constraints of interfacial tension that almost inevitably lead to spherical particles. In this chapter we describe a method by which microparticles with morphologies that are currently unobtainable by heterogeneous polymerization techniques can be produced by templating pre-existing structures and describe their interfacial activity.

6.2.1. Naturally occurring anisotropic particles

Nature shows a fascinating complexity in the morphological structure of small objects. Unicellular organisms such as diatoms are provided with a captivating nanopatterned biomineralized armor[1] whilst pollen grains and spores show intricate variety in shape, patterns, and chemical composition(see **Figure 6. 1**).[2] In many cases the anisotropy in structure generates advanced functionalities, for example optimization of adhesion and transport characteristics.

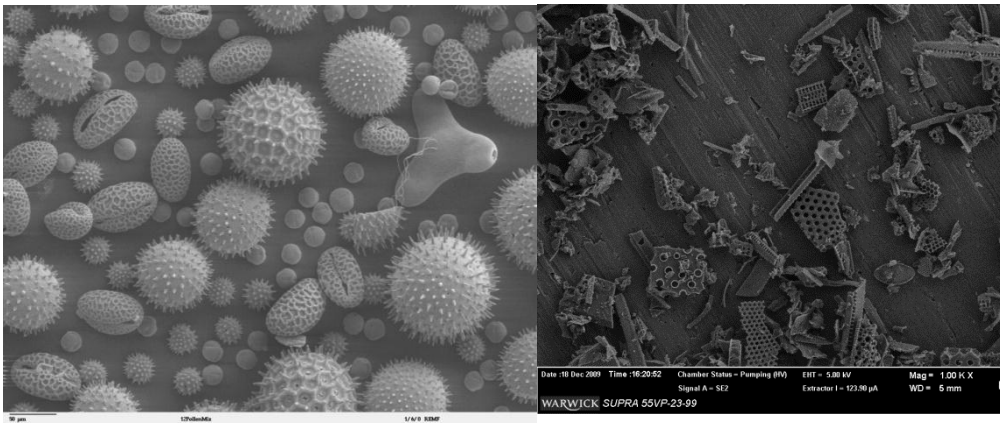

Figure 6. 1 *(Left)* SEM image of an array of pollen grains. Image courtesy of Dartmouth Electron Microscopy Facility. *(Right)* SEM image of diatomaceous earth (Celite).

6.2.2. Synthetic anisotropic particles

Drawing inspiration from the complexity of naturally occurring particles a revolution in the fabrication of manmade anisotropic colloidal particles is taking place, as variety in shape and chemical or morphological patchiness offers great engineering potential in advanced supracolloidal material design. Particles of amphiphilic Janus-type nature, for example, have the ability to self-assemble into suprastructures analogous to those formed by amphiphilic molecules,[3] the assembly process driven by hydrophobic attractive forces and governed by a geometric packing parameter. Noticeable commercialized examples are in the area of electronic paper and e-books, using bichromal dipolar microspheres imbedded in a soft fluidic matrix as tech-base,[4] or exploiting electrophoretic display technology in order to dynamically induce anisotropy in microcapsule content.[5] Numerous innovative techniques have been developed in order to produce anisotropic particles with wide-ranging morphologies from ellipsoids[6–8], cylinders[9–12] and dumbbell-like particles[13–17] to highly anisotropic particles fabricated by lithographical techniques (see **Figure 6. 2**).[18–20]

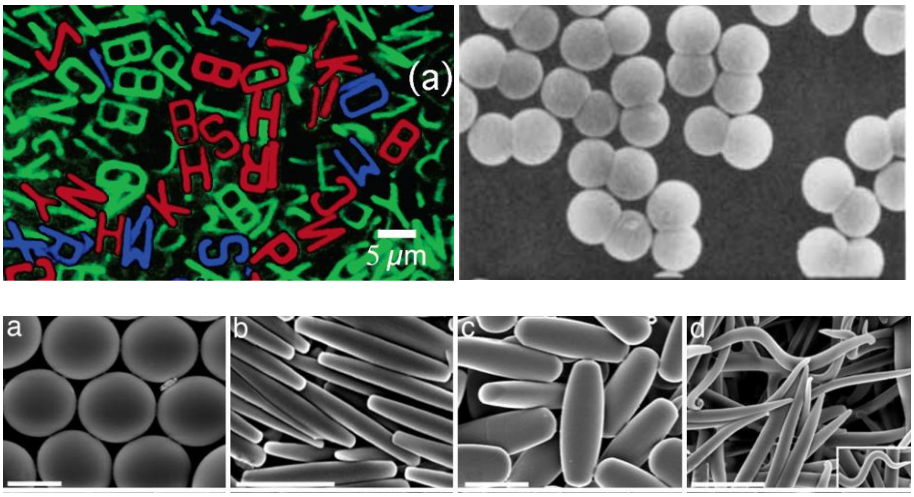

Figure 6. 2 Anisotropic particles made by synthetic methods *(Top left)* 'Alphabet soup' made by nanolithography[20] *(Top right)* Dumbbell like particles made by a seeded emulsion polymerization of lightly crosslinked polystyrene nanoparticles[21] *(Bottom)* Anisotropic nanoparticles made by stretching nanoparticles embedded in PVA matrix[6]

Despite these advances in the ability to synthesize highly anisotropic particles some residual issues have yet to be solved. The majority of techniques that describe the synthesis of controlled shape-designed particle morphologies are based on lithographical techniques which have major issues in terms of scalability and industrial application. Most alternative methods rely on chemical synthesis and/or self assembly of particle morphologies which can be high yielding and scalable but is restricted to the synthesis of simple shapes with round edges such as ellipsoids and dumbbells.[22] One potential method of solving both problems so that highly anisotropic particles can be formed in high yield is to template readily available pre-existing structures.

6.2.3. Biotemplating of anisotropic particles

The synthetic fabrication efforts described above pale into insignificance in terms of the complexity and scale of production when compared to microscopic particles made by nature. A promising route towards complex anisotropic colloids is to transform naturally occurring particles into synthetic hybrids.[23] Biological small objects are used as a template so that morphological complexity is preserved or replicated. In addition functionality can be tailored through chemical modification. Mann and coworkers used a variety of pollen grains as templates to fabricate inorganic replicas made from SiO_2, $CaCO_3$, and calcium phosphates by soaking the structures in a precursor solution which were later precipitated.[24] There have been numerous reports of using similar methods for other biological templates.[25–27] For example, the intricate structures of butterfly wings were used as a photonic scaffold for controlled assembly of CdS nanoparticles by activating the original wing to serve as a reactive site for the deposition of the inorganic nanocrystallites, producing materials that exhibited interesting optical properties (see **Figure 6. 3**).[28]

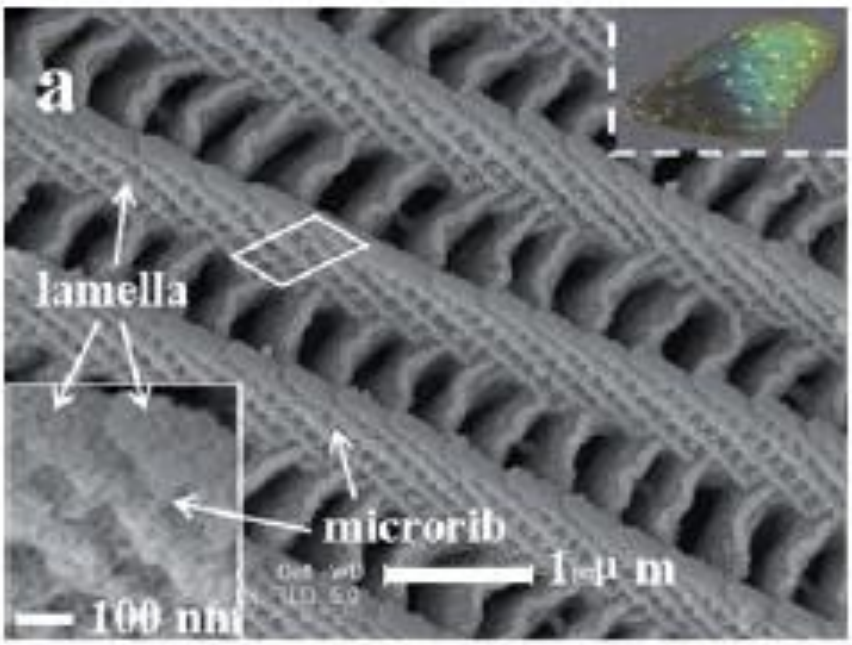

Figure 6. 3 FEG-SEM image of quantum dot nanoparticles coating the wing of a male *Euploea mulciber* butterfly. The upper right inset is a photograph demonstrating the photonic properties of the hybrid wing while the lower left shows high magnification image of the surface illustrating the quantum dot surface distribution.[28]

Instead of synthesizing inorganic replicas of biological objects herein we show that we can selectively coat *Lycopodium Clavatum* spores with crosslinked polymer nanoparticles through a free radical precipitation polymerization process. Lycopodium spores are commercially available in large quantities and have frequently proved to be useful throughout history in applications ranging widely from herbal remedies to pyrotechnics. These spores, as is common to many other pollinating particles, are of complex morphology and monomodal in size. The 30 μm Lycopodium particles used here have a unique structure with a polygon-like patterned surface consisting of high ridges. The chemical structure of the spores is rather ill-defined but can be separated into two distinct regions. The inner layer of the spore wall is composed of polysaccharides whereas the external ridge-like layer of the particle is made up of sporopollenin, an extremely resistant biopolymer derived from the oxidative polymerization of carotenoids and carotenoid esters.[29,30]

In this chapter we demonstrate the synthesis by bio-replication of anisotropic polymer particles by a seeded precipitation polymerization. The *in situ* formed polymer colloids self-assemble on specific parts of the spore surface forming an interpenetrating polymer mesh. We can tailor the fabrication of the "patchy" hybrid biological spores with control over the thickness of the mesh as well as its chemical composition and thus functionality. We investigated the ability of these "patchy" hybrid spores to adhere to liquid-liquid interfaces and serve as Pickering stabilizers. Their adhesion behaviour could be influenced upon variation of the chemical composition, and thus lyophilicity, of the polymer mesh. We show that the anisotropic polygon-like "patchy" morphology of the hybrid spores substantiates a marked and distinct wettability in comparison to isotropic microspheres.

6.3. Results and Discussion

6.3.1. Synthesis of templated microspheres by seeded precipitation polymerization

We successfully templated the biological spore particle by a precipitation polymerization of divinylbenzene in acetonitrile (see **Figure 6. 4**). The spores were dispersed into a solution containing divinylbenzene (DVB), azobisisobutyronitrile (AIBN) and acetonitrile. After degassing by nitrogen bubbling, the reaction vessel was sealed and gently tumbled in a rotary oven at 70°C.

Precipitation polymerization of divinylbenzene (DVB), commonly carried out in acetonitrile, is an established method for the synthesis of monodisperse, heavily crosslinked, micron sized particles with extensive amounts of work on core-shell and copolymer particles.[31–34] The growth mechanism of the particles throughout the reaction has been discussed in detail by Stöver and coworkers.[35] The initial homogeneous mixture of solvent, monomer(s), and initiator is heated so that oligomeric radicals form

in solution. Further propagation occurs in solution up to the point at which the fractal-like chains reach a critical molar mass upon which they aggregate and desolvate to form the particle nuclei. The formed nuclei capture oligomeric chains from solution throughout the polymerization and grow continuously as the reaction proceeds.

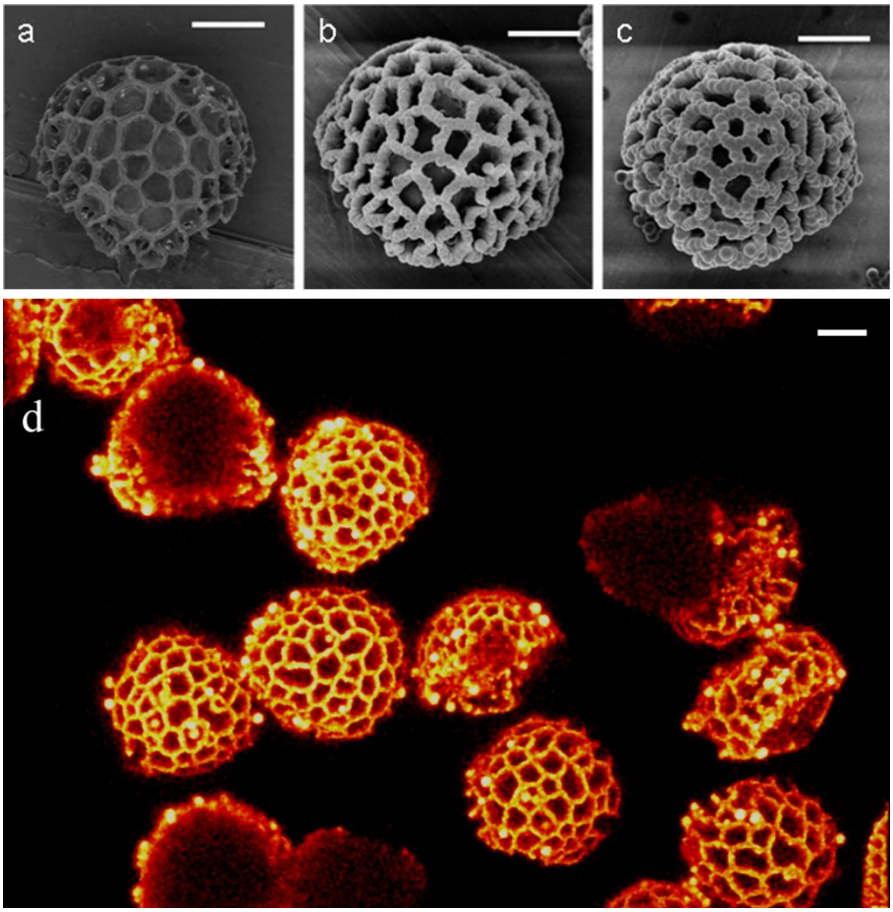

Figure 6. 4 Selective adsorption of polymer particles to the surface of Lycopodium spores at various points of the reaction. (a) 0 hours (b) 8 hours (c) 24 hours. The scale bar in all cases is 10 μm. (d) Confocal laser scanning image Z stack projection (64 z slices of 0.4 μm; total of 25.6 μm) of particles after DVB copolymerization at 70ºC for 24 hours with fluorescent tag hostasol methacrylate.

In our experiments the presence of the micron sized Lycopodium spores induced heterocoagulation of the polymer particles onto the surface of the spores resulting in complex polymer architectures (see **Figure 6. 4**). In all cases the polymer only adsorbed onto the outer polygon-like surface of the spore particles thereby forming an interpenetrating mesh. This was visualised with greater ease by confocal microscopy on hybrid Lycopodium particles that were fabricated through copolymerizing a small

amount of fluorescent monomer, in this case a hostasol functional methacrylate[36] (see **Figure 6. 4d**). The ridges of the spore particles are saturated but there is no evidence of adsorption inside the holes between the ridges. It is thought that this spatially selective heterocoagulation is the result of a long-range hydrophobic interaction between the spore ridge, composed of sporopollenin, and the emerging polymer particle mesh. Subsequent growth of the interpenetrating polymer mesh occurs as the oligomeric chains in solution are captured.

In order to confirm that the selective heterocoagulation was a result of favourable surface interactions between the polymer and the spore particle the spores were subjected to acetolysis using the method of Mackenzie *et al.*[37] which produces substantial numbers of hydrophilic carboxylate and alcohol surface groups.[38] When the modified spores were used under the same conditions under similar conditions (1:1 monomer to spore ratio with 5% monomer used in reaction medium) the polymer was no longer selective in the location of precipitation and substantial secondary nucleation was observed (see **Figure 6. 5**).

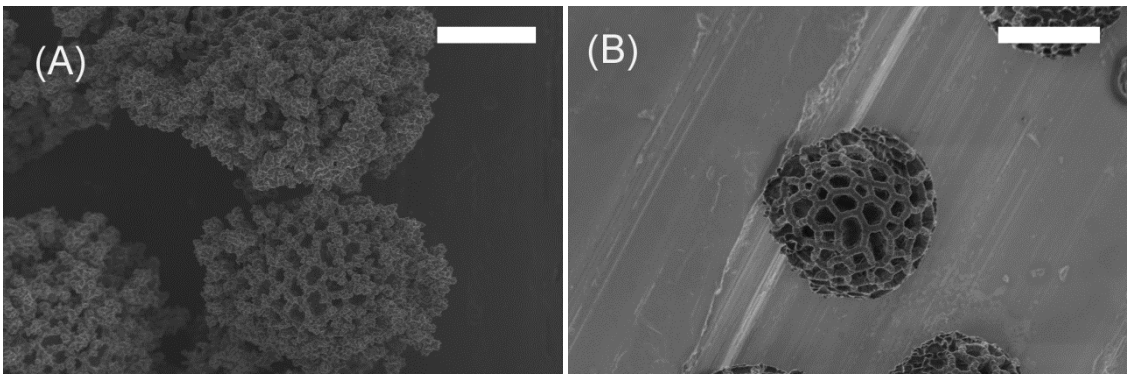

Figure 6. 5 (A) SEM image of templated particles using acetolyzed Lycopodium spores (B) SEM image of templated particles using non-acetolyzed spores. Both scale bars are 20 μm.

6.3.1.1. Polymerization kinetics

A series of precipitation polymerizations of divinylbenzene (5.0 vol%) was performed in acetonitrile in presence of azobisisobutyronitrile (AIBN) as thermal

radical initiator (3wt% to DVB). The weight ratio of Lycopodium spores to monomer was varied (L:M = 0, 0.5, 1.0 and 2.0 respectively) in order to investigate polymerization kinetics and the growth of the interpenetrating polymer mesh. Precipitation polymerizations of DVB carried out in absence of Lycopodium were colloidally unstable and coagulated after approximately 3 hours. Monomer conversion, X_M, monitored by ^{1}H NMR comparing the vinyl hydrogens of divinylbenzene to a known amount of ethyl acetate tracer, indicated the polymerization was first order with respect to divinylbenzene when initiator decomposition was taken into account in all cases (see **Figure 6. 1**) . The rate equation for this case is given by **Equation 6. 1**.

Equation 6. 1

$$-\ln(1-X_M) = 2k_p\sqrt{\frac{f[I]_0}{k_d k_t}}\,(1-\sqrt{e^{-k_d t}})$$

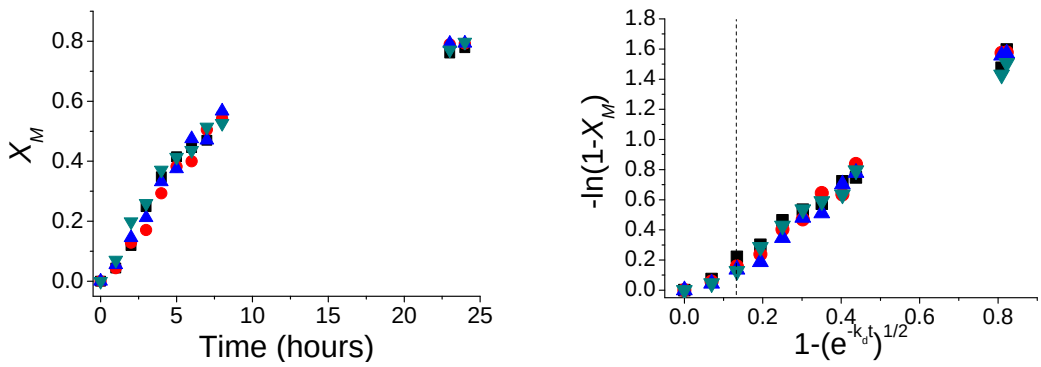

Figure 6. 6 *(Left)* Conversion versus time for seeded precipitation polymerization at varying ratios of Lycopodium spores to monomer *(Right)* First order kinetic plot taking into account decomposition of initiator at varying ratios of Lycopodium spores to monomer k_d=4×10^{-5} s^{-1}.[39] [DVB]=5 wt% [AIBN]=3 wt% Symbols correspond to Lycopodium to monomer L:M ratios of 0(■), 0.5(▲), 1(▼) and 2(◆).

The rate of reaction is not affected by the Lycopodium content, indicating that polymerization occurs almost exclusively in solution, and in all cases is in good agreement with literature values of $k_p/k_t^{1/2}$, determined from the gradient of the graph, which gave $k_p/k_t^{1/2}$ values of 6.0-6.5×10^{-2} (L/mol.s)$^{1/2}$ using an initiator efficiency of 1 compared to literature values of 4.85×10^{-2} (L/mol.s)$^{1/2}$ for *para*-DVB and 7.28×10^{-2} (L/mol.s)$^{1/2}$ for *meta*- DVB polymerized in toluene at 70°C, whereby an initiator

efficiency of 1 was assumed.[40] Note the graph in **Figure 6. 6** shows an induction period when the temperature is equilibrating in the reaction vessel denoted by the dotted line.

6.3.1.2. Particle growth kinetics

The formation and growth of the polymer mesh composed of interpenetrating polymer nanoparticles onto the surface of the Lycopodium spores was monitored by SEM as function of monomer conversion and expressed in approximate thickness. Experiments at an L:M of 0.5 showed rapid saturation of the ridges of the Lycopodium spores with interpenetrating polymer nanoparticles. Secondary homogeneous nucleation occurred after 2 hours, leading to the formation of a crop of dispersed spherical micron sized DVB particles, as detected by an increase in turbidity. Higher concentrations of the Lycopodium particles led to a slower increase in thickness of the polymer mesh, with secondary nucleation in the continuous phase completely suppressed for L:M = 2.0. In this case the larger surface area facilitated a greater volume of polymer to precipitate onto the ridges thus preventing secondary nucleation.

The growth (thickness) of the polymer mesh on the surface of the Lycopodium spores can easily be modelled when we ignore secondary homogeneous nucleation. Expressing the polymer mesh as a continuous non self-avoiding cylinder with radius *R* and length l, and estimating the total polymer mesh volume, *V*, by summation over the number of particles, N_{spore}, we can correlate monomer conversion using **Equation 6. 2**.

$$X_M \propto V \propto \pi R^2 N_{spore} l$$ **Equation 6. 2**

N_{spore} is calculated using a density value of 0.34 g.cm^{-3} for the Lycopodium spores.[41] An approximate value for *l*, the total length of the ridged surface of one spore, of 750 μm was obtained from SEM analysis of a batch of Lycopodium spores. In the absence of secondary nucleation a graph of X_M plotted against R^2N_{spore} should yield a

straight line with gradient πl (see Fig 2). It can be seen that for low L:M the plot deviates significantly from the theoretical line, where R^2N_{spore} is calculated by dividing the volume of polymer at a given time (calculated from kinetic experiments) by πl (l = 750 μm), indicating secondary nucleation. For the case of high values of L:M where little or no individual polymer particles were observed we see good agreement with the theoretical line.

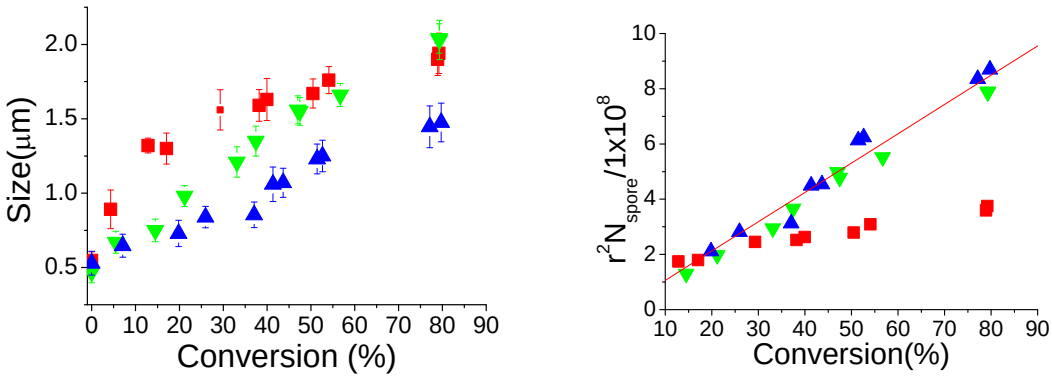

Figure 6. 7 *(Left)* Diameter of spore ridge with conversion at varying L:M values. Error bars correspond to standard deviation in measured diameter *(Right)* Growth of polymer on spore particle modelled as a continuous cylinder. The straight line is the theoretical increase of R^2N_{spore} with conversion calculated using l=750 μm. [DVB]=5 wt% [AIBN]=3 wt% to monomer. Symbols correspond to Lycopodium to monomer L:M ratios of 0.5(■), 1(▼) and 2(▲).

6.3.1.3. Templating alternative structures

In order to determine the versatility of the strategy is templating other complex colloidal particles we performed similar reactions using micron sized cellulose particles and diatomaceous earth (see **Figure 6. 8**). In both cases the deposition of the DVB nanoparticles onto the template surface was observed but there was also evidence of a new crop of particles which were not attached to the surface. The cause of this is probably due to the less favourable interaction between the polymer and the template surface that makes the heterocoagulation process less favoured compared to homocoagulation and thus secondary nucleation occurs.

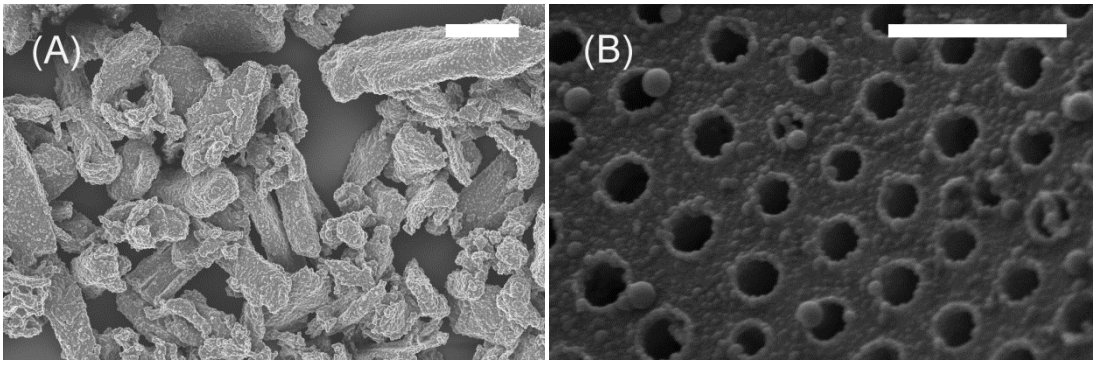

Figure 6. 8 SEM image of (A) Templated cellulose particles by seeded precipitation polymerization [DVB]=2wt% [AIBN]=3% to monomer DVB:Cellulose ratio 1:1. Scale bar is 30 μm. (B) Templated diatomaceous earth (Celite) by seeded precipitation polymerization [DVB]=2 wt% [AIBN]=3% to monomer DVB:Celite ratio 1:1. Scale bar is 5 μm

6.3.2. Interfacial activity of templated microparticles

The chemical composition of the polymer mesh wrapped around the Lycopodium spores could be readily altered upon copolymerization with functional monomers, in our case methacrylic acid (MAA), 2-hydroxyethyl methacrylate (HEMA), and methyl methacrylate (MMA) all in 1:1 weight ratio with respect to DVB. Polymerizations were stopped after 5 h in order to restrict secondary nucleation, using L:M = 1.0. The hybrid spores were subsequently cleaned by repeated sedimentation and washing with acetone followed by drying in a vacuum oven at 40°C. The prime reason to vary chemical composition was to influence the lyophilicity of the hybrids, in other words their affinity to wet either water or oil (hydrophilic versus hydrophobic). Control of this would allow fine-tuning of their adhesion properties to soft interfaces, and thus their efficacy as Pickering stabilizers. Binks *et al.*[41] previously reported that pristine Lycopodium spores can stabilize various oil-in-water emulsions. Our interest was to explore the role of the "patchy" polygon-like morphology of the spores. As a model system we examined the use of our hybrid "patchy" particles to stabilize emulsions of hexadecane and water. The particles were suspended in hexadecane (4wt%) and mixed with an equal volume fraction of water upon which emulsions were formed by handshaking and left for 1 hour (see **Figure 6. 9**).

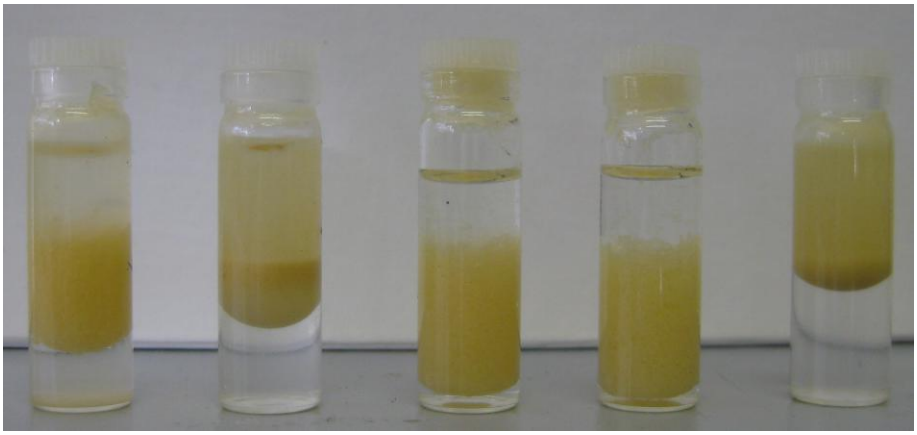

Figure 6. 9 Hexadecane in water emulsions stabilized by Lycopodium spores from left to right; bare spore, pDVB coated spore, pDVB-MAA copolymer, pDVB-HEMA copolymer, pDVB-MMA copolymer.

To our initial surprise the most hydrophobic hybrid particles, where the polymer only consisted of divinylbenzene, were unable to emulsify any oil. In sharp contrast the two components of the structured particles, the Lycopodium spore and a DVB sphere, are both excellent Pickering stabilizers. The wettability of the particles, which directly correlates to the interfacial adsorption activity, can therefore be described as a function of both the surface chemistry and the surface roughness.[42,43] A polymer mesh composed of DVB and MMA to lessen its hydrophobicity only led to negligible improvements. Copolymerization with more hydrophilic monomers, that is MAA and HEMA, led to stable oil-in-water emulsions that remained stable for a period of many weeks.

The wettability of the hybrid spores and hence their capability to serve as Pickering stabilizers was further investigated by determination of their apparent three phase contact angle, θ, using the "gel trapping" technique (see **Figure 6. 10**).[44] Lycopodium spores wrapped in a mesh of poly(DVB) did not wet the oil-water interface at all (image omitted). Upon incorporation of methyl methacrylate, a more hydrophilic monomer, the spores exhibited limited adhesion to the oil-water interface ($\theta \approx 10°$, **Figure 6. 10b**). When the hydrophilic co-monomers, HEMA and MAA, were used the contact angle was closer to 90° ($\theta \approx 105°$ and $\theta \approx 130°$ respectively), giving the emulsion increased stability.

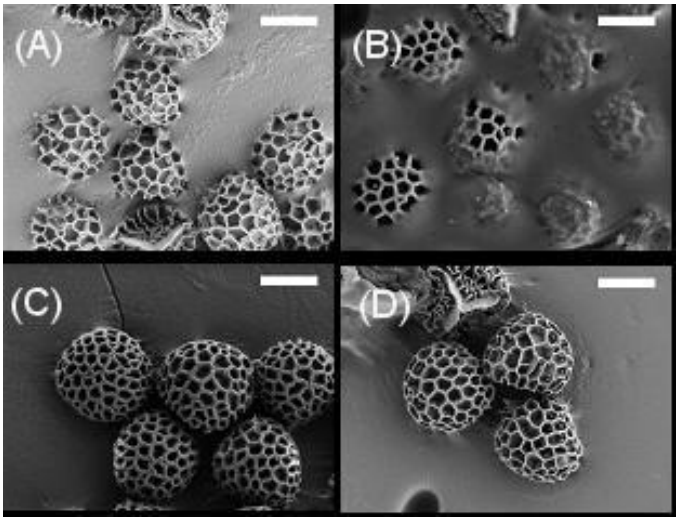

Figure 6. 10 SEM image of the Lycopodium spores position at the oil water interface for (a) bare Lycopodium (b) pDVB-co-pMMA coated Lycopodium (c) pDVB-co-pHEMA coated Lycopodium (d) pDVB-co-pMAA coated Lycopodium. Scale bar in all cases is 10 μm.

The results found experimentally agree with theoretical determination of the position of the spore at the interface. The position of a particle at a heterogeneous interface has traditionally been described by computing the free energy change based on interfacial tension as originally demonstrated by Pieranski.[45] The surface activity of non uniform particles has recently been investigated in detail by Nonomura *et al*.[46–48] who evaluated the interfacial energy as a function of a roughness factor. Using a similar approach we model the spore particles as a uniform Archimedean solid. For a non spherical particle the interfacial energy, E_T, is the sum of the energy of the particle oil interface, E_{PO}, the particle water interface, E_{PW}, and the missing oil water interface, E_{OW} (see **Equation 6. 3**).

Equation 6. 3

$$E_T \approx \sigma_{PO} S_T \left(\frac{1+z}{2}\right) + \sigma_{PW} S_T \left(\frac{1-z}{2}\right) - \sigma_{PO} \pi R^2 (1 - z^2)$$

Where σ is the interfacial tension between two phases, R is the particle radius, z is the vertical coordinate of the centre of the sphere (where z = 1 the particle resides in the oil phase and where z = -1 the particle resides in the aqueous phase) and S_T is the total surface area of the particle. This equation is derived by equating our spore particle to a

sphere with periodic patterned roughness and computing the energy as a fraction of the surface area of a sphere. For example for a smooth sphere $S_T = 4\pi R^2$ and the commonly used Pieranski expression is resolved. The missing oil water interface changes very little with a change in the surface roughness, and is neglected in the equation, resulting in a change in the interfacial energy as the particle anisotropy increases (see **Figure 6. 11**). For the Lycopodium spore we use a model buckyball type structure as a series of flat plates consisting of 12 pentagonal faces, 20 hexagonal faces and 90 edges with a width of 0.5 μm 180 faces with depth 3 μm to get an approximate surface area, S_T=6250 μm^2 compared to 3217 μm^2 for a sphere of similar radius.

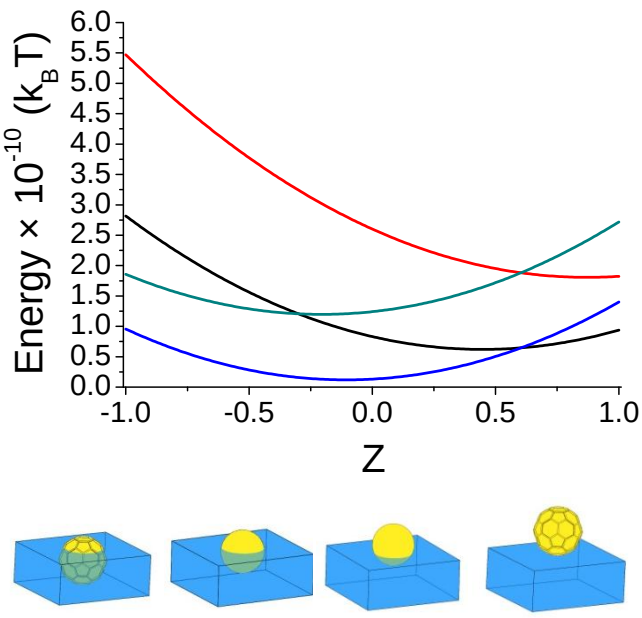

Figure 6. 11 Position of a sphere of polystyrene(—) and of polyHEMA(—) and a buckyball type structure of polystyrene(—) and polyHEMA(—)at the oil water interface and illustration of predicted contact angles for (from left to right) a buckyball type structure of polyHEMA, a polyHEMA sphere, a polystyrene sphere and a polystyrene buckyball structure. Interfacial tension values used were $\sigma_{HD/water}$=53.5 mNm^{-1} $\sigma_{HD/PSt}$=14 mNm^{-1} $\sigma_{water/PSt}$=32 mNm^{-1} $\sigma_{HD/PHEMA}$=18 mNm^{-1} $\sigma_{water/PHEMA}$=12 mNm^{-1} either calculated from the polymer surface energy or taken from literature.[49–51]

Knowing the value of S_T for the structure of interest we can use equation two to compute the free energy of the system through the liquid-liquid interface. The energy

minima, obtained by differentiation of **Equation 6. 3**, defines the vertical coordinate at equilibrium (**Equation 6. 4**).

$$z_{min} = \frac{S_T}{4\pi R^2}\frac{(\sigma_{PO} - \sigma_{PW})}{\sigma_{WO}}$$ **Equation 6. 4**

This allows us to explain for the observation that a sphere of poly(DVB) and a spore particle are adsorbed at the liquid-liquid interface but our hybrid spores of DVB, where both the interfacial tension term and the total surface area are large, are not. For the case of a polystyrene sphere, which is slightly more hydrophilic than DVB, the energy minima is found at z = 0.33 corresponding to a contact angle of approximately 70° whereas the corresponding buckyball type structure with identical interfacial tension values but an increased surface area has an energy minima at z=0.65 with contact angle approximately 50° which results in significantly reduced interfacial activity. This is shown graphically in **Figure 6. 11**. Similarly it is shown that for a more hydrophilic poly(HEMA) coated spore we expect a shift in contact angle to reflect the increase in surface area from the case of a sphere to a buckyball type structure. These theoretical results can be used to explain the experimentally determined position of the copolymer hybrid spores at the interface shown in **Figure 6. 10**. For polymer particles which are known to adsorb at interfaces we see their position at the interface accentuated towards either the oil phase, in the case of MMA and to the point of complete wetting for DVB, or towards the aqueous phase, for copolymers of HEMA and MAA due to the large increase in surface area.

6.4. Conclusions

We have developed an original method for selective coating of micrometer sized naturally occurring spore particles with smaller sub micrometer particles via an in situ precipitation polymerization. By fine tuning the monomer mixture the surface properties

of the spore particles can be easily altered and this has been demonstrated by use of the gel trapping technique to exert control over the three phase contact angle at the oil-water interface demonstrating that shape anisotropy has a huge impact on the stability of particle stabilized emulsion droplets. This technique offers the ability to template highly anisotropic structures that would otherwise be unobtainable by traditional heterogeneous polymerization techniques.

6.5. Experimental

6.5.1. Materials

Divinylbenzene (DVB, 80%, mixture of isomers), 2-hydroxyethylmethacrylate (HEMA, 98%) and methyl methacrylate (MMA, >99%) were purchased from Sigma-Aldrich and were filtered through a short column of basic alumina before use to remove inhibitor. Lycopodium powder, Celite 521, microcrystalline cellulose with an average particle size of 20 μm and phytagel were purchased from Sigma-Aldrich and were used without further purification. Azobisisobutyronitrile (AIBN) was purchased from Wako and used without further purification. All solvents were of reagent grade purity and were purchased from fisher scientific. Sylgard 184 was purchased from Farnell UK and used in a ratio of 9:1 with respect to curing agent.

6.5.2. Equipment

Scanning electron microscopy was performed on a Zeiss supra 55VP FEGSEM. Particles were coated with a thin layer of platinum prior to scanning. Confocal imaging was performed on a Zeiss LSM 510 confocal microscope. NMR measurements were performed on a Bruker DPX-300 300MHz spectrometer and the spectrum was analysed with Mestrec v2.3a. Experiments were performed in a SciGene Model 777 Microarray Oven consisting of two steel plates attached to a rotor in a thermostatted chamber.

6.5.3. Synthesis

In a typical experiment AIBN (10 mg, 3 wt% wrt monomer), the monomer(s) (300 mg) and Lycopodium spores (300 mg) were dispersed in acetonitrile (15 ml), degassed and sealed in a vial with screw cap lid. The mixture was placed in an oven with a rotating steel plate at 25 rpm and heated slowly over the course of 1 hour to 70ºC. The mixture was then left for 5 hours before being removed and left to cool. The particles were left to settle then the supernatant liquid was decanted and the particles resuspended in acetone and the process repeated 5 times. The particles were then left to dry in air.

Where alternative templating particles were used a typical experiment involved dissolving AIBN (10 mg, 3 wt% wrt monomer), DVB (300 mg) and templating particles, either microcrystalline cellulose or Celite (300 mg) were dispersed in acetonitrile (15 ml), degassed and sealed in a vial with screw cap lid and conducting the experiment as above.

6.5.4. Pickering emulsions

Particle stabilized emulsions were generated by mechanical shaking of a hexadecane water mixture. The spore particles were dispersed in hexadecane due to their hydrophobicity at a weight fraction of up to 4% and water was added (usually at a 1:1 ratio with respect to the oil phase). The vial was attached to a mechanical shaker for 10 minutes or alternatively shaken by hand for a similar amount of time. The emulsion type was inferred by placing a small amount of dye in the aqueous phase.

6.5.5. Kinetic experiments

AIBN (375 mg) and DVB (12.5 ml) were diluted to 250 ml in a volumetric flask with acetonitrile. 50 ml of this solution was added to a Schlenk tube containing varying

amounts of Lycopodium (0-5 g) and deoxygenated thoroughly by bubbling nitrogen through the solution. The flasks were sealed with rubber seals attached using jubilee clips and placed in a rotary oven at 70°C. An initial sample was removed for a reference at time zero. Conversion was monitored by NMR by comparison of the vinyl peaks of the monomer to an ethyl acetate tracer. 1 ml of the sample mixture was removed from the reaction vessel and cooled in ice. 0.3 ml of this sample was added to 0.3 ml of $CDCl_3$ and 0.05 ml ethyl acetate. In order to avoid the solvent peaks the range of the NMR spectrum was limited to between 3.5 and 8 ppm.

6.5.6. Derivation of rate equation

For the case of a free radical polymerization where initiator decomposition is taken into account we can deduce the appropriate rate equation:

$$-\frac{d[M]}{dt} = k_p[M][R^\bullet]$$

Where k_p is the polymerization rate constant of divinylbenzene, [M] is monomer concentration and [$R^\bullet$] is the radical concentration.

The overall concentration of radicals, equated to 0 by the steady state approximation, in solution is given as the rate of production of radicals by decomposition of the thermal initiator minus the rate of consumption of radicals by termination

$$\frac{d[R^\bullet]}{dt} = 2k_d f[I] - 2k_t[R^\bullet]^2 = 0$$

Where k_d is the initiator decomposition constant, f is the initiator efficiency, $[I]$ is the initiator concentration and k_t is the termination constant. The radical concentration is therefore given by

$$[R^{\bullet}] = \sqrt{\frac{k_d f[I]}{k_t}}$$

Substitution of this value back to the original rate equation gives us

$$-\frac{d[M]}{dt} = k_p[M]\sqrt{\frac{k_d f[I]}{k_t}}$$

The concentration of initiator at a given time is related to the initial concentration of initiator and the initiator decomposition rate at the reaction temperature

$$[I] = [I]_0 e^{-k_d t}$$

Where $[I]_0$ is the initiator concentration at time zero. Substituting this back into the rate equation we obtain

$$-\frac{d[M]}{dt} = k_p[M]\sqrt{\frac{k_d f[I]_0 e^{-k_d t}}{k_t}}$$

$$-\frac{d[M]}{[M]} = k_p\sqrt{\frac{k_d f[I]_0}{k_t}}\sqrt{e^{-k_d t}}\,dt$$

Integration of this equation leads to the final rate equation

$$-\ln\frac{[M]}{[M]_0} = 2k_p\sqrt{\frac{f[I]_0}{k_d k_t}}(1-\sqrt{e^{-k_d t}})$$

$$-\ln(1-X_M) = 2k_p\sqrt{\frac{f[I]_0}{k_d k_t}}(1-\sqrt{e^{-k_d t}})$$

Where X_M is the conversion of monomer expressed as a fraction.

6.5.7. Gel trapping technique

A 2wt% solution of phytagel was made up by dissolving in water at 80°C with vigorous stirring then left to cool to 50°C with light stirring until no bubbles remained in the system. This solution was placed in a Petri dish and where required oil at 50°C was layered on top. 0.5 ml of a 1wt% particle suspension in isopropanol was injected at the air-water or oil-water interface by syringe and the Petri dish was left to cool for 30 minutes at which point the gel had set. The oil layer was gently removed by pipette and replaced by a Sylgard 184 elastomer at a ratio of 9:1 PDMS:curing agent ratio, which had previously been degassed in a vacuum. The liquid PDMS was gently poured over the gel surface and left to cure for 2 days at room temperature. At this point the PDMS layer was peeled from the hydrogel surface and immersed in hot water for two minutes to remove any residual phytagel. The PDMS layer could then be imaged by electron microscopy after sputter coating a thin layer of platinum onto the surface.

6.6. References

1. Round, F.., Crawford, R.M. & F.G.Mann *The Diatoms - Biology and Morphology of the Genera*. (Cambridge University Press: 1990).

2. Heslop-Harrison, J. Pollen Wall Development. *Science* **161**, 230-237 (1968).

3. Whitelam, S. & Bon, S.A.F. Self-assembly of amphiphilic peanut-shaped nanoparticles. *The Journal of Chemical Physics* **132**, 074901 (2010).

4. Nisisako, T., Torii, T., Takahashi, T. & Takizawa, Y. Synthesis of Monodisperse Bicolored Janus Particles with Electrical Anisotropy Using a Microfluidic Co-Flow System. *Advanced Materials* **18**, 1152-1156 (2006).

5. Chen, Y. *et al.* Flexible active-matrix electronic ink display. *Nature* **423**, 423-426 (2003).

6. Champion, J. a, Katare, Y.K. & Mitragotri, S. Making polymeric micro- and nanoparticles of complex shapes. *Proceedings of the National Academy of Sciences of the United States of America* **104**, 11901-11904 (2007).

7. Ho, C.C., Keller, A., Odell, J.A. & Ottewill, R.H. Preparation of monodisperse ellipsoidal polystyrene particles. *Colloid & Polymer Science* **271**, 469-479 (1993).

8. Jiang, P., Bertone, J.F. & Colvin, V.L. A lost-wax approach to monodisperse colloids and their crystals. *Science* **291**, 453-7 (2001).

9. Badaire, S., Cottin-Bizonne, C., Woody, J.W., Yang, A. & Stroock, A.D. Shape selectivity in the assembly of lithographically designed colloidal particles. *Journal of the American Chemical Society* **129**, 40-41 (2007).

10. Ruhland, T.M., Gröschel, A.H., Walther, A. & Müller, A.H.E. Janus cylinders at liquid-liquid interfaces. *Langmuir* **27**, 9807-9814 (2011).

11. Alargova, R.G., Bhatt, K.H., Paunov, V.N. & Velev, O.D. Scalable Synthesis of a New Class of Polymer Microrods by a Liquid-Liquid Dispersion Technique. *Advanced Materials* **16**, 1653-1657 (2004).

12. Courbaron, A.-C., Cayre, O.J. & Paunov, V.N. A novel gel deformation technique for fabrication of ellipsoidal and discoidal polymeric microparticles. *Chemical communications* 628-30 (2007).

13. Kim, J.-W., Larsen, R.J. & Weitz, D.A. Uniform Nonspherical Colloidal Particles with Tunable Shapes. *Advanced Materials* **19**, 2005-2009 (2007).

14. Kim, J.-W., Lee, D., Shum, H.C. & Weitz, D.A. Colloid Surfactants for Emulsion Stabilization. *Advanced Materials* **20**, 3239-3243 (2008).

15. Wang, D., Dimonie, V.L., Sudol, E.D. & El-Aasser, M.S. Seeded dispersion polymerization. *Journal of Applied Polymer Science* **84**, 2710-2720 (2002).

16. Sheu, H.R., El-Aasser, M.S. & Vanderhoff, J.W. Uniform nonspherical latex particles as model interpenetrating polymer networks. *Journal of Polymer Science Part A: Polymer Chemistry* **28**, 653-667 (1990).

17. Mock, E.B., De Bruyn, H., Hawkett, B.S., Gilbert, R.G. & Zukoski, C.F. Synthesis of anisotropic nanoparticles by seeded emulsion polymerization. *Langmuir* **22**, 4037-43 (2006).

18. Gratton, S.E. a *et al.* The effect of particle design on cellular internalization pathways. *Proceedings of the National Academy of Sciences of the United States of America* **105**, 11613-8 (2008).

19. Rolland, J.P. *et al.* Direct Fabrication and Harvesting of Monodisperse , Shape Specific Nanobiomatrials. *Journal of the American Chemical Society* **127**, 10096-10100 (2005).

20. Hernandez, C.J. & Mason, T.G. Colloidal Alphabet Soup: Monodisperse Dispersions of Shape-Designed LithoParticles. *Journal of Physical Chemistry C* **111**, 4477-4480 (2007).

21. Sheu, H.R., El-Aasser, M.S. & Vanderhoff, J.W. Phase separation in polystyrene latex interpenetrating polymer networks. *Journal of Polymer Science Part A: Polymer Chemistry* **28**, 629-651 (1990).

22. Yang, S.-M., Kim, S.-H., Lim, J.-M. & Yi, G.-R. Synthesis and assembly of structured colloidal particles. *Journal of Materials Chemistry* **18**, 2177 (2008).

23. Sotiropoulou, S., Sierra-sastre, Y., Mark, S.S. & Batt, C.A. Biotemplated Nanostructured Materials. *Chemistry of Materials* **20**, 821-834 (2008).

24. Hall, S.R., Bolger, H. & Mann, S. Morphosynthesis of complex inorganic forms using pollen grain templates Porous micron-sized particles of silica , calcium carbonate or by template-directed synthesis employing intact pollen. *Chemical Communications* **44**, 2784-2785 (2003).

25. Guan, Z.S., Lu, C.H., Zhang, Y. & Zi, X.Z. Morphology-controlled Synthesis of SiO 2 Hierarchical Structures Using Pollen Grains as Templates. *Chinese Journal of Chemistry* **26**, 467-470 (2008).

26. Liu, S. & He, J. Facile Fabrication of Porous Titania Microtube Arrays by Replication of Human Hair. *Journal of the American Ceramic Society* **88**, 3513-3514 (2005).

27. Wang, Y. *et al.* Replication of biological organizations through a supercritical fluid route. *Chemical Communications* 2948-50 (2005).

28. Han, J., Su, H., Zhang, D., Chen, J. & Chen, Z. Butterfly wings as natural photonic crystal scaffolds for controllable assembly of CdS nanoparticles. *Journal of Materials Chemistry* **19**, 8741 (2009).

29. Shaw, G. & Yeadon, a. Chemical Studies on the Constitution of Some Pollen and Spore Membranes. *Grana Palynologica* **5**, 247-252 (1964).

30. Brooks, J. & Shaw, G. Chemical Structure of the Exine of Pollen Walls and a New Function for Carotenoids in Nature. *Nature* **219**, 532-533 (1968).

31. Yan, Q., Bai, Y., Meng, Z. & Yang, W. Precipitation polymerization in acetic acid: synthesis of monodisperse cross-linked poly(divinylbenzene) microspheres. *The Journal of Physical Chemistry. B* **112**, 6914-22 (2008).

32. Cui, H. *et al.* Highly Crosslinked Poly(styrene-co-divinylbenzene) Microspheres Prepared by Precipitation Polymerization: Effects of the Polymerization Parameters on the Characteristics of the Particles. *Journal of Applied Polymer Science* **111**, 3144-3149 (2009).

33. Perrier-Cornet, R., Héroguez, V., Thienpont, a, Babot, O. & Toupance, T. Functional crosslinked polymer particles synthesized by precipitation polymerization for liquid chromatography. *Journal of Chromatography. A* **1179**, 2-8 (2008).

34. Li, W.-hui & Stover, H.D.H. Porous Monodisperse Poly (divinylbenzene) Microspheres by Precipitation Polymerization. *Journal of Polymer Science Part A: Polymer Chemistry* **36**, 1543-1551 (1998).

35. Downey, J.S., Frank, R.S., Li, W.-H. & Stover, H.D.H. Growth Mechanism of Poly(divinylbenzene) Microspheres in Precipitation Polymerization. *Macromolecules* **32**, 2838-2844 (1999).

36. Tronc, F. *et al.* Fluorescent Polymer Particles by Emulsion and Miniemulsion Polymerization ´. *Journal of Polymer Science Part A: Polymer Chemistry* **41**, 766-778 (2003).

37. Barrier, S. *et al.* Viability of plant spore exine capsules for microencapsulation. *Journal of Materials Chemistry* **21**, 975 (2011).

38. Diego-Taboada, A. *et al.* Sequestration of edible oil from emulsions using new single and double layered microcapsules from plant spores. *Journal of Materials Chemistry* **22**, 9767 (2012).

39. Li, K. & Stöver, H.D.H. Synthesis of monodisperse poly(divinylbenzene) microspheres. *Journal of Polymer Science Part A: Polymer Chemistry* **31**, 3257-3263 (1993).

40. Nyhus, A.K., Hagen, S. & Berge, A. A Kinetic Study of the Polymerization of Pure meta- Divinylbenzene and Pure para-Divinylbenzene. *Journal of Polymer Science Part A: Polymer Chemistry* **37**, 3345-3359 (1999).

41. Binks, B.P., Clint, J.H., Mackenzie, G., Simcock, C. & Whitby, C.P. Naturally occurring spore particles at planar fluid interfaces and in emulsions. *Langmuir* **21**, 8161-7 (2005).

42. Binks, B.P. & Lumsdon, S.O. Influence of Particle Wettability on the Type and Stability of Surfactant-Free Emulsions. *Langmuir* **16**, 8622-8631 (2000).

43. Binks, B.P. & Lumsdon, S.O. Pickering Emulsions Stabilized by Monodisperse Latex Particles: Effects of Particle Size. *Langmuir* **17**, 4540-4547 (2001).

44. Paunov, V.N. Novel Method for Determining the Three-Phase Contact Angle of Colloid Particles Adsorbed at Air-Water and Oil-Water Interfaces. *Langmuir* **19**, 7970-7976 (2003).

45. Pieranski, P. Two-Dimensional Interfacial Colloidal Crystals. *Physical Review Letters* **45**, 569-572 (1980).

46. Nonomura, Y. & Komura, S. Surface activity of solid particles with extremely rough surfaces. *Journal of Colloid and Interface Science* **317**, 501-6 (2008).

47. Nonomura, Y., Komura, S. & Tsujii, K. Surface-active particles with microstructured surfaces. *Langmuir* **21**, 9409-11 (2005).

48. Nonomura, Y., Komura, S. & Tsujii, K. Adsorption of microstructured particles at liquid-liquid interfaces. *The Journal of Physical Chemistry. B* **110**, 13124-9 (2006).

49. Binks, B.P. & Clint, J.H. Solid Wettability from Surface Energy Components: Relevance to Pickering Emulsions. *Langmuir* **18**, 1270-1273 (2002).

50. Colver, P.J., Chen, T. & Bon, S.A.F. Supracolloidal Structures through Liquid-Liquid Interface Driven Assembly and Polymerization. *Macromolecular Symposia* **245-246**, 34-41 (2006).

51. Çaykara, T., Yerlikaya, Z. & Kantoglu, Ö. The Effect of Copolymer Composition on Surface Free-Energy of Poly(2-Hydroxyethyl Methacrylate-Crotonic Acid) Copolymers. *Journal of Macromolecular Science, Part A* **40**, 1173-1182 (2003).

Chapter 7: Conclusions

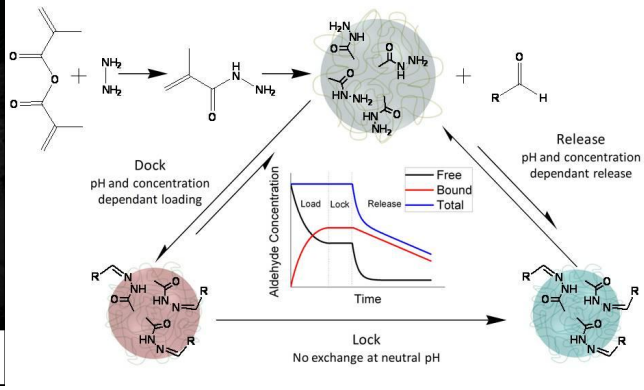

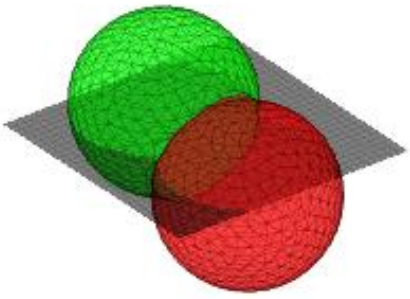

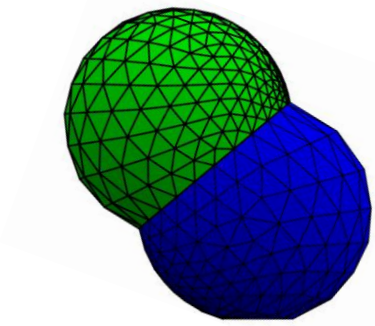

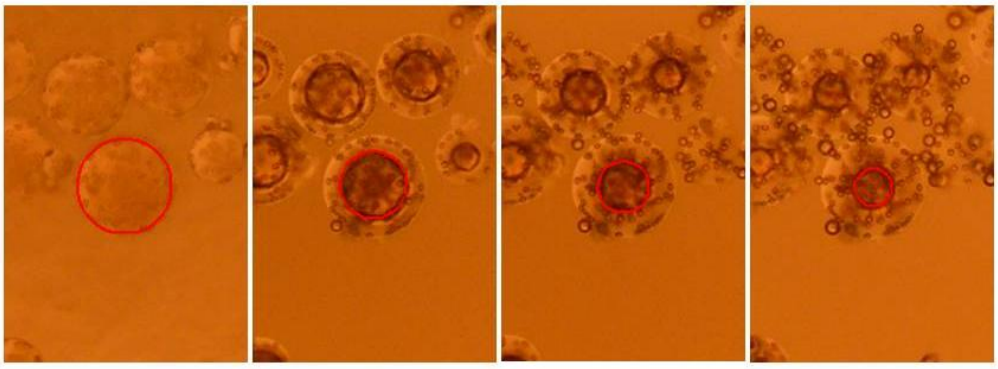

This chapter describes the main conclusions of the work included in this thesis. The outlook for future work and further application of the underlying principles that have been investigated within this body of work are described.

Colloids are used ubiquitously in home and personal care products but in many areas the full potential of colloidal particles is yet to be exploited. The wide range of applications described in chapter 1 is certainly not comprehensive and future applications of colloidal particles will no doubt be enhanced by our increasing ability to synthesize particles tailored to function. This thesis has attempted to describe new synthetic techniques for the production of colloidal polymers that have been designed with application specific properties.

Chapter 2 described a new route towards synthesis of particles that are capable of wet deposition from solution onto fibrous and otherwise non-reactive substrates. We showed that by attaching small adhesive patches onto an otherwise non-adhesive particle deposition can be drastically enhanced. This kind of technology is of vital interest to various industrial processes, particularly that of paper manufacture where traditionally flocculating polymers or chemical/physical interactions have been used to increase deposition efficiency. *Further investigations into efficient attachment of adhesive polymers onto particles to be deposited and the effect of the adhesive polymer (glass transition temperature and size with respect to the main particle) are vital in order to further this work and develop it into a functional product.*

Chapter 3 described the synthesis of hydrazide functionalized polymer microgels. These particles were shown to be capable of dynamic release of carbonyl containing compounds and the response to pH and concentration gradients was described. It was shown that fragrance release could be extended for long periods in the presence of the microgel particles. *The hydrazide functional polymer has the potential to be of great use to a variety of applications, specifically in biological applications but in order to be used practically extensive safety tests on the polymer and its long term stability must be examined. The particles were synthesized by dispersion polymerization in the presence*

of large amounts of polymeric stabilizers and for scaling up further work into synthesis of the microgel particles and the polymer in general should be undertaken.

Chapter 4 described the synthesis of highly porous particles with tailored surface chemistry in order to remove oil for fibrous substrates. The rate at which the oil was absorbed by the particles was shown to increase with increasing average pore size. By incorporation of magnetic iron oxide nanoparticles into the porous polymer network it was possible to obtain particles that can be easily removed from the surface of the hair fibres by magnetic force. *In order to develop this further into a product capable of commercialization further tests into the use of the particles in aerosol formulations should be undertaken and the testing of the particles for the end application must be achieved.*

Chapter 5 described the development of a computational program designed in order to predict the ability of particulates to emulsify certain systems. To exemplify the use of the program cubic particles were tested and the orientations were shown to be well described by the theory. The surface activities of several classes of particles were calculated and in many cases were shown to deviate from the molecular analogues. *The program has the potential to be a useful tool in the synthesis by design of highly anisotropic particles as Pickering stabilizers. It is hoped that through use of the program and by following the set of general guidelines set out in this chapter new classes of highly efficient Pickering stabilizers will be generated*

Chapter 6 discussed the synthesis of highly anisotropic colloidal particles synthesized by polymer templating of naturally occurring spore particles. The surface activity of these highly anisotropic particles was found to be drastically reduced compared to the smooth analogues of these particles. *This chapter demonstrated that*

increasing surface roughness decreased the wettability of the particles. This could be of potential interest in the synthesis of particles designed for use in superhydrophobic coatings and as antifoam agents where activity is enhanced by reduced wettability. The method of templating pre-existing particles will be of interest to colloid scientists in achieving particle morphologies that cannot be obtained by traditional heterogeneous polymerization techniques.